CENTRO DE NEUROCIENCIAS DE CUBA
DEPARTAMENTO DE NEUROESTADÍSTICA

CARACTERIZACIÓN ESPACIO-TIEMPO-FRECUENCIA DE LA ACTIVIDAD ELÉCTRICA DE REDES NEURONALES

Trabajo de Tesis para optar por el grado de

Doctor en Ciencias Físicas

EDUARDO MARTÍNEZ MONTES

Ciudad de la Habana

2009

CENTRO DE NEUROCIENCIAS DE CUBA
DEPARTAMENTO DE NEUROESTADÍSTICA

CARACTERIZACIÓN ESPACIO-TIEMPO-FRECUENCIA DE LA ACTIVIDAD ELÉCTRICA DE REDES NEURONALES

Trabajo de Tesis para optar por el grado de

Doctor en Ciencias Físicas

Autor: Lic. EDUARDO MARTÍNEZ MONTES

Tutor: Inv. Tit., Dr. Pedro Antonio Valdés Sosa, Dr. C

Ciudad de la Habana

2009

AGRADECIMIENTOS

Utilizando un orden cronológico inverso, quisiera agradecer a todos los que han aportado a la realización de esta tesis. Primeramente a los oponentes y tribunales de la Defensa y la Pre-Defensa por la seriedad y el rigor, tanto en la evaluación del contenido como de la forma del trabajo. A mi tutor Pedro A. Valdés Sosa y a todos los coautores de los artículos que forman el núcleo de esta tesis, por la educación, la amistad y la oportunidad de trabajar a su lado. A Lídice por su tiempo, dedicación y ayuda tanto en la revisión de la Tesis como en la organización y trámites para llevarla a buen término. A mis compañeros del Centro de Neurociencias de Cuba, especialmente a Mayrim, Bornot, Tin, Mayita, Pavel y Lester por sus ayudas explícitas e implícitas, pero siempre necesarias. A mi familia por el apoyo incondicional, fundamentalmente a los más allegados: mi mamá, mi papá, mi hermana y mi suegra. Y muy especial agradecimiento a mi esposa por el amor, la motivación, el incentivo, las discusiones científicas, los consuelos, el eterno apoyo y la paciencia para postergar tantos planes y necesidades indefinidamente, digo, hasta que “acabe la Tesis”.

A Laura y Frank Alberto

SÍNTESIS

El Electroencefalograma (EEG) es el registro de las series temporales del potencial eléctrico medido en el cuero cabelludo. Refleja la actividad eléctrica sincronizada de grandes poblaciones de neuronas interconectadas en redes. La actividad de estas redes se relaciona con los procesos cerebrales normales o patológicos, por lo que el análisis del EEG es importante para el estudio, con alta resolución temporal, de dichos procesos. En esta tesis nos proponemos desarrollar nuevos métodos de análisis del EEG que permitan una caracterización de las propiedades espaciales, temporales y espectrales de la actividad de las redes neuronales. En particular, se proponen nuevas medidas estadísticas para cuantificar los cambios en la dinámica cerebral relacionada a eventos en el dominio tiempo-frecuencia; se introducen dos nuevos métodos para la descomposición espacio-tiempo-frecuencia de actividades espontáneas, esporádicas y relacionadas a eventos y se proponen algoritmos para incorporar a esta descomposición restricciones con bases fisiológicas y físicas, así como datos procedentes de imágenes de resonancia magnética funcional. Las metodologías propuestas demostraron su utilidad para la identificación de las redes neuronales con el uso de datos reales y simulados, superando limitaciones de los métodos clásicos de análisis del EEG.

ÍNDICE

INTRODUCCIÓN GENERAL

El estudio no invasivo del funcionamiento cerebral se ha hecho posible en las últimas décadas con el desarrollo de las técnicas de neuroimágenes, en particular aquellas relacionadas con las imágenes de resonancia magnética (IRM) y con las mediciones de la actividad electromagnética del cerebro a través del electro y magnetoencefalograma (EEG y MEG). A pesar de la alta resolución espacial de las IRM, sólo el EEG y MEG proveen mediciones de la actividad eléctrica cerebral con la resolución temporal requerida para el estudio de la dinámica de los procesos cerebrales. El EEG es el registro del potencial eléctrico con electrodos distribuidos sobre el cuero cabelludo. Actualmente es el método más común tanto en las neurociencias clínicas como en la investigación debido a su menor costo y fácil implementación.

Las series de tiempo del EEG se modelan como un **proceso estocástico** $V(r,t)$, (donde r representa las coordenadas de los electrodos y t los instantes de tiempo) que es altamente complejo, no lineal y no estacionario. Su dinámica debe estudiarse con el uso de métodos estadísticos [Lopes da Silva 1993, Dummermuth y col. 1987] dado que el EEG es el reflejo de la actividad eléctrica (sincronizada espacial y temporalmente) de grandes poblaciones de neuronas interconectadas entre sí, formando redes neuronales [Niedermeyer y col. 1999, Varela y col. 2001]. La actividad de estas redes está relacionada con los diversos procesos neurales, por lo que se asume que las áreas cerebrales cuyas actividades eléctricas tienen similares propiedades espaciales, dinámicas y espectrales, forman parte de una red neuronal involucrada en el procesamiento de una información común [Lopes da Silva 1993, Varela y col. 2001,

Martínez-Montes y col. 2006]. **Por tanto, el problema fundamental del análisis cuantitativo del EEG es la identificación de las redes neuronales involucradas en distintos procesos cerebrales, a partir del estudio de las propiedades espacio-tiempo-frecuencia de su actividad eléctrica**.

En el EEG, se reconocen esencialmente dos tipos de actividades relevantes para el estudio del funcionamiento cerebral:

a) **EEG espontáneo:** Actividad eléctrica registrada mientras el sujeto está en reposo y en ausencia de estímulos externos, ya sea normal o patológica. Tradicionalmente se han identificado actividades oscilatorias (ritmos cerebrales) denominadas según la banda de frecuencia de las oscilaciones. Su aparición y los cambios en su amplitud han sido relacionados con diferentes estados cognitivos como la atención visual, el dolor y con patologías como tumores, desórdenes sensoriales, lesiones de tallo cerebral y desmielinización [Niedermeyer y col. 1999]. Otro tipo de actividad espontánea es la que llamaremos "actividad esporádica", ya que aparece como consecuencia de procesos cerebrales internos. Dos ejemplos de estos son los "husos de sueño" y la actividad epiléptica, cuyas propiedades han sido bien definidas en la práctica clínica.

b) **Dinámica Cerebral Relacionada a Eventos (DCRE):** Actividad que aparece como respuesta a estímulos externos o eventos internos. Los cambios en la DCRE son actualmente tema de gran interés en las investigaciones de neuropsicología, ya que ellos están relacionados directamente con las funciones sensoriales, cognitivas y de consciencia cerebral [Handy 2005, Tallon-Baudry y col. 1997, Mazaheri y col. 2005, Ward 2003, Mäkinen y col. 2005]. Los cambios más estudiados son: i) el Potencial Relacionado a Eventos (PRE, ver Anexo C), que es un transiente de voltaje de pequeña

amplitud [Handy 2005]; ii) la actividad inducida (ver Anexo C), que son los cambios en la amplitud de oscilaciones en determinada banda de frecuencia [Varela y col. 2001, Pfurtscheller y col. 1999] y iii) los cambios en la fase de las oscilaciones, conocido como fenómeno de restablecimiento parcial de fase (RPF, ver Anexo C) [Hanslmayr y col. 2007, Mazaheri y col. 2006, Klimesch y col. 2006].

La alta dimensionalidad del EEG ha llevado a que el modelo más popular para su análisis corresponda a una descomposición en funciones cuyas propiedades en espacio, tiempo y frecuencia sean conocidas o más fáciles de caracterizar. Este modelo puede expresarse genéricamente con la ecuación:

$$V(r,t) = \sum_k g_{k,f}(r,t) + \varepsilon(r,t) \qquad (1)$$

Cada función $g_{k,f}$ contiene la actividad de la componente *k*-ésima dependiendo del espacio (*r*), el tiempo (*t*) e implícitamente de la frecuencia (*f*). El término $\varepsilon(r,t)$ representa el ruido o errores aleatorios no modelados en la descomposición. En este contexto, las metodologías de análisis del EEG pueden agruparse según las dimensiones estudiadas:

1. Análisis en el dominio del tiempo: Localización en el tiempo de la actividad de interés y estudio de su distribución espacial. Ej. Potenciales Relacionados a Eventos (PREs). Dados *N* segmentos o ensayos de EEG, $V_i(r,t)$ ($i = 1,..,N$), el PRE se calcula como su promedio: $\bar{V}(r,t) = \sum_{i=1}^{N} V_i(r,t) / N$. Luego, se define (visualmente o con métodos estadísticos) una ventana de tiempo T_0 (N_t instantes) alrededor del pico de interés y se obtiene la topografía $a(r) = \sum_{t \in T_0} \bar{V}(r,t) / N_t$. Esta metodología no permite distinguir si el PRE es una actividad aditiva (superpuesta) al EEG oscilatorio "de fondo"

o aparece como parte de cambios en las fases de este último. Otros métodos aplicados en el dominio del tiempo a las actividades espontáneas consisten en el ajuste de modelos autorregresivos [Jimenez y col. 1995] y el uso de la teoría de caos determinista [Quian-Quiroga 1998]. Sin embargo, estos métodos asumen que la señal es estacionaria por lo que su utilidad en el análisis del EEG no ha sido totalmente establecida [Quian-Quiroga 1998, Valdés-Sosa y col. 1999].

2. Análisis en el dominio de la frecuencia: Localización de la frecuencia de la oscilación de interés a través del cálculo del espectro. Ej. Estudio de ritmos espontáneos. Dados N segmentos medidos en $t_n = t_0 + n\Delta$, (con $n = 0,..,N_t - 1$ y período de muestreo Δ), sus transformadas de Fourier conforman el proceso estocástico $\tilde{V}_i(r,f) \in \mathbb{C}$ ($i = 1,..,N$), con $\tilde{V}_i(r,f_m) = \sum_{n=0}^{N_t-1} V_i(r,t_n) e^{-j2\pi f_m t_n / N_t}$, $f_m = m / N_t\Delta$ y $m = 0,..,N_t - 1$. El espectro se estima según $S(r,f) = \sum_{i=1}^{N} \tilde{V}_i(r,f)\tilde{V}_i^*(r,f) / N$, donde * denota la conjugación compleja. Luego se define (visualmente o con métodos estadísticos) una banda de frecuencia de interés F_0 (N_f frecuencias) y se obtiene la topografía $a(r) = \sum_{f \in F_0} S(r,f) / N_f$. Nótese que esta topografía tiene unidades de voltaje al cuadrado. Este análisis tiene las limitaciones de asumir que la señal de EEG es estacionaria y desechar la información de las fases de las oscilaciones, al estudiar solamente el espectro. Para disminuir los efectos de bordes, usualmente se multiplica la señal en cada segmento por una función que cae a cero en las fronteras, dando lugar a otros estimadores del espectro, como el método de Hanning y el *multitaper* de Thomson [Thomson 1982, Dummermuth y col. 1987].

3. Análisis espacio-temporal: Descomposición de la señal en componentes que conllevan las características espaciales y temporales por separado. Ej. Determinación simultánea de la forma temporal de un PRE y su correspondiente distribución topográfica. En los dominios del tiempo y la frecuencia, el análisis de la actividad de interés se hace independientemente para cada electrodo de medición. En el análisis espacio-temporal, se asume que cada red neuronal produce una actividad eléctrica con un patrón espacial fijo y su correspondiente dinámica. Por tanto, se propone la descomposición del EEG en N_k componentes, cada una formada por la combinación de una topografía característica $a_k(r)$ con su correspondiente evolución temporal $c_k(t)$:

$$V(r,t) = \sum_{k=1}^{N_k} a_k(r) c_k(t) + \varepsilon(r,t) \qquad (2)$$

Utilizando una notación matricial el EEG se representa por la matriz $\mathbf{V}_{(N_r \times N_t)}$ y esta ecuación se reescribe como $\mathbf{V} = \mathbf{A}\mathbf{C}^T + \mathbf{E}$, donde $\mathbf{A}_{(N_r \times N_k)}$ y $\mathbf{C}_{(N_t \times N_k)}$ son las matrices cuyas columnas representan las topografías y series de tiempo características de cada componente, respectivamente. **E** es la matriz de ruido. Este enfoque permite identificar actividades cuyas distribuciones espacial y temporal aparecen combinadas en los datos, por lo que se dice que extrae las características espacio-temporales de las redes neuronales. Sin embargo, esta descomposición no es única y es necesario imponer restricciones a las matrices **A** y **C** para obtener una solución. Los métodos de Análisis de Componentes Principales (CP) y de Componentes Independientes (CI) son los más usados en este enfoque y se distinguen por exigir ortogonalidad e independencia estadística entre las columnas de **A** y **C**, respectivamente [Soong y col. 1995, Makeig y

col. 2002]. Sin embargo, estas restricciones matemáticas no siempre llevan a soluciones fisiológicamente fundadas e interpretables.

4. Análisis tiempo-frecuencia: Descomposición de las series de tiempo en funciones base con características tiempo-frecuencia conocidas o más fáciles de estudiar.

Primer enfoque: Obtención de la evolución temporal del espectro de la señal. El método más simple consiste en la estimación del espectro de Fourier para segmentos consecutivos del EEG (espectro variante en el tiempo). Este es superado por la modelación del EEG de la forma:

$$V(r,t) = \frac{1}{\|g\|} \sum_f \sum_{t'} x(r,t',f) g(t-t') e^{j2\pi ft} \qquad (3)$$

Donde $g(t-t')$ representa una función de "ventana", o sea, con valores no nulos sólo en una vecindad de t' y con norma $\|g\| = \sqrt{\sum_t |g(t)|^2}$. Los coeficientes $x(r,t,f) \in \mathbb{C}$ son obtenidos por la transformada de Fourier de Tiempo Corto (discreta):

$$x(r,t,f) = \sum_{t'} V(r,t') g(t'-t) e^{-j2\pi ft'} \qquad (4)$$

La distribución de la energía de la señal en el dominio tiempo-frecuencia se conoce como **espectrograma** $S(r,t,f) = |x(r,t,f)|^2$ [Boashash 2003]. El uso de diferentes funciones *g* ha dado lugar a diversos espectrogramas, destacándose los métodos de ventanas deslizantes [Makeig 1993], análisis de Gabor [Feichtinger y col. 1998] y análisis "*wavelet*" [Tallon-Baudry y col. 1997], este último el más usado actualmente en el estudio de la Dinámica Cerebral Relacionada a Eventos. El análisis del espectrograma tampoco permite cuantificar los cambios en las fases de las oscilaciones ni distinguir entre los posibles mecanismos de generación del PRE. Además, la dimensión espacial no es afectada por la transformación tiempo-frecuencia por lo que la distribución

espacial también es obtenida luego de seleccionar *ad hoc* la banda de frecuencias F_0 y la ventana de tiempo T_0 de interés: $a(r) = \sum_{f \in F_0} \sum_{t \in T_0} S(r,t,f) \Big/ N_t N_f$.

Segundo enfoque: Descomposición de la señal en una base sobrecompleta (diccionario) de funciones con localizaciones tiempo-frecuencia conocidas (átomos tiempo-frecuencia). Este enfoque ha sido utilizado principalmente en la identificación de actividades esporádicas y se basan en el modelo:

$$V(r,t) = \sum_{k(t',f)} x_k(r) d_k(t) + \varepsilon(r,t) \qquad (5)$$

donde los átomos $d_{k(t',f)}(t)$ son funciones oscilatorias de frecuencia *f*, moduladas por una "ventana" centrada en el tiempo t' (por ejemplo las funciones de Gabor o *wavelets* de Morlet) [Durka 2007]. Los coeficientes tiempo-frecuencia $x_{k(t',f)}(r)$ pueden ser reales o complejos, en dependencia de los átomos. El uso de diccionarios sobrecompletos o redundantes es necesario para garantizar una buena resolución tiempo-frecuencia [Durka 2007]. Sin embargo, esto implica la no-unicidad de la descomposición, por lo que las metodologías de este enfoque se distinguen por las restricciones y algoritmos utilizados para obtener una representación de la señal en sólo unos pocos átomos relevantes o los correspondientes a la actividad de interés. Entre los métodos desarrollados sobresalen el "*Matching Pursuit*" [Durka y col. 1995], el "*Basis Pursuit*" y el "método de marcos" [Chen y col. 2001]. Este enfoque se ha restringido al análisis de un sólo electrodo por lo que no toma en cuenta las características espaciales de las actividades analizadas.

5. Análisis espacio-tiempo-frecuencia: Identificación simultánea de las propiedades espaciales, temporales y espectrales de la actividad de las redes neuronales. Este problema se ha intentado resolver con la combinación de algunos de los métodos

explicados arriba. Como ejemplo relevante, en Koenig y col. 2001, se introduce el método de descomposición "Tiempo-Frecuencia Topográfico" (ver Anexo C). En este se realiza la descomposición del EEG en un diccionario tiempo-frecuencia (en cada electrodo por separado) y luego se aplica un método de clusterización para obtener unas pocas topografías fisiológicamente relevantes. Otro intento ha sido el análisis tiempo-frecuencia de las componentes obtenidas de la descomposición espacio-temporal del EEG [Makeig y col. 2002]. Estos estudios heredan las limitaciones de los métodos utilizados en cada paso y no proveen una caracterización simultánea en espacio, tiempo y frecuencia de la señal de EEG.

En la Tabla 1, se resumen los métodos de análisis del EEG según el dominio y el tipo de actividad estudiada, así como sus principales limitaciones y referencias bibliográficas. En esta Tesis nos proponemos introducir metodologías que completen esta Tabla, buscando, en primer lugar, superar las limitaciones del estudio de la Dinámica Cerebral Relacionada a Eventos a partir del análisis directo de los cambios en la distribución de los coeficientes tiempo-frecuencia complejos.

En segundo lugar, abordaremos el uso de métodos para la caracterización simultánea espacio-tiempo-frecuencia de la actividad eléctrica de las redes neuronales. Esta puede obtenerse con la adaptación al análisis del EEG de metodologías utilizadas en otras ramas del procesamiento de señales. Por un lado, introduciremos la generalización del método de descomposición tiempo-frecuencia *Matching Pursuit* para el análisis de actividades esporádicas del EEG en todos los electrodos simultáneamente [Gribonval 2003]. Por otro lado, investigaremos el uso del modelo de descomposición tensorial

conocido como PARAFAC (del inglés, *Parallel Factor analysis*) [Harshman 1970, Carroll y col. 1970], para el análisis del espectrograma del EEG espontáneo o relacionado a eventos. Interpretando el espectrograma de todos los electrodos como un tensor de tercer orden, el modelo PARAFAC toma la forma:

$$S(r,t,f) = \sum_k a_k(r) b_k(f) c_k(t) + \varepsilon(r,t,f) \qquad (6)$$

La obtención de las funciones *a*, *b* y *c* proveería una caracterización simultánea y separada en espacio, tiempo y frecuencia de la energía de la señal del EEG.

Tabla 1. Metodologías de análisis del EEG según el dominio de análisis y las actividades de estudio. Las referencias y limitaciones fundamentales de cada método aparecen entre paréntesis. Las letras T, F y E representan los dominios del tiempo, la frecuencia y el espacio respectivamente. CP/CI se refiere a los análisis de Componentes Principales e Independientes y TFTC significa Transformada de Fourier de Tiempo Corto.

Dominio de Análisis	Actividades esporádicas	Dinámica Cerebral Relacionada a Eventos	Ritmos cerebrales espontáneos
T	Series de Tiempo / Teoría de Caos *(Supone señal estacionaria y libre de ruido)* [Quian-Quiroga 1998]	Promediación *(Supone PRE como actividad aditiva)* [Handy 2005]	Teoría de Caos *(Supone señal estacionaria y libre de ruido)* [Quian-Quiroga 1998]
F	Análisis Espectral *(supone señal estacionaria, analiza sólo amplitud)* [Gotman y col. 1981]	Análisis Espectral / Autorregresivos *(supone señal estacionaria, analiza sólo amplitud)* [Nuwer 1994, Gersch 1970]	Análisis Espectral *(supone señal estacionaria, analiza sólo amplitud)* [Dummermuth y col. 1987]
E – T	CP/ CI/ Teoría de Caos *(asumen señal estacionaria y restricciones no fisiológicas)* [Lehnertz y col. 1995]	CP / CI *(Descomposición no única, restricciones no fisiológicas)* [Onton y col. 2006]	CP / CI *(Descomposición no única, restricciones no fisiológicas)* [Lagerlund y col. 1997]
T – F	*Matching Pursuit* / Gabor / *wavelets* *(analiza sólo amplitud en un electrodo)* [Durka y col. 1995, Quian-Quiroga 1998]	*Wavelets* de Morlet *(analiza sólo amplitud en un electrodo)* [Tallon-Baudry y col. 1997]	TFTC / CP *(analiza sólo amplitud en un electrodo)* [Moosmann y col. 2003, Kayser y col. 2000]
T – F – E	¿?	¿?	¿?

En tercer lugar, nos proponemos obtener descomposiciones PARAFAC más interpretables desde el punto de vista fisiológico y con alta resolución espacial, a través de la introducción de restricciones apropiadas y de su combinación con datos de imágenes de resonancia magnética funcional (IRMf) con el método de Mínimos Cuadrados Parciales Tensorial. En la Tabla 2 hemos insertado en el mapa de los métodos de análisis del EEG, los espacios que trataremos de cubrir con las metodologías propuestas en cada uno de los objetivos específicos de este trabajo.

Tabla 2. Dominio de análisis y actividades de estudio de las distintas metodologías de análisis de EEG con los objetivos de este trabajo insertados (y el Artículo correspondiente). Las letras T, F y E representan los dominios del tiempo, la frecuencia y el espacio respectivamente. CP/CI se refiere a los análisis de Componentes Principales e Independientes y TFTC significa Transformada de Fourier de Tiempo Corto.

Dominio de Análisis	Actividades esporádicas	Dinámica Cerebral Relacionada a Eventos	Ritmos cerebrales espontáneos
T	Teoría de Caos	Promediación	Teoría de Caos
F	Análisis Espectral	Análisis Espectral	Análisis Espectral
E – T	CP / CI / Caos	CP / CI	CP / CI
T – F	*Matching Pursuit*	*Wavelets*/**Objetivo 1 (Artículo 1)**	TFTC
T – F – E	**Objetivo 2 (Artículos 2 y 3)**	**Objetivo 3 (Artículo 4)**	**Objetivo 4 (Artículos 5 y 6)**
T – F – E +IRMf			**Objetivo 5 (Artículo 7)**

Planteamiento del problema

Superar las limitaciones de los métodos tradicionales de análisis del EEG para obtener una mejor caracterización en espacio, tiempo y frecuencia de los cambios en la actividad eléctrica de las redes neuronales involucradas en distintos procesos cerebrales.

Hipótesis

El uso de métodos diseñados específicamente para el análisis multidimensional del EEG permite la caracterización espacial, espectral y temporal de las redes neuronales implicadas en el funcionamiento cerebral.

Objetivo general

La introducción de medidas estadísticas y métodos de descomposición multidimensional para el análisis espacio-tiempo-frecuencia de la actividad eléctrica transiente, inducida, esporádica y rítmica de larga duración de las redes neuronales involucradas en el funcionamiento cerebral.

Objetivos específicos

1.- Diseño de medidas estadísticas que permitan diferenciar la actividad transiente e inducida, así como la reorganización parcial de fase de las oscilaciones cerebrales, basándose en estadígrafos definidos sobre la nube de coeficientes complejos de la representación tiempo-frecuencia del EEG relacionado a estímulos.

2.- Introducción de un método de descomposición espacio-tiempo-frecuencia para el análisis de actividades esporádicas, basado en la combinación de versiones multicanales del algoritmo *Matching Pursuit* con soluciones inversas distribuidas.

3.- Introducción de un método de descomposición espacio-tiempo-frecuencia para el estudio de actividades oscilatorias espontáneas o inducidas, basado en el análisis multilineal PARAFAC del espectrograma del EEG.

4.- Introducción de descomposiciones tensoriales espacio-tiempo-frecuencia más interpretables desde el punto de vista fisiológico mediante el uso de un algoritmo que

permita imponer múltiples restricciones cuadráticas y no cuadráticas al modelo PARAFAC.

5.- Combinación de datos de IRMf con la actividad espontánea oscilatoria en el EEG para el mejoramiento de la resolución espacial en la caracterización espacio-tiempo-frecuencia de redes neuronales, mediante el uso del método de Mínimos Cuadrados Parciales Tensorial.

Organización de la tesis

Los cinco objetivos específicos de este trabajo están cubiertos en 7 artículos publicados en revistas indexadas en la *Web of Science*. Cada artículo se enmarca en su propio problema específico y detalla las motivaciones y revisión bibliográfica particular (ver Tabla 2). A cada objetivo se dedicará un capítulo con secciones Introducción, Métodos y Resultados y discusión parcial. En ellos no se pretende duplicar la información técnica (ecuaciones, gráficas y referencias) de los artículos, sino complementar su contenido para una mejor comprensión de su aporte al problema general abordado en esta Tesis. El texto íntegro de los artículos originales (en inglés) aparecerá en el Anexo A. Finalmente presentamos un capítulo con la Discusión General, seguido de las Conclusiones, las Referencias Bibliográficas y los Anexos B, C y D conteniendo las abreviaturas utilizadas, un glosario español-inglés de los términos más importantes que aparecen en los artículos con la correspondiente traducción utilizada en la Tesis y una lista de los Eventos Científicos en que se han presentado los resultados de este trabajo, respectivamente.

CAPÍTULO I

ANÁLISIS TIEMPO-FRECUENCIA DE LA DINÁMICA CEREBRAL RELACIONADA A EVENTOS.

CAPÍTULO I. ANÁLISIS TIEMPO-FRECUENCIA DE LA DINÁMICA CEREBRAL RELACIONADA A EVENTOS

1.1 Introducción

El análisis clásico de la dinámica cerebral relacionada a eventos (DCRE) se ha enfocado en la determinación de los cambios en latencia y amplitud de los potenciales relacionados a eventos (PREs) y de la actividad inducida. El primer problema se ha abordado bajo la suposición de que el PRE es una actividad evocada por el estímulo que se superpone a las oscilaciones "de fondo" (ver Anexo C). Esto conlleva a una relación temporal fija entre el PRE y la presentación del estímulo, por lo que se le denomina actividad "bloqueada en tiempo" (ver Anexo C). Un punto de vista alternativo plantea que la presentación del estímulo induce cambios en la actividad oscilatoria de fondo solamente. El método tradicional de análisis no permite distinguir cuál de estos mecanismos origina el PRE, por lo que los méritos de cada punto de vista están actualmente en fuerte debate y escrutinio.

Por otro lado, el estudio de la actividad inducida se ha basado en la evaluación estadística de medidas obtenidas de la transformación tiempo-frecuencia del EEG. El análisis tiempo-frecuencia permite obtener la distribución de energía (espectro o densidad espectral) del EEG para distintos valores de frecuencia y en cada instante de tiempo. Existen distintos métodos para obtener esta descomposición como son las transformadas de Fourier de tiempo corto (ver Anexo C), de *wavelet* Morlet (ver Anexo C), de Gabor y de Hilbert, las cuales son representaciones equivalentes del EEG en coeficientes complejos para cada frecuencia e instante de tiempo [Kiebel y col. 2005]. El

análisis actual se restringe a la búsqueda de los cambios significativos en el espectrograma o en la amplitud de las oscilaciones (valor absoluto de los coeficientes complejos) utilizando tanto estadígrafos paramétricos como no paramétricos [Makeig 1993, Kiebel y col. 2005, Tallon-Baudry y col. 1996]. Este enfoque tampoco permite distinguir entre los diferentes mecanismos que originan el PRE, ya que excluye el estudio de los cambios en la fase de las oscilaciones de fondo.

Los primeros intentos de medir la alineación de fases en la actividad de fondo consistieron en el uso del factor de bloqueo de fase (*phase-locking factor*, ver Anexo C) [Tallon-Baudry y col. 1996], también llamado Coherencia Interensayo (ITC, del inglés *Intertrial Coherence*, ver Anexo C) [Makeig y col. 2002, Yamagishi y col. 2003, Edwards y col. 2005, Mørup y col. 2006]. Esta es una medida de la uniformidad de la distribución de las fases de los coeficientes complejos para diferentes ensayos o repeticiones del experimento. Sin embargo, algunos trabajos han cuestionado la validez de esta medida para distinguir entre la presencia de un PRE aditivo al EEG de fondo o aparecido como parte de un fenómeno de restablecimiento parcial de fase [Yeung y col. 2004, Cuspineda-Bravo y col. 2006].

En este capítulo proponemos nuevas medidas estadísticas para evaluar los cambios en la DCRE. Estas se derivan directamente de los coeficientes complejos, tomando en cuenta tanto su amplitud como su fase. De esta forma, pretendemos superar las limitaciones del análisis actual, en particular, la imposibilidad de distinguir entre los posibles mecanismos originarios del PRE.

1.2 Métodos

1.2.1 *Representación de la DCRE en el plano tiempo-frecuencia*

Los coeficientes de la transformación tiempo-frecuencia del EEG se pueden hallar según la ecuación 4 (ver Introducción), aunque en la práctica, se calculan mediante la convolución de la señal con cada una de las funciones de la familia de *wavelets* de Morlet:

$$x_i(r,t,f) = \sum_{t'} V_i(r,t')w(t-t',f) \qquad (7)$$

donde el índice *i* representa el ensayo del experimento. La función "madre" de la familia de *wavelets* de Morlet tiene una forma gaussiana tanto en el tiempo (semiancho σ_t) como en la frecuencia (semiancho σ_f), dada por $w(t,f) = (\sigma_t\sqrt{\pi})^{-1/2} e^{-t^2/2\sigma_t^2} e^{i2\pi ft}$, de donde $\sigma_f = 1/2\pi\sigma_t$.

Según el principio de incertidumbre del análisis de señales (a veces denominado Heisenberg-Gabor [Durka 2007, Boashash 2003]) la localización temporal y la frecuencia de oscilación de una señal no pueden determinarse con precisión arbitraria simultáneamente. Matemáticamente, este puede expresarse en términos de medidas de la localización en tiempo (Δt) y frecuencia (Δf) de la energía de la señal, de la forma: $\Delta t \Delta f \geq 1/4\pi$. Esta relación explica la interdependencia de las resoluciones en tiempo y frecuencia de esta transformación: a medida que una aumenta, la otra disminuye. En el caso de la transformación *wavelet*, los semianchos ($\Delta t = \sigma_t$, $\Delta f = \sigma_f$) cumplen con la igualdad, de forma que la función de Morlet (en general, cualquier función oscilatoria modulada por una gaussiana) permite una representación tiempo-frecuencia de la señal con la combinación óptima de resolución en tiempo y en frecuencia. A la vez, la base de

funciones *wavelets* se caracteriza por mantener la razón f/σ_f constante, de forma que la resolución espectral es menor para frecuencias mayores. Esta razón define el número de ciclos o períodos de la *wavelet* y en el análisis del EEG se recomienda el uso de un valor mayor que 5 (equivalente a un número de ciclos mayor que $5/\pi$), para garantizar una estimación aceptable de la energía de la señal en cualquier frecuencia.

Cada una de las actividades relacionadas a eventos puede representarse por los coeficientes *wavelets* en el plano complejo. En un experimento típico de estimulación cognitiva se realizan muchas repeticiones del estímulo y se obtienen segmentos de la actividad eléctrica cerebral desde 200 a 400 ms antes del estímulo hasta 600 ó 1000 ms después. Cada repetición o ensayo muestra actividad oscilatoria que contiene la actividad relacionada al estímulo. La presentación aleatoria del estímulo durante el experimento provoca que la actividad oscilatoria de fondo que aparece en el período pre-estímulo aparezca con un rango de amplitudes y de fases en los distintos ensayos. Por tanto, los coeficientes complejos correspondientes a cada ensayo para un instante de tiempo en el pre-estímulo y una frecuencia dados, representan una nube en el plano complejo con una distribución quasi-esférica (fases uniformes) alrededor del origen (figura 1a del Artículo 1).

Si la actividad evocada por el estímulo corresponde a una actividad aditiva a las oscilaciones de fondo, en un instante de tiempo post-estímulo la nube de puntos complejos mostrará la misma distribución esférica (fases uniformes) pero alrededor de un valor medio diferente del origen (figura 1b del Artículo 1). En el caso de que el evento evoque un restablecimiento de fase de las oscilaciones de fondo, en el período post-estímulo los coeficientes mantendrán el mismo módulo que en el pre-estímulo pero

sus fases tendrán valores cercanos (figura 1c del Artículo 1). Por último, si el estímulo provoca el aumento o disminución de la amplitud de las oscilaciones de una frecuencia determinada, la nube de coeficientes aumentará el rango de amplitudes sin variar las fases ni la media en el origen (figura 1d del Artículo 1).

1.2.2 *Medidas estadísticas a partir de los coeficientes tiempo-frecuencia complejos*

En el Artículo 1 (Anexo A) mostramos que la búsqueda de cambios significativos en la DCRE puede hacerse con el uso de tests estadísticos sobre los coeficientes tiempo-frecuencia. Estos se basan en que los distintos tipos de actividades son fácilmente distinguibles según la distribución de los coeficientes en el plano complejo. De esta forma, podemos evaluar la presencia de una actividad media en el post-estímulo (PRE), utilizando directamente la media de los coeficientes complejos como medida estadística. En cada frecuencia e instante de tiempo dados, la desviación de esta medida de su valor promedio en el período pre-estímulo puede estimarse con el uso del estadígrafo **t complejo** [Brillinger 2001], según la ecuación 3 del Artículo 1.

En segundo lugar, la actividad inducida puede medirse por los cambios en la variabilidad de la distribución de puntos alrededor de su valor medio. Esto contrasta con la práctica actual donde se mide el cambio en el valor medio del módulo de los coeficientes. En este último caso cualquier medida de la actividad inducida dependería de la actividad media, ya que la traslación de la nube implicaría cambios en los módulos de los coeficientes medidos desde el origen, aún en ausencia de cambios en la amplitud de las oscilaciones. Por tanto, proponemos usar directamente la varianza de los coeficientes complejos como medida de la amplitud de las oscilaciones con respecto a su

valor medio e independiente de este. La desviación de esta magnitud con respecto a sus valores promedios en el período pre-estímulo para cada frecuencia se puede cuantificar con un estadígrafo similar a la **t de Student**, como se muestra en la ecuación 4 del Artículo 1.

Por último, nos proponemos evaluar la presencia de una distribución de fases no uniforme en la nube de puntos complejos, como reflejo de la ocurrencia del fenómeno de restablecimiento parcial de fase (RPF). Actualmente, la presencia de RPF se valida con la Coherencia Interensayo (ITC del inglés, *Intertrial Coherence*), que se obtiene según la ecuación 1 del Artículo 1. Sin embargo, esta medida ofrece valores similares (significativamente distintos de cero) tanto en casos de RPF como de PRE aditivo (paneles centrales de las figuras 1b, 1c y 7 del Artículo 1). Esto se debe a que las fases de los coeficientes complejos son medidas a partir del origen y no reflejan la distribución de los puntos alrededor de su valor medio, lo cual hace que el ITC dependa de este último. Al restar el valor medio a cada uno de los coeficientes el ITC se anula, sin embargo se puede distinguir entre los casos de PRE aditivo y RPF, ya que el primero ofrece una distribución esférica mientras que el segundo muestra una distribución bimodal (figura 2 del Artículo 1). Esto nos permite proponer dos medidas de RPF basadas en la existencia de una distribución de fases no esférica alrededor del valor medio. La primera consiste en el test de igualdad de los autovalores (ver Anexo C) de la matriz de covarianzas entre la parte real e imaginaria de los coeficientes complejos (ecuación 5 del Artículo 1). Esta puede interpretarse como una correlación generalizada que detecta la orientación lineal de los coeficientes en el plano complejo. La segunda medida consiste en el valor absoluto del segundo momento trigonométrico (ver Anexo

C) de las fases de los coeficientes medidas con respecto al valor medio de la nube (ecuación 6 del Artículo 1). Este es una medida de la no uniformidad de una distribución de fases bimodal, como la que aparece en el caso de RPF al centrar los coeficientes (figura 2b del Artículo 1).

1.3 Resultados

En el Artículo 1 se presenta la simulación de 200 segmentos de EEG correspondientes a dos escenarios: uno de RPF y otro de PRE aditivo. En ambos la actividad de fondo consistió en oscilaciones de 6 y 10 Hz. En el caso del RPF las fases de las oscilaciones de 10 Hz se reorganizaron en el momento del estímulo, por lo que al promediar aparece una actividad no nula en el período post-estímulo. Esta actividad media se sumó escalada a cada uno de los ensayos del caso de PRE aditivo, de forma que aparecía igualmente en la promediación de estos. En ambos casos se diseñó un aumento de la amplitud de las oscilaciones de 6 Hz con el estímulo (actividad inducida).

El estadígrafo para la media mostró cambios significativos con respecto al pre-estímulo similares en ambos casos como era de esperar. Asimismo, en ambos casos el estadígrafo para la varianza reveló correctamente cambios significativos en la actividad inducida en los 6 Hz. El ITC mostró cambios significativos en el post-estímulo en ambos casos, lo cual evidencia su incapacidad para distinguir los dos mecanismos originarios del PRE. Sin embargo, los estadígrafos para la fase sólo tomaron valores significativos en el caso de RPF, aunque la medida de correlación generalizada mostró algunos efectos de borde significativos (figura 1.1 de la Tesis y figuras 5 y 6 del Artículo 1).

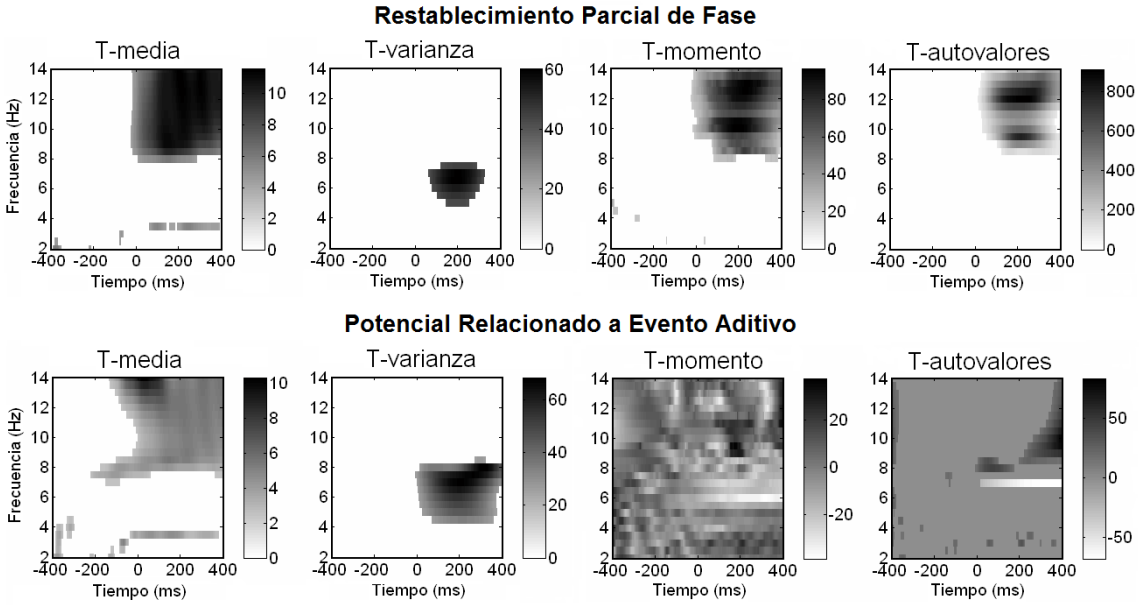

Figura 1.1. Gráficos tiempo-frecuencia de las medidas propuestas para validar cambios en: la actividad evocada media (T-media); la actividad inducida (T-varianza); la distribución de fases con el segundo momento trigonométrico (T-momento) y con el test de igualdad de autovalores de la matriz de covarianzas entre las partes real e imaginaria de los coeficientes complejos (T-autovalores). La fila superior corresponde a los datos simulados con un fenómeno de restablecimiento parcial de fase y la inferior con la suma de un potencial relacionado a eventos sobre las oscilaciones de fondo (ver Artículo 1 del Anexo A).

En el análisis de datos reales de atención visual, los estadígrafos para la media y la varianza revelaron cambios cuya localización tiempo-frecuencia concordó con reportes previos. Sin embargo, los estadígrafos para la fase, contrario a análisis previos de los mismos datos con el ITC [Delorme y col. 2004], no mostró claras evidencias de la presencia de RPF como responsable de la actividad evocada (figura 1.2 de la Tesis y figura 8 del Artículo 1).

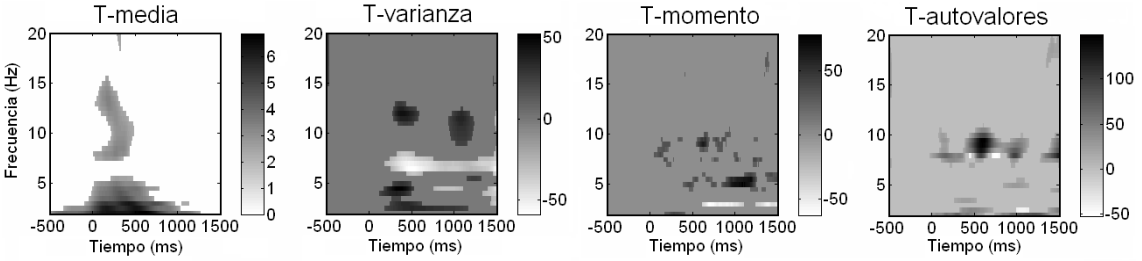

Figura 1.2. Gráficos tiempo-frecuencia de las medidas propuestas para validar cambios en las diferentes actividades de la DCRE, aplicadas a los datos reales obtenidos de un experimento de atención visual (ver Artículo 1 del Anexo A).

1.4 Discusión parcial de los resultados

Este estudio muestra la utilidad de las medidas propuestas para validar los cambios en la DCRE, sin embargo, algunas limitaciones de estos estadígrafos deben ser discutidas. El estadígrafo propuesto para medir los cambios en la actividad media demostró ser útil para este propósito con el uso de datos simulados y reales. Sin embargo, una limitación de este es que no es adecuado para distinguir entre los diferentes mecanismos que pueden originar dicha actividad media.

Otro estadígrafo introducido permitió medir correctamente cambios en la varianza de la amplitud de los coeficientes complejos, lo cual es un reflejo del aumento (o disminución) de la amplitud de las oscilaciones después del estímulo. Este fenómeno se conoce como sincronización (o desincronización) relacionada a eventos y es actualmente uno de los más investigados debido a su relación con innumerables estados cognitivos y procesamiento de alto nivel [Pfurtscheller y col. 1999, Tallon-Baudry y col. 1997, Tallon-Baudry y col. 1999, Amidzic y col. 2001, Herrmann y col. 2004]. Este estadígrafo demostró ser más sensible que el de la media en la localización tiempo-

frecuencia de la actividad inducida, aunque también se afecta con la baja resolución espectral y la potencia del test es menor. Un estudio más riguroso de las propiedades y la validez de este test estadístico debe realizarse a partir de simulaciones que involucren diversas situaciones de sincronización y desincronización simultáneamente. Por ejemplo, podrían existir cambios en la varianza de los coeficientes complejos cuando estos tienen aproximadamente la misma fase (o sea, en el caso de reorganización de la fase después del estímulo) que no se deberían a la presencia de actividad inducida.

Por otro lado, en nuestro estudio obtuvimos evidencias de que el ITC no es adecuado para medir el restablecimiento de fase debido al estímulo. Esta medida fue muy similar al estadígrafo propuesto para la media (figura 10 del Artículo 1), tanto en simulaciones como en datos reales, por lo que no puede distinguir entre los posibles mecanismos que originan esta actividad. Este resultado está en correspondencia con estudios anteriores que han encontrado que el ITC no ofrece una respuesta inequívoca de la presencia de un proceso de restablecimiento parcial de fase (RPF) como mecanismo originario de un potencial evocado [Yeung y col. 2004]. Al estudio de este fenómeno se le ha dedicado mucha atención en los últimos años [Hanslmayr y col. 2007, Mazaheri y col. 2006, Klimesch y col. 2006, Luu y col. 2004], encontrándose resultados contradictorios precisamente por el uso de medidas diversas en la medición del mismo.

Los estadígrafos propuestos para la medición de RPF están basados en la idea de que la distribución no uniforme de fases persiste incluso cuando se sustrae la media de los coeficientes a cada uno de ellos. Por tanto, no dependen de la actividad media, lo cual ayuda a evitar la influencia de esta actividad en la estimación de su mecanismo originario. Sin embargo, estos estadígrafos sí dependen de la estimación correcta de las

fases de los coeficientes complejos, lo cual puede afectar la resolución en la localización tiempo-frecuencia del RPF. Esta dependencia debe estudiarse con mayor profundidad en trabajos futuros, utilizando datos reales de EEG.

Debemos subrayar que aún cuando estas medidas son capaces de validar la presencia de cambios en la distribución de fases de las oscilaciones en una frecuencia y un tiempo determinados con respecto al pre-estímulo, no siempre podemos asegurar que estos reflejen un transiente de fase ordenado, realmente provocado por el estímulo dado. Creemos que dada la complejidad de las señales reales de EEG y la posibilidad de que diferentes tipos de cambios en la dinámica cerebral ocurran en la misma ventana tiempo-frecuencia, sólo el uso de modelos adecuados del EEG, junto con las medidas apropiadas de la evolución temporal de la fase, puede ofrecer una respuesta definitiva a este problema.

CAPÍTULO II

ANÁLISIS ESPACIO-TIEMPO-FRECUENCIA DE ACTIVIDADES ESPONTÁNEAS ESPORÁDICAS: *MATCHING PURSUIT* Y SOLUCIÓN INVERSA

CAPÍTULO II. ANÁLISIS ESPACIO-TIEMPO-FRECUENCIA DE ACTIVIDADES ESPONTÁNEAS ESPORÁDICAS: *MATCHING PURSUIT* Y SOLUCIÓN INVERSA

2.1 Introducción

En el Capítulo anterior introducimos nuevas medidas estadísticas que permiten caracterizar las actividades relacionadas a eventos en cuanto a su localización en tiempo y su contenido espectral. Sin embargo, con estas medidas no podemos conocer la localización espacial de las redes neuronales responsables de las actividades analizadas. La caracterización espacial de dichas redes neuronales ha sido abordada anteriormente a partir del análisis tiempo-frecuencia de cada electrodo por separado [Tallon-Baudry y col. 1997], o en la combinación de métodos de descomposición espacio-temporal con los métodos tiempo-frecuencia [Koenig y col. 2001, Makeig y col. 2002].

En esta Tesis introduciremos nuevos métodos de descomposición de la actividad eléctrica del EEG para la caracterización simultánea en espacio, tiempo y frecuencia. Para esto proponemos dos enfoques que se diferencian en la capacidad resolutiva tiempo-frecuencia y pueden ser utilizados en dependencia del tipo de actividad a analizar: uno de mayor resolución temporal para el análisis de actividad esporádica y otro con mayor resolución espectral, para el análisis de actividades rítmicas de larga duración y la actividad inducida.

En este Capítulo abordaremos el primer enfoque, el cual consiste en la aplicación de versiones multicanales del *Matching Pursuit* para el análisis tiempo-frecuencia de

actividades esporádicas. Aunque algunas versiones multicanales del *Matching Pursuit* ya se han introducido en la literatura [Gribonval 2003], hasta donde sabemos, nosotros proponemos por primera vez su uso en el análisis del EEG. Además, proponemos la combinación de este método con otros de localización espacial con alta resolución de las de fuentes generadoras de dichas actividades.

Los antecedentes de este enfoque están en la combinación del análisis espectral clásico con los métodos de solución inversa (ver Anexo C) del EEG [Michel y col. 2004]. Las actividades de interés eran escogidas visualmente por especialistas y a través de la transformada de Fourier, se seleccionaba la banda de frecuencias más representativa de dicha actividad. El cálculo de la energía de esta banda de frecuencias (integral o promedio del espectro) en cada electrodo definía una topografía cuyas fuentes neurales se estimaban con métodos de solución inversa en el dominio de la frecuencia [Bosch-Bayard y col. 2001]. Sin embargo, el proceso de integración o promediación del espectro conlleva a que la topografía obtenida contenga tanto la energía de la actividad de interés como de otras actividades (incluyendo posibles artefactos) con frecuencias similares. Las fuentes obtenidas por este método son muy variables en cada segmento por lo que es necesario un post-procesamiento estadístico para distinguir cuáles activaciones son relevantes [Valdés-Sosa y col. 1998, Bosch-Bayard y col. 2001, Martínez-Montes y col. 2005].

2.2 Métodos

2.2.1 *Descomposición tiempo-frecuencia con el método Matching Pursuit*

El método *Matching Pursuit* (MP) consiste en la descomposición de una serie de tiempo (o señal) en una base de funciones con localización tiempo-frecuencia bien definida,

similar a la ecuación 5. Este método fue propuesto por Mallat y Zhang [Mallat y col. 1993] como una solución iterativa sub-óptima al problema de la representación de una señal en un diccionario redundante o sobrecompleto (ver Anexo C) de funciones denominadas átomos. El MP es un algoritmo adaptativo que consiste en encontrar el átomo del diccionario de máxima correlación con la señal y sustraer su contribución de la misma, repitiendo luego el procedimiento a partir del residuo obtenido (ver algoritmo en la ecuación 2 del Artículo 2).

La descomposición MP del EEG conlleva a extraer un número pequeño de átomos que caractericen la actividad de interés, de forma que en su análisis no interfieran otras actividades no relacionadas con el proceso cerebral en estudio. En la práctica, el uso de átomos de Gabor, junto con bases de Fourier y Deltas de Dirac es muy popular, ya que conforman diccionarios sobrecompletos con alta resolución tiempo-frecuencia. Esto permitiría la aplicación del MP a prácticamente cualquier actividad típica del EEG, desde espigas epilépticas, pasando por husos de sueño, hasta ritmos cerebrales de larga duración [Durka 2007]. Sin embargo, su gran costo computacional lo ha limitado al análisis a la señal de un solo electrodo, de forma que no es posible reconstruir la distribución espacial de los átomos extraídos. El desarrollo en la última década de la potencia de cómputo de las computadoras personales, permite la implementación de versiones multicanales del MP para la caracterización simultánea en espacio, tiempo y frecuencia de las actividades presentes en el EEG.

2.2.2 *Combinación de Matching Pursuit multicanal y métodos de solución inversa*

En el Artículo 2 (Anexo A) se introduce una formulación multicanal del MP (MMP) que escoge en cada paso el átomo tiempo-frecuencia que mejor explica la señal promedio entre todos los electrodos (ver algoritmo en la ecuación 5 del Artículo 2). El diccionario utilizado consistió en bases sobrecompletas de funciones de Gabor reales. Estas pueden escribirse como la parte real de las correspondientes funciones de Gabor complejas (que al igual que la *wavelet* de Morlet, consisten en sinusoides moduladas por gaussianas), con parámetros explícitos de localización en tiempo (t_c), frecuencia (*f*) y fase (φ):

$$g_c(t,f) = Ze^{-\pi(t-t_c)^2/\sigma_t^2}\cos(2\pi f(t-t_c)+\varphi) \quad (8)$$

donde Z es una constante de normalización [Durka 2007]. El uso de funciones reales de Gabor en lugar de las *wavelets* de Morlet obedece a dos razones fundamentales. En primer lugar, estas no exigen una dependencia entre la frecuencia y el semiancho temporal σ_t. Esto permite una representación de la señal con igual resolución temporal y espectral en todo el rango de frecuencias, lo cual es conveniente para la caracterización de actividades esporádicas con parámetros tiempo-frecuencia conocidos. En segundo lugar, las propiedades analíticas de las funciones de Gabor permiten el cálculo de los productos escalares con cualquier señal de forma rápida, lo que convierte al MP en un método factible para el análisis de largos registros de EEG con las actuales computadoras personales [Barwińsky 2004].

El producto escalar de un átomo escogido con la señal en cada electrodo define los pesos con que se representa este átomo en cada canal (ecuación 5 del Artículo 2). Estos pesos resultan en una topografía, lo cual completa la caracterización espacio-tiempo-

frecuencia de la actividad identificada por el átomo. A partir de esta topografía (con unidades de voltaje) podemos localizar las redes neuronales generadoras de la actividad representada por el átomo. Esto se logra con la solución del llamado Problema Inverso del EEG, consistente en la estimación de la densidad de corriente primaria (DCP) generada por las masas neuronales a partir de los voltajes medidos en la superficie del cuero cabelludo. Este es un problema mal planteado debido a la no unicidad de la solución [Nunez 1981]. Sin embargo, el uso de información adicional o restricciones sobre las características fisiológicas y físico-matemáticas de la DCP permite hallar soluciones únicas. Ejemplos de estas "soluciones inversas" (ver Anexo C) son la Tomografía Eléctrica de Baja Resolución (LORETA) [Pascual-Marqui y col. 1994], Mínima Norma [Hämäläinen y col. 1994], tomografía de resolución variable (VARETA) [Bosch-Bayard y col. 2001, Martínez-Montes y col. 2002], el método BMA (del inglés, *bayesian model averaging*) [Trujillo-Barreto y col. 2004] y otros basados en modelos de mínimos cuadrados penalizados múltiples (ver Anexo C) [Vega-Hernández y col. 2008]. La ecuación 6 del Artículo 2 representa la formulación del problema inverso para los pesos espaciales obtenidos con el MMP. De esta forma, el uso de una metodología que combine el MMP con métodos de solución inversa permite la localización de las redes neuronales en tiempo, frecuencia y espacio.

2.3 Resultados

La metodología propuesta fue aplicada en el análisis de actividades esporádicas de datos reales de EEG. Primeramente, esta fue usada para la localización de las redes generadoras de los husos de sueño (ver Anexo C). En el Artículo 2 mostramos que la localización de las fuentes cerebrales a partir de átomos simples es un procedimiento

más robusto que la localización tradicional a partir de bandas espectrales, en concordancia con estudios anteriores con datos simulados [Martínez-Montes y col. 2005]. Utilizando la solución inversa LORETA, se encontraron dos fuentes para los husos de sueño, una en la región cingular anterior y otra occipital (figura 2.1 de la Tesis y figuras 2 a la 5 del Artículo 2). Estas coinciden con las reportadas previamente con el análisis tradicional [Anderer y col. 2001] donde fue necesario la localización *ad hoc* de la frecuencia de los husos y un elaborado post-procesamiento estadístico. Además, el MMP permitió distinguir las dos fuentes encontradas como redes generadoras de husos de distintas frecuencias, lo cual fue imposible en el trabajo de Anderer y col. 2001.

La segunda aplicación de esta metodología consistió en el análisis del EEG de un paciente epiléptico y la localización del foco de esa actividad (ver Artículo 3 del Anexo A). Utilizamos un diccionario redundante de funciones de Gabor complejas, así como la suma de los cuadrados de los productos escalares con cada uno de los electrodos como medida a maximizar para escoger el átomo que mejor explica la señal (ecuación 4 del Artículo 3). El método LORETA se usó para la localización de las fuentes de los átomos correspondientes a la actividad epiléptica. Estas mostraron el foco epiléptico en el área temporal, de acuerdo con el encontrado durante la cirugía con el electrocorticograma intraoperatorio (ver Anexo C), validado clínicamente por la ausencia de epilepsia después de la operación (figura 2.2 de la Tesis y figuras 2 a la 5 del Artículo 3).

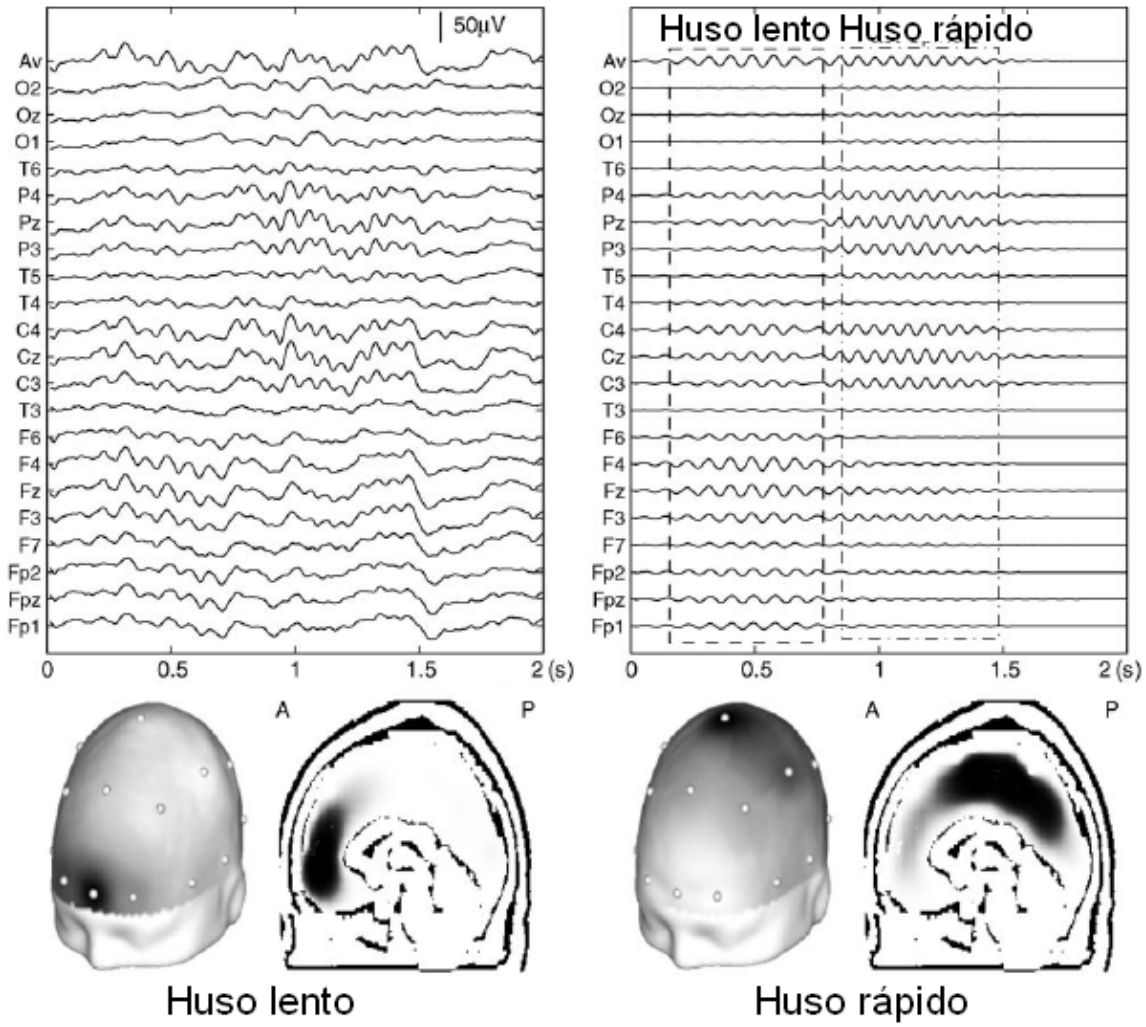

Figura 2.1. Descomposición *Matching Pursuit* multicanal (MMP) y solución inversa de dos tipos de husos de sueño. La fila superior muestra 2 segundos de 21 canales de EEG (izquierda) y la dinámica de dos átomos de Gabor extraídos con MMP como representantes de la actividad de los husos de sueño lento (centrado en 0.5 s y 11 Hz) y rápido (centrado en 1 s y 14 Hz). La fila inferior muestra las topografías y tomografías correspondientes a estos átomos. El huso lento muestra fuentes frontales mientras el rápido muestra fuentes más centro-parietales.

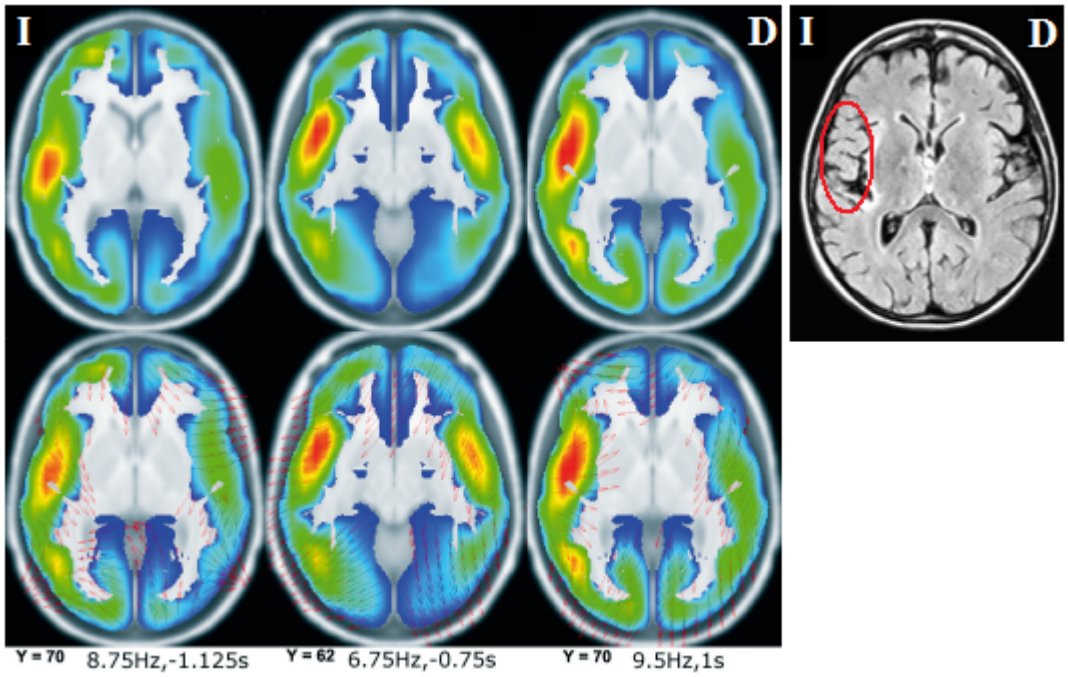

Figura 2.2. Imágenes tomográficas (solución inversa LORETA) de tres átomos identificados con MMP como representantes de la actividad epiléptica, cuya localización en tiempo y frecuencia se muestra en el borde inferior, así como el corte axial utilizado para la visualización. Las áreas en rojo y amarillo muestran mayores valores absolutos de densidad de corriente primaria (DCP) y el azul representa una DCP nula. La fila inferior muestra con flechas rojas la orientación estimada para las fuentes. En la esquina superior derecha se muestra la imagen anatómica de resonancia magnética del paciente antes de ser operado. Nótese la correspondencia de la zona afectada señalada por el epileptólogo (elipse roja) con las fuentes en la zona temporal encontradas con LORETA a partir de los átomos tiempo-frecuencia extraídos con MMP.

2.4 Discusión parcial de los resultados

Aunque en este trabajo el MP se utiliza sólo en la identificación espacio-tiempo-frecuencia de actividades esporádicas como los husos de sueño y actividad epiléptica, este puede ser aplicado a otras actividades si se utilizan diccionarios con los átomos

adecuados. Esta flexibilidad, junto con una relativa ausencia de parámetros arbitrarios, hace que el MP tenga un alto grado de compatibilidad con el análisis visual clásico del EEG (todavía utilizado ampliamente) [Durka 2007].

Dos versiones multicanales del MP fueron propuestas. En la primera (Artículo 2), se utiliza un diccionario de átomos de Gabor reales y en cada iteración se extrae el átomo que mejor explique la señal promedio de todos los electrodos. Esto implica la suposición de que las actividades de interés aparecen con la misma fase en todos los electrodos y permite una implementación eficiente. En la segunda versión multicanal se posibilita la extracción de actividades que aparezcan con fases distintas en cada electrodo a través del uso de un diccionario de funciones de Gabor complejas. El átomo escogido es aquel que hace máxima la suma de los cuadrados de su producto escalar con cada uno de los electrodos (ecuación 4 del Artículo 3). Contrario a la primera, en esta versión se evita la desventaja de una posible (aunque improbable) anulación de actividades de interés durante la promediación de la señal en todos los electrodos. También presenta mejores propiedades de convergencia, aunque con mayor costo computacional. En un futuro, otras variantes multicanales del MP pueden ser exploradas, con diferentes diccionarios y criterios para escoger el mejor átomo en cada iteración.

En la práctica, nuestra metodología mostró la ventaja de poder localizar correctamente las fuentes de los husos de sueño de forma automática, en correspondencia con el conocimiento general sobre los mismos y con estudios anteriores de husos identificados visualmente [Anderer y col. 2001]. En el enfoque clásico se hallan los generadores de husos a partir de promediar bandas de frecuencia que pueden incluir energía de otras actividades no relacionadas con el huso de sueño. Por tanto, se obtiene una gran

variabilidad en las fuentes estimadas para cada huso, llevando a la necesidad de un post-procesamiento estadístico para determinar cuáles áreas son realmente relevantes en la generación de los husos de sueño. Con nuestra metodología, la localización de los generadores de los husos fue mucho más robusta, obteniéndose las mismas fuentes a partir de átomos simples, sin la necesidad de post-procesamiento estadístico.

En el caso de la epilepsia, las fuentes identificadas correspondieron a las halladas con la medición directa de la actividad eléctrica en la corteza cerebral durante la operación y verificada posteriormente como la responsable de la actividad epiléptica a partir de la valoración clínica. Este único caso ilustra las potencialidades de la metodología propuesta para la localización de la actividad epiléptica, pero no constituye una validación conclusiva de su utilidad en el diagnóstico clínico.

Una metodología similar a la presentada consiste en la localización espacial de las actividades extraídas con el análisis de Componentes Independientes [Tang y col. 2002]. Sin embargo, contrario a las actividades encontradas con el MP, las componentes independientes no necesariamente están relacionadas con alguna de las estructuras conocidas del análisis clásico del EEG. Además, están basadas en fuertes suposiciones no fisiológicas como la independencia estadística de las actividades en estudio.

Por último, cabe mencionar que la metodología presentada hereda las deficiencias de la solución inversa utilizada, en este caso LORETA, discutidas ampliamente en la literatura [Pascual-Marqui y col. 1994, Trujillo-Barreto y col. 2004]. Por tanto, el uso de otros métodos inversos que superen estas desventajas (por ejemplo sLORETA [Pascual-Marqui 2002] o BMA [Trujillo-Barreto y col. 2004]) proveerían más exactitud y confiabilidad en la localización de las fuentes de las actividades estudiadas.

CAPÍTULO III

ANÁLISIS ESPACIO-TIEMPO-FRECUENCIA DE ACTIVIDAD RELACIONADA A EVENTOS Y RITMOS ESPONTÁNEOS: PARAFAC

CAPÍTULO III. ANÁLISIS ESPACIO-TIEMPO-FRECUENCIA DE ACTIVIDAD RELACIONADA A EVENTOS Y RITMOS ESPONTÁNEOS: PARAFAC

3.1 Introducción

En el capítulo anterior vimos que el *Matching Pursuit* multicanal permite la caracterización espacio-tiempo-frecuencia de estructuras oscilatorias fijas a través de su modelación como átomos de Gabor. Sin embargo, a pesar de la flexibilidad de este método, en el EEG existen dinámicas más complejas (que pueden incluir modulaciones en amplitud y frecuencia), que serían muy difíciles de modelar como parte de una misma red si se utiliza una base de funciones oscilatorias con características tiempo-frecuencia fijas.

En este capítulo abordaremos el segundo enfoque para la caracterización espacio-tiempo-frecuencia del EEG, consistente en el uso de métodos "basados en los datos", sin necesidad de fijar *a priori* las características espaciales, espectrales y temporales de las actividades en estudio. Esto es particularmente relevante en el estudio de las actividades de larga duración como la actividad inducida y los ritmos espontáneos, donde la evolución temporal en una escala de tiempo mayor (modulaciones en amplitud y frecuencia) es independiente de las características intrínsecas de la red y puede estar determinada por estímulos externos o por la interacción con otras redes cerebrales.

De la Introducción vimos que los métodos "basados en los datos" más populares en el análisis del EEG han sido el análisis de Componentes Principales (CP) e Independientes

(CI). Estos son conocidos como métodos de reducción de dimensionalidad y se han aplicado sólo a la descomposición del EEG en dos de las tres dimensiones intrínsecas de la actividad eléctrica cerebral, imponiendo restricciones matemáticas difíciles de interpretar desde el punto de vista fisiológico. Este tipo de métodos pueden generalizarse para realizar el análisis multidimensional (ver Anexo C) del espectrograma de actividades espontáneas o relacionadas a eventos. Un modelo adecuado para la descomposición multilineal de arreglos de datos multidimensionales (ver Anexo C) es el llamado Análisis de Factores Paralelos (PARAFAC, del inglés *Parallel Factor*) que fue propuesto independientemente por Harshman [Harshman 1970] y por Carroll y Chang [Carrol y col. 1970] quienes lo llamaron Descomposición Canónica. La principal ventaja de este método respecto a CP y CI es que la descomposición es única bajo condiciones débiles [Sidiripoulos y col. 2000]. Un estudio riguroso de este modelo ha sido realizado por Bro [Bro 1998], quien también lo implementó en un paquete de programas en Matlab disponible en internet (http://www.models.kvl.dk/users/rasmus/).

3.2 Métodos

3.2.1 *Análisis de factores paralelos (PARAFAC)*

PARAFAC es una generalización del análisis de CP a datos de más de dos dimensiones, con la ventaja de que la descomposición es única sin la necesidad de exigir que las componentes sean ortogonales o estadísticamente independientes. Por ejemplo, ajustado a un arreglo tridimensional (tensor de tercer orden) este modelo permite una descomposición de la forma:

$$\mathbf{T}(x,y,z) = \sum_k a_k(x) b_k(y) c_k(z) + \varepsilon(x,y,z) \qquad (9)$$

La factores $a_k(x)$, $b_k(y)$ y $c_k(z)$ son vectores que representan las características de la componente (o átomo) *k*-ésima a lo largo de cada una de las dimensiones *x*, *y*, *z*. La descomposición PARAFAC consiste en hallar estas características y es única cuando la suma de los k-rangos de las matrices $\mathbf{A} = [a_1(x),...,a_{Nk}(x)]$, $\mathbf{B} = [b_1(y),...,b_{Nk}(y)]$ y $\mathbf{C} = [c_1(z),...,c_{Nk}(z)]$ es mayor que $2Nk+2$, donde Nk es el número de átomos [Sidiripoulos y col. 2000].

En el Artículo 4 (Anexo A) proponemos por primera vez el uso de PARAFAC para el análisis del espectrograma del EEG multicanal. Este último conforma un tensor de tercer orden (con dimensiones tiempo, frecuencia y espacio) es descompuesto en una suma de componentes, cada una de las cuales consiste en el producto tensorial de vectores que corresponden a las características o factores (ver Anexo C) espacial, espectral y temporal (ecuación 2 y figura 1 del Artículo 4). Esporádicas aplicaciones del modelo PARAFAC a datos de EEG han tenido en cuenta sólo las dimensiones espacio y tiempo, y adicionalmente otras como los diferentes sujetos y/o dosis de medicamentos [Achim y col. 1997, Estienne y col. 2001, Field y col. 1991]. Una interpretación especial de este modelo es el llamado Modelo de Componentes Topográficas, el cual ofrece una justificación del uso de estos métodos de descomposición en el contexto del análisis de potenciales evocados, basada en consideraciones biofísicas [Möcks 1988a, Möcks 1988b].

El modelo PARAFAC es estimado con el uso del algoritmo conocido como Mínimos Cuadrados Alternantes (MCA, ver Anexo C) [Bro 1998]. Este consiste en la estimación iterativa de cada uno de los factores con una regresión de mínimos cuadrados usando los otros dos factores fijos. Por tanto, una vez que se tienen los factores estimados en un

segmento de datos donde se conoce que existe la actividad de interés, uno o dos de estos pueden utilizarse fijos en la descomposición de nuevos datos para exigir la extracción de la misma actividad (ecuaciones 3 y 4 del Artículo 4). Este procedimiento de monitoreo o exploración (ver Anexo C) de nuevos datos permitiría encontrar artefactos tecnológicos o fisiológicos como movimientos oculares o parpadeo.

3.3 Resultados

En el Artículo 4 presentamos la aplicación del análisis PARAFAC al espectrograma multicanal del EEG recogido durante períodos alternados de reposo con ojos cerrados y tareas de cálculo mental. El estado con ojos cerrados conlleva a la aparición de ritmo alfa, mientras que se conoce de la aparición de ritmo theta frontal durante el cálculo mental [Sasaki y col. 1996]. Por tanto, en la dimensión temporal se organizaron cinco segmentos de reposo y cinco de tarea escogidos aleatoriamente.

La figura 3.1 muestra como el análisis PARAFAC es capaz de separar los distintos ritmos con su evolución temporal y localización espacial. Consistentemente en cinco sujetos, se encontraron dos componentes (o redes neuronales) cuyas características espectrales mostraban picos alrededor de 7 y 11 Hz, que identificamos como “átomo theta” y “átomo alfa”, respectivamente (figura 2 del Artículo 4). En los factores temporales, la actividad theta aumentaba durante la realización de la tarea y era menor en el estado de reposo, mientras que la actividad alfa mostró el comportamiento opuesto (figura 3 del Artículo 4). La distribución topográfica obtenida mostró los mayores valores de voltaje en electrodos frontales para la actividad theta y en la zona occipital para la actividad alfa (paneles a y b de la figura 4 del Artículo 4).

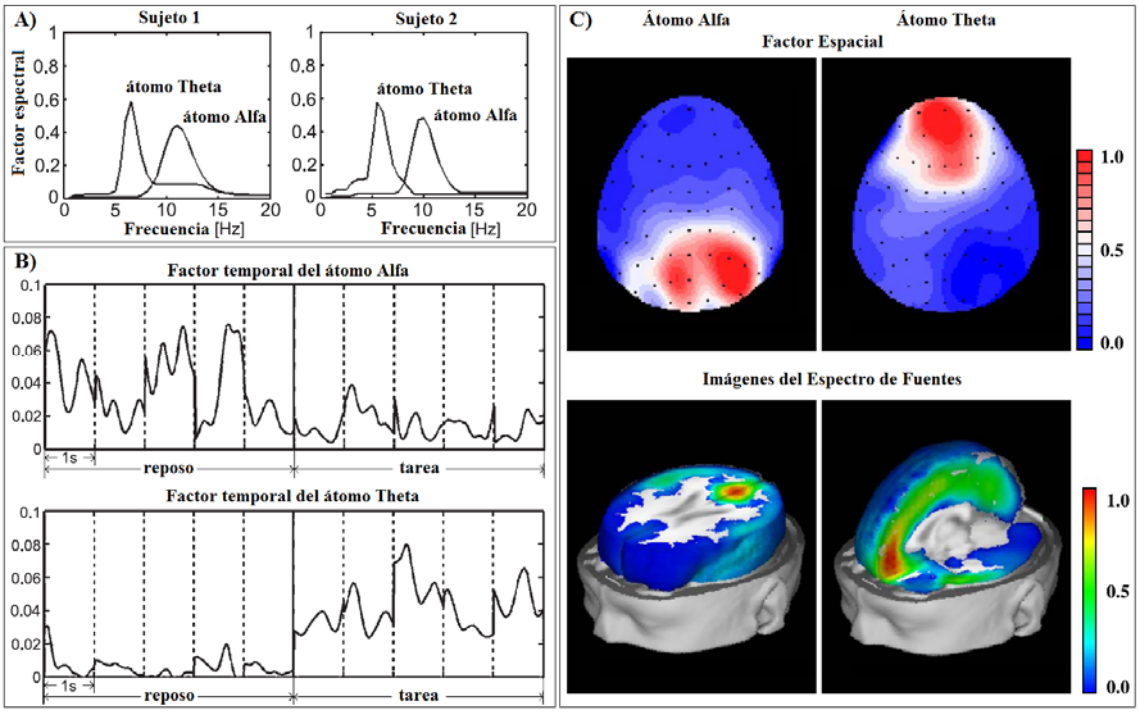

Figura 3.1. Descomposición PARAFAC de datos recogidos durante reposo y tarea de cálculo mental. A) Factores espectrales de dos sujetos típicos, mostrando la presencia de un átomo "alfa" (pico alrededor de 10 Hz) y otro "theta" (pico alrededor de 6 Hz). B) Factor temporal para cada átomo en segmentos consecutivos de reposo y tarea. Nótese que el átomo Alfa presenta mayores valores en el estado de reposo y menores durante la tarea, mientras que el Theta muestra el comportamiento contrario. C) Factor espacial (arriba) y sus correspondientes soluciones inversas (abajo) mostrando las fuentes del átomo alfa en la zona occipital y las del átomo teta en la zona singular anterior. Los factores espectrales y espaciales están normalizados, mientras el temporal retiene las dimensiones del espectrograma (mV^2). El espectro de fuentes, originalmente en nA^2/cm^4 se muestra normalizado para su mejor visualización.

A partir de esta topografía obtuvimos la localización tomográfica de las redes neuronales con la adaptación de métodos de solución inversa para hallar el espectro de la densidad de corriente primaria. Las fuentes generadoras aparecieron en el surco calcarino para la

red alfa y en la corteza frontal medial para la red theta de forma estable en los distintos sujetos (paneles c y d de la figura 4 del Artículo 4). En el Artículo 4 además, se ejemplifica la utilidad del análisis PARAFAC en la detección y eliminación de artefactos en el EEG (figura 8 del Artículo 4). Asimismo, se muestra la comparación de los planos tiempo-frecuencia reconstruidos de la descomposición de Componentes Principales con la de PARAFAC (figura 6 del Artículo 4).

3.4 Discusión parcial de los resultados

Una interpretación fisiológica de la aplicación del modelo PARAFAC al espectrograma del EEG es intuitiva: las redes neuronales correspondientes a cada componente tienen una actividad oscilatoria caracterizada por un espectro fijo (característica espectral), modulado en el tiempo (según la característica temporal) y con una distribución espacial fija respecto a los sensores en el cuero cabelludo (característica espacial).

Además de la unicidad, otra ventaja de esta metodología con respecto a los métodos tradicionales es la posibilidad de seleccionar el número óptimo de componentes para la descripción adecuada de los datos de EEG. Entre los diversos métodos que existen para esta selección, utilizamos el Corcondia (del inglés *Core Consistency Diagnostic*), el cual fue desarrollado específicamente para PARAFAC, y ofrece una medida de lo apropiado de la suposición de trilinealidad en un ajuste dado (ver sección 1 del suplemento del Artículo 5 del Anexo A). Esta selección es crítica y a menudo problemática en muchos de los métodos de descomposición como los análisis Componentes Principales (CP) y Componentes Independientes (CI) [Bro 1998]. Por otro lado, en comparación con el análisis de CP, la descomposición PARAFAC ofreció una descripción más concisa e

interpretable de los datos en una manera cualitativamente más simple y sin necesidad de restricciones adicionales.

En general, se ha demostrado que si los datos son aproximadamente trilineales, la relación señal-ruido (ver Anexo C) es apropiada y se usa el número correcto de componentes, PARAFAC permite encontrar el verdadero fenómeno subyacente en los datos [Harshman 1972, Kruskal 1976, Kruskal 1977]. En este trabajo no se realizó una verificación formal de la trilinealidad de los datos analizados. Sin embargo, aunque no constituyen una prueba definitiva, existen algunos aspectos en los que podemos basarnos para validar el modelo: a) la obtención de los mismos resultados utilizando distintos valores iniciales, así como distintos criterios de convergencia; b) la interpretabilidad de los resultados, en correspondencia con estudios previos en este tipo de experimentos y c) la relativamente pequeña variabilidad de los mismos entre distintos sujetos.

El modelo PARAFAC no es adecuado si los datos no son multilineales, ni en el caso en que la señal cambie de frecuencia continuamente en el tiempo ya que se requeriría un gran número de componentes para su ajuste, de forma que no se cumpla la condición de unicidad. En situaciones como estas, una serie de fenómenos no deseados pudieran aparecer en el análisis PARAFAC. Por ejemplo, en ocasiones es posible obtener dos o más componentes con características muy similares, lo que se conoce como degeneración (ver Anexo C). Esta se debe generalmente a un sobreajuste y puede ser eliminada con la selección del número correcto de componentes. Por otro lado, en presencia de altos niveles de ruido o de diferencias de escala entre subconjuntos de los datos el análisis PARAFAC ofrece factores donde aparece una misma actividad explicada en varias componentes, lo que se conoce como *cross-talk* (ver Anexo C). Por

ejemplo, en la dimensión espectral, cuando una componente no logra explicar toda la varianza en una banda de frecuencias determinada aparecen picos remanentes en esa banda en otras componentes. Aunque en nuestro caso encontramos este efecto en algunos de los sujetos analizados, la afectación general de este en el análisis del EEG merecería estudios más completos. Para evitar estas dificultades, es necesario realizar un cuidadoso pre-procesamiento de los datos, incluyendo la exploración de elementos atípicos (*outliers*, ver Anexo C), así como la selección del número óptimo de componentes y un escalamiento apropiado de los datos.

CAPÍTULO IV

ANÁLISIS PARAFAC CON RESTRICCIONES: MÍNIMOS CUADRADOS ALTERNANTES PENALIZADOS

CAPÍTULO IV. ANÁLISIS PARAFAC CON RESTRICCIONES: MÍNIMOS CUADRADOS ALTERNANTES PENALIZADOS

4.1 Introducción

Como discutimos en el capítulo anterior, en presencia de elementos atípicos, escalamiento irregular o altos niveles de ruido en los datos, la descomposición PARAFAC muestra efectos no deseados que entorpecen su interpretación. Entre estos efectos están la obtención de características ruidosas, sobreajuste, degeneración y el llamado "*cross-talk*" entre componentes. Las estrategias seguidas para disminuir estos efectos se han basado principalmente en un adecuado pre-procesamiento de los datos (escalado, centrado, eliminación de elementos atípicos), y en otros procedimientos para determinar el número correcto de componentes a extraer y disminuir la dependencia de soluciones iniciales [Bro 1998, Stegeman 2007].

En este capítulo abordamos otra estrategia que consiste en la incorporación de información *a priori* o restricciones sobre las propiedades fisiológicas, físicas o matemáticas para evitar la ambigüedad en la identificación de las redes neuronales. Desde el punto de vista matemático, se pueden utilizar restricciones de tipo "exactas" (por ejemplo exigir que la suma de los coeficientes de una regresión sea igual a uno) o "aproximadas" (como exigir que la norma de los coeficientes sea la mínima posible). En la implementación disponible de PARAFAC [Andersson y col. 2000] sólo se tiene la posibilidad de exigir restricciones exactas de ortogonalidad, no negatividad y unimodalidad de las componentes extraídas. Sin embargo, en el estudio de sistemas

complejos como el cerebro a través de datos ruidosos como el EEG, el uso de restricciones exactas no es lo ideal.

4.2 Métodos

4.2.1 *PARAFAC con restricciones a través de los Mínimos Cuadrados Alternantes Penalizados*

La estimación de los factores en PARAFAC se hace con regresiones sucesivas de mínimos cuadrados, en los cuales pueden introducirse restricciones aproximadas en forma de funciones de penalización (página 3 del Artículo 5 del Anexo A). Este tipo de restricciones es adecuado ya que permite un compromiso entre el ajuste de la descomposición única y la restricción requerida. Nuevos avances en el campo de los mínimos cuadrados penalizados han permitido el uso de funciones de penalización no convexas, (no cuadráticas), continuas y con singularidad en el origen (ver Anexo C). Estas funciones permiten obtener soluciones estables y esparcidas (*sparse*, ver Anexo C), o sea, con pocos coeficientes no nulos [Fan y col. 2001]. Los modelos no lineales resultantes son estimados con algoritmos de Newton-Raphson modificados como la Aproximación Cuadrática Local [Fan y col. 2001] y el método de Minorización-Maximización [Hunter y col. 2005]. Estos se basan en la aplicación iterativa de regresiones cuadráticas y han sido extendidos recientemente para usar varias funciones de penalización simultáneamente, o sea, para estimar modelos de mínimos cuadrados penalizados múltiples [Valdés-Sosa y col. 2006]. Con estos modelos podrían obtenerse una gran variedad de soluciones con diferentes propiedades. Por ejemplo, el uso de la función "norma L2" (cuadrática, ver Anexo C) conduce a la estimación de forma analítica de la solución conocida como Ridge, la cual es generalmente suave. El uso de

la penalización basada en la "norma L1" (ver Anexo C) da lugar a la solución Lasso (del inglés, *Least Absolute Shrinkage Selection Operator*) [Tibshirani 1996], que ofrece soluciones muy esparcidas. Una variante de esta es el Lasso Fusion [Land y col. 1996] que usa la norma L1 del vector obtenido de aplicar un operador de primeras diferencias a los coeficientes de regresión. Otro penalizador atractivo resulta de la combinación de un término de penalización basado en la norma L2 (para exigir suavidad) y otro basado en la norma L1 (para exigir esparcidad). Este penalizador se denomina Elastic Net [Zou y col. 2005]. El enfoque de los modelos de mínimos cuadrados penalizados múltiples ha sido aplicado satisfactoriamente por nuestro grupo en la solución del problema inverso del EEG [Vega-Hernández y col. 2008] y la estimación de la conectividad funcional a partir de datos de IRMf [Sánchez-Bornot y col. 2008].

En el Artículo 5 (Anexo A) proponemos la sustitución de cada paso de regresión de mínimos cuadrados en el algoritmo Mínimos Cuadrados Alternantes (MCA) por uno de mínimos cuadrados penalizados para crear un nuevo algoritmo llamado Mínimos Cuadrados Alternantes Penalizados (ver Anexo C). Este permite la descomposición PARAFAC utilizando tanto funciones de penalización cuadráticas, como no convexas y no lineales en general, que puedan proveer soluciones suaves, esparcidas, e incluso con estas propiedades combinadas. Algunas de estas restricciones serían muy difíciles de implementar dentro de enfoques populares como el EM (del inglés, *Expectation-Maximization*) y el VBEM (del inglés *Variational Bayes EM*) y darían lugar a algoritmos muy lentos [Mørup 2005], por lo que utilizamos la generalización del algoritmo Aproximación Cuadrática Local para llevar a cabo la regresión penalizada. El nivel de restricción puede ser modulado a través de los parámetros de peso de las

funciones de penalización, cuyos valores óptimos también pueden ser escogidos por medio de la técnica de validación cruzada [Golub y col. 1979] o utilizando criterios de información como el de Akaike [Akaike 1974] o el Bayesiano [Schwartz 1978]. La descripción matemática del algoritmo propuesto se detalla en la sección 2 del Artículo 5.

4.2.2 *Penalizador Entropía-Ridge*

Siguiendo este mismo enfoque, en el Artículo 6 (Anexo A) proponemos el uso de otras restricciones basadas en medidas de complejidad de la actividad eléctrica de las redes neuronales. En particular, introducimos una nueva función de penalización basada en la Entropía Informacional para identificar, con el análisis PARAFAC, las redes neuronales cuya actividad tiene mínima entropía espectral (ver Anexo C). La entropía espectral es una medida de la coherencia de la red neuronal, en el sentido de que sus oscilaciones tengan una frecuencia bien definida. La Entropía Informacional (ver Anexo C) del vector $\boldsymbol{\beta}$ (con $\beta_j > 0,\ \forall\, j$ y $\sum_j \beta_j = 1$) se define como $H(\boldsymbol{\beta}) = -k\sum_j \beta_j \ln \beta_j$, donde k es una constante positiva [Shannon 1948]. Esta magnitud toma valor máximo cuando todos los elementos β_j son iguales y mínimo (cero) cuando sólo uno de ellos es distinto de cero. En el caso de que $\boldsymbol{\beta}$ sea el espectro o densidad espectral (normalizado) de una señal, la entropía espectral es una medida de la agudeza del mismo, o sea, de la estrechez de la banda de frecuencias fundamentales.

El uso de la función no lineal $H(\boldsymbol{\beta})$ como penalizador produciría soluciones esparcidas para $k < 2$ pero que estarían sesgadas para valores grandes de los coeficientes β_j. Sin embargo, podemos obtener una solución esparcida y no sesgada si combinamos esta función con un penalizador cuadrático (Ridge), de la forma:

$$p(\boldsymbol{\beta}) = -\sum_j \left(\beta_j \ln \beta_j - \beta_j^2 / 2 \right) \tag{10}$$

A este penalizador le hemos denominado Entropía-Ridge y su gráfico puede verse en la figura 1 del Artículo 6 (Anexo A). Su uso en el análisis PARAFAC del espectrograma del EEG, conllevaría a la obtención de factores espectrales esparcidos y con un pico estrecho (y con cierta suavidad) alrededor de la frecuencia fundamental de oscilación. Esto puede interpretarse como la identificación de las redes neuronales que oscilan con una frecuencia bien definida, o sea con mínima entropía espectral.

4.3 Resultados

En el Artículo 5 se evaluó la descomposición multilineal penalizada y se compararon sus resultados con los del PARAFAC no restringido en la caracterización espacio-tiempo-frecuencia de tres ritmos (alfa, theta y gamma) presentes en el EEG recogido durante el estado de reposo (ver Anexo C). En un primer resultado, con el uso de un penalizador cuadrático se obtuvieron características espectrales con distintos niveles de suavidad, una propiedad conveniente para la mejor identificación de los ritmos presentes en el EEG (figura 2 del Artículo 5). También se simularon datos a partir de actividades con diferentes escenarios de evolución temporal esparcida, que semejan fenómenos fisiológicos intermitentes como las espigas de epilepsia (ver Anexo C), las actividades en respuesta a estímulos del tipo "pulso rectangular" (ver Anexo C) en bloques, y otras de evolución suave a pedazos como la modulación típica de los ritmos cerebrales espontáneos (figura 4.1 y figuras 3 y 4 del Artículo 5). El uso de las restricciones adecuadas en la descomposición de estos datos simulados, permitió obtener características temporales esparcidas mucho más cercanas a las reales que las obtenidas con la solución (única) dada por el PARAFAC no penalizado.

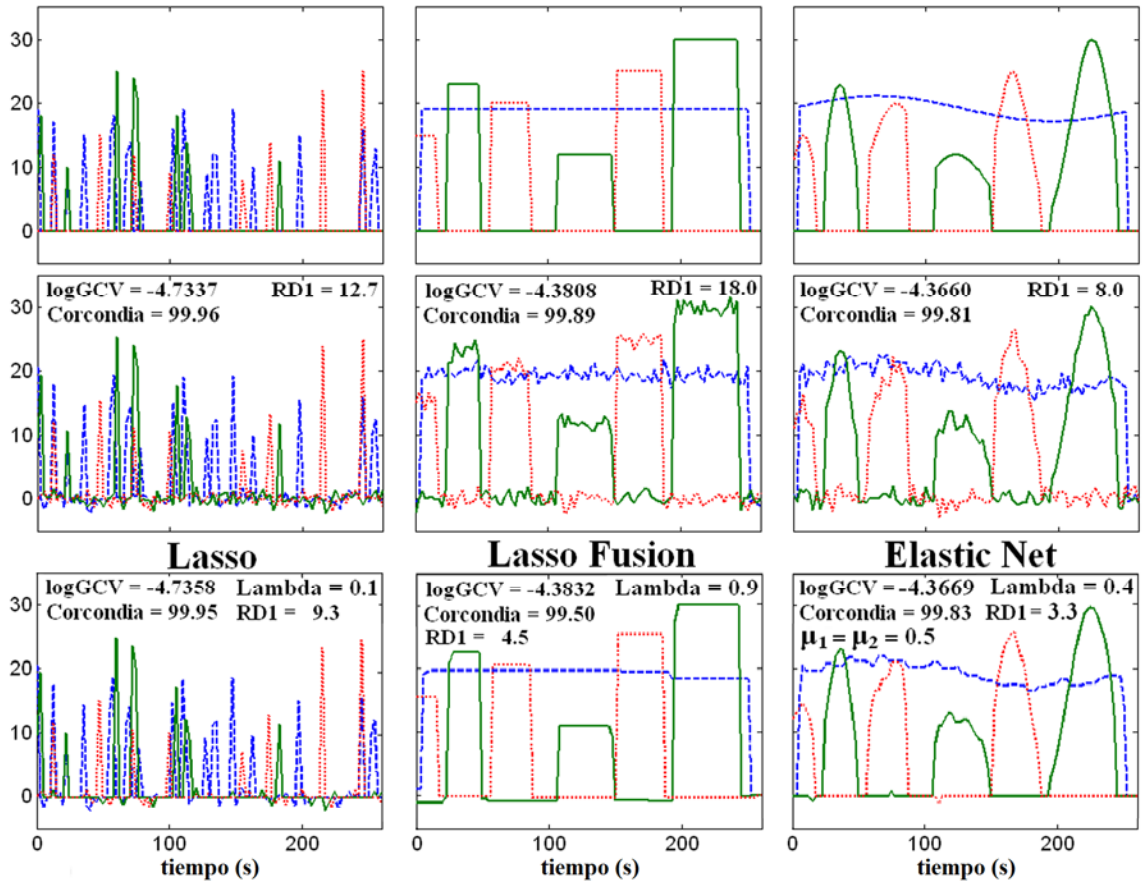

Figura 4.1. Fila superior: factores temporales simulados con distintos grados de esparcidad y suavidad, semejando comportamientos dinámicos de datos fisiológicos reales. Fila media: factores temporales estimados con el uso de PARAFAC sin restricciones. Nótese la característica ruidosa en todos los casos y la imposibilidad de obtener valores nulos. Fila inferior: factores temporales estimados con el uso de PARAFAC penalizado con las restricciones adecuadas en cada caso. En las estimaciones se reportan el logaritmo de la función de validación cruzada (logGCV), Corcondia, el parámetro de regularización (Lambda) y la distancia relativa (RD1) entre el factor estimado y el simulado, en porciento.

En el Artículo 6 (Anexo A) introducimos una función de penalización no lineal basada en la Entropía Informacional para realizar la descomposición PARAFAC penalizada del

espectro variante en el tiempo de un EEG recogido en estado de reposo (figura 1 del Artículo 6). Este está orientado a la identificación en espacio, tiempo y frecuencia de las redes cerebrales con mínima entropía espectral. El uso de esta penalización proveyó características espectrales mucho más esparcidas, unimodales y con valores no negativos, mostrando una sola banda de frecuencia con energía distinta de cero.

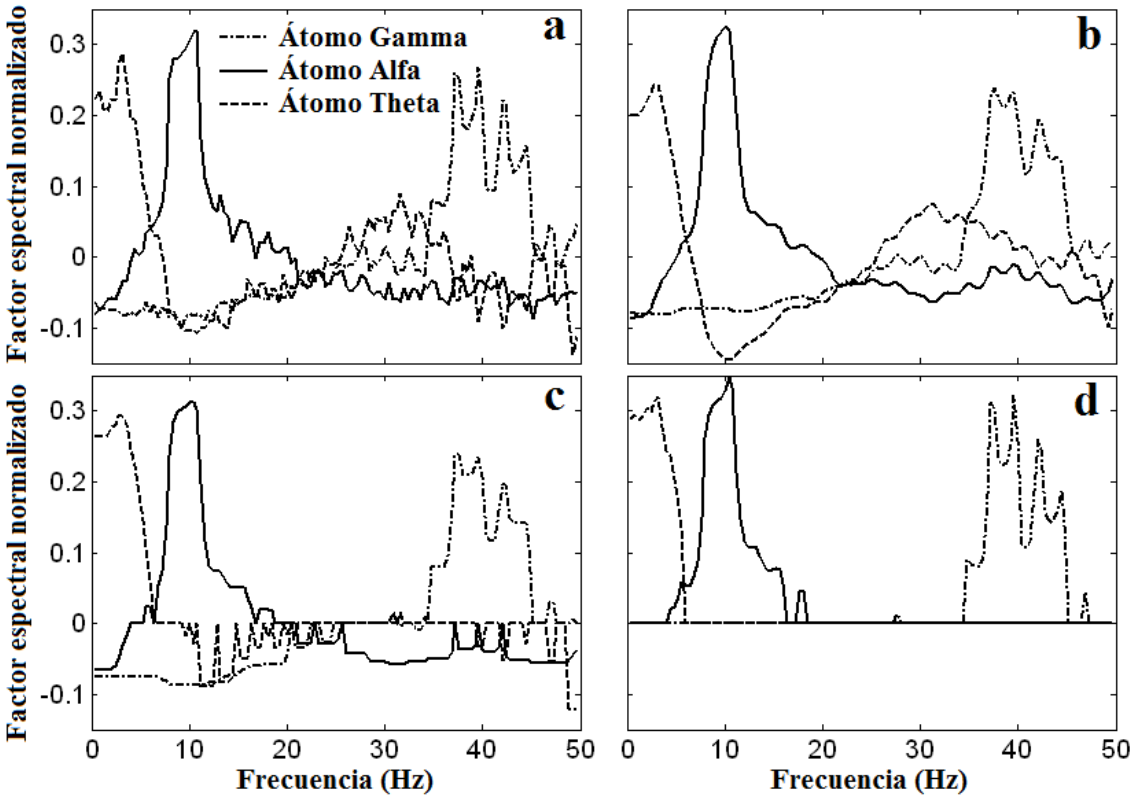

Figura 4.2. Factores espectrales estimados con a) PARAFAC no penalizado. Para los tres átomos identificados los espectros muestran valores negativos, comportamiento ruidoso y "*cross-talk*". b) PARAFAC con restricciones de suavidad. c) PARAFAC con penalización tipo Elastic Net. d) PARAFAC con penalización Entropía-Ridge.

También ilustramos que el uso de restricciones de suavidad y de la penalización Elastic Net ofrece mejores soluciones que la descomposición PARAFAC no penalizada, aunque las características espectrales estimadas no están exentas de mostrar valores negativos y algún comportamiento oscilatorio en frecuencias lejanas al pico principal (figura 4.2 de la Tesis y figuras 3 y 4 del Artículo 6).

4.4 Discusión parcial de los resultados

En este trabajo, la imposición de funciones de penalización cuadráticas en la descomposición PARAFAC del espectro variante en el tiempo del EEG en reposo permitió obtener factores espectrales suaves. También, con penalizaciones no cuadráticas se estimaron satisfactoriamente distintos tipos de características temporales esparcidas que semejan patrones encontrados en la práctica experimental. Otras funciones de penalización no lineales que puedan ser localmente aproximadas de forma cuadrática pueden también ser utilizadas dentro del formalismo propuesto.

El enfoque propuesto hereda la virtud del PARAFAC no restringido de ofrecer una solución única bajo condiciones débiles. Incluso, el uso de penalizaciones ayuda en aquellos casos en que el nivel de ruido de los datos limita la convergencia. En principio, también hereda las desventajas, como la dependencia de los estimadores iniciales y la posibilidad de obtener soluciones degeneradas y *cross-talk*. Sin embargo, el uso de restricciones puede contribuir a evitar tanto el *cross-talk* como las soluciones degeneradas y los factores iniciales pueden obtenerse fácilmente de la solución no restringida.

En sentido general, aunque obtuvimos evidencias de que el algoritmo de mínimos cuadrados alternantes penalizados ofrece soluciones más robustas que el de mínimos

cuadrados alternantes ordinario, un estudio más riguroso sobre esta cuestión debe llevarse a cabo en el futuro. Por otro lado, en este modelo cada penalización conlleva el uso de un parámetro de peso que controla el grado de la restricción. Estos pueden ser sintonizados a mano pero, en el caso del PARAFAC, el uso de la medida Corcondia [Bro 1998] y de una aproximación de la función de validación cruzada [Golub y col. 1979] puede ayudar en la estimación de un valor óptimo para ellos.

En este trabajo también se introdujo el penalizador Entropía-Ridge, consistente en la combinación de la Entropía Informacional y la norma L2. Este penalizador permitió obtener soluciones esparcidas y no sesgadas, así como la disminución de valores negativos y del efecto *cross-talk* entre las características espectrales de las redes neuronales. Su uso en la descomposición PARAFAC del espectro variante en el tiempo del EEG es interpretado como la extracción de componentes cuyos factores espectrales son suaves a pedazos y con mínima entropía espectral. Esto significa la identificación de aquellas redes que oscilan en una banda estrecha de frecuencias.

Aunque no está totalmente clara la relación fisiológica del estado de mínima entropía espectral con el de procesamiento cognitivo, algunos estudios han demostrado la validez de esta medida como marcador electrofisiológico de la presencia de crisis epilépticas y otros procesos cerebrales [Rosso y col. 2006]. Podríamos conjeturar que las redes neuronales logran un estado de mínima entropía espectral durante el procesamiento de información específica, por ejemplo participando estrictamente en determinado proceso cognitivo o cuando alcanzan un estado basal intrínsecamente oscilatorio como el ritmo alfa. Este estudio puede ser considerado como un intento inicial de incluir medidas descriptoras de la complejidad de las actividades cerebrales como restricciones en el

análisis de los datos de neuroimágenes. El uso de otras posibles medidas de complejidad en la búsqueda de las redes funcionales responsables de procesos cognitivos o espontáneos debe ser llevado a cabo en próximas investigaciones.

CAPÍTULO V

ANÁLISIS CONJUNTO DE EEG E IRMF: MÍNIMOS CUADRADOS PARCIALES TENSORIAL

CAPÍTULO V. ANÁLISIS CONJUNTO DE EEG E IRMF: MÍNIMOS CUADRADOS PARCIALES TENSORIAL

5.1 Introducción

Tanto la descomposición PARAFAC como la obtenida con el *Matching Pursuit* multicanal ofrecen una caracterización espacial de las redes a nivel topográfico, o sea con una resolución definida por el arreglo de electrodos en la superficie del cuero cabelludo. A partir de esta topografía, una mayor resolución espacial puede obtenerse con métodos de solución del problema inverso del EEG, como se mostró en los Artículos 2, 3 y 4 de esta Tesis. Sin embargo, la característica espacial obtenida de esta forma hereda las limitaciones de la solución inversa utilizada, y depende del modelo asumido para las fuentes generadoras de la actividad neural. Un enfoque alternativo para obtener características espaciales con alta resolución resulta del análisis combinado de datos de EEG y de otras técnicas de neuroimágenes [Horwitz y col. 2002].

La búsqueda de métodos que combinen información proveniente de dos o varias mediciones es relevante, dada la ausencia de una técnica de neuroimágenes que ofrezca una combinación óptima de resolución espacial y temporal [Churchland y col. 1988]. En particular, se hace muy atractiva la fusión del EEG, de muy alta resolución temporal, con datos de Imágenes de Resonancia Magnética funcional (IRMf) con muy alta resolución espacial. Esta última técnica registra cambios en la magnetización local debido a variaciones en la oxigenación de la sangre, que se conoce como señal BOLD (del inglés *Blood Oxygenation Level Dependent*). Recientemente se han podido vencer los obstáculos tecnológicos para realizar las mediciones de ambas técnicas

simultáneamente [Goldman y col. 2000]. Esto hace posible el estudio de las relaciones dinámicas entre la señal BOLD y la actividad eléctrica medida en el cuero cabelludo, ya que ambos datos reflejan la actividad de los mismos procesos cerebrales subyacentes.

En este capítulo, introducimos un método "basado en los datos" para el análisis conjunto de datos de EEG e IRMf que conlleva a una caracterización espacio-tiempo-frecuencia de la actividad de redes neuronales con alta resolución espacial. Estudios anteriores han llevado a cabo el análisis de correlación entre una serie de tiempo representativa de la potencia espectral del ritmo alfa en el EEG con la señal BOLD de cada elemento de volumen (voxel, ver Anexo C) independientemente [Goldman y col. 2002, Moosmann y col. 2003]. Los mapas tomográficos de correlación o tomogramas (ver Anexo C) ofrecen una caracterización espacial con alta resolución de las áreas involucradas en la generación de la actividad alfa medida en el EEG. Sin embargo, la serie de tiempo representativa de la actividad alfa es hallada a partir de escoger *ad hoc* la banda de frecuencia correspondiente al ritmo alfa, así como los electrodos con mayor energía en esta banda, lo cual introduce un sesgo subjetivo en el análisis.

En este sentido, se hace conveniente el uso de métodos "basados en los datos" que expliquen mejor las relaciones espacio-temporales entre datos de IRMf y las componentes oscilatorias del EEG, sin formarse una hipótesis *a priori* de cuáles son las actividades de interés y sus localizaciones en frecuencia y espacio. Una alternativa consiste en la correlación de la señal BOLD con las características temporales obtenidas de la descomposición espacio-tiempo-frecuencia del EEG, las cuales estarían automáticamente asociadas al espectro característico de la red estudiada y no a una banda particular de frecuencias. Sin embargo, existen métodos capaces de extraer

automáticamente los componentes espectrales del EEG que tienen máxima correlación temporal con las señales BOLD. Entre estos se encuentra la regresión de Mínimos Cuadrados Parciales (MCP), introducida en el análisis de IRMf por McIntosh y colaboradores [McIntosh y col. 1996] y también utilizada para el análisis espacio-temporal de potenciales relacionados a eventos [Lobaugh y col. 2001] y de datos conjuntos de EEG y MEG [Düzel y col. 2001]. Con la generalización de esta técnica al análisis de datos multidimensionales, podríamos identificar las combinaciones lineales de voxeles en la matriz de IRMf (variable dependiente) que tienen máxima covariancia con los factores temporales de la descomposición multilineal del espectro variante en el tiempo o espectrograma del EEG (variables independiente).

5.2 Métodos

5.2.1 *Mínimos Cuadrados Parciales Tensorial*

La técnica de MCP ha sido extendida al análisis de datos multidimensionales, obteniendo un nuevo modelo conocido como Mínimos Cuadrados Parciales Tensorial (MCPT, ver Anexo C) [Bro 1996]. Este modelo consiste en la descomposición multilineal de los datos dependientes e independientes de modo que los factores estimados en una dimensión común tengan máxima covarianza. A diferencia del PARAFAC, en el MCPT se extraen las componentes de una en una, lo cual asegura la unicidad de la solución, aunque también es necesario un convenio para establecer los signos y escala de los factores estimados.

En el Artículo 7 (Anexo A) introducimos el uso del modelo MCPT en el análisis de datos de EEG e IRMf medidos conjuntamente durante el estado de reposo. Hasta donde sabemos, esta es la primera vez que se aplica dicho modelo en el análisis de datos de

neurociencias. Como variable independiente, definimos el espectro variante en el tiempo del EEG, obtenido de la aplicación del método *multitaper* de Thomson [Thomson 1982] a segmentos del EEG de 2,5 segundos, período en el cual se recogió la señal BOLD en un conjunto de voxeles dentro del cerebro. El espectro variante en el tiempo del EEG resulta en un tensor de tercer orden con las dimensiones espacial (electrodos), espectral (frecuencias) y temporal (segmentos). Luego, se convoluciona temporalmente con una función teórica de respuesta hemodinámica [Friston y col. 1998] para llevarlo a la misma escala temporal de las IRMf, asumidas como variable dependiente. Por su parte, estas últimas conforman una matriz (tensor de segundo orden) de número de voxeles por número de volúmenes recogidos, los cuales coinciden con los segmentos temporales y que llamaremos solamente "instantes de tiempo". El modelo se expresa de la forma:

$$\left.\begin{array}{c} S(e,t,f)=\sum_k a_k(e)b_k(t)c_k(f)+\varepsilon(e,t,f) \\ F(v,t)=\sum_k u_k(v)q_k(t)+\xi(v,t) \end{array}\right\} \text{bajo la condición } \max\left\{\sum_{t=1}^{T} b_k(t)q_k(t)\right\}, \forall k$$

y el algoritmo utilizado se resume en el Apéndice A del Artículo 7. Para cada componente *k*, los vectores a_k ,b_k y c_k son los factores espacial, temporal y espectral del EEG, mientras que los vectores u_k y q_k son los factores espacial y temporal de las IRMf (figura 1 del Artículo 7). Esta descomposición es también única, y permite la caracterización de las redes neuronales cuya actividad eléctrica está temporalmente correlacionada con la actividad metabólica. Además de la caracterización espacio-tiempo-frecuencia dada por la descomposición del EEG, el factor espacial correspondiente de la descomposición de las IRMf ofrece un mapa tomográfico de alta resolución espacial de las áreas anátomo-funcionales de la red neuronal. Esta tomografía

puede ser comparada con la obtenida con el uso de métodos de localización de fuentes a partir de los factores espaciales del EEG.

5.3 Resultados

En el Artículo 7 aplicamos el modelo MCPT a datos de EEG e IRMf recogidos simultáneamente durante el estado de reposo con ojos cerrados. Como vimos, en este estado es de esperar la presencia predominante del ritmo alfa, junto con otros ritmos espontáneos en el EEG. Como resultado del análisis, los factores espectrales del EEG permitieron identificar las componentes "alfa", "theta" y "gamma", de acuerdo a las frecuencias de los picos principales (figura 5.1a de la Tesis y figura 2 del Artículo 7). Los factores espaciales del EEG de las componentes alfa, theta y gamma mostraron activaciones mayores en los electrodos occipitales, frontales y centro-parietales, respectivamente (figura 5.1b de la Tesis y figura 6 del Artículo 7). Solamente el átomo alfa mostró una evolución temporal significativamente correlacionada con la evolución temporal de las IRMf (figura 5.1c de la Tesis y figura 3 del Artículo 7). Para este átomo, las imágenes del espectro de las fuentes obtenidas a partir del factor espacial del EEG mostraron sólo activaciones en la corteza parieto-occipital (figura 5.1d de la Tesis y figura 6 del Artículo 7), mientras que las áreas representadas en la característica espacial de las IRMf incluyeron la corteza parieto-occipital, con correlación negativa y el tálamo e ínsulas con correlación positiva (figura 5.1e de la Tesis y figura 5 del Artículo 7).

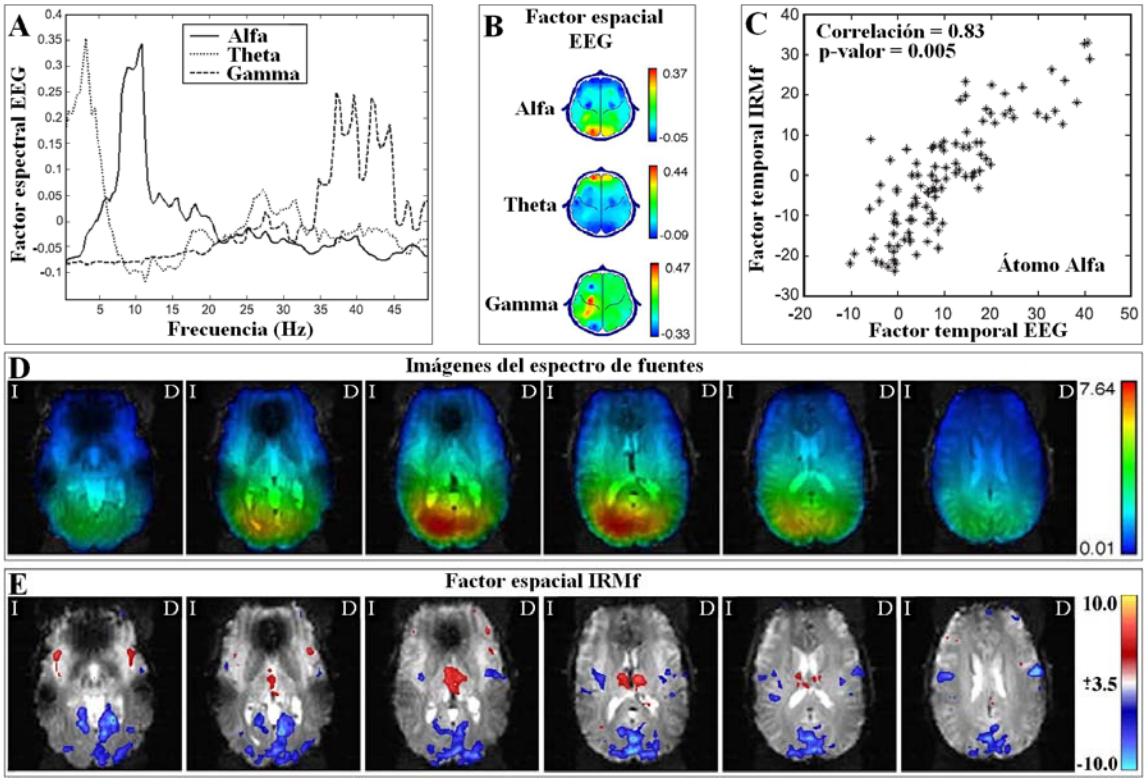

Figura 5.1. Resultados del análisis con MCPT de datos de EEG e IRMF recogidos conjuntamente en estado de reposo. A) Factores espectrales del EEG, que permiten identificar tres átomos (Alfa (~10 Hz). Theta (~6 Hz) y Gamma (~40 Hz)). B) Factores espaciales del EEG para los tres átomos. C) Correlación entre los factores temporales del EEG y de las IRMf para el átomo Alfa. D) Imágenes del espectro de las fuentes del átomo Alfa obtenidas con métodos de solución inversa a partir del factor espacial del EEG. E) Imagen estadística del factor espacial de las IRMf para el átomo Alfa, que muestra las áreas donde la dinámica de la señal BOLD está significativamente correlacionada con la evolución temporal del espectro de la actividad alfa del EEG. Nótese la correlación negativa en áreas de la corteza occipital y positiva en el tálamo. Esta imagen muestra las áreas posiblemente involucradas en la generación de la actividad alfa con mayor resolución espacial que las imágenes mostradas en D.

5.4 Discusión parcial de los resultados

En este capítulo hemos introducido un nuevo método de análisis conjunto de datos de EEG e IRMf. Este método se basa en la descomposición multilineal simultánea de ambos datos de forma que se extraigan las componentes cuyos factores temporales del EEG y las IRMf tengan máxima covarianza. La descomposición se hace de forma similar a la del modelo PARAFAC por lo que aquí se heredan tanto las virtudes como las limitaciones de dicho método, discutidas en los capítulos 3 y 4 de esta Tesis. Además de la unicidad de la descomposición, el uso de herramientas estadísticas apropiadas, junto con la interpretabilidad fisiológica y la replicabilidad en varios sujetos permiten concluir que los resultados obtenidos son robustos y fisiológicamente relevantes, aunque no podemos asegurar que correspondan al verdadero fenómeno físico subyacente.

Un resultado consistente en nuestro análisis fue la identificación de tres redes neuronales presentes en el EEG del estado de reposo, responsables de actividades oscilatorias en las bandas de frecuencia correspondientes a los ritmos alfa, theta y gamma. Sin embargo, de estas, solamente la red alfa mostró una correlación temporal significativa entre la evolución temporal de su espectro y el curso temporal de las IRMf. Este hecho demuestra lo inconveniente de reducir el análisis a una sola banda de frecuencia y determinados electrodos *ad hoc*, como se ha realizado en estudios anteriores [Goldman y col. 2002].

Los resultados obtenidos están en concordancia con otros estudios similares usando el análisis de correlación voxel a voxel [Goldman y col. 2002, Moosmann y col. 2003]. En particular, el factor espacial de las IRMf encontrado con MCPT para la componente alfa mostró correlaciones temporales positivas con el EEG en áreas como el tálamo y las

ínsulas, mientras que las correlaciones negativas se encontraron en las cortezas parieto-occipital y somatosensorial. Esta correlación negativa sugiere que las redes con actividad alfa sincronizada requieren de una actividad metabólica menor en este estado. Asimismo, la disminución de la amplitud de las oscilaciones alfa debido a la resincronización temporal de los potenciales post-sinápticos de los circuitos neurales involucrados, conllevaría a un aumento de la actividad metabólica reflejada en la señal BOLD.

Por otro lado, el espectro de las fuentes neurales obtenido a partir de la característica espacial del EEG del átomo alfa, mostró solamente activación en la región parieto-occipital. Aunque esto se corresponde con los estudios realizados en la localización de las fuentes del ritmo alfa [Valdés-Sosa y col. 1998, Casanova y col. 2000], representa una disociación con la característica espacial de las IRMf, donde otras fuentes profundas (como el tálamo) aparecen como parte de la red neuronal. Esta aparente contradicción puede ser un resultado de la incapacidad del método de solución inversa utilizado para encontrar las fuentes de actividad eléctrica en áreas profundas, en cuyo caso la utilidad de otros métodos de solución inversa que no tengan este problema debería investigarse. Otra posibilidad es que la diferencia se deba al hecho de que las fuentes de corriente primaria en el tálamo tienen una contribución muy pequeña o despreciable al EEG medido, dada su lejanía a los sensores. En este caso, la correlación significativa observada entre la actividad metabólica en el tálamo y el ritmo alfa en el EEG debe ser indirecta. Por ejemplo, la señal BOLD en el tálamo puede estar correlacionada negativamente con la de la corteza parieto-occipital y esta, a su vez, negativamente correlacionada con la amplitud del ritmo alfa. De este modo, las ínsulas, el tálamo y las

áreas parieto-occipitales formarían parte de la red neuronal generadora de las oscilaciones en la banda de frecuencias alfa, aunque sólo estas últimas contribuirían al "ritmo alfa del EEG". Estudios que tengan en cuenta la causalidad de las conexiones entre estas mediciones pudieran ofrecer más información sobre este fenómeno.

CAPÍTULO VI

DISCUSIÓN GENERAL

CAPÍTULO VI. DISCUSIÓN GENERAL

6.1 Actualidad del trabajo

La búsqueda de las redes neuronales involucradas en las diferentes funciones cerebrales es un tema de interés sostenido en las investigaciones actuales en neurociencias. Los métodos desarrollados en esta Tesis se enfocan en la solución de este problema a partir del análisis del EEG y han sido publicados en revistas de alto impacto en los últimos cinco años. En particular, las medidas estadísticas para detectar cambios en la dinámica cerebral relacionada a eventos y para distinguir entre diferentes mecanismos de los potenciales evocados contribuyen a un debate sobre el origen de los PREs, al cual se dedica gran parte de la literatura científica actual [Hanslmayr y col. 2007, Mazaheri y col. 2006, Klimesch y col. 2006, Mäkinen y col. 2005, Yeung y col. 2004]. El enfoque de análisis multidimensional propuesto a partir de modelos como el PARAFAC y el MCPT, ha sido utilizado en diversas aplicaciones dentro de las neurociencias [Beckmann y col. 2005, Mørup y col. 2006, De Vos y col. 2007]. La generalización de algoritmos para utilizar diversos tipos de restricciones en el análisis de la actividad cerebral es también de interés creciente en la comunidad científica, dado el reconocimiento de la necesidad de nuevos métodos para abordar el estudio de sistemas complejos. En esta dirección se encamina el trabajo de la descomposición espacio-tiempo-frecuencia penalizada y la introducción de un penalizador para encontrar las redes con mínima entropía espectral. Por último, la posibilidad tecnológica de medir simultáneamente la actividad eléctrica (con el EEG) y metabólica (con IRMf) ha llevado al desarrollo de métodos para el análisis de este tipo de datos. En este contexto, el

método aquí propuesto para el análisis conjunto de datos de EEG e IRMf se inserta dentro de los esfuerzos actuales por integrar la actividad eléctrica cerebral de alta resolución temporal con la actividad metabólica medida con alta resolución espacial [Horwitz 2002, Goldman y col. 2002, Moosmann y col. 2003].

6.2 Aporte científico

En esta Tesis se presenta el uso de modelos y métodos no reportados previamente en su aplicación al análisis de datos de neuroimágenes, con el fin de caracterizar la actividad eléctrica del cerebro en espacio, tiempo y frecuencia. Se introducen cuatro medidas estadísticas para el análisis de cambios en la dinámica cerebral, basados en la información tanto de fase como de amplitud que brindan las representaciones tiempo-frecuencia complejas de los datos. Entre estas, se proponen por primera vez en la literatura medidas que son capaces de diferenciar entre dos teorías sobre el origen de los potenciales evocados, independientemente de la actividad media evocada.

Otro aporte metodológico es el uso del método *Matching Pursuit* en versiones multicanales para obtener representaciones espacio-tiempo-frecuencia de actividades esporádicas en el EEG. Además, por primera vez se reporta el uso de métodos de análisis multidimensional, como el PARAFAC, para la identificación simultáneamente en tiempo, espacio y frecuencia de las redes neuronales responsables del EEG espontáneo y relacionado a eventos, así como aquellas cuya actividad neural tiene alta correlación con la actividad metabólica.

Hasta donde sabemos, este trabajo también es el primero en proponer un algoritmo general que permite el uso de una gran variedad de restricciones y la combinación de ellas en el análisis multidimensional (PARAFAC) del EEG. Esto es particularmente

importante en neurociencias, donde la naturaleza estocástica de los datos hace necesario el uso de información adicional para obtener resultados interpretables y fisiológicamente plausibles.

Con los nuevos algoritmos, una gran variedad de funciones lineales y no lineales son posibles de utilizar, incluyendo la Entropía Informacional que es por primera vez utilizada como información *a priori* para encontrar las redes neuronales que funcionan en un estado de mínima entropía espectral. Este enfoque puede ser útil en el estudio de otros tipos de actividad patológica, como la encontrada en casos de epilepsia y Alzheimer, donde los cambios en la complejidad de la actividad neural podrían reflejar el estado funcional o de salud del cerebro [Quian-Quiroga 1998, Jeong 2004, Rosso y col 2006].

Otro aporte resulta la introducción del método de Mínimos Cuadrados Parciales Tensorial para el análisis de datos conjuntos de EEG e IRMf. Esta metodología provee por primera vez un análisis de reducción de dimensionalidad, que permite la fusión de la información contenida en ambas neuroimágenes sin la necesidad de escoger subjetivamente los electrodos o bandas de frecuencias de interés ni de especificar un modelo paramétrico que relacione las magnitudes medidas con ambas técnicas.

La mayoría de los métodos desarrollados en esta Tesis pueden ser adaptados para el análisis de datos de otras ramas como por ejemplo, la quimiometría, la industria alimenticia, la separación a ciegas de señales electrónicas en antenas, la antropometría y en otras aplicaciones a la medicina, como el diagnóstico de cáncer, estudios de toxicidad y detección de crisis epilépticas, entre otras. Estos métodos se han implementado como paquetes de programas en Matlab [The MathWorks Inc. 2007] y se incorporarán en un

futuro cercano a sistemas informáticos de análisis de EEG y otras neuroimágenes que se comercializan junto con los equipos médicos producidos por nuestro Centro.

6.2 Limitaciones de la metodología

La imposibilidad del estudio *in vivo* con técnicas invasivas ha llevado a un gran desarrollo de tecnologías inocuas para medir la actividad cerebral, con la desventaja de que estas sólo ofrecen mediciones indirectas de los procesos subyacentes. Este trabajo ofrece una aproximación al estudio del funcionamiento cerebral a través del análisis de datos de neuroimágenes y como tal, es importante conocer los límites de aplicabilidad de los métodos propuestos.

En el análisis de la Dinámica Cerebral Relacionada a Eventos, hemos introducido medidas para evaluar separadamente los diferentes tipos de actividades relacionadas con el funcionamiento cerebral. Sin embargo, recientemente estudios experimentales en animales y humanos apoyan la contribución simultánea de los diferentes mecanismos en la generación de los tres tipos de actividades (potencial evocado, restablecimiento de fase y actividad inducida) [Shah y col. 2004, Düzel y col. 2005]. Por tanto, en nuestro punto de vista, se debe asumir una visión más amplia del problema de la generación de la actividad evocada, en la cual ambos mecanismos (actividad aditiva y RPF) puedan coexistir con distintos grados de interacción. La correcta modelación de la dinámica cerebral, junto con el uso de nuevas técnicas estadísticas parece ser el enfoque correcto para el análisis de este tipo de datos.

Por otro lado, los métodos desarrollados para el análisis espacio-tiempo-frecuencia se han restringido a la descomposición del EEG a nivel topográfico. Las fuentes originarias de la actividad cerebral pueden ser obtenidas como un paso posterior con el uso de

métodos de solución inversa. Sin embargo, creemos que es posible utilizar la relación espacial conocida entre la densidad de corriente primaria dentro del cerebro y el potencial eléctrico en el cuero cabelludo para plantear modelos de descomposición que permitan la caracterización espacio-tiempo-frecuencia de las fuentes generadoras directamente (en un sólo paso).

En este sentido hemos planteado el uso del método de MCPT para el análisis conjunto de datos de EEG e IRMf que permite utilizar la alta resolución de estas últimas para hallar las áreas cerebrales que podrían formar parte de las redes generadoras de los ritmos espontáneos del EEG. Sin embargo, una limitación de este análisis es que no permite distinguir si las estructuras de las redes generadoras de un determinado ritmo, están oscilando en el mismo rango de frecuencias. Tampoco es probable que este análisis permita localizar completamente las estructuras profundas (no reflejadas en el EEG) cuya actividad cambia en una escala temporal fina, lo cual establece la existencia de actividad neural no detectable con mediciones simultáneas de EEG e IRMf. Experimentos futuros con registro conjunto de IRMf y la actividad eléctrica con electrodos profundos pudieran ser la solución a esta cuestión. Finalmente, también es posible que existan interacciones no lineales entre las características temporales, espectrales y espaciales de las redes funcionales que este análisis no pueda explicar.

De manera general, en el enfoque utilizado en esta Tesis los modelos explican la relación macroscópica y fenomenológica entre los procesos de interés y la señal medida, pero no la forma en que estos procesos se llevan a cabo a partir de la interacción de la actividad de cada célula. En este sentido, los parámetros de estos modelos no pueden ser directamente asociados a procesos fisiológicos y los métodos de análisis propuestos no

ofrecen respuestas sobre los mecanismos biofísicos que producen la actividad eléctrica de las redes identificadas. Es posible que la combinación de los métodos aquí propuestos con otros modelos biofísicos del funcionamiento cerebral en una escala espacial más fina sea el enfoque adecuado para encontrar la relación entre la actividad básica neuronal y el comportamiento complejo de las redes funcionales responsables de los procesos de consciencia y cognición.

CONCLUSIONES

En este trabajo hemos presentado el uso de nuevos modelos y métodos de análisis de la actividad eléctrica cerebral para el estudio de las redes neuronales subyacentes. Los métodos han estado orientados a la identificación de estas redes mediante la caracterización en espacio, tiempo y frecuencia de su actividad eléctrica. En general, podemos concluir que las metodologías introducidas ofrecieron, de manera confiable, información relevante sobre la actividad de las redes neuronales involucradas en diversos estados cognitivos y espontáneos. De modo particular, podemos concluir que:

1. Los estadígrafos de la media, la varianza y la distribución de fases constituyen medidas que permiten cuantificar los cambios en la actividad media, la actividad inducida y la reorganización de fases en el dominio tiempo-frecuencia, respectivamente.
2. a) Versiones multicanales del método *Matching Pursuit* permiten identificar en espacio, tiempo y frecuencia actividades esporádicas como los husos de sueño y la actividad epiléptica.

   b) La aplicación del método de solución inversa LORETA a las características espaciales obtenidas por la descomposición *Matching Pursuit* multicanal ofrece una localización espacial con alta resolución de las redes generadoras de actividades simples sin el post-procesamiento estadístico inevitable en el análisis de fuentes clásico.
3. La descomposición multilineal PARAFAC del espectrograma del EEG permite la obtención de forma única de los factores característicos en tiempo, frecuencia y

espacio de las redes neuronales involucradas en tareas cognitivas y actividad espontánea.

4. a) El algoritmo Mínimos Cuadrados Penalizados Alternantes permite la imposición de restricciones en la descomposición PARAFAC con el uso tanto de funciones convexas (cuadráticas) y no convexas, así como combinación de ellas, dando lugar a una gran variedad de posibilidades para incluir información adicional sobre las características de las redes buscadas.

   b) El uso de funciones no convexas como restricciones en la descomposición PARAFAC permiten obtener características temporales que semejan las obtenidas experimentalmente en el caso de actividades fisiológicas reales.

   c) La descomposición PARAFAC con el uso de una función de penalización no convexa basada en la Entropía Informacional posibilita la caracterización espacio-tiempo-frecuencia de las redes funcionando en estados de mínima entropía espectral.

5. El método de Mínimos Cuadrados Parciales Tensorial para el análisis conjunto de datos de EEG e IRMf, ofrece una localización espacial de las áreas pertenecientes a las redes responsables de los distintos ritmos cerebrales espontáneos con mayor resolución que la obtenida de la descomposición PARAFAC del EEG solamente.

Recomendaciones

Las diferentes metodologías utilizadas presentan limitaciones que abren nuevas interrogantes y recomendaciones para trabajos futuros. Entre ellas podemos mencionar:

1. Validar los estadígrafos propuestos para evaluar los cambios en la Dinámica Cerebral Relacionada a Eventos en otros datos reales y situaciones simuladas más complejas. Asimismo, comparar los resultados obtenidos con diferentes métodos de análisis

tiempo-frecuencia, para estudiar la dependencia de estos estadígrafos con las propiedades y parámetros de estas transformaciones.

2. Explorar las posibles mejoras en la localización de las fuentes de actividades identificadas con el *Matching Pursuit* multicanal, con el uso de métodos de solución inversa que superen las limitaciones del método LORETA.
3. Estudiar métodos más adecuados para estimar el número de componentes correcto y los parámetros de pesos óptimos en la descomposición PARAFAC con penalizaciones no cuadráticas.
4. Estudiar nuevas medidas de complejidad de la actividad neural y su relación con los procesos cerebrales para su uso como restricciones en la identificación de las redes neuronales.
5. Desarrollar las herramientas estadísticas apropiadas para evaluar la significación de los resultados del análisis PARAFAC penalizado así como su implementación dentro de un formalismo bayesiano que podría ayudar en la selección de descomposiciones penalizadas óptimas.
6. Aplicar los métodos desarrollados al estudio del funcionamiento cerebral a partir de datos de otras técnicas de neuroimágenes que puedan cumplimentar los estudios aquí realizados.
7. Validar los métodos con uso clínico potencial a través de estudios rigurosos de sus resultados en la aplicación a diversos datos reales, así como la evaluación de los límites de su aplicabilidad.

REFERENCIAS BIBLIOGRÁFICAS

1. Achim, A., Bouchard, S.: Toward a dynamic topographic components model. Electroencephalography and Clinical Neurophysiology 103, 381–385 (1997).
2. Akaike, H.: A new look at the statistical model identification. IEEE Transactions on Automatic Control 19, 716-723 (1974).
3. Amidzic, O., Riehle, H.J., Fehr, T., Wienbruch, C., Elbert, T.: Pattern of focal gamma-bursts in chess players. Nature 412, 603 (2001).
4. Anderer, P., Klösch, G., Gruber, G., Trenker, E., Pascual-Marqui, R., Zeitlhofer, J., Barbanoj, M. J., Rappelsberger, P., Saletu, B.: Low-resolution brain electromagnetic tomography revealed simultaneously active frontal and parietal sleep spindles sources in the human cortex. Neuroscience 103, 3, 581–592 (2001).
5. Andersson, C.A., Bro, R.: The N-way Toolbox for MATLAB. Chemometrics and Intelligent Laboratory Systems 52, 1-4 (2000).
6. Barwińsky, M.: Product-based metric for Gabor functions and its implications for the Matching Pursuit algorithm. M.Sc. Thesis, Warsaw University, Institute of Experimental Physics, (2004). http://eeg.pl/Members/mbarwinski/m.sc.-on-matching-pursuit-theory
7. Beckmann, C., Smith, S.: Tensorial extensions of independent component analysis for multisubject fmri analysis. NeuroImage 25, 294–311 (2005).
8. Boashash, B. Time frequency signal analysis and processing. Elsevier, London, (2003).

9. Bosch-Bayard, J., Valdes-Sosa, P., Virues-Alba, T., Aubert-Vazquez, E., John, E.R., Harmony, T., Riera-Díaz, J.J., Trujillo-Barreto, N.: 3D statistical parametric mapping of EEG source spectra by means of variable resolution electromagnetic tomography (VARETA). Clinical Electroencephalography 32, 2, 47-61 (2001).
10. Brillinger, D.R.: Times Series: Data Analysis and Theory. SIAM, Philadelphia, (2001).
11. Bro, R.: Multi-way Analysis in the Food Industry: Models, Algorithms and Applications. PhD Thesis. University of Amsterdam (NL) and Royal Veterinary and Agricultural University (DK), (1998).
12. Bro, R.: Multi-way calibration. Multi-linear PLS. Journal of Chemometrics 10, 47–61 (1996).
13. Carroll, J.D., Chang, J.: Analysis of individual differences in multidimensional scaling via an N-way generalization of 'Eckart-Young' decomposition. Psychometrika 35, 283– 319 (1970).
14. Casanova, R., Valdés-Sosa, P.A., García, F., Aubert, E., Riera, J., Korin, W., Lins, O.: Frequency domain distributed inverse solutions. In: Aine, C.J., Okada, Y., Stroink, G., Swithenby, S.J., Wood, C.C. (Eds.), Biomag 96, Proceedings of the 10th International Conference on Biomagnetism. Springer-Verlag, New York, (2000).
15. Chen, S.S., Donoho, D.L., Saunders, M.A.: Atomic decomposition by basis pursuit. SIAM Review 43, 1, 129–59 (2001).
16. Churchland, P.S., Sejnowski, T.J.: Perspectives on cognitive neuroscience. Science 242, 4879, 741–745 (1988).

17. Cuspineda-Bravo, E.R., Sánchez-Bornot, J.M., Valdés-Sosa, P.A.: Measuring event-related dynamics [abstract]. Presented at the 12th Annual Meeting of the Organization for Human Brain Mapping, Florence, Italy. NeuroImage 27, 1, (2006).
18. De Vos, M., Vergult, A., De Lathauwer, L., De Clercq, W., Van Huffel, S., Dupont, P., Palmini, A., Van Paesschen, W.: Canonical decomposition of ictal scalp EEG reliably detects the seizure onset zone. NeuroImage 37, 3, 844–54 (2007).
19. Delorme, A., Makeig. S.: EEGLAB: An open-source toolbox for analysis of EEG dynamics. Journal of Neuroscience Methods 134, 9–21 (2004).
20. Düzel, E., Habib, R., Schott, B., Schoenfeld, A., Lobaugh, N., McIntosh, A.R., Scholz, M., Heinze, H.J., 2003. A multivariate, spatiotemporal analysis of electromagnetic time– frequency data of recognition memory. NeuroImage 18, 185–197 (2001).
21. Düzel, E., Neufang, M., Heinze, H.J.: The oscillatory dynamics of recognition memory and its relationship to event-related responses. Cerebral Cortex 15, 1992–2002 (2005).
22. Dummermuth, G., Molinari, L. Spectral analysis of EEG background activity. En: Gevins, A., Remond, A. (Eds). Handbook of electroencephalography and clinical neurophysiology. Vol 1: Methods of analysis of brain electrical and magnetic signals. Elsevier, Amsterdam, (1987).
23. Durka, P.: Matching pursuit and unification in EEG analysis. Artech House, London, (2007).
24. Durka, P.J., Blinowska, K.J.: Analysis of EEG transients by means of matching pursuit. Annals of Biomedical Engineering 23, 608–611 (1995).

25. Edwards, E., Soltani, M., Deouell, L.Y., Berger, M.S., Knight, R.T.: High gamma activity in response to deviant auditory stimuli recorded directly from human cortex. Journal of Neurophysiology 94, 4269–4280 (2005).
26. Estienne, F., Matthijs, N., Massart, D.L., Ricoux, P., Leibovici, D.: Multi-way modelling of high-dimensionality electroencephalographic data. Chemometrics and Intelligent Laboratory Systems 58, 59–71 (2001).
27. Fan, J.Q., Li, R.Z.: Variable selection via nonconcave penalized likelihood and its oracle properties. Journal of American Statistical Association 96, 456, 1348-1360 (2001).
28. Feichtinger, H.G., Strohmer, T. (eds). Gabor Analysis and Algorithms: Theory and Applications. Birkhäuser, Boston, (1998).
29. Field, A.S., Graupe, D.: Topographic component (Parallel Factor) analysis of multichannel evoked potentials: practical issues in trilinear spatiotemporal decomposition. Brain Topography 3, 407–423 (1991).
30. Friston, K.J., Fletcher, P., Josephs, O., Holmes, A., Rugg, M.D., Turner, R.: Event-related fMRI: characterizing differential responses. Neuroimage 7, 30-40 (1998).
31. Gersch, W.: Spectral analysis of EEG's by autoregressive decomposition of time series. Mathematical Biosciences 7, 205–222 (1970).
32. Goldman, R.I., Stern, J.M., Engel, J., Cohen, M.S.: Acquiring simultaneous EEG and functional MRI. Clinical Neurophysiology 111, 1974–1980 (2000).
33. Goldman, R.I., Stern, J.M., Engel, J., Cohen, M.S.: Simultaneous EEG and fMRI of the alpha rhythm. NeuroReport 13, 18, 2487–2492 (2002).

34. Golub, G., Heath, M., Wahba, G.: Generalized cross-validation as a method for choosing a good ridge parameter. Technometrics 21, 215-223 (1979).
35. Gotman, J., Ives, J.R., Gloor, P.: Frequency content of EEG and EMG at seizure onset: possibility of removal of EMG artifact by digital filtering, Electroencephalography and Clinical Neurophysiology 52, 626–639 (1981).
36. Gribonval, R.: Piecewise linear source separation. En: Proc. SPIE 03.Vol. 5207, Wavelets: Applications in Signal and Image Processing. San Diego, California, (2003).
37. Hämäläinen, M., Ilmoniemi, R.: Interpreting magnetic fields of the brain: minimum norm estimates. Medical & Biological Engineering & Computing 32, 35–42 (1994).
38. Handy, T.C. Event-Related Potentials: A methods handbook. MIT Press, Cambridge, (2005).
39. Hanslmayr, S., Klimesch, W., Sauseng, P., Gruber, W., Doppelmayr, M., Freunberger, R., Pecherstorfer, T., Birbaumer, N.: Alpha phase reset contributes to the generation of ERPs. Cerebral Cortex 17, 1–8 (2007).
40. Harshman, R.A.: Determination and proof of minimum uniqueness conditions for PARAFAC1. UCLA Working Papers in Phonetics 22, 111–117 (1972).
41. Harshman, R.A.: Foundations of the PARAFAC procedure: models and conditions for an 'explanatory' multi-modal factor analysis. UCLA Working Papers in Phonetics 16, 1– 84 (1970).
42. Herrmann, C.S., Munk, M.H.J., Engel, A.K.: Cognitive functions of gamma-band activity: memory match and utilization. TRENDS in Cognitive Sciences 8, 8, 347-355 (2004).

43. Horwitz, B., Poeppel, D.: How can EEG/MEG and fMRI/PET data be combined? Human Brain Mapping 17, 1–3 (2002).
44. Hunter, D.R., Li, R.: Variable selection using MM algorithms. Annals of Statistics 33, 1617-1642 (2005).
45. Jeong, J.: EEG dynamics in patients with Alzheimer´s disease. Clinical Neurophysiology 115, 1490-1505 (2004).
46. Jimenez, J.C., Biscay, R., Montoto, O.: Modeling the electroencephalogram by means of spatial spline smoothing and temporal autoregression. Biological Cybernetics 72, 249-259 (1995).
47. Kayser, J., Tenke, C.E., Debener, S.: Principal components analysis (PCA) as a tool for identifying EEG frequency bands: I. Methodological considerations and preliminary findings. Psychophysiology 37, S54 (2000).
48. Kiebel, S.J., Tallon-Baudry, C., Friston, K.J.: Parametric analysis of oscillatory activity as measured with EEG/MEG. Human Brain Mapping 26, 170–177 (2005).
49. Klimesch, W., Hanslmayr, S., Sauseng, P., Gruber, W.R.: Distinguishing the evoked response from phase reset: a comment to Mäkinen et al. NeuroImage 29, 808–811 (2006).
50. Koenig, T., Marti-Lopez, F., Valdes-Sosa, P.: Topographic time-frequency decomposition of the EEG. Neuroimage 14, 383–390 (2001).
51. Kruskal, J.B.: More factors than subjects, test and treatments: an indeterminacy theorem for canonical decomposition and individual differences scaling. Psychometrika 41, 281-293 (1976).

52. Kruskal, J.B.: Three-way arrays: rank and uniqueness of trilinear decomposition with applications to arithmetic complexity and statistics. Linear Algebra and its Applications 18, 95– 138 (1977).
53. Lagerlund, T.D., Sharbrough, F.W., Busacker, N.E.: Spatial filtering of multichannel electroencephalographic recordings through principal component analysis by singular value decomposition. Journal of Clinical Neurophysiology 14, 73– 83 (1997).
54. Land, S., Friedman, J.: Variable fusion: a new method of adaptive signal regression. Technical Report. Department of Statistics, Stanford University, Stanford, (1996).
55. Lehnertz, K., Elger, C.: Spatio-temporal dynamics of the primary epileptogenic area in temporal lobe epilepsy characterized by neuronal complexity loss. Electroencephalography and Clinical Neurophysiology 95, 108-117 (1995).
56. Lobaugh, N.J., West, R., McIntosh, A.R.: Spatiotemporal analysis of experimental of experimental differences in event-related potential data with partial least squares. Psychophysiology 38, 517–530 (2001).
57. Lopes da Silva, F.H. EEG analysis: theory and practice. En: Niedermeyer, E., Lopes da Silva, F.H. (Eds). Electroencephalography: Basic Principles, Clinical Applications and Related Fields. Baltimore, Williams and Wilkins 3rd ed., (1993).
58. Luu, P., Tucker, D.M., Makeig, S.: Frontal midline theta and the error-related negativity: neurophysiological mechanisms of action regulation. Clinical Neurophysiology 115, 1821–1835 (2004).

59. Makeig, S., Westerfield, M., Jung, T.P., Enghoff, S., Townsend, J., Courchesne, E., Sejnowskii, T.J.: Dynamic brain sources of visual evoked responses. Science, 295, 690-694 (2002).

60. Makeig, S.: Auditory event-related dynamics of the EEG spectrum and effects of exposure to tones. Electroencephalography and Clinical Neurophysiology 86, 283–293 (1993).

61. Mäkinen, V., Tiitinen, H., May, P.: Auditory event-related responses are generated independently of ongoing brain activity. NeuroImage 24, 4, 961–968 (2005).

62. Mallat, S., Zhang, Z.: Matching pursuit with time–frequency dictionaries. IEEE Transactions on Signal Processing 41, 3397–3415 (1993).

63. Martínez-Montes, E., Bosch-Bayard, J., Matysiak, A., Durka, P., Rodríguez-Puentes, Y.: Adaptive time-frequency approximations vs. spectral integrals as preprocessing for EEG inverse solutions [abstract]. Presented at the 11th Annual Meeting of the Organization for Human Brain Mapping, June 12-16, Toronto, Canada. Available on CD-Rom in NeuroImage 26, 1 (2005).

64. Martínez-Montes, E., Lage-Castellanos, A., Canales-Rodríguez, E., Iturria-Medina, Y., Valdés-Sosa, P.A.: El cerebro como sistema complejo: estimación de la conectividad cerebral. Revista Cubana de Física 23, 2, 97-106 (2006).

65. Martínez-Montes, E., Trujillo-Barreto, N.J., Melie-García, L.: Variable Resolution Electromagnetic Tomography: a new type of inverse solution based on Bayesian Theory. Revista CNIC Ciencias Biológicas 33, 3, 129-135 (2002).

66. Mazaheri, A., Jensen, O.: Posterior {alpha} activity is not phase-reset by visual stimuli. Proceedings of the National Academy of Sciences 103, 2948–2952 (2006).

67. Mazaheri, A., Picton, T.W.: EEG spectral dynamics during discrimination of auditory and visual targets. Cognitive Brain Research 24, 81–96 (2005).

68. McIntosh, A.R., Bookstein, F.L., Haxby, J.V., Grady, C.L.: Spatial pattern analysis of functional brain images using Partial Least Squares. NeuroImage 3, 143–157 (1996).

69. Michel, C.M., Murray, M.M., Lantz, G., Gonzalez, S., Spinelli, L., Grave de Peralta, R.: EEG source imaging. Clinical Neurophysiology, 115, 2195–2222, (2004).

70. Möcks, J.: Decomposing event-related potential: a new topographic components model. Biological Psychology 26, 199–215 (1988a).

71. Möcks, J.: Topographic components model for event-related potentials and some biophysical considerations. IEEE Transactions on Biomedical Engineering 35, 482–484 (1988b).

72. Moosmann, M., Ritter, P., Krastel, I., Brink, A., Thees, S., Blankenburg, F., Taskin, B., Obrig, H., Villringer, A.: Correlates of alpha rhythm in functional magnetic resonance imaging and near infrared spectroscopy. Neuroimage 20, 1, 145–158 (2003).

73. Mørup, M., Hansen, L.K., Hermann, C.S., Parnas, J., Arnfred, S.M.: Parallel factor analysis as an exploratory tool for wavelet transformed event-related EEG. NeuroImage 29, 3, 938–947 (2006).

74. Mørup, M.: Analysis of brain data using multi-way array models on the EEG. MSc Thesis. Technical University of Denmark, 2005.

75. Niedermeyer, E., Lopes da Silva, F.H. Electroencephalography: Basic Principles, Clinical Applications and Related Fields. Urban and Schwarzengreg: Baltimore, MD, (1999).
76. Nunez, P., Electric fields of the brain. Oxford University Press, 1981.
77. Nuwer, M.R., Lehmann, D., Lopes da Silva F.H., Matsuoka, S., Sutherling, W., Vivert, J.F.: IFCN guidelines for topographic and frequency analysis of EEGs and EPs. Report of and IFCN committee. Electroencephalography and Clinical Neurophysiology 91, 1-5 (1994).
78. Onton, J., Makeig, S.: Information-based modeling of event-related brain dynamics. Progress in Brain Research 159, 99-120 (2006).
79. Pascual-Marqui, R., Michel, C., Lehman, D.: Low resolution electromagnetic tomography: a new method to localize electrical activity in the brain. International Journal of Psychophysiology 18, 49–65 (1994).
80. Pascual-Marqui, R.D.: Standardized low resolution brain electromagnetic tomography (sLORETA): technical details. Methods & Findings in Experimental & Clinical Pharmacology 24D, 5-12 (2002).
81. Pfurtscheller, G., Lopes da Silva, F.: Event-related EEG/MEG synchronization and desynchronization: basic principles. Clinical Neurophysiology 110, 1842–1857 (1999).
82. Quian-Quiroga, R.: Quantitative analysis of EEG signals: Time-frequency methods and Chaos theory. PhD Thesis. Medical University Lübeck, Alemania, (1998).

83. Rosso, O.A., Martin, M.T., Figliola, A., Keller, K., Plastino, A.: EEG analysis using wavelet-based information tools. Journal of Neuroscience Methods 153, 2, 163-182 (2006).

84. Sánchez-Bornot, J.M., Martínez-Montes, E., Lage-Castellanos, E., Vega-Hernández, M., Valdés-Sosa, P.A.: Uncovering sparse brain effective connectivity: voxel/based approach using penalized regression. Statistica Sinica 18, 4, 1501-1518 (2008).

85. Sasaki, K., Tsujimoto, T., Nishikawa, S., Nishitani, N., Ishihara, T.: Frontal mental theta wave recorded simultaneously with megnetroencephalography and electroencephalography. Neuroscience 26, 79–81 (1996).

86. Schwartz, G.: Estimating the dimension of a model. Annals of Statistics 6, 461-464 (1978).

87. Shah, A.S., Bressler, S.L., Knuth, K.H., Ding, M., Mehta, A.D., Ulbert, I., Schroeder, C.E.: Neural dynamics and the fundamental mechanisms of event-related brain potentials. Cerebral Cortex 14, 476–483 (2004).

88. Shannon, C.E.: A mathematical theory of communication. Bell System Technical Journal 27, 379-423 and 623-656 (1948).

89. Sidiropoulos, N.D., Bro, R.: On the uniqueness of multilinear decomposition of N-way arrays. Journal of Chemometrics 14, 229–239 (2000).

90. Soong, A.C., Koles, Z.J.: Principal-component localization of the sources of the background EEG. IEEE Transactions on Biomedical Engineering 42, 59– 67 (1995).

91. Stegeman, A.: Comparing Independent Component Analysis and the Parafac model for artificial multi-subject fMRI data. Technical Report, Available online at http://www.ppsw.rug.nl/~stegeman/main_pub.htm, (2007).

92. Tallon-Baudry, C., Bertrand, O., Delpuech, C., Pernier, J.: Oscillatory g-band (30–70 Hz) activity induced by a visual search task in humans. Journal of Neuroscience 17, 722–734 (1997).

93. Tallon-Baudry, C., Bertrand, O., Delpuech, C., Pernier, J.: Stimulus specificity of phase-locked and non-phase-locked 40 Hz visual responses in human. Journal of Neuroscience 16, 4240–4249 (1996).

94. Tallon-Baudry, C., Bertrand, O.: Oscillatory gamma activity in humans and its role in object representation. Trends in Cognitive Sciences 3, 4, 151–162 (1999).

95. Tang, A.C., Pearlmutter, B.A., Malaszenko, N.A., Phung, D.B., Reeb, B.C.: Independent components of magnetoencephalography: Localization. Neural Computation 14, 1827–1858 (2002).

96. The MathWorks, Inc.: MATLAB 2007b, 24 Prime Park Way, Natick MA, 2007, http://www.mathworks.com/products/matlab/.

97. Thomson, D.J.: Spectrum estimation and harmonic analysis. Proceedings of the IEEE (Special issue on spectrum estimation) 70, 1055–1096 (1982).

98. Tibshirani, R.: Regression shrinkage and variable selection via the lasso. Journal of the Royal Statistical Society Series B 58, 267-288 (1996).

99. Trujillo-Barreto, N.J., Aubert, E., Valdés-Sosa, P.: Bayesian model averaging in EEG/MEG imaging. NeuroImage 21, 1300–1319 (2004).

100. Valdés-Sosa, P.A., Bosch, J., Virués, T., Aubert, E., Fermín, E., González, E.: EEG source frequency domain SPM. NeuroImage 7, 4, 636 (1998).

101. Valdés-Sosa, P.A., Jimenez, J.C., Riera, J., Biscay, R., Ozaki, T.: Nonlinear EEG analysis based on a neural mass model. Biological Cybernetics 81, 415-424 (1999).

102. Valdés-Sosa, P.A., Sánchez-Bornot, J.M., Vega-Hernández, M., Melie-García, L., Lage-Castellanos, A., Canales-Rodríguez, E.: Granger Causality on Spatial Manifolds: Applications to Neuroimaging. En: Schelter, B., Winterhalder, M., Timmer, J. (eds) Handbook of time series analysis: Recent theoretical developments and applications, pp. 461-492. Wiley-VCH, Weinheim (2006).

103. Varela, F., Lachaux, J.P., Rodriguez, E., Martinerie, J.: The brainweb: phase synchronization and large-scale integration. Nature Review Neuroscience 2, 229–239 (2001).

104. Vega-Hernández, M., Martínez-Montes, E., Sánchez-Bornot, J.M., Lage-Castellanos, A., Valdés-Sosa, P.A.: Penalized Least Squares methods for solving the EEG Inverse Problem. Statistica Sinica 18, 4, 1535-1551 (2008).

105. Ward, L.M.: Synchronous neural oscillations and cognitive processes. Trends in Cognitive Sciences 7, 12, 553–559 (2003).

106. Yamagishi, N., Callan, D.E., Goda, N., Anderson, S.J., Yoshida, Y., Kawato, M.: Attentional modulation of oscillatory activity in human visual cortex. NeuroImage 20, 98–113 (2003).

107. Yeung, N., Bogacz, R., Holroyd, C., Cohen, J.: Detection of synchronized oscillations in the electroencephalogram: an evaluation of methods. Psychophysiology 41, 822–832 (2004).

108. Zou, H., Hastie, T.: Regularization and variable selection via the elastic net. Journal of the Royal Statistical Society Series B 67, 301-320 (2005).

ANEXO A. ARTÍCULOS

Artículo 1.

Martínez-Montes, E., Cuspineda-Bravo, E.R., El-Deredy, W., Sánchez-Bornot, J.M., Lage-Castellanos, A., Valdés-Sosa, P.A.: Exploring event-related brain dynamics with tests on complex valued time-frequency representations. Statistics in Medicine, 27, 2922–2947 (2008).

STATISTICS IN MEDICINE
Statist. Med. 2008; **27**:2922–2947
Published online 13 December 2007 in Wiley InterScience
(www.interscience.wiley.com) DOI: 10.1002/sim.3132

Exploring event-related brain dynamics with tests on complex valued time–frequency representations

Eduardo Martínez-Montes[1,*,†], Elena R. Cuspineda-Bravo[2], Wael El-Deredy[3], José M. Sánchez-Bornot[1], Agustín Lage-Castellanos[1] and Pedro A. Valdés-Sosa[4]

[1]*Neurostatistics Department, Cuban Neuroscience Center, Havana, Cuba*
[2]*Clinical Neuroimaging Department, Cuban Neuroscience Center, Havana, Cuba*
[3]*Division of Psychology, University of Manchester, U.K.*
[4]*Department of Neuroinformatics, Cuban Neuroscience Center, Havana, Cuba*

SUMMARY

A question subject to intense debate is whether scalp-recorded event-related brain potentials are due to phase resetting of the ongoing electroencephalogram (EEG) or rather to the superimposition of time-locked components on background activity. The two hypotheses are usually assessed by means of statistics in the time–frequency domain, for example, through wavelet transformation of multiple EEG trials that yield for each time and frequency a scatter plot of complex values coefficients. Currently, intertrial phase correlation (phase locking or phase coherence) is taken as evidence for phase resetting at a given frequency and latency. Here we present a formal analysis using a complex t-statistic to illustrate that such measures are, in effect, tests for the mean vector of the repeated trials, and as such on their own are inappropriate measures of phase resetting. We also propose simple t-like statistics for testing changes in (i) the mean (presence of an event-related potential), (ii) the amplitude variance (presence of (de)synchronization) and (iii) the concentration of phases (phase locking). The first two statistics are found to be proper measures of the presence of a non-zero mean activity and induced activity, respectively. In the third case, two different tests are introduced: one based on measuring the alignment of coefficients in the complex plane and another derived from the argument that phase locking persists when the mean of the coefficients is removed. Both statistics gave unambiguous evidence of the presence of phase locking suggesting that they constitute promising tools in the analysis of event-related brain dynamics. Copyright © 2007 John Wiley & Sons, Ltd.

KEY WORDS: event related brain dynamics; EEG; intertrial coherence; complex statistics; phase locking; local FDR

INTRODUCTION

The electroencephalogram (EEG) is the time series of brain electric activity measured on the scalp, produced by the sum of postsynaptic potentials of large populations of neurons, synchronized in

*Correspondence to: Eduardo Martínez-Montes, Neurostatistics Department, Cuban Neuroscience Center, Ave. 25, esq 158, #15202, Cubanacán, Playa, P.O. Box: 6414, Havana 11600, Cuba.
†E-mail: eduardo@cneuro.edu.cu

Received 31 August 2006
Accepted 5 October 2007

time and space. The spontaneous normal EEG is characterized by rhythmic activity with different frequencies [1]. In the presence of stimuli or events, the EEG displays changes at different frequencies and latencies, tracking the different stages and conditions of cognitive processing. Event-related responses provide an exceptionally high temporal resolution tool for studying brain function and dysfunction during cognitive performances, and reflecting the stages of information processing in the brain, while event-related frequency changes are considered an important indicator of the underlying brain processes, mechanisms and dynamics [2–7].

In the classical point of view, the analysis of event-related brain dynamics (ERBD) is based on the assumption that the EEG is composed of the ongoing (or background) activity formed mainly by rhythms, and the stimulus presentation evokes new strictly time-locked event-related neural activity which is superimposed on the background activity. An alternative view suggests that the presentation of the stimulus induces changes of the background rhythmic dynamics only. The merits of each viewpoint are currently subject to intense debate and scrutiny, based on their ability to distinguish the three types of activity:

(1) Additive activity time locked to the presentation of the stimulus and superimposed on background EEG. Averaging over the repeated responses to stimulus presentation yields a noise-free version of the event-related potential (ERP).
(2) Partial phase resetting (PPR) of ongoing EEG, the time-locked components of which are responsible for the ERP.
(3) Induced EEG amplitude and frequency changes that are event-related but not time-locked, and which do not appear in the ERP.

In general, the presence of these types of activity can be assessed by means of statistics computed in the time–frequency domain. Time–frequency analysis is carried out by means of some form of time-localized Fourier decomposition of single trials. The most common approaches are the use of short-term Fourier transform, Morlet wavelet, Gabor or the Hilbert transform, all of which are equivalent representations of the time series in terms of complex coefficients at each time and frequency [8]. Other tools such as Matching Pursuit, have also been used for the study of induced activity in the time–frequency domain [9]. Current analysis of ERBD predominantly uses parametric (t-statistics) and non-parametric (Wilcoxon) statistics to test for significant changes in the power (or its logarithm or square root transformations) of these complex coefficients [8, 10, 11].

As such, these statistics do not distinguish between the different originating mechanisms of the response ERP, since e.g. a phase resetting of the ongoing activity would produce a change in the mean activity (ERP) without significant increase in the power spectrum. In this sense, the phase-locking factor [11] and the intertrial coherence (ITC) [12–15] were introduced as a measure of the uniformity of the distribution of the phase (or coherence) of the complex coefficients for different trials. Nevertheless, some works have raised questions on the validity of this measure for distinguishing between the presence of PPR or an additive ERP [16, 17].

In this paper, we will show that the search for significant changes in ERBD can be addressed with the use of statistical tests on the complex-valued coefficients that arise from time–frequency transformation of the data. This contrasts with the current practice, which analyzes only the energy or the power of these coefficients. We will use simple real statistics (derived from the formal statistics for complex variables) for testing the presence in the post-stimulus period of non-zero mean activity, induced activity and phase concentration with respect to the pre-stimulus period.

DOI: 10.1002/sim

The validity of these statistics as measures of the corresponding effects, as well as the suitability of ITC for measuring PPR, will be studied with the use of simulated and real data. A relevant (but not definitive) comparison between ITC and tests for the mean will also be addressed to show that ITC is equivalent to a measure of the mean activity in the case of ERBD analysis.

The structure of the paper is as follows: the section Methods contains a formal mathematical description of the three types of aforementioned activities in terms of the cloud of complex wavelet coefficients. Subsections dedicated to the ITC and newly proposed statistics for the mean, variance and phase distribution of the cloud of coefficients also appear. The last two subsections are devoted to the local false discovery rate (FDR) technique employed in assessing significance of the tests and to the description of the simulated and real data used in the analysis. In section Results, the analysis of simulated and real data with the proposed statistics is presented and in the next section (Discussion) these results are interpreted and discussed. Finally, a section is dedicated to conclusions of the work.

METHODS

Mathematical description of the three types of ERBD activities

The Morlet wavelet transform (MWT) has been used to compute the instantaneous power and phase of EEG signals [18]. The MWT gives the coefficients of a decomposition of the signal as a weighted sum of wavelet functions; thus, it is also referred to as the wavelet coefficients. It can also be seen as a convolution of the data with the wavelet function which is a windowed, complex sinusoid, with the distinctive property that the width of the Gaussian window is coupled to the frequency of the sinusoid in the form: $\sigma_t = z_0/(2\pi f)$. This is the main difference with windowed Fourier transform (short-term Fourier transform) for which the window can be any other than Gaussian and the variance is not restricted [8]. The parameter z_0 is user-specified and fixes the number of cycles. In this work we used $z_0 = 7$ following [2, 7] as a good choice for obtaining a suitable time–frequency resolution.

Let the wavelet coefficients for ith trial at frequency f and time t be denoted by w_{ift}. Let us assume that in an instant of the pre-stimulus period these coefficients for all trials are distributed as a cloud in the complex plane (Figure 1(a)) in which amplitudes vary in a range but phases are uniformly distributed in $[0, 2\pi)$. Each of the three types of post-stimulus ERBD mentioned above can be characterized by changes in the distribution of this cloud of complex coefficients in the following way:

Activity strictly phase locked to the event (*additive ERP*): This type of component causes a shift of the cloud of complex coefficients from the origin after stimulus; that is, the appearance of a non-zero mean μ_{ft} for the x_{ift} (Figure 1(b)). μ_{ft} is usually estimated by the sample mean $\overline{x}_{ft} = (1/L)\sum_{i=1}^{L} x_{ift}$. This activity implies changes in the EEG power spectrum, estimated as $P_{ft} = (1/L)\sum_{i=1}^{L} |x_{ift}|^2$, where $|x_{ift}|$ denotes the absolute value of the complex number. Since the translation of the cloud does not change the allocation of points with respect to the sample mean, when this mean is removed the distribution of phases will be the same as that of pre-stimulus (Figure 2(a)).

Activity due to EEG PPR: Explained by a partial event-related phase reorganization of oscillatory activity in ongoing EEG (Figure 1(c)). It causes the cloud of complex coefficients to concentrate around a certain angle or phase without change in amplitude and therefore without change in the

DOI: 10.1002/sim

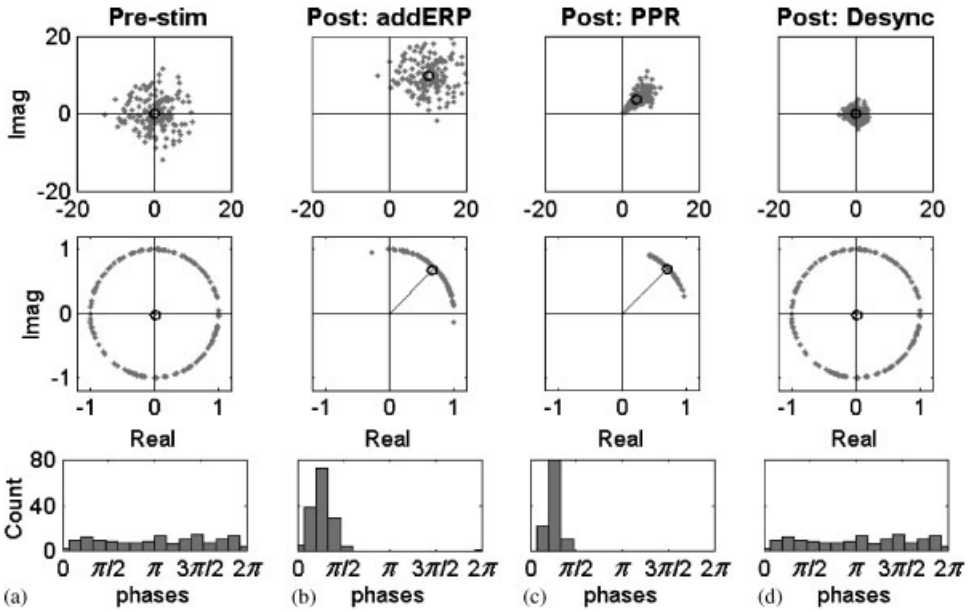

Figure 1. Illustration of different ERBD scenarios according to the cloud of wavelet coefficients (150 trials) in the complex plane for a particular frequency and time point (top view). The projection of points to the unit circle (middle panel) allows one to study the uniformity of phases, shown as a histogram in the bottom view: (a) Pre-stimulus instant, the cloud of coefficients is randomly distributed in the four quadrants; the mean sample is close to zero and distribution of phases is almost uniform. (b) Post-stimulus instant of an additive ERP, the event evokes a time-locked response, with activity superimposed on the ongoing EEG. The cloud is translated to a non-zero mean, while the distribution around the mean remains the same. However, distribution of phases as measured from the origin is far from being uniform. (c) Post-stimulus instant of partial phase resetting effect, the event evokes a reorganization of the phase of the oscillations. The wavelet coefficients take a preferred phase, without variation in amplitude. This scenario also results in a non-zero mean of the ERP and, obviously, non-uniform distribution of phases. (d) Post-stimulus instant of induced activity, the event evokes a change in amplitude of the coefficients but neither in the phase nor in the mean. This example shows a decrease in amplitude of the coefficients which is called desynchronization at that frequency. In all cases the black circle represents the sample mean. In the middle panel the distance from the origin to this circle is the ITC measure.

EEG power spectrum. As this effect evokes a non-zero mean activity after stimulus, condition $\overline{x}_{ft} \neq 0$ also holds. However, it is important to explore phase reorganization as a departure from a uniform distribution of phases of coefficients after having subtracted the mean since PPR is not destroyed by this operation (Figure 2(b)). The evidence for phase resetting is currently based on moderate increases in the ITC which measures the uniformity of the distribution of angles, but with respect to the origin and not to the center $\overline{x}_{ft}$ of the cloud of coefficients (Figure 1, middle panel).

Induced activity: Event-related changes in the EEG power spectrum not due to changes in the mean or PPR. It shows up as changes in the variance σ^2_{ft} of the absolute values of complex coefficients x_{ift} (Figure 1(d)), but without evoking changes in the mean $\overline{x}_{ft}$. The variance σ^2_{ft} is related to the EEG power spectrum; hence, this activity is usually found by comparing power in

DOI: 10.1002/sim

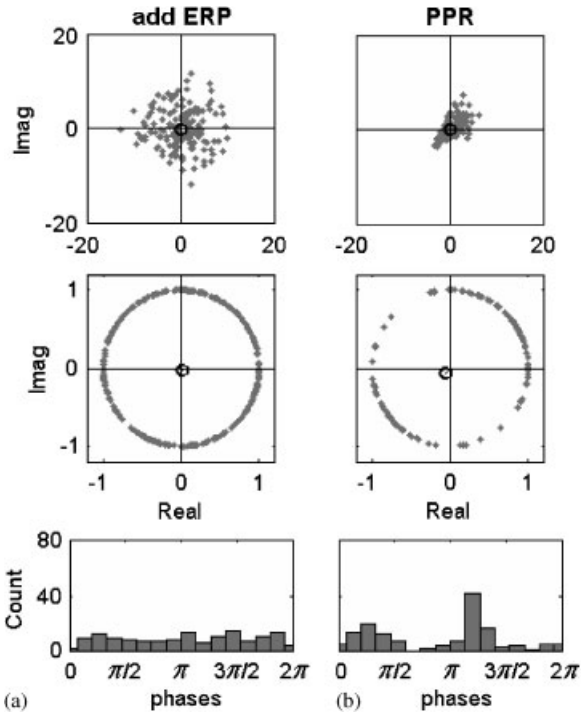

Figure 2. The same plots as in Figure 1(b) and (c) after removing the sample mean from each coefficient. (a) Scenario of additive ERP, note that the cloud coincides with that of the pre-stimulus instant shown in Figure 1(a). (b) Scenario for partial phase resetting effect, the preferred phase does not disappear, but the mean of the cloud of coefficients is now zero. The distribution of phases is not uniform but bimodal and, therefore, the ITC is also very small.

the pre- and post-stimulus EEG spectra. Increases in the variance σ^2_{ft} are termed 'synchronization' and decreases "desynchronization' [9, 19, 20].

Intertrial coherence

It is currently assumed that the most direct evidence of the presence of an ERP due to PPR is an uneven distribution of the phase of oscillations across trials in a period following the event of interest. Phase information from Fourier or wavelet analyses has been used in two ways to assess phase synchronization [12]. A first, qualitative approach is to plot the EEG data after sorting them according to their spectral phase at a particular frequency, so that visual inspection can be used to determine whether ERP components coincide with periods in which EEG activity at that frequency tends to be in phase across trials.

A second, more quantitative approach is to measure the correlation across trials in the EEG spectral phase for particular frequency ranges. The presence of this intertrial phase coherence is considered evidence for the hypothesis that an ERP peak is generated by phase resetting of EEG

DOI: 10.1002/sim

oscillations [12]. It can be measured by the so-called ITC, also known as phase-locking factor [11] and phase-locking index [21]. The ITC is defined as

$$\mathrm{ITC}_{ft} = \left| \frac{1}{L} \sum_{i=1}^{L} \mathrm{e}^{\mathrm{j}\varphi_{ift}} \right| = \left| \frac{1}{L} \sum_{i=1}^{L} \frac{x_{ift}}{|x_{ift}|} \right| \tag{1}$$

where φ_{ift} are the phases of the wavelet coefficients x_{ift} and L is the total number of trials. This measure corresponds to the amplitude of the sample mean of the projection of wavelet coefficients to the unit circle in the complex plane, represented in the middle panel of Figure 1 as a line between the origin and the sample mean (black circle). It can be seen that the test $H_0 : \mathrm{ITC}_{ft} = 0$ is equivalent to the Rayleigh test for uniformity of phases [22]. However, several studies (and we will add evidence on this) have pointed out that this does not imply that ITC is a satisfactory, unambiguous measure of the presence of PPR [16, 17].

The main problem is easily illustrated in Figures 1 and 2. Figure 1(b) and (c) show that an evoked non-zero mean activity is reflected as a non-zero sample mean of the cloud of complex wavelet coefficients in a post-stimulus instant, and it can be represented as a translation of the cloud as a whole or as a reorganization of phases of each point without changing its absolute value. ITC measure in these cases is shown in the middle panel as the length of the line joining the origin and the black circle representing the sample mean of the projection of points to the unit circle. It can be seen that it can be similarly large for both situations, thus making this measure strongly dependent on the position of the sample mean. However, these two situations are easily differentiated by the distribution of points around its sample mean; therefore, removing this from each point is a direct way for subsequently assessing the real distribution of phases. This procedure is illustrated in Figure 2. It can be seen that in the case of an additive ERP, removing the mean will transform the cloud to have the same shape of the pre-stimulus one and the ITC will drop sharply since there is no preferred phase. In the case of PPR, the alignment of points along a preferred direction is retained, but phases, as measured from the origin, present a bimodal distribution. This makes ITC to be very small too, showing that it is not a good measure for distinguishing between these two originating mechanisms of the ERP.

In this study, for comparison purposes, we will report a t-like statistics offering information on the difference between ITC_{ft} and the mean in the baseline period. This statistics will be called T-ITC and is given by

$$T_{ft}^{\mathrm{ITC}} = \sqrt{N-1} \frac{(\mathrm{ITC}_{ft} - \overline{\mathrm{ITC}}_{f}^{\mathrm{pre}})}{\mathrm{STD}_{\mathrm{ITC}_{ft}}^{\mathrm{pre}}} \tag{2}$$

Here, the mean and standard deviation in the N time points $(t_1, \ldots, t_N)$ of the pre-stimulus period are found as $\overline{\mathrm{ITC}}_{f}^{\mathrm{pre}} = (1/N) \sum_{t=t_1}^{t_N} \mathrm{ITC}_{ft}$ and $\mathrm{STD}_{\mathrm{ITC}_{ft}}^{\mathrm{pre}} = \sqrt{\sum_{t=t_1}^{t_N} (\mathrm{ITC}_{ft} - \overline{\mathrm{ITC}}_{f}^{\mathrm{pre}})^2 / (N-1)}$. Although equation (2) resembles a t-statistics, we cannot assure that this statistics follows a t-student distribution. Therefore, significant values will be assessed with the use of the local FDR (to be explained in a subsequent section), which at the same time deal with the problem of multiple testing in the time–frequency plane.

Moreover, we also report the ITC and corresponding confidence interval computed with the use of EEGLAB 4.512 developed by Delorme and Makeig [23], since this is a Matlab Toolbox that has been extensively used in the analysis of ERBD and is freely available at http://www.sccn.ucsd.edu/eeglab/. With this toolbox, significant deviation of ITC from the baseline

DOI: 10.1002/sim

is assessed by using a bootstrap method for creating an empirical 'baseline' distribution, whose specified percentiles are taken as significance thresholds [23].

Statistics for the mean and the variance of the time–frequency coefficients

So far, we see that different situations in ERBD can be easily characterized by the complex wavelet coefficients. Hence, tools for testing changes in the brain dynamics using the complex coefficients instead of its absolute values will provide easier interpretation of the results and discrimination of those different scenarios. Our goal is to propose simple real statistics that allow testing for changes in the distribution of the cloud of complex wavelet coefficients after the occurrence of a stimulus/event.

Firstly we are interested in finding the differences between the sample mean of the cloud of L wavelet coefficients for each time point and frequency ($\overline{x}_{ft}$) and the average of these sample means for the pre-stimulus period $\overline{x}_f^{\text{pre}}$. The former is found by $\overline{x}_{ft}=(1/L)\sum_{i=1}^{L} x_{ift}$ and the latter is defined as $\overline{x}_f^{\text{pre}}=(1/N)\sum_{t=t_1}^{t_N}\overline{x}_{ft}$, where $t_1,\ldots,t_N$ are the N time points belonging to the pre-stimulus period. Let the sample variance of the complex coefficients be given by the real magnitude $\sigma_{ft}^2=(1/(L-1))\sum_{i=1}^{L}(x_{ift}-\overline{x}_{ft})(x_{ift}-\overline{x}_{ft})^*=(1/(L-1))\sum_{i=1}^{L}|x_{ift}-\overline{x}_{ft}|^2$, where $*$ and $|\cdot|$ indicate complex conjugation and absolute value of a complex number, respectively. Then, a statistic for the mean (hereinafter T-mean statistic) of the complex coefficients is proposed as

$$T_{ft}^{\mu}=\sqrt{L-1}\,\frac{\sqrt{(\overline{x}_{ft}-\overline{x}_f^{\text{pre}})(\overline{x}_{ft}-\overline{x}_f^{\text{pre}})^*}}{\sqrt{\sigma_{ft}^2}}=\sqrt{L-1}\,\frac{|\overline{x}_{ft}-\overline{x}_f^{\text{pre}}|}{\sigma_{ft}} \tag{3}$$

This can be seen as the absolute value of the complex t-statistics [24], having a one-tail distribution since only positive values are possible. If the wavelet coefficients are complex normally distributed, then the variance σ_{ft}^2 is chi-square distributed and T_{ft}^{μ} is the absolute value of the complex t-statistics, such that $(T_{ft}^{\mu})^2\sim F_{2,2(L-1)}$. However, here we do not assume gaussianity of the coefficients since significance levels will be found by means of the local FDR, which is a distribution-free technique (see section Local FDR).

Secondly, we want to measure changes produced only in the variance of the cloud of complex coefficients after the stimulus. In this case, similarly, the idea is to compare the variance for all frequencies and time points *vs* the average of the variance in the pre-stimulus period. The mean and standard deviation of the sample variance in the pre-stimulus are found as $\overline{\sigma}_f^{2\text{pre}}=(1/N)\sum_{t=t_1}^{t_N}\sigma_{ft}^2$ and $\text{STD}_{\sigma_{ft}^2}^{\text{pre}}=\sqrt{\sum_{t=t_1}^{t_N}(\sigma_{ft}^2-\overline{\sigma}_f^{2\text{pre}})^2/(N-1)}$. Then, a statistic for the variance (to be called T-variance statistic) of the complex coefficients is proposed as

$$T_{ft}^{\sigma}=\sqrt{N-1}\,\frac{(\sigma_{ft}^2-\overline{\sigma}_f^{2\text{pre}})}{\text{STD}_{\sigma_{ft}^2}^{\text{pre}}} \tag{4}$$

Note that σ_{ft}^2 measures the variance of distances in the complex plane between each coefficient and the sample mean of the cloud of coefficients. Therefore, the T-variance statistic will provide evidence of changes in the EEG power spectrum, without taking into account changes due to the non-zero ERP. Currently, to test for changes in the power spectrum, one firstly needs to remove the

DOI: 10.1002/sim

effects due to the ERP mean. With this statistic, this is not necessary since the variance does not depend on the mean. Therefore, this test assesses the appearance of induced activity, which only produces changes in amplitude of the oscillations, without phase resetting and without change in the mean across trials. In the same way of the T-mean statistic, we are not concerned about the real distribution of this statistic since a free-distribution approach for assessing significance levels will be used (see section Local FDR). Importantly, we can note that it can present positive and negative values, offering the possibility of distinguishing between synchronization and desynchronization.

Statistics for the concentration of phases

Analyzing Figure 1(c), one can conclude that correlation between real and imaginary part of the wavelets coefficients is a good measure of the concentration of the cloud around a particular phase. However, it is easy to note that in the case of PPR, if phases reorganize around $0, \pi/2, \pi$ and $3\pi/2$, (i.e. along one of the axis in the complex plane) correlation values will be low. Moreover, since phase changes linearly with time for each frequency ($\varphi = 2\pi f t + \varphi_0$), this situation will certainly take place if the phase resetting period is long enough. Another reason for the non-suitability of pure correlation is that if there is a very small variability in amplitude, the coefficients can appear aligned along an axis not passing through the origin, thus not really reflecting phase concentration.

The idea of correlation can, however, be used in an orientation-free representation analyzing the alignment of the points in the complex plane. A possible way of doing this is by comparing the two eigenvalues $(\lambda^1_{ft}, \lambda^2_{ft})$ of the covariance matrix between real and imaginary parts of the L coefficients. A statistical measure of the similarity of these eigenvalues is given by $\psi_{ft} = (L - \frac{15}{6}) \log((\lambda^1_{ft} + \lambda^2_{ft})^2 / 4\lambda^1_{ft}\lambda^2_{ft})$ [25], which uses Bartlett's approximation and asymptotically distributes as a chi-square variate with 2 degrees of freedom. In this work, similarly to previous proposals, we will use a t-like statistics for comparing this measure in the whole time–frequency plane with its mean value in the pre-stimulus period. Let the mean and standard deviation of this measure in this period be defined as $\overline{\psi}^{\text{pre}}_f = (1/N) \sum_{t=t_1}^{t_N} \psi_{ft}$ and $\text{STD}^{\text{pre}}_{\psi_{ft}} = \sqrt{\sum_{t=t_1}^{t_N} (\psi_{ft} - \overline{\psi}^{\text{pre}}_f)^2 / (N-1)}$; then the statistic for the equality of eigenvalues of the (real *vs* imaginary part) covariance matrix (to be called T-eigenvalue statistic) is given by

$$T^{\psi}_{ft} = \sqrt{N-1} \frac{(\psi_{ft} - \overline{\psi}^{\text{pre}}_f)}{\text{STD}^{\text{pre}}_{\psi_{ft}}} \tag{5}$$

On the other hand, we can use the phases of the wavelet coefficients to look for a proper measure of its non-uniform circular distribution. As explained above, in the absence of a stimulus, the EEG is assumed to be composed of spontaneous brain rhythms. In this pre-stimulus period the wavelet coefficients for different trials of the experiment will have uniformly distributed phases (Figure 1(a)). A non-zero ERP after a stimulus can be caused by a shift of the whole cloud or a change of each coefficient's phase (Figures 1(b) and (c)). The simple Rayleigh test is not useful for differentiating between these two situations since the distribution of phases will depend on the position of the mean. However, a direct way of getting around this is translating the complex coefficients in order to have sample mean equal zero, i.e. removing the sample mean from each coefficient (Figure 2). In this situation, a test for the uniformity of phases seems to be appropriate for testing the presence of a preferred phase, but if this is the case, phases will show a bimodal distribution (Figure 2(b), bottom panel) and the usual Rayleigh test is not valid.

DOI: 10.1002/sim

Bimodal distributions of phases in which the two modes are roughly π radians apart have been studied and considered for developing appropriate statistical tools [22]. If $\overline{\varphi}_{ift}$ are the phases of wavelets coefficients after removing the sample mean, then, we can define $\varphi^*_{ift}=\overline{\varphi}_{ift}$ if $0<\overline{\varphi}_{ift}\leqslant\pi$; $\varphi^*_{ift}=\overline{\varphi}_{ift}-\pi$ if $\pi<\overline{\varphi}_{ift}\leqslant 2\pi$, which will have a unimodal distribution in the range $[0,\pi]$. In this case it is known that a proper test for uniformity is based on the second trigonometric moment given by $m_2(f,t)=(1/L)\sum_{i=1}^{L}\mathrm{e}^{\mathrm{j}2\varphi^*_{ift}}=R_{2ft}\mathrm{e}^{\mathrm{j}\theta_{2ft}}$ [22]. Here R_{2ft} and θ_{2ft} are the absolute value and the phase of m_2 for each time and frequency. The relation with the ITC can be easily seen if we express R_{2ft} as

$$R_{2ft}=\left|\frac{1}{L}\sum_{i=1}^{L}\mathrm{e}^{\mathrm{j}2\varphi^*_{ift}}\right| \tag{6}$$

This measure takes values between 0 and 1 and obviously, it does not depend on the non-zero sample mean, since this is removed before evaluating it. Also, note that $R_{2ft}(\varphi^*_{ift})=R_{2ft}(\overline{\varphi}_{ift})$, since $\mathrm{e}^{\mathrm{i}2\theta}=\mathrm{e}^{\mathrm{i}2(\theta-\pi)}$. Thus, in practice the transformation of the angles is not necessary and the measure can be evaluated directly in the phases of the wavelet coefficients after removing the non-zero sample mean.

If phases $\overline{\varphi}_{ift}$ are uniformly distributed, the distribution of R_{2ft} can be approximated as a chi square for large L. On the other hand, a more complicated distribution is found when assuming that phases follow a bimodal Von Mises-type distribution [22]. However, using the procedure described above we can evaluate this measure for each time point and frequency and compute a t-like statistics similar to those explained in the previous section. Defining the mean and the variance of R_{2ft} in the pre-stimulus period as $\overline{R}^{\mathrm{pre}}_{2f}=(1/N)\sum_{t=t_1}^{t_N}R_{2ft}$ and $\mathrm{STD}^{\mathrm{pre}}_{R_{2ft}}=\sqrt{\sum_{t=t_1}^{t_N}(R_{2ft}-\overline{R}^{\mathrm{pre}}_{2f})^2/(N-1)}$, respectively, a statistic for the uniformity of phase distribution (T-phase statistic) around the sample mean of the complex coefficients is proposed as

$$T^{R_2}_{ft}=\sqrt{N-1}\frac{(R_{2ft}-\overline{R}^{\mathrm{pre}}_{2f})}{\mathrm{STD}^{\mathrm{pre}}_{R_{2ft}}} \tag{7}$$

This statistic will be a measure of the deviance of uniformity of phases in the whole time range from the average uniformity of phases in the pre-stimulus period for each frequency.

Again, we do not need to derive the real distributions of statistics proposed to test the concentration of phases, since the local FDR will be used for simultaneously correcting multiplicity and finding the significance threshold. A summary of the t-like statistics for measuring the different event-related effects is given in Table I.

Local FDR

Assessing significant changes in mean, variance and phase concentration between pre- and post-stimuli wavelet coefficients through the use of t-like statistics produces a large number of false positives due to the multiple comparisons problem. A simple approach to dealing with it is the well-known Bonferroni correction, but this has been shown to be too conservative [26]. Another approach is the FDR procedure introduced by Benjamini and Hochberg in 1995 [27]. This method identifies, through the analysis of the histogram of individual p-values, which are the significant tests such that the expected value of the ratio of the number of false rejections to the total number of rejections is kept below a user-specified control value.

DOI: 10.1002/sim

Table I. Summary of the measures and *t*-like statistics proposed.

Measure	*t*-like statistics	Name in text	Distribution	Reference
$\mathrm{ITC}_{ft}=\left\lvert\frac{1}{L}\sum_{i=1}^{L}\frac{x_{ift}}{\lvert x_{ift}\rvert}\right\rvert$	$T^{\mathrm{ITC}}_{ft}=\sqrt{N-1}\frac{(\mathrm{ITC}_{ft}-\overline{\mathrm{ITC}}^{\mathrm{pre}}_{f})}{\mathrm{STD}^{\mathrm{pre}}_{\mathrm{ITC}_{ft}}}$	*T*-ITC	$\mathrm{ITC}\sim\chi^2$, for large L	[11, 22]
$\overline{x}_{ft}=\frac{1}{L}\sum_{i=1}^{L}x_{ift}$	$T^{\mu}_{ft}=\sqrt{L-1}\frac{\lvert\overline{x}_{ft}-\overline{x}^{\mathrm{pre}}_{f}\rvert}{\sqrt{\sigma^2_{ft}}}$	*T*-mean (Complex *t*-statistics)	$(T^{\mu}_{ft})^2\sim F_{2,2(L-1\ )}$	[24]
$\sigma^2_{ft}=\frac{1}{L-1}\sum_{i=1}^{L}\lvert x_{ift}-\overline{x}_{ft}\rvert^2$	$T^{\sigma}_{ft}=\sqrt{N-1}\frac{(\sigma^2_{ft}-\overline{\sigma}^{2\mathrm{pre}}_{f})}{\mathrm{STD}^{\mathrm{pre}}_{\sigma^2_{ft}}}$	*T*-variance	$\sigma^2_{ft}\sim\chi^2_{2(L-1)}$	[24, 25]
$\psi_{ft}=(L-\frac{15}{6})\log(f)$ $f=(\lambda^1_{ft}+\lambda^2_{ft})^2/4\lambda^1_{ft}\lambda^2_{ft}$	$T^{\psi}_{ft}=\sqrt{N-1}\frac{(\psi_{ft}-\overline{\psi}^{\mathrm{pre}}_{f})}{\mathrm{STD}^{\mathrm{pre}}_{\psi_{ft}}}$	*T*-eigenvalue	$\psi_{ft}\sim\chi^2_2$	[25]
$R_{2ft}=\left\lvert\frac{1}{L}\sum_{i=1}^{L}\left(\frac{(x_{ift}-\overline{x}_{ft})}{\lvert x_{ift}-\overline{x}_{ft}\rvert}\right)^2\right\rvert$	$T^{R_2}_{ft}=\sqrt{N-1}\frac{(R_{2ft}-\overline{R}^{\mathrm{pre}}_{2f})}{\mathrm{STD}^{\mathrm{pre}}_{R_{2ft}}}$	*T*-phase	$R_{2ft}\sim\chi^2$, for large L	[22]

Complex wavelet coefficients are represented by x_{ift}, with $i=1\ldots L$ trials. The null hypothesis H_0 in all cases is that the measure in each time–frequency point is equal to its average value in the pre-stimulus period of N time points. The latter is generically represented by $\overline{\langle\mathrm{measure}\rangle}^{\mathrm{pre}}_{f}$ and the standard deviation of each measure in the pre-stimulus period is denoted by $\mathrm{STD}^{\mathrm{pre}}_{\langle\mathrm{measure}\rangle}$. The symbol $|x|$ denotes the absolute value of a complex number x while λ^1_{ft} and λ^2_{ft} are the eigenvalues of the covariance matrix between real and imaginary parts of the wavelet coefficients. The theoretical distributions for the measures are given, assuming that the wavelet coefficients follow a complex normal distribution. Theoretical distributions of the *t*-like statistics are more difficult to derive; therefore, significant rejections of H_0 are assessed by using a distribution-free technique: local FDR.

In this paper we will use a third method, based on Bayesian statistics, developed by Efron [28], which is called 'local' FDR. In this approach, the histogram of the multiple tests is modeled as a mixture of an 'uninteresting distribution' (null hypothesis) and an 'interesting distribution' (alternative hypothesis), assuming the former to prevail in the data. The mixture and the uninteresting distribution are estimated with non-parametric methods, thus the higher the number of tests to be compared, the better the performance of local FDR is expected to be. In our case, the comparison is made among all time–frequency points defined by the wavelet transformation of the data; therefore, a high time–frequency resolution is better to obtain reliable results with the use of the local FDR technique. It is also very important to note that this is a distribution-free technique (unlike original FDR) since significant tests are found based on the empirical null distribution estimated from the histogram of multiple tests. Therefore, it is suitable for assessing significance when the real or theoretical distribution of the statistic is unknown, as is the case of the statistics proposed here. This approach was shown to be useful for assessing statistically significant brain functional connectivity with the use of multivariate autoregressive models [29]. Moreover, its lower computational cost makes it preferable over other approaches, such as bootstrapping, jacknife and permutation tests, which might also be useful in this kind of analysis.

With the local FDR, the user can specify a desired value for the probability of each test to belong to the null hypothesis (uninteresting distribution), which is the density of the FDR but cannot be interpreted as the actual fraction of false-positive tests in all selected significant time–frequency

DOI: 10.1002/sim

points. However, this density can be integrated in the selected tail region of the mixture distribution to obtain the q-value [26, 30] which is effectively an estimator of the actual false-positive proportion in the selected region. Moreover, from these densities a power diagnostic statistic can also be estimated [30]. Therefore, fixing the q-value, instead of the local FDR density, and reporting the power of the test are statistically sounder (and intuitive) in medical and psychological research, in the line of recent arguments on the misuse of null-hypothesis significance-testing procedures [31]. In the present study, we will require that $q=0.05$ in the analysis of both synthetic and real data. This means that we expect an average of 5 per cent of false positives in the set of significant time–frequency points if the experiment is repeated many times. Additionally we will report the estimated power for that experiment. We used the R code developed by Efron for the local FDR method, which is available from the CRAN website (http://cran.r-project.org/src/contrib/Descriptions/localFDR.html).

Data description

Synthetic data. In order to evaluate the performance of the newly proposed statistics, two sets of simulated data was prepared. The objective was to obtain real-like EEG oscillations in which the aforementioned event-related changes in the dynamics are present by construction. The two data sets were prepared as follows:

(1) *PPR case*: A total of 100 trials of alpha (10 Hz) and theta (6 Hz) rhythms were obtained as sinusoids in a pre-stimulus period of 400 ms, with a sampling rate of 200 Hz. The amplitudes of these oscillations were sampled from gaussian distributions with means $\mu^{\text{alpha}}_{\text{amp-pre}}=0$ and $\mu^{\text{theta}}_{\text{amp-pre}}=0$; and variances $\sigma^{2\text{alpha}}_{\text{amp-pre}}=1$ and $\sigma^{2\text{theta}}_{\text{amp-pre}}=0.1$. The phases of both oscillations were uniformly sampled in the interval $[0, 2\pi)$.

For the post-stimulus period (400 ms) the amplitude of the alpha rhythm was not changed but phases were resampled now from a gaussian distribution with mean $\mu^{\text{alpha}}_{\text{phase-post}}=\pi/3$ and variance $\sigma^{2\text{alpha}}_{\text{phase-post}}=\pi/16$. This simulates a reorganization of the phase (phase resetting) for the alpha rhythm after stimulus onset at 0 ms, which conveys the appearance of a non-zero mean ERP activity in the post-stimulus period without changing the amplitude of the alpha oscillation.

The phase of the theta rhythm was not changed and the amplitude was resampled from a gaussian distribution with $\mu^{\text{theta}}_{\text{amp-post}}=0$ and variance $\sigma^{2\text{theta}}_{\text{amp-post}}=1$. This implies a change (increase) in the amplitude without changing the mean activity and without phase reorganization, which implies the presence of induced activity in the theta rhythm. Figure 3 shows these EEG series, the mean power spectrum in the time–frequency plane and the cloud of wavelet coefficients for theta (6 Hz) and alpha (10 Hz) frequencies, at time points in the pre-stimulus (−200 ms) and in the post-stimulus (200 ms) periods.

(2) *Additive ERP case*: Again 100 trials of alpha (10 Hz) and theta (6 Hz) rhythms were obtained in a pre-stimulus period in the same way of previous simulation.

For the post-stimulus period neither the amplitude nor the phase of the alpha rhythm was changed. The mean ERP obtained from the previous simulation was added to each trial, therefore, the non-zero ERP in this case is exactly the same as the ERP of the PPR case, but they have different originating mechanisms. The theta rhythm was changed in the same way as the PPR case; hence, it also presents induced activity in this case. Figure 4 similarly shows these simulated EEG series, its mean power spectrum in the time–frequency plane and the cloud of wavelet coefficients

DOI: 10.1002/sim

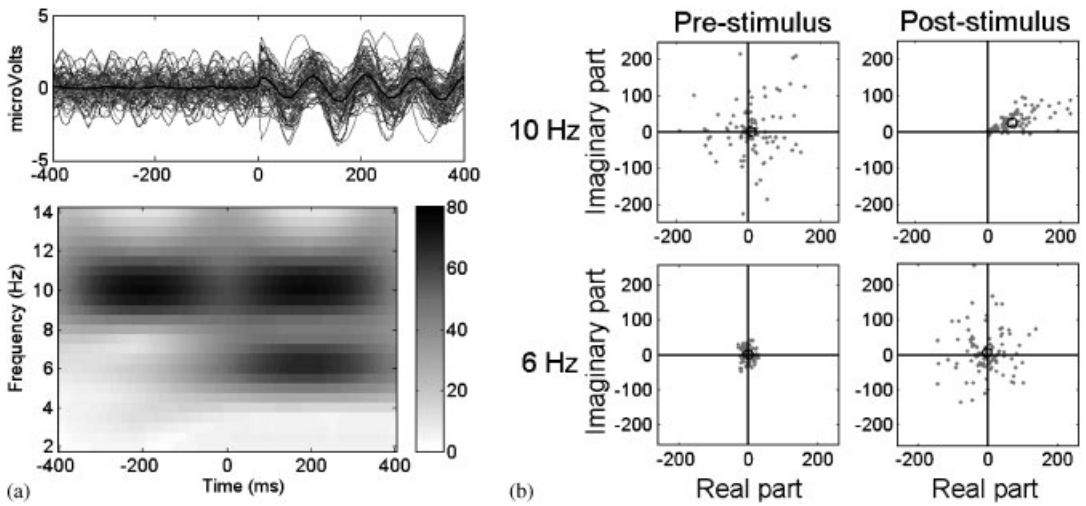

Figure 3. Simulation of a partial phase resetting effect at 10 Hz and induced activity at 6 Hz, after stimulus at 0 ms. (a) Upper panel: time series of the 100 trials. Oscillations (10 and 6 Hz) in the pre-stimulus period (−400 to 0 ms) have uniform distribution of phases and normal distribution of amplitudes. After stimulus, the 10 Hz oscillation reorganizes phases to have normal distribution, without changing the amplitudes, which provokes a non-zero mean activity (bold black line). Oscillations of 6 Hz keep the same distribution of phases but increase the variance of the normal distribution of amplitudes. Lower panel: Time–frequency plot of the mean power of the wavelet coefficients. Activity at 10 Hz has the same power in the pre- and post-stimulus periods, since the phase resetting effect does not imply changes in the power of the oscillations. The decrease around onset is a border effect of the time–frequency transformation procedure. At 6 Hz there is an increase in the power after stimulus, corresponding to the induced activity. (b) Clouds of wavelet coefficients in the complex plane for 10 Hz (phase reorganization) and 6 Hz (induced activity). For both cases, pre-stimulus corresponds to −200 ms and post-stimulus to 200 ms.

for theta (6 Hz) and alpha (10 Hz) frequencies, at time points in the pre-stimulus (−200 ms) and in the post-stimulus (200 ms) periods.

These simulations follow the ideas presented in [32] for obtaining data with the same ERP generated by different mechanisms, i.e. phase resetting or superimposed activity. In both cases, the rhythms were combined in each trial and little noise was added for a signal-to-noise ratio of 30. The MWT (with $z_0 = 7$) was applied to each trial of the noisy data in the frequency range from 2 to 14 Hz, with a step of 0.5 Hz. The complex coefficients obtained for each time point and frequency were subject to the subsequent analysis.

Real data. In order to evaluate the hypotheses studied with the simulated data, a set of real data was subject to the same analysis. We decided to use the sample data coming with the EEGLAB toolbox, since it is extensively studied in the EEGLAB tutorial (freely available online at http://www.sccn.ucsd.edu/eeglab/). These data correspond to a visual spatial attention experiment, where the event is the appearance of a green-colored square on the left side of the display. The subject had to attend the selected location on the computer screen and had to respond only when a square was presented at this location, and ignore circles when they were presented either at the attended location or at unattended locations. For more details about the experiment, see [33].

DOI: 10.1002/sim

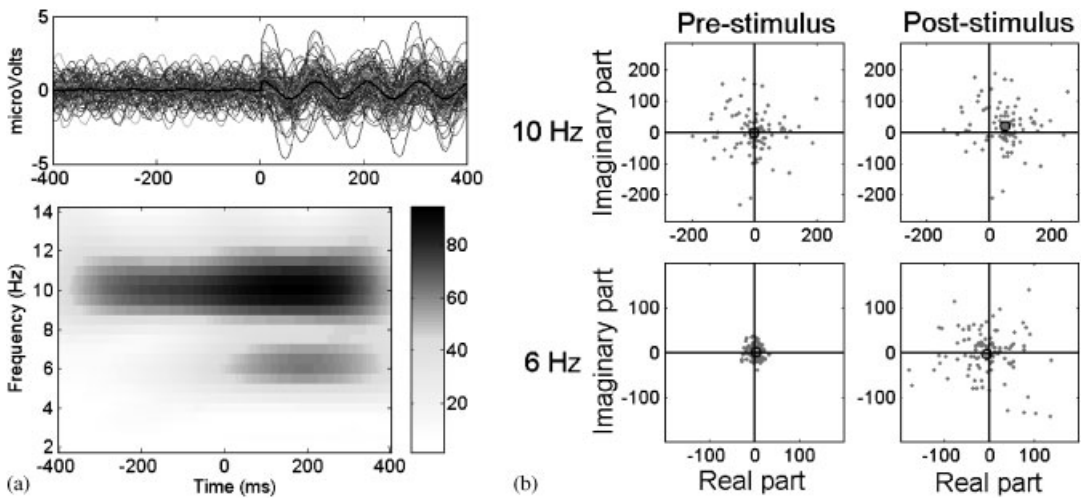

Figure 4. Simulation of an additive ERP time locked to the event and induced activity at 6 Hz. (a) Upper panel: time series of the 100 trials. Oscillations (10 and 6 Hz) in the pre-stimulus period (−400 to 0 ms) have uniform distribution of phases and normal distribution of amplitudes. After stimulus, the variance of the normal distribution of amplitudes of the 6 Hz oscillation is increased and the same ERP mean found for the PPR case (oscillating at 10 Hz) was added to the oscillatory background activity (bold black line). Lower panel: time–frequency plot of the mean power of the wavelet coefficients. Activity at 10 Hz increases in the post-stimulus period due to the presence of an additive ERP. At 6 Hz there is an increase in the power after stimulus, corresponding to the induced activity. (b) Clouds of wavelet coefficients in the complex plane for 10 Hz (additive ERP) and 6 Hz (induced activity). For both cases, pre-stimulus corresponds to −200 ms and post-stimulus to 200 ms.

A total of 80 epochs (trials) of 3 s for a single subject were used for the analysis, corresponding to presentation of a target square in the attended location followed by a button response. For the purpose of presentation of results, we chose the electrode 27 (POz) following the EEGLAB tutorial because this is the channel with highest alpha band power (around 10 Hz). For these data the analysis was carried out in the frequency range from 2 to 20 Hz, with a step of 0.5 Hz.

RESULTS

Synthetic data

Testing for the mean and variance of the time–frequency coefficients. The tests for the mean and variance of the cloud of complex coefficients were performed for both PPR and additive ERP cases. For a visual inspection of the distribution of wavelet coefficients in the complex plane—for the frequencies of interest 6 and 10 Hz—we chose two time instants, one belonging to the pre-stimulus period (−200 ms) and the other to the post-stimulus period (200 ms). Figure 3(b) shows the clear phase reorganization for the PPR case at 10 Hz, which also implies that the mean of the coefficients is not zero. On the other hand, for the additive ERP case, Figure 4(b) shows the same 'spread' distribution of coefficients at 10 Hz for pre- and post-stimuli, but in the latter they are

DOI: 10.1002/sim

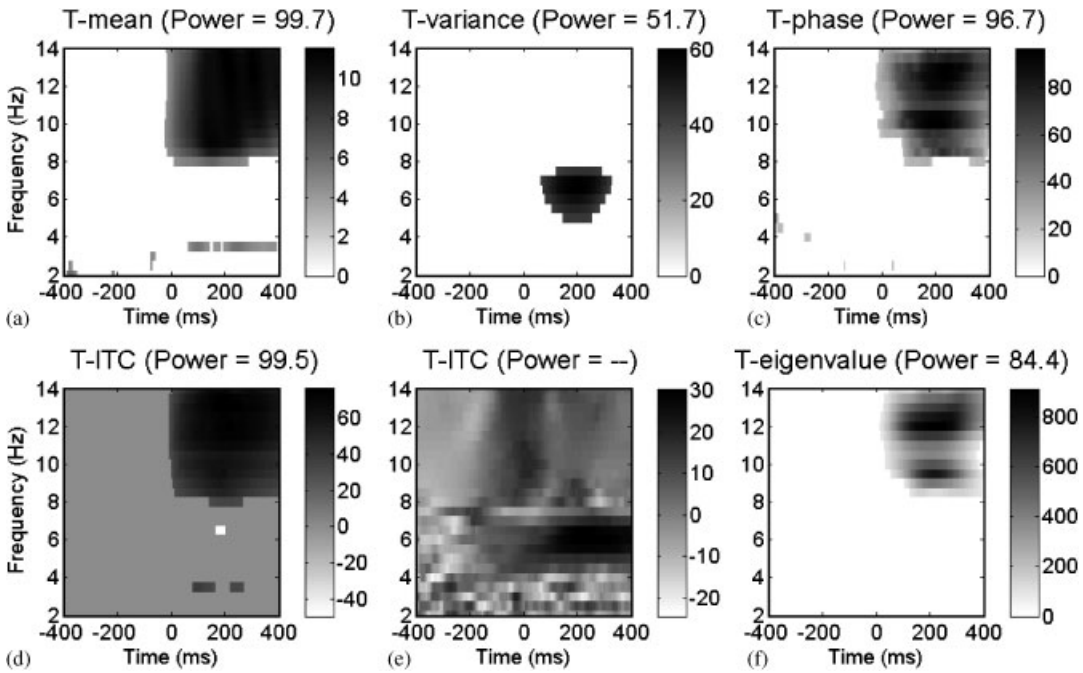

Figure 5. Time–frequency plots of statistics on the cloud of wavelet coefficients for the PPR case (synthetic data). (a) T-mean statistic (equation (3)); (b) T-variance statistic (equation (4)); (c) T-phase statistic (equation (7)); (d) T-ITC (equation (2)) and (f) T-eigenvalue (equation (5)). Only significant values are plotted as assessed by local FDR, requiring a 5 per cent of false-positive results ($q=0.05$). The power of each test is reported. Note that although T-variance, T-phase and T-eigenvalue statistics can take positive and negative values, the colorbar shows only the positive part since there were no significant negative values. (e) T-ITC computed from the data after removing the mean ERP from each single trial. This is not thresholded, since there was no significant point at the level of $q=0.05$. For these data the T-mean statistic was also not significant at any time–frequency point (not shown) and the other three statistics did not change, since they do not depend on the mean activity.

moved out of the zero mean. As expected, the cloud of wavelet coefficients at 6 Hz in both cases are not moved out of the origin after stimulus, but its variance is clearly increased.

Figures 5 and 6 (panels (a) and (b)) show the plots of the statistics T^{μ}_{ft} and T^{σ}_{ft} in the time–frequency plane for PPR and additive ERP cases, respectively. The plots only show significant values as assessed by the local FDR method. As expected, both cases present significant non-zero mean around 10 Hz after stimulus. Owing to the smaller variance of the cloud of coefficients in the PPR case (established by the simulated strong phase resetting effect) the corresponding T-mean statistic presents higher values than in the case of additive ERP in the post-stimulus time–frequency range. On the other hand, significant changes in the variance appear around 6 Hz in both cases, showing the presence of induced theta activity.

Testing for phase concentration of the time–frequency coefficients. Panels (c) and (f) of Figure 5 show plots of the statistics $T^{R_2}_{ft}$ and T^{ψ}_{ft}, respectively, for the PPR simulated case. Significant values are found by local FDR in the post-stimulus period in the range of frequencies of 10 ± 2 Hz.

DOI: 10.1002/sim

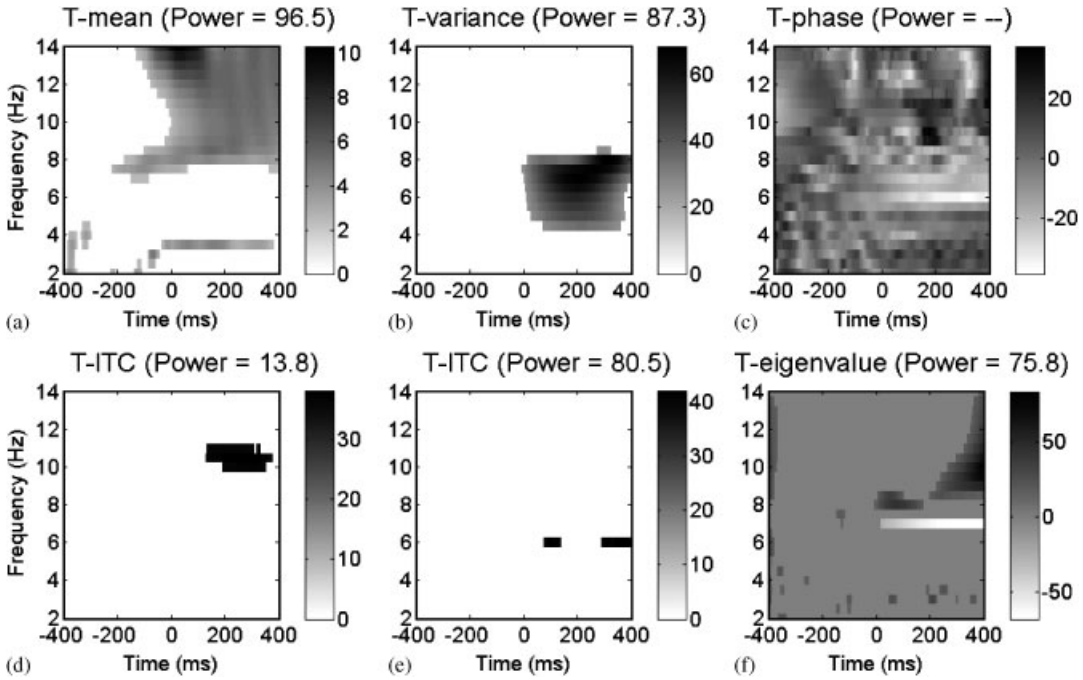

Figure 6. Time-frequency plots of statistics on the cloud of wavelet coefficients for the additive ERP case (synthetic data). (a) T-mean statistic (equation (3)); (b) T-variance statistic (equation (4)); (c) T-phase statistic (equation (7)); (d) T-ITC (equation (2)) and (f) T-eigenvalue (equation (5)). Only significant values are plotted as assessed by local FDR, requiring a 5 per cent of false-positive results ($q=0.05$), except in the case of the T-phase which showed no significant points even at the level of $q=0.1$. The power of each test is reported. Note that although T-variance can take positive and negative values, the colorbar shows only the positive part since there were no significant negative values. (e) T-ITC computed from the data after removing the mean ERP from each single trial. For these data, the T-mean statistic was not significant at any time–frequency point at the level of $q=0.05$ (not shown) and the other three statistics did not change, since they do not depend on the mean activity.

Figure 6(c) and (f) shows these statistics for the case of a simulated additive ERP. Contrary to the PPR case, there was no significant value of $T_{ft}^{R_2}$ in the whole time–frequency plane as assessed by local FDR, clearly indicating that there is no significant difference between distribution of phases around the mean in the pre- and post-stimulus periods. The T-eigenvalue statistic, in turn, shows some significant positive values around 10 Hz (but at very late latencies) and negative values in the post-stimulus at 7 Hz, which can be due to border effects of the wavelet transformation. Note that in none of the cases, the simulated induced activity at 6 Hz shows significant differences between pre- and post-stimuli regarding phase concentration as expected by construction. Figures 5 and 6 also show the T-ITC measure in the whole time–frequency plane (panel (d)), which shows significant values around 10 Hz in the post-stimulus period for both the PPR and the additive ERP case.

As discussed in the Methods, translating the cloud of complex coefficients to have the sample mean at the origin does not change the configuration of points around the mean; hence, the preference for a particular phase is not destroyed if it exists. Having this in mind, we decided

DOI: 10.1002/sim

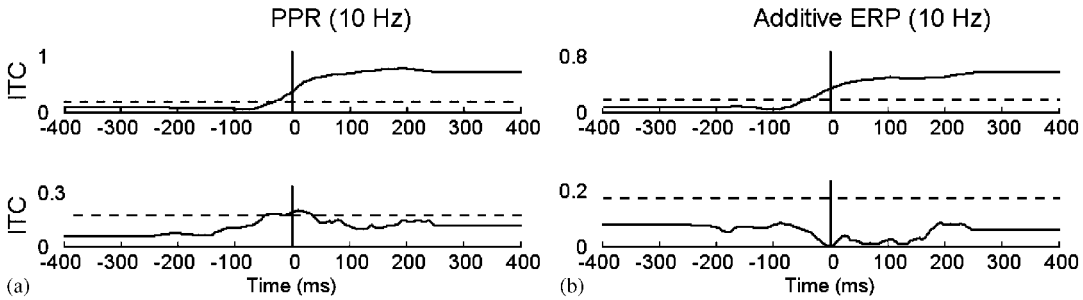

Figure 7. Intertrial coherence (ITC) computed by EEGLAB 4.51 at 10 Hz for the PPR (a) and additive ERP (b) cases (synthetic data). In both cases the bottom plot corresponds to the same data after removing the mean activity from each single trial. Dashed lines represent the 0.05 significance level. ITC shows significant values for both cases and looses significance when the mean is removed, although the partial phase resetting remains. Only in a very small time window just after the onset the ITC at 10 Hz shows significant values for the PPR case.

to explore the suitability of ITC as a measure of uniformity of phases, using the same data after subtracting the mean activity from each single trial. Figures 5 and 6 (panel (e)) show the corresponding plots of T-ITC for the zero-mean data. Figure 7 shows the ITC computed by EEGLAB at 10 Hz for both simulated data, before and after removing the mean activity. The threshold found for a p-value of 0.05 is shown with dashed lines.

It is evident that ITC drops sharply in the whole time–frequency plane in both cases. However, in the PPR case (where the phase resetting effect still holds), a small time window after the onset shows slightly significant values around 10 Hz (Figure 7(a), bottom panel)). This seems to be associated with the phase reorganization that occurred at 0 ms, but it is not consistent in the whole post-stimulus period where, by construction, the same phase concentration remains for all time instants. Similarly, as expected, the T-mean statistic does not show any significant value in the whole time–frequency plane when applied to the mean-removed data in both simulated cases. On the contrary, the T-variance, the T-phase and the T-eigenvalue statistics computed for the mean-removed data were exactly the same as shown in Figures 5 and 6, since they do not depend on the mean ERP activity.

Real data

Assessing the presence of a strictly phase-locked mean activity and induced activity. Figure 8(a) shows the time–frequency plot of the T-mean statistic given by equation (3). This statistic is significantly different from zero mainly in the post-stimulus period, in a range of frequencies from 2 to 15 Hz, assessing the presence of a mean ERP strictly phase-locked to events. There is one component showing significant non-zero mean around 10 Hz which peaks around 300 ms and another non-zero mean activity wider in time at frequencies lower than 6 Hz.

Figure 8(b) on the other hand, shows the time–frequency plot of the T-variance statistic given by equation (4). The presence of induced activity is assessed around 10 Hz, a second after the event. This appears as an increase in the variance of the wavelet coefficients which can be interpreted as synchronization of the activity at 10 Hz. Also, some traces of earlier desynchronization (decrease in the post-stimulus variance with respect to the pre-stimulus variance) can be seen at lower frequencies. Both plots were thresholded by using local FDR with 5 per cent of false-positive

DOI: 10.1002/sim

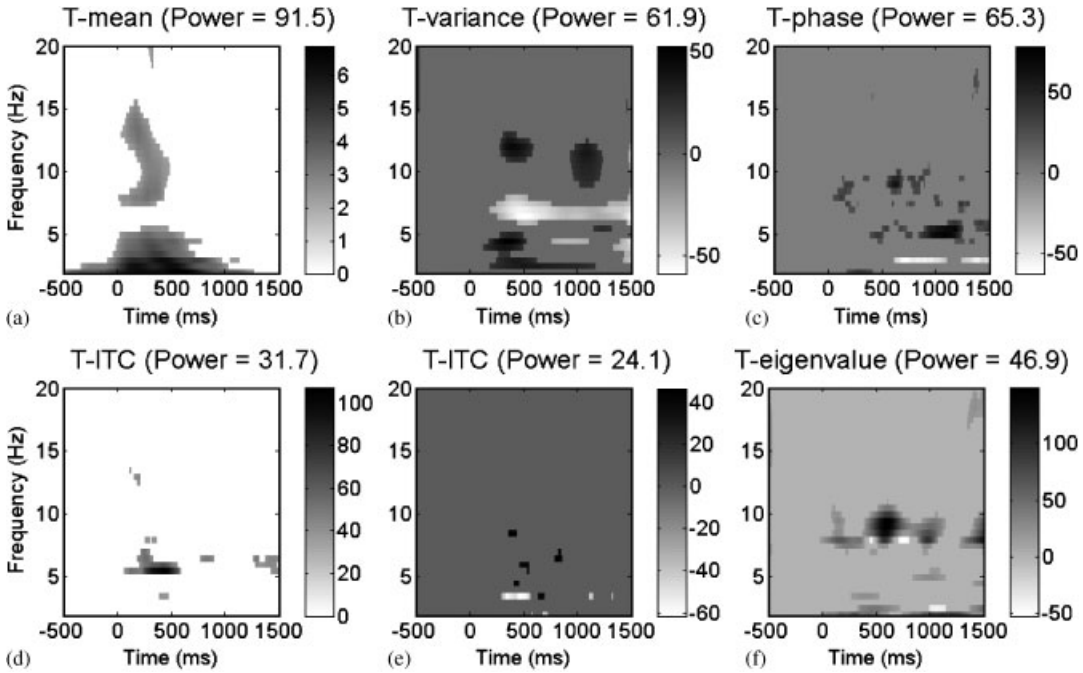

Figure 8. Time–frequency plots of statistics on the cloud of wavelet coefficients for the EEGLAB sample data set. (a) T-mean statistic (equation (3)); (b) T-variance statistic (equation (4)); (c) T-phase statistic (equation (7)); (d) T-ITC (equation (2)) and (f) T-eigenvalue (equation (5). Only significant values are plotted as assessed by local FDR, requiring a 5 per cent of false-positive results ($q=0.05$). The power of each test is reported. (e) T-ITC computed from the data after removing the mean ERP from each single trial. For these data, the T-mean statistic was not significant at any time–frequency point at the level of $q=0.05$ (not shown) and the other three statistics did not change, since they do not depend on the mean activity.

results. Since we are not interested in the neurophysiologic interpretation we decided to analyze a small frequency range; therefore, it is obvious that we cannot tell anything about induced activity at higher frequencies (gamma band) which is currently of particular interest in this kind of experiments.

Assessing the presence of concentration of phases. Figure 8(c) shows the time–frequency plot of the T-phase statistic (equation (7)), thresholded by local FDR in order to give a 5 per cent of false positives. Several spots appear in the whole time–frequency plane, although none of them can be related with the studied changes due to the stimulus [33]. However, it is interesting to see positive values around 600 ms (9 Hz), 1000 ms (5 Hz) and also negative values in low frequencies (from 500 ms) which means that phases of oscillations at that frequency are more uniformly distributed in post-stimulus than in the pre-stimulus period. In panel (f) of Figure 8, the T-eigenvalue for these data is shown. It is also difficult to associate the spots to the event in study, although it shows also a main significant positive change around 500–600 ms at 9 Hz.

On the other hand, Figure 8(d) shows the time–frequency plot of the T-ITC for the real data, which has only a few significant positive changes around 5 Hz and 300–400 ms, which is more

DOI: 10.1002/sim

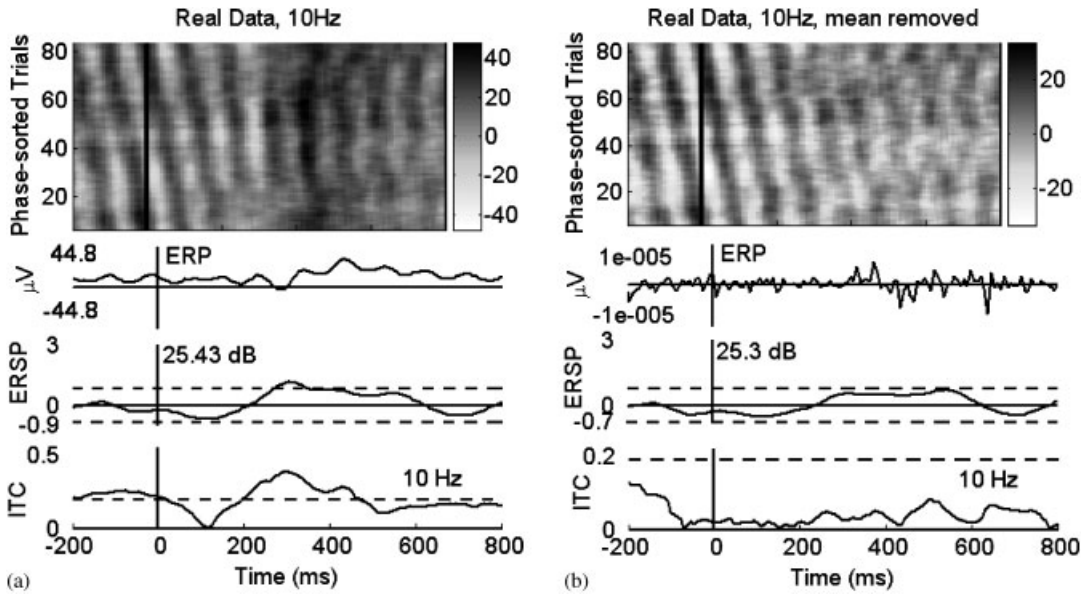

Figure 9. (a) ERP image obtained with EEGLAB 4.51 for the real data and (b) for the same data after removing the mean post-stimulus ERP from each single trial. All magnitudes represented were found at 10 Hz. From top to bottom: phase-sorted trials, ERP mean activity in microVolts, ERSP (mean change in the spectral power from pre-stimulus activity) and intertrial coherence. In the two last plots, the dashed lines represent 0.05 significance levels. Vertical lines correspond to onset.

consistent with the plot of the T-mean statistic as in the analysis of simulated data. Following the same idea, we computed this statistic after removing the mean ERP from each single trial and showed it in panel (e) of Figure 8. EEGLAB 4.51 was also used for computing the mean ERP, the ITC and the mean change in spectral power from baseline (ERSP) at 10 Hz, in the range from -200 to 800 ms for normal real data and for the data after removing the average ERP from each single trial. Results are shown in Figure 9, together with a plot of trials, sorted by phase at 10 Hz (typical *erp image* of EEGLAB, [23]). Figure 9(a) shows significant increments of ITC around 300 ms, corresponding to the N300 ERP component and with a small increment in ERSP, which would be interpreted as a PPR [12, 33]. However, Figure 9(b) shows that when the mean activity is removed, the significant increase in the ITC disappears completely. Note that the scale of ERP is greatly different; since, the activity after subtracting the mean is almost inexistent (noise).

DISCUSSION

Simulated data analysis

Testing for the mean ERP and induced activity. In order to assess the presence of a non-zero mean ERP activity, it is straightforward to test for the mean of the cloud of time–frequency coefficients in the complex plane. The T-mean statistic proposed here is the absolute value of the difference between the mean of the wavelet coefficients for each time–frequency point and their average

DOI: 10.1002/sim

values in the pre-stimulus period. It was shown that this statistic is a good measure of the presence of the mean as assessed with the use of simulated data (Figures 5(a) and 6(a)). As expected, there was no time–frequency point giving significant non-zero mean after removing the mean ERP from each single trial in both simulated cases. The power of the test was above 90 per cent in all cases, which gives evidence on the suitability of this test for the aforementioned purpose.

However, one limitation of this statistic is that it cannot be used to distinguish the originating mechanism of the ERP activity, since it gave similar results for the case in which ERP was due to a phase resetting and for the case in which the ERP was added to the unchanged ongoing EEG. Another limitation is that it cannot tell anything about the position of the mean in the complex plane, i.e. it does not have information about the phase of the mean activity, just about its absolute value. Finally, in the analysis of the synthetic data this statistic showed significant changes in the mean in a relatively wide range of frequencies (8–14 Hz), while the mean is known to be only at 10 Hz. This might be a consequence of the use of small frequency range for wavelet transformation and a poor frequency resolution. Further studies on this subject should be carried out for testing its ability to show correctly the time–frequency content of the mean ERP.

On the other hand, the T-variance statistic showed to be useful for assessing the presence of induced activity (Figures 5(b) and 6(b)). It found correctly the simulated induced activity independently of the generating mechanism of the mean ERP in another frequency band. This statistic seems to be more sensitive (than the T-mean statistic) in the time–frequency localization of the induced activity, although usual effects of the poor frequency resolution were also observed (Figures 5(b) and 6(b)) and the power of the test was lower.

This real statistic allows for a comparison of the variance of the complex coefficients in each time–frequency point with the average variance in the pre-stimulus period. Then it gives information about increases and decreases in the variance of the wavelet coefficients, which are related to synchronization and desynchronization of the EEG oscillations, respectively. Moreover, it does not depend on the presence of a non-zero mean activity, thus giving the same picture when applied to the mean-removed simulated data.

It has been recently argued that evoked and induced responses are more related than was thought and that a mixture of mechanisms could be generating them [34]. However, even when in this sense we did not simulate suitable data, e.g. in which induced and evoked activities appear in the same frequency bands, we have proved the presence of both types of activities through unequivocal statistical measures. The simulations used in this work were focused on differentiating between two different originating mechanisms of the mean ERP activity. For a closer study of the performance and properties of the proposed test for the variance, other kinds of simulations involving several situations of synchronization and desynchronization should be analyzed. In particular, it could be possible to find changes in the variance of the cloud of points when clear phase reorganization appears after stimulus. These changes will not be due to induced activity and might be reflected as significant by the proposed statistic for the variance. Our analysis of simulated data did not give evidence of such an effect, as can be seen in Figures 5(b) and 6(b), where there are no significant changes in the variance at 10 Hz. However, as stated above, more complex (real-like) situations, in which PPR and induced activity coexist perhaps in the same frequency band, should be studied.

ITC does not measure phase resetting. ITC was computed for both simulated cases, showing that it is not an adequate measure of phase resetting. ITC was quite similar to the T-mean statistic in the whole time–frequency plane in both simulated cases (compare Figures 10(a) with 5(a) and 10(b) with 6(a)), where the T-ITC statistic also showed significant values at 10 Hz, which implies

DOI: 10.1002/sim

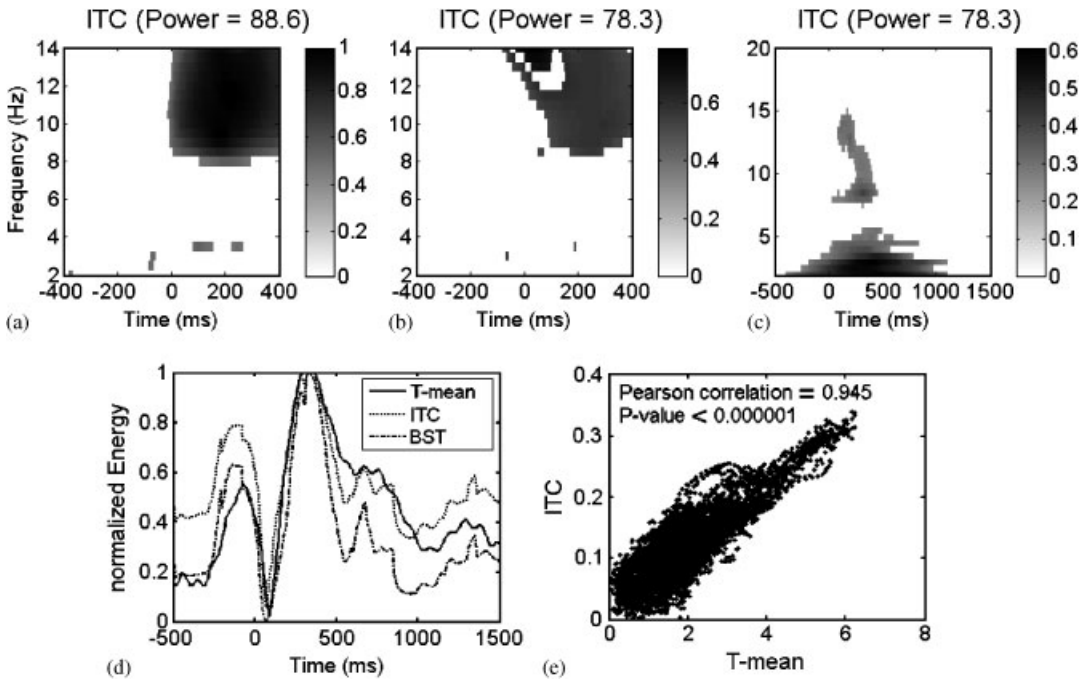

Figure 10. Time–frequency plot of ITC computed for the simulated PPR (a) and additive ERP (b) cases, as well as for the real data (c). Only significant values are plotted as assessed by local FDR, requiring a 5 per cent of false-positive results ($q=0.05$). The power of each test is reported. (d) Normalized plots of the time series at 10 Hz. *T*-mean statistic and ITC are represented as solid and dotted lines, respectively. The statistic of the bivariate sign test (BST) for the complex coefficients is also shown (dot-dashed line) for illustrative purposes. (e) *T*-mean statistic *vs* ITC for all frequencies and time points. There is a statistically significant ($p<10^{-6}$) linear correlation of 0.945.

that it cannot distinguish if the ERP is due to a phase resetting or a superimposed activity. This is also supported by the results obtained in the analysis of the simulated data after removing the mean ERP. It is clear that this procedure takes the cloud of wavelet coefficients to have zero mean without changing the spatial distribution in the complex plane. Hence, a preferred phase of the complex coefficients is preserved in the case of phase resetting. However, after removing the mean ERP the significant post-stimulus increases in the T-ITC and ITC at 10 Hz disappeared (Figures 5(e) and 7(a)). Moreover, the T-ITC statistic around 6 Hz (induced activity) did not show a significant increase in the post-stimulus period for any of the simulated cases (Figures 5(d) and 6(d)). Besides, in the case of the additive ERP, when the mean was removed, a significant change in ITC appeared at 6 Hz, which means that changes in the amplitudes of the wavelet coefficients can also affect the ITC measure, making it even more inappropriate for the study of ERBD changes. The results presented here are in concordance with the study of Yeung and colleagues [16], in which they test a set of currently used methods, including evaluation of ITC, for assessing the presence of PPR as the mechanism originating ERP peaks. Using simulated and empirically derived ERP peaks, they showed that none of these methods could effectively disambiguate competing views of ERP generation.

DOI: 10.1002/sim

Additionally, we have seen in our study that ITC closely resembles our statistic for the mean activity. Figure 10, panels (a)–(c), present the ITC time–frequency plots, thresholded by local FDR to show only 5 per cent of false positives, which closely resembles the corresponding plots of the T-mean (Figures 5(a), 6(a) and 8(a)). Also, Figure 10(d) shows normalized plots of the T-mean statistic and ITC for wavelets coefficients of the real data at 10 Hz. For illustrative purposes, the normalized plot of the bivariate sign test BST statistic [35] is also shown, which is done in the complex plane for testing the location of the distribution of points.

An analysis of the correlations between ITC and the proposed T-mean statistic was also performed using all values of both magnitudes for all frequencies and time points. The scatter plot of ITC *vs* T-mean statistic is shown in Figure 10(e). Correlations between these two measures were significant for all frequencies between 2 and 20 Hz, stating the equivalence between ITC and this statistic (Pearson correlation $= 0.945$, p-value $= 0.000001$). ITC was even more similar to a BST for the mean of the cloud of wavelet coefficients at 10 Hz (Figure 10(a)) and was also significantly correlated to BST for all frequencies. Correlation values between ITC and BST (not shown) were higher than those obtained in the correlation between ITC and the T-mean statistic, which supports the conclusion that ITC might be actually a version of a multivariate sign test for the location of the center of the distribution of wavelet coefficients in the complex plane.

Testing for phase resetting. Much attention has been dedicated in the past few years to the study of the phase resetting effect as a possible originating mechanism of different known ERPs, especially in the alpha band [3, 36–40]. Contradictory results are found mainly due to the use of different measures for assessing the presence of phase resetting. These measures depend strongly on the underlying theoretical assumptions on the nature of EEG and MEG ongoing oscillations and our work cannot completely avoid this pitfall. However, some criteria seem to have wide acceptance as necessary conditions for the presence of this effect as a generating mechanism for the ERP. Among these criteria are (i) the presence of ongoing oscillations in the data (something that can be phase reset), (ii) the presence of a 'realistic-looking' ERP (something originated by this phase resetting), (iii) no increase in the post-stimulus power (phase resetting of an oscillation does not change the amplitude) and (iv) common sources of the pre- and post-stimulus activities (the same neuronal mass is producing the oscillations that are phase reset). It should be said that the last two points are more difficult to assess since induced activity can appear in the same frequency and the sources depend on the reliability of the method used and the extraction of the correct activity.

The main problem then is to find a sufficient condition for phase resetting. The more direct ideas followed have been to look for the presence of phase locking in the post-stimulus with respect to the pre-stimulus. Previous works have used the phase-locking factor or ITC and similar measures [12, 37, 41, 42], the entropy [43, 44], the circular variance [45] and measures of linear standard deviations of the amplitude of the EEG trials [3, 36, 39]. However, there is no complete consensus as to which is the correct measure for phase concentration [16, 38, 40]. This work supports these critics as discussed in the previous subsection. In addition, a main contribution of this work is to present the idea that the presence of phase locking should persist if the non-zero mean (ERP) is removed from each single trial. This helps one to avoid the influence of the mean ERP itself on the estimation of its generating mechanism. In this paper, on the basis of the distribution of the cloud of complex coefficients after removing the mean, we followed two ideas for measuring phase locking for each time and frequency: (i) the measurement of the alignment of the points along a phase through the eigenvalues of the covariance matrix of real and imaginary parts and (ii) the use of the second trigonometric moment, which accounts for the bimodality of the

DOI: 10.1002/sim

distribution of the phases (if there exists a preferred phase) that appears after removing the non-zero mean.

Nevertheless, a question can still be raised if an estimated change in phase locking at a particular time and frequency with respect to a pre-stimulus status is actually related to an ordered, event-related phase transient. We believe that, given the complexity of the real EEG signals and the possibility of different kinds of changes occurring in the same time–frequency window, only the use of adequate models of the EEG signal, together with proper measures of the phase evolution in time, can lead to a definite solution to this problem. Some studies on the evolution of phases have been proposed, with particular interest in the use of the instantaneous frequency [46]. However, more work is needed for validating its usefulness in the analysis of real (noisy) data. On the other hand, besides some attempts [34], models containing explicitly the components that characterize phase reset, additive, induced and other activities separately are still unexplored.

In this study, we used the two measures in the form of t-like statistics for assessing the presence of phase locking in the whole time–frequency plane for simulated scenarios. Both statistics could correctly assess the presence of phase resetting around 10 Hz in the corresponding synthetic data (Figure 5(c) and (f)) and not in the simulated additive ERP case (Figure 5(c) and (f)), although the T-eigenvalue was shown to be affected by border effects of the wavelet transformation. In the same sense, the T-phase always showed more powerful tests than the T-eigenvalue; thus, we can conclude that it is a more robust measure for the study of phase resetting. These statistics do not depend on the mean ERP activity. However, they do depend on how well the phases of the wavelet coefficients are estimated, which can affect their sensitivity and time–frequency resolution. Future work should be devoted to studying the dependence of these measures on these properties in real EEG data.

Real data analysis

Testing for the mean ERP and induced activity. In the analysis of the sample data accompanying EEGLAB 4.51, which corresponds to a visual spatial attention experiment, the T-mean statistic showed a significant non-zero activity around 10 Hz and at lower frequencies (Figure 8(a)). The former appears as a short ERP mean, peaking at approximately 300 ms, which corresponds to that reported as an N300 in the analysis of this data in the EEGLAB tutorial. On the other hand, slower activity appears in longer periods, even before the stimulus onset. These long increases in the mean could be related to artifacts or to the poor time resolution of the wavelet procedure at low frequencies.

As concluded from the analysis of synthetic data, in this case, we cannot say anything about the nature of the origin of the mean activity at 10 Hz. However, a visual comparison between two distributions of the cloud of wavelet coefficients at 10 Hz, one corresponding to 400 ms before stimulus and the other to 300 ms after onset (i.e. near the peak of the evoked potential), shows a clear move out the zero mean, but the distribution of angles does not seem to be non-uniform in both cases. This could be understood as light evidence supporting the additive ERP hypothesis, but might also fit into what is called 'PPR' [12, 19]. Therefore, we would like to stress that a proper statistical measure of the phase resetting effect should be evaluated for rising conclusions on this question. This point will be discussed in the next subsection.

The use of the T-variance statistic is shown in Figure 8(b). It is interesting to note that there are several significant changes in the time–frequency plane. Synchronizations appear in two separate spots around 12 Hz and in the 3–5 Hz range, at 400–500 ms and lately around 11 Hz at 1.1 s after

DOI: 10.1002/sim

onset. Desynchronization also starts in the latencies after the ERP peak, at 400 ms around 7 Hz and extends to the whole window of 1.5 s after stimulus onset. It is not the purpose of this paper to study the neurophysiologic interpretation of such activities in this kind of experiment. As we already mentioned, they have received the name of induced activity due to the fact that it is not evoked directly by the stimulus but induced probably through nonlinear effects and by autonomous mechanisms, such as changes in the activity of local interactions between main neurons and interneurons that control the frequency components of the ongoing EEG [20, 34].

Testing for phase resetting. In Figure 9(a) it can be seen that the ITC computed by EEGLAB shows a significant increase from 200 to 450 ms after onset, peaking at around 300 ms in correspondence with the N300 peak of the ERP. This increase is also accompanied by a significant increase ($p<0.05$) in ERSP in a very small time window around 300 ms. It is important to note that this same case is presented in the EEGLAB tutorial, in which the increase in ERSP is not significant since they asked for a p-value lower than 0.01. Increases in ITC accompanied by no changes in the ERSP are usually interpreted as a presence of phase reorganization causing the appearance of the mean ERP [12]. In this case, however, the increase in ERSP is not clearly negligible, hence, it can be argued that ERP could arise from PPR that could be combined with a stimulus-locked increase in ERSP. This interpretation is wrong if the ITC measure does not provide statistically reliable evidence of the phase reorganization effect, as was claimed by Yeung *et al*. [16] and was demonstrated by our analysis of synthetic data.

In addition, ITC has been proposed to be a measure of phase resetting which is independent of the existence of a strictly phase-locked ERP activity and of ongoing EEG oscillations. If this is true, this measure should not be affected by removal of the mean ERP since—as proved in the analysis of simulated data—this procedure does not destroy the phase reorganization. However, significant increases in ITC and ERSP at 10 Hz disappeared in the analysis of the real data, after removing the mean ERP from each single trial (Figure 9(b)). It is also to be noted that the supposed reorganization of phases, shown by the plot of phase-sorted trials (top of Figure 9(a)) around 300 ms, disappeared when the mean ERP was removed (top of Figure 9(b)). This can be explained by the fact that a phase-locked superimposed ERP will effectively appear in this kind of plots as a vertical band even when there is no reorganization of the phases. In this sense, plots based on sorting trials according to phase or any other parameter do not provide statistical evidence of the presence of any of the aforementioned effects that one can face in the ERBD.

The statistics proposed here for measuring changes in the distribution of phases showed small areas in the time–frequency plane with significant changes in the distribution of phases with regard to that of the pre-stimulus (Figures 8(c) and (f)). The main positive changes appear around 9 Hz at 500 ms, and around 5 Hz, at 1000 ms. They seem difficult to be related to the event in study, hence, we could conclude that these data do not provide evidence on the possibility that a phase resetting effect is causing the mean ERP observed for visual attention.

CONCLUSIONS

The goal of this paper has been twofold. Firstly, we have provided further evidence on the inappropriateness of the ITC as a measure of the presence of a phase resetting effect in the generation of an ERP. With simulations, we showed that ITC does not offer unambiguous evidence on whether the ERP is generated by an additive effect or a PPR. Moreover, we showed that ITC

DOI: 10.1002/sim

is probably just an indirect measure of the presence of a non-zero mean activity, since it usually disappears when the analysis is done in zero-mean data, independently of the uniformity of the distribution of phases.

Secondly, we have proposed measures for assessing the different kinds of event-related changes in the brain dynamics with respect to the pre-stimulus activity: the mean ERP, the induced activity and the concentration (or distribution) of the phases of the oscillations. These measures are based on using the whole information given by the complex wavelet coefficients that represent the data in the time–frequency space and not only on their absolute values as in current practice [2, 8–11]. We found that the statistics for the mean and the variance of the complex coefficients are proper measures of the presence of a non-zero mean activity and induced activity, respectively. The latter can even distinguish between synchronization and desynchronization. On the other hand, we proposed two different ways of looking for a phase resetting effect. The first one is based on measuring the alignment of the coefficients in the complex plane and the other on measuring the non-uniformity of the distribution of phases after removing the mean, but taking into account the bimodal character of this distribution. Both statistics were shown to give unambiguous evidence of the presence of phase locking, although in our study, the second one turned out to give more reasonable and robust results, always showing more powerful statistical tests. These results suggest that these statistics constitute promising tools in the analysis of ERBD. The Matlab code for preparing the simulations as well as the measures used in this work can be obtained upon request to the authors.

Recently, a series of experimental studies in animals and humans have been supporting the presence of the three types of activities (evoked, PPR and induced) in different states of cognitive processes even at a higher level of analysis [47, 48]. Thus, in our point of view, a wider vision of the problem of the generation of ERP activity should be assumed, in which both mechanisms can be possible and even they can have different degrees of interaction in the formation of the ERBD. The methodological tools being used nowadays for the analysis of ERBD might not be a complete toolbox for studying the underlying processes. However, researches in the field of statistics together with a correct modeling of its dynamics seem to be the correct approach to the successful analysis of these data.

ACKNOWLEDGEMENTS

The authors would like to thank two anonymous reviewers for their comments, which contributed largely to the better presentation of the ideas and results of this article.

REFERENCES

1. Niedermeyer E, Lopes da silva FH. *Electroencephalography*: *Basic Principles*, *Clinical Applications and Related Fields*. Urban and Schwarzengreg: Baltimore, MD, 1999.
2. Tallon-Baudry C, Bertrand O, Delpuech C, Pernier J. Oscillatory gamma-band (30–70 Hz) activity induced by a visual search task in humans. *Journal of Neuroscience* 1997; **17**:722–734.
3. Mäkinen V, Tiitinen H, May P. Auditory event-related responses are generated independently of ongoing brain activity. *NeuroImage* 2005; **24**:961–968. DOI: 10.1016/j.neuroimage.2004.10.020.
4. Mazaheri A, Picton TW. EEG spectral dynamics during discrimination of auditory and visual targets. *Cognitive Brain Research* 2005; **24**:81–96. DOI: 10.1016/j.cogbrainres.2004.12.013.
5. Ward LM. Synchronous neural oscillations and cognitive processes. *Trends in Cognitive Sciences* 2003; **7**(12): 553–559. DOI: 10.1016/j.tics.2003.10.012.

6. Bentley DE, Derbyshire SWG, Youell PD, Jones AKP. Caudal cingulate cortex involvement in pain processing: an inter-individual laser evoked potential source localisation study using realistic head models. *Pain* 2003; **102**(3):265–271. DOI: 10.1016/S0304-3959(02)00405-0.
7. Gruber T, Müller M. Oscillatory brain activity dissociates between associative stimulus content in a repetition priming task in the human EEG. *Cerebral Cortex* 2005; **15**(1):109–116. DOI: 10.1093/cercor/bhh113.
8. Kiebel SJ, Tallon-Baudry C, Friston KJ. Parametric analysis of oscillatory activity as measured with EEG/MEG. *Human Brain Mapping* 2005; **26**:170–177. DOI: 10.1002/hbm.20153.
9. Durka PJ, Zygierewicz J, Klekowicz H, Ginter J, Blinowska K. On the statistical significance of event-related EEG desynchronization and synchronization in the time–frequency plane. *IEEE Transactions on Biomedical Engineering* 2004; **51**:1167–1175. DOI: 10.1109/TBME.2004.827341.
10. Makeig S. Auditory event-related dynamics of the EEG spectrum and effects of exposure to tones. *Electroencephalography and Clinical Neurophysiology* 1993; **86**:283–293. DOI: 10.1016/0013-4694(93)90110-H.
11. Tallon-Baudry C, Bertrand O, Delpuech C, Pernier J. Stimulus specificity of phase-locked and non-phase-locked 40 Hz visual responses in human. *Journal of Neuroscience* 1996; **16**:4240–4249.
12. Makeig S, Westerfield M, Jung T, Enghoff S, Towsen J, Courchesne E, Sejnowski J. Dynamic brain sources of visual evoked responses. *Science* 2002; **295**:690–694.
13. Yamagishi N, Callan DE, Goda N, Anderson SJ, Yoshida Y, Kawato M. Attentional modulation of oscillatory activity in human visual cortex. *NeuroImage* 2003; **20**:98–113. DOI: 10.1016/S1053-8119(03)00341-0.
14. Edwards E, Soltani M, Deouell LY, Berger MS, Knight RT. High gamma activity in response to deviant auditory stimuli recorded directly from human cortex. *Journal of Neurophysiology* 2005; **94**:4269–4280. DOI: 10.1152/jn.00324.2005.
15. Mörup M, Hansen LK, Hermann CS, Parnas J, Arnfred SM. Parallel factor analysis as an exploratory tool for wavelet transformed event-related EEG. *NeuroImage* 2006; **29**(3):938–947. DOI: 10.1016/j.neuroimage.2005.08.005.
16. Yeung N, Bogacz R, Holroyd C, Cohen J. Detection of synchronized oscillations in the electroencephalogram: an evaluation of methods. *Psychophysiology* 2004; **41**:822–832. DOI: 10.1111/j.1469-8986.2004.00239.x.
17. Cuspineda-Bravo ER, Sánchez-Bornot JM, Valdés-Sosa PA. Measuring event-related dynamics [abstract]. *Presented at the 12th Annual Meeting of the Organization for Human Brain Mapping*, Florence, Italy, vol. 27(1), June 2006. Available on CD-Rom in NeuroImage; **31**(suppl. 1).
18. Tallon Baudry C, Kreiter A, Bertrand O. Sustained and transient oscillatory responses in the gamma and beta bands in a visual short-term memory task in humans. *Visual Neuroscience* 1999; **16**:449–459.
19. Makeig S, Debener S, Onton J, Delorme A. Mining event-related brain dynamics. *Trends in Cognitive Sciences* 2004; **8**(5):204–210. DOI: 10.1016/j.tics.2004.03.008.
20. Pfurtscheller G, Lopes da Silva FH. Event-related EEG/MEG synchronization and desynchronization: basic principles. *Clinical Neurophysiology* 1999; **110**:1842–1857. DOI: 10.1016/S1388-2457(99)00141-8.
21. Klimesch W, Schack B, Schabus M, Doppelmayr M, Gruber W, Sauseng P. Phase-locked alpha and theta oscillations generate the P1–N1 complex and are related to memory performance. *Cognitive Brain Research* 2004; **19**:302–316. DOI: 10.1016/j.cogbrainres.2003.11.016.
22. Mardia KV. *Statistics of Directional Data*. Academic Press: London, 1972.
23. Delorme A, Makeig S. A EEGLAB: an open source toolbox for analysis of single-trial EEG dynamics including independent component analysis. *Journal of Neuroscience Methods* 2004; **134**:9–21. DOI:10.1016/j.jneumeth.2003.10.009.
24. Brillinger DR. *Times Series*: *Data Analysis and Theory*. SIAM: Philadelphia, PA, 2001.
25. Mardia K, Kent J, Bibby J. *Multivariate Analysis*. Academic Press: San Diego, CA, 1979.
26. Storey JD. The positive false discovery rate: a Bayesian interpretation and the *q*-value. *Annals of Statistics* 2003; **31**(6):2013–2035. DOI: 10.1214/aos/1074290335.
27. Benjamini Y, Hochberg Y. Controlling the false discovery rate: a practical and powerful approach to multiple testing. *Journal of the Royal Statistical Society. Series B* (*Methodological*) 1995; **57**(1):289–300.
28. Efron B. Large-scale simultaneous hypothesis testing: the choice of a null hypothesis. *Journal of American Statistical Association* 2004; **99**:96–104. DOI 10.1198/016214504000000089.
29. Valdés-Sosa PA, Sánchez-Bornot JM, Lage-Castellanos A, Vega-Hernández M, Bosch-Bayard J, Melie-García L, Canales-Rodríguez E. Estimating brain functional connectivity with sparse multivariate autoregression. *Philosophical Transactions of the Royal Society B* 2005; **360**(1457):969–981. DOI: 10.1098/rstb.2005.1654.
30. Efron B. Size, power, and false discovery rates. *Annals of Statistics* 2007; **35**(4):1351–1377.
31. Trafimow D. Hypothesis testing and theory evaluation at the boundaries: surprising insights from Bayes's theorem. *Psychological Review* 2003; **110**(3):256–535. DOI: 10.1037/0033-295X.110.3.526.

32. Penny WD, Kiebel SJ, Kilner JM, Rugg MD. Event-related brain dynamics. *Trends in Neurosciences* 2002; **25**(8):387–389. DOI: 10.1016/S0166-2236(02)02202-6.
33. Makeig S, Westerfield M, Jung TP, Covington J, Townsend J, Sejnowski TJ, Courchesne E. Functionally independent components of the late positive event-related potential during visual spatial attention. *Journal of Neuroscience* 1999; **19**:2665–2680.
34. Oliver D, Kilner JM, Friston KJ. Mechanisms of evoked and induced responses in MEG/EEG. *NeuroImage* 2006; **31**(4):1580–1591. DOI: 10.1016/j.neuroimage.2006.02.034.
35. Oja H, Randles R. Multivariate nonparametric tests. *Statistical Science* 2004; **19**:598–605. DOI: 10.1214/088342304000000558.
36. Hanslmayr S, Klimesch W, Sauseng P, Gruber W, Doppelmayr M, Freunberger R, Pecherstorfer T, Birbaumer N. Alpha phase reset contributes to the generation of ERPs. *Cerebral Cortex* 2007; **17**:1–8. DOI: 10.1093/cercor/bhj129.
37. Mazaheri A, Jensen O. Posterior {alpha} activity is not phase-reset by visual stimuli. *Proceedings of the National Academy of Sciences* 2006; **103**:2948–2952. DOI: 10.1073/pnas.0505785103.
38. Klimesch W, Hanslmayr S, Sauseng P, Gruber WR. Distinguishing the evoked response from phase reset: a comment to Mäkinen *et al*. *NeuroImage* 2006; **29**:808–811. DOI: 10.1016/j.neuroimage.2005.08.041.
39. Luu P, Tucker DM, Makeig S. Frontal midline theta and the error-related negativity: neurophysiological mechanisms of action regulation. *Clinical Neurophysiology* 2004; **115**:1821–1835. DOI: 10.1016/j.clinph.2004.03.031.
40. Yeung N, Bogacz R, Holroyd CB, Nieuwenhuis S, Cohen JD. Theta phase resetting and the error-related negativity. *Psychophysiology* 2007; **44**:39–49. DOI: 10.1111/j.1469-8986.2006.00482.x.
41. Fuentemilla Ll, Marco-Pallarés J, Grau C. Modulation of spectral power and of phase resetting of EEG contributes differentially to the generation of auditory event-related potentials. *NeuroImage* 2006; **30**:909–916. DOI: 10.1016/j.neuroimage.2005.10.036.
42. Tass PA. Stochastic phase resetting of stimulus-locked responses of two coupled oscillators: transient response clustering, synchronization, and desynchronization. *Chaos* 2003; **13**(1):364–376. DOI: 10.1063/1.1505813.
43. Tass PA, Rosenblum MG, Weule J, Kurths J, Pikovsky A, Volkmann J, Schnitzler A, Freund HJ. Detection of *n*:*m* phase locking from noisy data: application to magnetoencephalography. *Physics Review Letters* 1998; **81**:3291–3294. DOI: 10.1103/PhysRevLett.81.3291.
44. Fell J, Dietl T, Grunwald T, Kurthen M, Klaver P, Trautner P, Schaller C, Elger CE, Fernández G. Neural bases of cognitive ERPs: more than phase reset. *Journal of Cognitive Neuroscience* 2004; **16**(9):1595–1604. DOI: 10.1162/0898929042568514.
45. Fell J, Klaver P, Lehnertz K, Grunwald T, Schaller C, Elger CE, Fernández G. Human memory formation is accompanied by rhinal–hippocampal coupling and decoupling. *Nature Neuroscience* 2001; **4**:1259–1264. DOI: 0.1038/nn759.
46. Hurtado JM, Rubchinsky LL, Sigvardt KA. Statistical method for detection of phase-locking episodes in neural oscillations. *Journal of Neurophysiology* 2004; **91**:1883–1898. DOI: 10.1152/jn.00853.2003.
47. Shah AS, Bressler SL, Knuth KH, Ding M, Mehta AD, Ulbert I, Schroeder CE. Neural dynamics and the fundamental mechanisms of event-related brain potentials. *Cerebral Cortex* 2004; **14**:476–483. DOI: 10.1093/cercor/bhh009.
48. Düzel E, Neufang M, Heinze HJ. The oscillatory dynamics of recognition memory and its relationship to event-related responses. *Cerebral Cortex* 2005; **15**:1992–2002. DOI: 10.1093/cercor/bhi074.

Artículo 2.

Durka, P.J., Matysiak, A., Martínez-Montes, E., Valdés-Sosa, P.A., Blinowska, K.J. Multichannel matching pursuit and EEG inverse solutions. Journal of Neuroscience Methods 148, 49–59 (2005).

ELSEVIER

Journal of Neuroscience Methods 148 (2005) 49–59

JOURNAL OF NEUROSCIENCE METHODS

www.elsevier.com/locate/jneumeth

Multichannel matching pursuit and EEG inverse solutions

Piotr J. Durka[a,*], Artur Matysiak[a], Eduardo Martínez Montes[b], Pedro Valdés Sosa[b], Katarzyna J. Blinowska[a]

[a] *Department of Biomedical Physics, Institute of Experimental Physics, Warsaw University, ul. Hoża 69, 00-681 Warszawa, Poland*
[b] *Cuban Neuroscience Center, Ave 25 #15202 esquina 158 Cubanacan, Playa, Area Code 11600, Habana, Cuba*

Received 23 December 2004; received in revised form 5 April 2005; accepted 6 April 2005

Abstract

We present a new approach to the preprocessing of the electroencephalographic time series for EEG inverse solutions. As the first step, EEG recordings are decomposed by multichannel matching pursuit algorithm—in this study we introduce a computationally efficient, sub-optimal solution. Then, based upon the parameters of the waveforms fitted to the EEG (frequency, amplitude and duration), we choose those corresponding to the the phenomena of interest, like e.g. sleep spindles. For each structure, the corresponding weights of each channel define a topographic signature, which can be subject to an inverse solution procedure, like e.g. Loreta, used in this work.

As an example, we present an automatic detection and parameterization of sleep spindles, appearing in overnight polysomnographic recordings. Inverse solutions obtained for single sleep spindles are coherent with the averages obtained for 20 overnight EEG recordings analyzed in this study, as well as with the results reported previously in literature as inter-subject averages of solutions for spectral integrals, computed on visually selected spindles.

Keywords: Multichannel matching pursuit; Lareta; EEG inverse solutions; Sleep spindles

1. Introduction

In recent decades electroencephalography is losing field to the new brain imaging techniques like MRI/fMRI and PET. This is mainly due to the fact that these *imaging* techniques provide information directly related to the well-known anatomy of the brain at a scale of few millimeters, which is more appealing and easier to interpret for the clinicians.

Nevertheless, EEG (together with MEG) still has the highest temporal resolution, and provides information directly related to the *function* of the brain—all from a relatively cheap and non-invasive technique. Therefore, several attempts were directed at relating the structures, known from the EEG traces, to the anatomical locations of their cerebral generators. Unfortunately, this so-called EEG inverse problem is ill-posed and underdetermined (cf. (Koles, 1998)). There is an infinity of possible electric current density distributions in the brain which may generate the same potential on the scalp surface. Choosing a unique solution requires a priori information, independently of the EEG data, which are usually an arbitrary choice of additional constraints.

There can be different kinds of constraints, the most used being of anatomical and physical–mathematical nature. The former consist basically on restricting the solution to some physiologically supported area, which can be a particular structure or the whole gray matter. The latter vary from considering the solution to be a sum of current dipoles to choosing the distributed solution with minimum norm or maximum smoothness. On the other hand, the task of solving an ill-posed problem by adding additional information about the solution has been firstly treated by the Tikhonov regularization (Hämäläinen and Ilmoniemi, 1994; Pascual-Marqui et al., 1994; Wang et al., 1992). Recently, the Bayesian approach has gained adepts because of its possibilities in introducing a priori information in a natural and flexible way (Schmidt et al., 1999; Trujillo-Barreto et

* Corresponding author. Tel.: +48 22 5532126; fax: +48 22 6226154.
E-mail addresses: durka@fuw.edu.pl (P.J. Durka), amatys@fuw.edu.pl (A. Matysiak), eduardo@cneuro.edu.cu (E.M. Montes), peter@cneuro.edu.cu (P.V. Sosa), kjbli@fuw.edu.pl (K.J. Blinowska).

0165-0270/$ – see front matter © 2005 Elsevier B.V. All rights reserved.
doi:10.1016/j.jneumeth.2005.04.001

al., 2004). Other approaches and combinations of the previously mentioned with time series and Fourier analysis have appeared in this field as well. According to constraints and algorithms used, different solutions are being promoted by different groups: LAURA, EPIFOCUS (Grave de Peralta-Menendez and Gonzales-Andino, 2002), ELECTRA (Grave de Peralta-Menendez et al., 2000)—and probably the most popular LORETA (Pascual-Marqui et al., 1994), with variants such as sLORETA (Pascual-Marqui, 2002), VARETA (Bosch-Bayard et al., 2001) and Bayesian Model Averaging solution (Trujillo-Barreto et al., 2004).

Just from the abundance of different solutions, one can see that the issue is complicated and far from stable conclusions, since none of the methods mentioned above gives fully satisfactory results in all kinds of EEG data. In this regard, an inverse solution is preferred according to the case of study. Some of them are suitable for applications in which a small region of the brain is active (as is the case for example in evoked potential studies) and others when the current density spread out in wider areas (e.g. spontaneous EEG, tumors, epilepsy). On the other hand, most of them, particularly Loreta, present usually physiologically non-interpretable sources, called ghost sources, and an inherent incapacity for recovering deep sources (Trujillo-Barreto et al., 2004). This bias on the recovering of the source amplitude is particular important when there exist more than one active source. The solution tends to present the cortical one (or nearer the electrodes) larger than the others, usually masking some strong activations in important deep structures of the brain. This is one of the motivations for the continuous developing of new methodologies for inverse solutions, although it has been shown that the bias can be overcome with a statistical postprocessing of the solution (Bosch-Bayard et al., 2001).

1.1. Motivation of this study

The scalp EEG is generally considered to be a linear sum of multiple neural masses or generators' electrical activity (Lopes Da Silva, 1999). Each of these generators, apart from its different localization, usually has a particular spectral content (probably with a signature very far from a delta function), and even a particular temporal evolution of its spectrum. This fact has brought neuroscientists to the task of decomposing the EEG into a sum of what can be called atoms of the electrical activity of the brain. Most of atomic decompositions of the EEG have taken into account two of the three inherent dimensions of this data, such as the space–time decompositions by principal and independent component analysis (PCA and ICA: Cichocki and Amari (2002), Hyvarinen et al. (2001), Lagerlund et al. (1997)), time–frequency analysis with the use of windowed Fourier transform (Makeig, 1993), wavelet transformation (Bartnik et al., 1992; Bertrand et al., 1994; Tallon-Baudry et al., 1997) and matching pursuit algorithm (Durka and Blinowska, 1995). Recently, new attempts of finding a multidimensional (space–time–frequency) atomic decomposition of the EEG have been made, in the way of having a complete description of the electrical activity of the underlying neural masses (König et al., 2001; Martínez-Montes et al., 2004; Miwakeichi et al., 2004).

On the other hand, inverse solutions have been mostly applied to instantaneous data (i.e. time points of the EEG data are treated separately), although some advances have been made to incorporate the temporal information for obtaining more reliable solutions (Galka et al., 2004; Yamashita et al., 2004). In the frequency domain, inverse solutions can be used as well due to the linearity of Fourier transform. However, in this case, clear delineation of the sources of activity usually requires heavy statistical post-processing of repetitions or many subjects data. This is probably due to the fact that the model underlying the inverse solution relates directly to energies of one or few generators, measured at the scalp. Unfortunately, spectral integrals used as the input to these procedures incorporate also large amount of unrelated activity. For example, in Anderer et al. (2001) spectral analysis was performed on 1.25 s time epochs with 0.8 Hz resolution in frequency; the content of these 1.25 s × 0.8 Hz boxes, which is due to the activity of sleep spindles

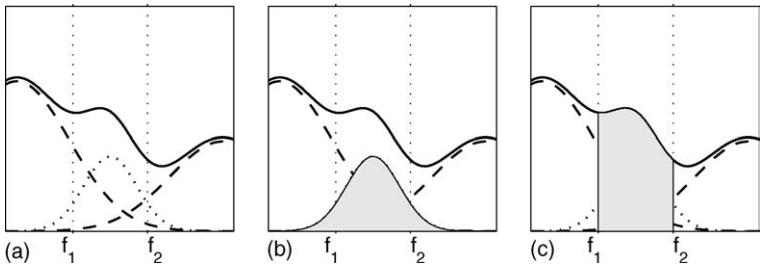

Fig. 1. Spectral power (vertical) vs. frequency (horizontal) of three hypothetical structures with frequency centers lying inside (dotted) and outside (dashed line) the f_1–f_2 interval. Due to the uncertainty principle, their spectral contents overlap. Solid line presents their sum, i.e. total spectral power, as estimated e.g. by Fourier transform. In (b) we mark (shaded) the actual power carried by structure of frequency originating between f_1 and f_2, as estimated e.g. by adaptive time–frequency approximation. Plot (c) highlights the power obtained from a spectral integral from f_1 to f_2. We observe that neighboring structures from outside the interval of interest may contribute significantly to the activity estimated within the interval, while some of the power carried by the structure inside the interval of interest falls outside and does not contribute to the spectral estimate.

generators, may at best statistically dominate other contributions. This effect, illustrated in Fig. 1, is a direct consequence of the uncertainty principle in signal analysis (Mallat, 1999).

In this study we will present a new approach for source localization of single structures with definite spatial–time–frequency properties. As a first step, EEG recordings are decomposed into a sum of atoms, each being the product of spatial (topographic) signature and waveforms having determined time–frequency localization. This is achieved by the multichannel matching pursuit algorithm, which is a generalization of the matching pursuit to analyzing several signals simultaneously, i.e. multidimensional data. The second step consists of using the topographic signatures of atoms of interest as input for obtaining 3D localization of its cerebral sources. This can be done through the use of any of the known inverse solution methods. In searching of simplicity and clear understanding of the method, we will use the widely known low resolution electromagnetic tomography (LORETA). It will be shown that application of selective and high-resolution estimates of generators activity, symbolically presented in Fig. 1b and described in Section 2.1, significantly improves the robustness of EEG inverse solutions. As will be presented in the following sections, it allows for a repeatable localization of single structures, based upon their time–frequency signatures.

2. Methods

2.1. Multichannel matching pursuit (MMP)

Matching pursuit algorithm (MP) with time–frequency dictionaries was proposed by Mallat and Zhang (1993) as a suboptimal iterative solution to the problem of optimal representation of monochannel signal in a redundant dictionary. Bias-free version, proposed by Durka et al. (2001), relies on randomization of the parameters of Gabor functions forming the dictionary. Real valued Gabor function can be expressed as

$$\mathbf{g}_\gamma(t) = K(\gamma)\mathrm{e}^{-\pi((t-u)/s)^2}\cos(\omega(t-u)+\phi), \tag{1}$$

where $\gamma = \{u, \omega, s, \phi\}$ and $K(\gamma)$ is such that $||\mathbf{g}_\gamma|| = 1$. Dictionary contains also Dirac and Fourier bases. From this dictionary, in each step we choose the atom representing optimally the nth residuum $R^n f$ of the signal f, left from previous iterations. For a monochannel signal f it can be written as

$$\begin{cases} R^0 f = f \\ R^n f = \langle R^n f, g_{\gamma_n}\rangle g_{\gamma_n} + R^{n+1} f \\ g_{\gamma_n} = \arg\max_{g_{\gamma_i}\in D} |\langle R^n f, g_{\gamma_i}\rangle| \end{cases} \tag{2}$$

This greedy algorithm can fail to properly decompose certain signals, containing simple combination of dictionary's functions. Theoretical examples of such failures are given e.g. by Chen et al. (2001), DeVore and Temlyakov (1996), Durka (2003). However, this suboptimality does not seem to pose problems in the parameterization of the EEG time series, as proved by 10 years of successful applications.[1] Recently it was shown that such "failures" may be explored to distinguish rhythmic discharges from series of unrelated/desynchronized spikes (Durka, 2004).

Multichannel extension of the MP algorithm (MMP) can be achieved in many ways. It is imaginable e.g. to allow for slightly different phases of the Gabor atoms (1) in different channels—phase optimization is usually a separate step in the numerical implementations. Differences in these phases might possibly reveal the direction of the information flow between channels, as in the AR-based directed transfer function (Kamiński and Blinowska, 1991)—in this case this flow would be attributed to a specified, single structure.[2] Since in this study the MMP was intended as preprocessing for instantaneous EEG inverse solutions, we keep the phases constant across the channels, assuming each atom corresponds to the same activity in all of them, as discussed in the next section.

Criterion for selecting the atom which "best" fits the residuum in all channels $\mathbf{f}^i$ of the multichannel signal $\mathbf{f}$ can be taken as

$$\max_{g_{\gamma_n}\in D} \sum_i |\langle R^n \mathbf{f}^i, g_{\gamma_n}\rangle|^2 \tag{3}$$

(Gribonval, 2003). This choice relates to the maximum of the energy of the multichannel signal, explained in one iteration. However, we may also choose e.g.

$$\max_{g_{\gamma_n}\in D} \sum_i |\langle R^n \mathbf{f}^i, g_{\gamma_n}\rangle|. \tag{4}$$

Algorithms based upon (3) and (4) may differ in convergence, but a structure from the dictionary, clearly present in $\mathbf{f}$, should be parameterized equally by both implementations, possibly in a different iteration. Slight differences in estimated parameters may stem from the nonlinearity of the algorithm.

In this study we choose the MMP maximizing the plain sum of products: $\max_{g_{\gamma_i}\in D} |\sum_i \langle R^n \mathbf{f}^i, g_{\gamma_i}\rangle|$. Owing to the linearity of the residuum operator R (Properties 1– 2 presented in Appendix A), this choice allows for an efficient implementation. Instead of finding in each step the product of each dictionary's waveform with all the channels, and then finding the maximum of the sum of these products (as in Eq. (4)) or their squares (as in Eq. (3)), in each step we decompose the signal constructed as the sum of all the channels residua, and then find the product of the globally optimal waveform with each channel. Denoting the average of all the N_e channels as

[1] For a review see e.g. Durka and Blinowska (2001) and Durka (2003) plus a recent work on ERD/ERS (Durka et al., 2004).

[2] However it is not obvious whether the information, contained in the EEG time series collected with the standard resolution, would suffice to estimate such a magnitude from single epochs.

$\bar{\mathbf{f}} = \frac{1}{N_e}\sum_{i=1}^{N_e}\mathbf{f}^i$, we define the algorithm as:

$$\begin{cases} R^0\bar{\mathbf{f}} = \bar{\mathbf{f}} \\ R^n\bar{\mathbf{f}} = \langle R^n\bar{\mathbf{f}}, \mathbf{g}_{\gamma_n}\rangle \mathbf{g}_{\gamma_n} + R^{n+1}\bar{\mathbf{f}} \\ \mathbf{g}_{\gamma_n} = \arg\max_{\mathbf{g}_\gamma \in D} |\langle R^n\bar{\mathbf{f}}, \mathbf{g}_\gamma\rangle| \\ R^n\mathbf{f}^i = \langle R^n\mathbf{f}^i, \mathbf{g}_{\gamma_n}\rangle \mathbf{g}_{\gamma_n} + R^{n+1}\mathbf{f}^i \end{cases} \quad (5)$$

This decomposition conserves the energy of representation (Property 3 in Appendix A); however, its convergence may be severely impaired in special cases, when given waveform is present in different channels with exactly opposite phases, with weights causing its total cancellation in the average signals $R^n\mathbf{f}$. Nevertheless, if this cancellation is not *complete*, and a clear trace of the atom g_{γ_n} is still present in $R^n\mathbf{f}$, then it should be correctly parameterized by the products $\langle R^n\mathbf{f}^i, \mathbf{g}_\gamma\rangle$—probably in a later iteration as compared to the algorithm maximizing the sum of moduli or squares, since $\sum|\langle R^n\mathbf{f}^i, g_{\gamma_n}\rangle| \geq |\sum\langle R^n\mathbf{f}^i, g_{\gamma_n}\rangle|$. As mentioned above, additional differences in $\langle R^n\mathbf{f}^i, g_{\gamma_n}\rangle$ for different n may also stem from the nonlinearity of the MP algorithm, but in general, except for a very special cases of total cancellation of a structure in the average of all channels, γ_n and $\langle R^n\mathbf{f}^i, g_{\gamma_n}\rangle$ obtained from this approach should be equivalent to those returned by an algorithm maximizing (3) or (4). We may say that this flavor of MMP favours structures with equal phases in all the channels.[3]

As a reward, this procedure reduces the computational complexity by the factor N_e (that is number of channels). In this study $N_e = 21$, but in general for inverse solutions a larger number of derivations (e.g. 128) is suitable. Speed of computations is still an important factor in practical applications, since the unbiased implementations of MP (Durka et al., 2001) make it difficult to apply some most natural numerical optimizations (this work is still in progress), and unbiased MP is still computationally intensive.

Due to operating on the average of channels, this version of the algorithm cannot be directly applied to the data presented in the average reference. In this study, we performed the MMP computations on the original EEG signals, which are referenced to the linked ears (A1 + A2). The output of this procedure are the time–frequency atoms representing the structures of interest, and the corresponding coefficients for each electrode are given by the products $\langle R^n\mathbf{f}^i, g_{\gamma_n}\rangle$. This vector represents a topographic (spatial) signature (see examples in lower panel of Fig. 2) of the nth atom, and completes the picture of a space–time–frequency decomposition of the EEG data. As will be explained in the next section, these topographic signatures conserve the magnitude of the original data (since the gabor atoms are normalized) and the reference to linked ears. Then these topographic signatures are taken as the input for a source localization procedure.

[3] This feature will be more relevant e.g. for compression, where the index of the iteration n may be used as a cutoff criterion.

2.2. Inverse solution

Three-dimensional reconstruction of the current densities inside the brain, obtained from the inverse solutions, is commonly termed brain electrical tomography (BET). The term "tomography" is also explicitly present in the acronym of the method used in this study: LORETA stands for "LOw Resolution Electromagnetic TomogrAphy". However, due to the problems mentioned in the Introduction, it may lead to serious misunderstandings when e.g. directly comparing the clinical applicability of BET and CT. Therefore, in the following we will avoid the use of the term "tomography", and will use "inverse solution" or "source estimation/localization" indistinctly.

The relation between scalp surface EEG measurements and the primary current density is described by a linear equation:

$$\mathbf{a} = \mathbf{K}\mathbf{j} + \mathbf{e} \quad (6)$$

Here, $\mathbf{a}$ denotes the vector containing the scalp electric potentials at N_e electrodes. The vector $\mathbf{j}$ has thrice the number of voxels elements, corresponding to the x, y and z components of the primary current density vector in each voxel of a grid defined inside the brain. The matrix $\mathbf{K}$, linking the current density with the measurements, is called the lead field matrix. It can be calculated by applying Maxwell's equations to a particular head model (Nunez, 1981). The vector $\mathbf{e}$ is an additive random element representing unmodeled effects such as observation noise. In the case of the data being a matrix $\mathbf{A}$ with N columns (representing e.g. time points, trials, atoms), this formulation will be the same with corresponding N columns in a matrix $\mathbf{J}$.

The inverse problem is defined as the estimation of current density $\mathbf{j}$ from a given measurement $\mathbf{a}$ and constitutes an ill-conditioned (sensitive to noise) and ill-posed problem in the sense of Hadamard (Hadamard, 1923), since it has non-unique solution. This is easy to see from the fact that the number of scalp electrodes is much smaller than the number of voxels for which the current density has to be estimated. Therefore, the imposition of additional constraints on the solution is needed to obtain a unique solution. This can be done by several approaches such as the Regularization Theory of Tikhonov like Loreta (Pascual-Marqui et al., 1994) and Bayesian Theory (Trujillo-Barreto et al., 2004) and/or using anatomical and other physical constraints like assuming the current density to consist only of single current dipoles (De Munck, 1989; Scherg and von Cramon, 1986; Scholz and Schwierz, 1994).

Another aspect to take into account is the ambiguity of voltage differences with respect to the reference. Although this is not a problem for the inverse solution procedure if the lead field is computed with the same reference used for recording the data, it has been shown (Pascual-Marqui, 1995) that Loreta solution is valid for Eq. (6) when the scalp voltage differences as well as the lead field are taken to have average

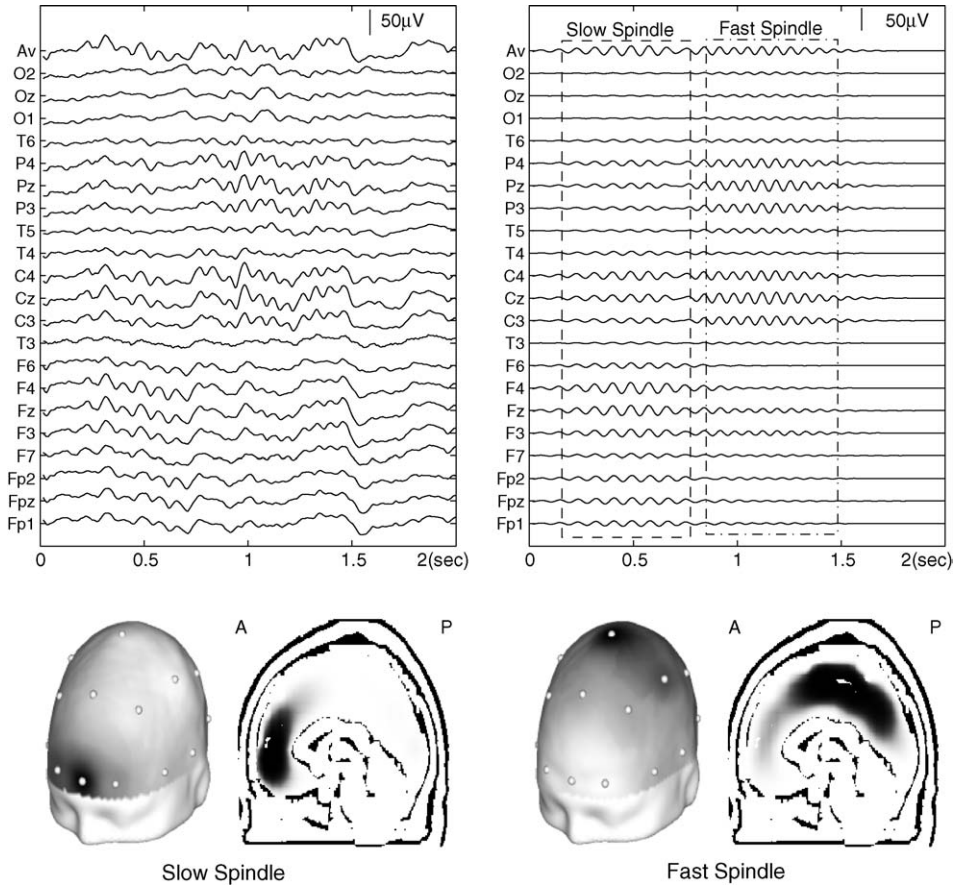

Fig. 2. Upper left: 2 s of sleep EEG from 21 standard electrodes (uppermost trace—average). Upper right: time courses of two Gabor atoms (Eq. (1)), conforming to the criteria of sleep spindles (Section 2.3), fitted to the EEG presented on the left by the multichannel matching pursuit (Section 2.1). The first atom (slow spindle) is centered around 0.5 s and 11 Hz. Center of the second atom (fast spindle) is around 1 s and 14 Hz. Lower left: representation of the topographic signature of the slow spindle, pronounced in the frontal derivations, and the corresponding Loreta image. Lower right: the same for the fast spindle, pronounced in the parietal derivations.

reference. This relates to the fact that some practical or technical solutions for the reference in measuring the EEG, such as the linked ears, do not represent a physical reference, i.e it cannot be located in a particular position in space. That is why the use of average reference is a common practice as preprocessing of the data for solving the EEG inverse problem and it is easily achieved by pre multiplication of both the data and the lead field by the matrix $\mathbf{H} = \mathbf{I} - \mathbf{1}\mathbf{1}^T/N_e$. Here $\mathbf{I}$ is the identity matrix of size N_e, $\mathbf{1}$ is a N_e-vector of ones, and $\mathbf{1}^T$ denotes its transpose.

In this study we used the implementation of an inverse solution (hereinafter Loreta solution), developed in the Cuban Neuroscience Center, which uses three concentric spheres model with solution space constrained to cortical gray matter and hippocampus (based upon the human brain atlas by Talairach and Tournoux (1988)). The lead field was computed as defined by Riera and Fuentes (1998), and Loreta algorithm (Pascual-Marqui et al., 1994) was used with an automatic setting of regularization parameter based on the minimization of the generalized cross-validation function. The average Probabilistic MRI Atlas produced by the Montreal Neurological Institute (Collins et al., 1994; Evans et al., 1993, 1994; Mazziotta et al., 1995) was used for computation and representation of Loreta inverse solutions.

This methodology was applied for source localization of single atoms with specific time–frequency characteristics, found from adaptive decomposition of EEG time series by MMP (Section 2.1). In a matrix notation, MMP representation of a spatio-temporal EEG recording $\mathbf{F}$[4] in N_a atoms is expressed as the product of two matrices plus the $N_a + 1$ residual:

$$\mathbf{F}_{N_e \times N_t} = \mathbf{A}_{N_e \times N_a} \mathbf{G}_{N_a \times N_t} + R^{N_a+1} \mathbf{F}_{N_e \times N_t} \quad (7)$$

The rows of matrix $\mathbf{G}$ are the $\mathbf{g}_{\gamma_n} (n = 1 \ldots N_a)$ fitted by MMP to the signal $\mathbf{F}$. The ith element of nth column of matrix $\mathbf{A}$ is the scalar product $\langle R^n \mathbf{f}^i, \mathbf{g}_{\gamma_n} \rangle$.

The square of these elements gives the energy explained by the nth atom fitted in the ith channel, since dictionarys

[4] In the other sections and equations, multichannel signal forming the matrix $\mathbf{F}$ is denoted by $\mathbf{f}$, and the one-dimensional signal in channel i as $\mathbf{f}^i$ $(i = 1 \ldots N_e)$.

functions $\mathbf{g}_{\gamma_n}$ are normalized. From the linearity of the procedure (see Appendix A) it is easy to see that these signatures will have the same reference as the original EEG data. In this study, the data is referenced to the linked ears and therefore, so will be the topographic signatures. Values of these topographies can be positive or negative.

In the second (separate) step of the proposed method, the spatial 3D localization of the sources of single atoms is carried out from each topography according to Eq. (6). For this purpose, the topographic signatures are taken to have average reference as required by LORETA (Pascual-Marqui, 1995), but this does not imply any further assumption or transformation on the data than those already made in the first step (MMP decomposition).

2.3. Parameterization of sleep spindles

In the last decade matching pursuit with Gabor dictionary was successfully applied in monochannel analysis of several types of EEG signals—for review see e.g. (Durka, 2003; Durka and Blinowska, 2001). Reliability of detection and parameterization of sleep spindles in single EEG channels was presented by Żygierewicz et al. (1999) and Durka et al. (2002). In this study, structures corresponding to sleep spindles were automatically chosen from the matching pursuit decompositions of artifact-free epochs of stage 2, as Gabor functions with frequency from 11.5 to 14.5 Hz and width from 0.5 to 2 s. Minimum peak-to-peak amplitude of a structure classified as sleep spindle was determined separately for each recording, to take into account inter-subject differences in EEG amplitude, depending e.g. on age, sex (Danker-Hopfe et al., 2004; Larsen et al., 1995) and quality of sleep (Armitage et al., 2000). Due to the one-to-one relation between the sleep spindles and fitted Gabor atoms (cf. Żygierewicz et al. (1999) and Fig. 2), this procedure provides an automatic parameterization of all the sleep spindles, present in given recording, in terms of their: time positions, lengths, frequencies and amplitudes in each channel (that is topographies, as discussed in Section 2.1).

2.4. Experimental data

We analyzed 20 overnight polysomnographic recordings, recorded at Medical University of Warsaw, Chair of Psychiatry, as a control group of another study. Polygraphic monitoring consisted of EEG activity collected from 21 electrodes, according to the international 10–20 system, electrooculogram (EOG) from two channels, and submentalis electromyogram. Filters were set between 0.15 and 30.0 Hz. The impedance at each electrode was below 5000 Ω. Sleep stages and artifacts were identified visually (stages according to the standardized manual for sleep scoring (Rechtschaffen and Kales, 1968)). Informed consent was obtained from all subjects. The study was approved by the University Ethics Committee.

3. Results

Sleep spindles were automatically detected in artifact-free epochs of stage 2. Each of the 20 available multichannel overnight EEG recordings (Section 2.4) was decomposed by the MMP algorithm described in Section 2.1. Atoms corresponding to sleep spindles were selected from this decomposition according to the parameters described in Section 2.3, and intensity images were obtained for each of these structures separately by means of the procedure described in Section 2.2. Fig. 3 presents Loreta images obtained for single sleep spindles: in each of the frequency bands, covering the spindles band in 0.5 Hz steps, one sleep spindle was randomly chosen from one of the analyzed recordings.

Based upon preliminary inspection of Loreta images as in Fig. 3, as well as their averages per subject, we divided the available recordings in two groups:

(1) In five of these subjects, Loreta images showed higher values for slower spindles consistently concentrated in the anterior regions.
(2) In the remaining 15 subjects, topographical distinction between the fast and slow spindles was not so clear.

The average number of spindles detected per one overnight recording in the first group was 578 (std. dev. 120), in the second group—692 (std. dev. 316). Figs. 4 and 5 present averages of single Loreta images—like the one presented in Fig. 3—separately for the subjects from these two groups. These images are constructed as vertical slices of the raw Loreta solution for the given structure, without any statistical postprocessing of the results. We observe the general consistency of these average images with the images obtained for single sleep spindles (Fig. 3), as well as their concordance with previous results, in particular those presented by (Anderer et al., 2001). In that study, construction of average images (corresponding to Figs. 4 and 5) from inverse solutions applied to spectral integrals required additional steps:

- visual selection of sleep spindles,
- their assignment to different classes of topographic distribution (also visual),
- substracting from the obtained images corresponding distributions, computed for the visually selected non-spindle EEG epochs.

In this paper, we automatically included all the spindles conforming to the general criteria—several hundreds per subject, comparing to an order of magnitude less of the structures, carefully selected by Anderer et al. (2001). As a result, images presented in that study look slightly sharper than Figs. 4 and 5.

4. Discussion

This paper implements a complete algorithm, starting from the raw EEG data and classical definition of sleep

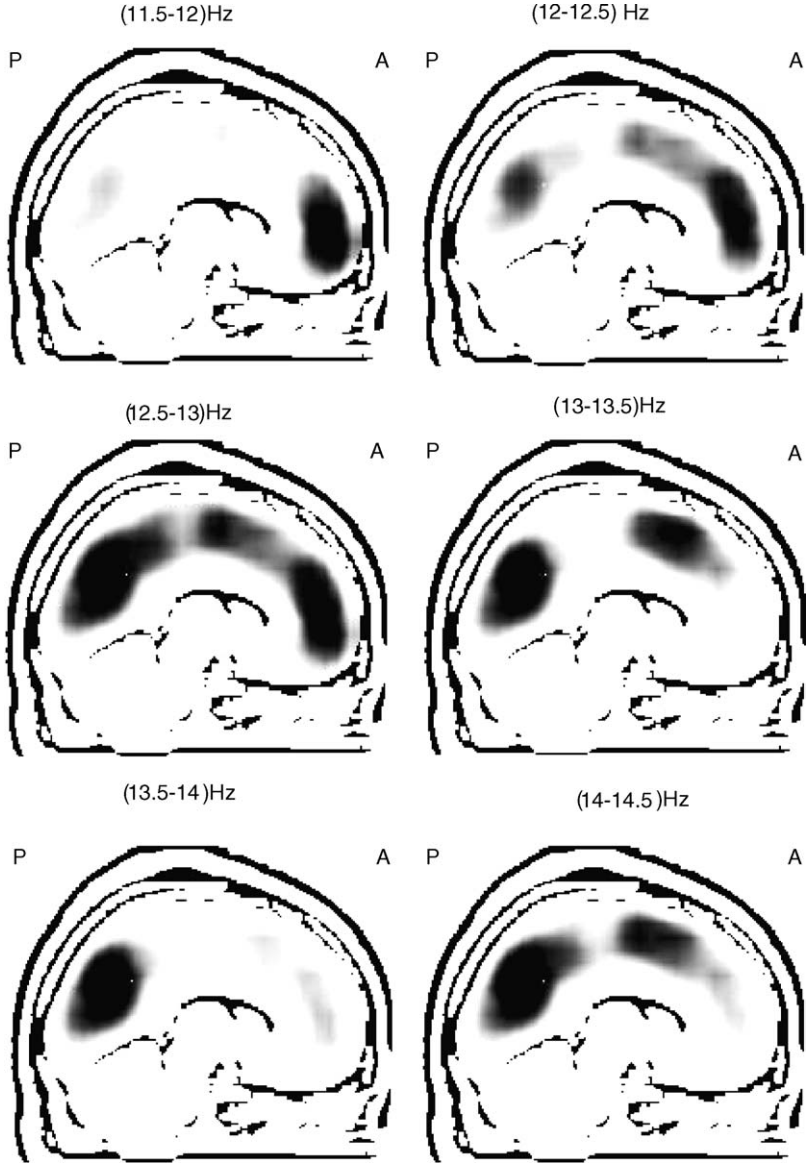

Fig. 3. Loreta images calculated for six single sleep spindles, chosen at random from the frequency intervals from 11.5–12 Hz (top left) to 14–14.5 Hz (bottom right). In each of these ranges one spindle was randomly chosen from the structures automatically detected and parameterized via the MMP. Corresponding panels present Loreta images computed for these single sleep spindles.

spindles, giving as the output automatic detection and description of structures conforming to these criteria. Each of the detected spindles is localised in time, frequency and space. Advantages of this paradigm include spatial localisation of single sleep spindles, straightforward extension to other kinds of structures, high degree of compatibility with the visual EEG analysis and a relative freedom from arbitrary parameters.

However, the idea of using topographic signatures of time–frequency atoms as the input for inverse solutions is not entirely new. Matching pursuit with a limited dictionary of wavelets was used for analysis of evoked potentials by Geva (1998), and localization of the sources of these atoms was carried out by a linear exhaustive search. Sources were constrained to a particular grid of the brain and supposed to be single or symmetrical pair of current dipoles. In a different study, another kind of inverse solution, called Source Spectra Imaging (SSI), was used for finding the spectra of the current density distribution, after obtaining topographic signatures from three-dimensional decomposition of the spontaneous EEG time-varying spectrum (Martínez-Montes et al., 2004; Miwakeichi et al., 2004). On the other side, multichannel extension of the MP was previously discussed by Gribonval (2003). It was applied to the separation of sources from stereo signals (Gribonval, 2002).

A different preprocessing for the inverse solutions can be based upon Independent Component Analysis (Tang et al., 2002). Contrary to the atoms identified within the proposed

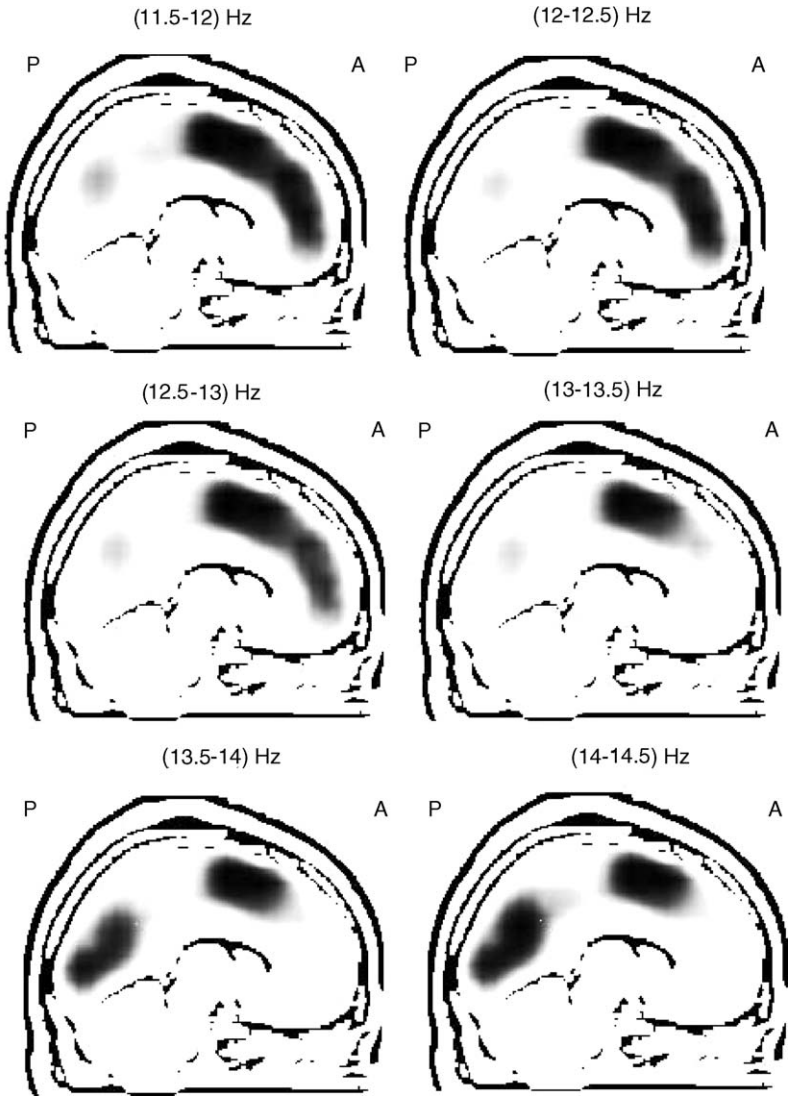

Fig. 4. Average Loreta images calculated for sleep sindles for the five recordings of subjects exhibiting clear prevalence of slow spindles in frontal regions. Separate averages constructed for spindles occurring in the frequency intervals from 11.5–12 Hz (top left) to 14–14.5 Hz (bottom right). No statistics or bias correction was employed in forming these images.

approach, independent components are not a priori related to any structures known from the clinical analysis of EEG. Also, ICA is based upon several strong assumptions, e.g. linearity and stability of the mixing process and some statistical independence of the sources.

In this study we combine adaptive time–frequency parameterization of EEG structures and EEG source localization. Resulting solution is not restricted to a sum of single current dipoles as in (Geva, 1998), and avoids strong assumptions on the independence of generators activity, made by the SSI solution (Miwakeichi et al., 2004). Sub-optimal implementation of the multichannel matching pursuit, based upon decomposition of the average residuum in each iteration, allows for a significant gain in the speed of computations. It seems that its suboptimality does not deteriorate the detection of relevant EEG structures; however, possible advantages of the other discussed implementations remain to be tested in this context.

Results obtained hereby on 20 overnight EEG recordings are coherent with the general knowledge about sleep spindles, and with particular results obtained by Anderer et al. (2001) with critical involvement of the visual analysis. As a new element, illustrating the increase of sensitivity compared to the previous approaches, we obtain possibility of localizing single structures. These results were obtained by a plain, raw an automatic combination of MMP and Loreta, with an explicit implementation of the traditional definition of sleep spindles. It was intended only as presentation of the possibilities and basic experimental verification. A wide margin for improvements remains open for applications, addressing directly some physiological or

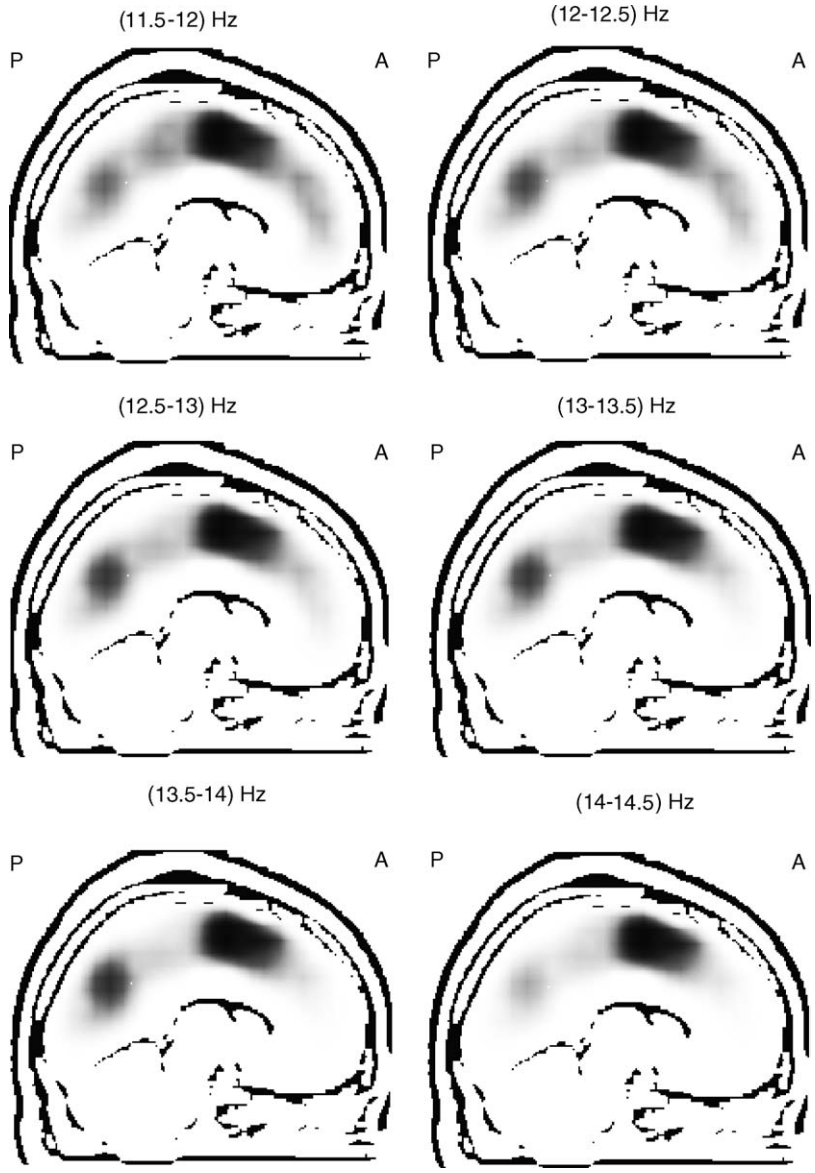

Fig. 5. The same as in Fig. 4, averaged for the 15 recordings of subjects exhibiting "less clear" spatial distinction between fast and slow spindles.

clinical issues: starting from the careful selection of the EEG epochs and tuning the parameters defining relevant structures (in this study sleep spindles), to the final statistical post-processing.

Some issues, like e.g. correction for the localization bias of the Loreta solution, remain to be solved within the proposed framework. It will be also valuable to test MMP as preprocessing to other inverse EEG solutions.

4.1. Reproducible research

An implementation of the MMP algorithm, described in Section 2.1 (with complete source in C), is available from http://eeg.pl, section "Software". Matlab code for the Loreta inverse solution is available upon request from Eduardo Martínez Montes (eduardo@cneuro.edu.cu).

Acknowledgments

We thank Prof. Waldemar Szelenberger from the Warsaw Medical School for providing the EEG data, Marek Barwiński for efficient implementation of the fast matching pursuit algorithm, and Dr. Jorge Bosch-Bayard for offering his technical experience on the inverse solution procedure. Piotr J. Durka, Artur Matysiak and Katarzyna J. Blinowska were supported by the grant of Committee for Scientific Research (Poland) to the Institute of Experimental Physics, Warsaw University.

Appendix A. Properties of the proposed implementation of multichannel matching pursuit

Property 1 (Linearity). *The sum of residua is equal to residuum of the sum, which implies that* R^n *is a linear*

operator.

$$R^n\bar{\mathbf{f}} = R^n\frac{1}{N_e}\sum_{i=1}^{N_e}\mathbf{f}^i = \frac{1}{N_e}\sum_{i=1}^{N_e}R^n\mathbf{f}^i = \overline{R^n\mathbf{f}} \tag{8}$$

Proof. From the fact that operator R^0 is an identity operator (i.e. $R^0\mathbf{f} = \mathbf{f}$) we have:

$$R^0\sum_{i=1}^{N_e}\mathbf{f}^i = \sum_{i=1}^{N_e}R^0\mathbf{f}^i \tag{9}$$

The linearity of product operator $\langle *, *\rangle$ implies

$$\left\langle\frac{1}{N_e}\sum_{i=1}^{N_e}R^n\mathbf{f}^i, \mathbf{g}_{\gamma_n}\right\rangle = \frac{1}{N_e}\sum_{i=1}^{N_e}\langle R^n\mathbf{f}^i, \mathbf{g}_{\gamma_n}\rangle \tag{10}$$

From the above, for the 0th iteration the residuum operator R^0 is a linear operator.

$$\begin{aligned}\frac{1}{N_e}\sum_{i=1}^{N_e}(R^0\mathbf{f}^i - \langle R^0\mathbf{f}^i, \mathbf{g}_{\gamma_0}\rangle\mathbf{g}_{\gamma_0}) &= \frac{1}{N_e}\sum_{i=1}^{N_e}R^1\mathbf{f}^i \\ &= R^1\frac{1}{N_e}\sum_{i=1}^{N_e}\mathbf{f}^i\end{aligned} \tag{11}$$

By induction for $n >$ 0th iteration we have:

$$\begin{aligned}\frac{1}{N_e}\sum_{i=1}^{N_e}(R^n\mathbf{f}^i - \langle R^n\mathbf{f}^i, \mathbf{g}_{\gamma_n}\rangle\mathbf{g}_{\gamma_n}) &= \frac{1}{N_e}\sum_{i=1}^{N_e}R^{n+1}\mathbf{f}^i \\ &= R^{n+1}\frac{1}{N_e}\sum_{i=1}^{N_e}\mathbf{f}^i\end{aligned} \tag{12}$$

□

Property 2. *The sum of products across all channels is equal to product of the sum*

$$\langle R^n\bar{\mathbf{f}}, \mathbf{g}_{\gamma_n}\rangle = \frac{1}{N_e}\sum_{i=1}^{N_e}\langle R^n\mathbf{f}^i, \mathbf{g}_{\gamma_n}\rangle \tag{13}$$

Proof. It is a simple conclusion from linearity of the residuum operator R^n. □

Property 3 (Energy conservation). *The energy of the decomposed signal is conserved across all channels*

$$\|\bar{\mathbf{f}}\|^2 = \sum_{n=0}^{N_a}\left|\frac{1}{N_e}\sum_{i=1}^{N_e}\langle R^n\mathbf{f}^i, \mathbf{g}_{\gamma_n}\rangle\right|^2 + \left\|\frac{1}{N_e}\sum_{i=1}^{N_e}R^{N_a+1}\mathbf{f}^i\right\|^2 \tag{14}$$

$$\|\mathbf{f}^i\|^2 = \sum_{n=0}^{N_a}|\langle R^n\mathbf{f}^i, \mathbf{g}_{\gamma_n}\rangle|^2 + \|R^{N_a+1}\mathbf{f}^i\|^2 \tag{15}$$

Proof. The orthogonality of $R^{n+1}\bar{\mathbf{f}}$ or $R^{n+1}\mathbf{f}^i$ with $\mathbf{g}_{\gamma_n}$ implies energy conservation for the average signal $\mathbf{f}$ and its every channel $\mathbf{f}^i$. □

References

Anderer P, Klösch G, Gruber G, Trenker E, Pascual-Marqui R, Zeitlhofer J, et al. Low-resolution brain electromagnetic tomography revealed simultaneously active frontal and parietal sleep spindles sources in the human cortex. Neuroscience 2001;103(3):581–92.

Armitage R, Hoffmann R, Fitch T, Trivedi M, Rush A. Temporal characteristics of delta activity during nrem sleep in depressed outpatients and healthy adults: group and sex effects. Sleep 2000;23(5):607–17.

Bartnik EA, Blinowska KJ, Durka PJ. Single evoked potential reconstruction by means of wavelet transform. Biol Cybern 1992;67:175–81.

Bertrand O, Bohorquez J, Pernier J. Time–frequency digital filtering based on an invertible wavelet transform: an application to evoked potential. IEEE Trans Biomed Eng 1994;41:77–88.

Bosch-Bayard J, Valdes-Sosa P, Virues-Alba T, Aubert-Vazquez E, John ER, Harmony T, et al. 3D statistical parametric mapping of EEG source spectra by means of variable resolution electromagnetic tomography (VARETA). Clin Electroenceph 2001;32.

Chen SS, Donoho DL, Saunders MA. Atomic decomposition by basis pursuit. SIAM Rev 2001;43(1):129–59.

Cichocki A, Amari S. Adaptive blind signal and image processing. Wiley; 2002.

Collins D, Neelin P, Peters R, Evans A. Automatic 3D intersubject registration of mr volumetric in standardized Talairach space. J Comput Assist Tomogr 1994;18:192–205.

Danker-Hopfe H, Kunz D, Gruber G, Klosch G, Lorenzo J, Himanen S, et al. Interrater reliability between scorers from eight european sleep laboratories in subjects with different sleep disorders. J Sleep Res 2004;13(1):63–9.

De Munck J. Random dipoles as a model for spontaneous EEG and MEG activity. In: Williamson SJ, editor. Advances in biomagnetism. New York: Plenum; 1989. p. 595–8.

DeVore RA, Temlyakov VN. Some remarks on greedy algorithms. Adv Comp Math 1996;5:173–87.

Durka PJ. From wavelets to adaptive approximations: time–frequency parametrization of EEG, Biomed Eng Online 2003;2(1).

Durka PJ. Adaptive time–frequency parametrization of epileptic EEG spikes. Phys Rev E 2004;69:051914.

Durka PJ, Blinowska KJ. Analysis of EEG transients by means of matching pursuit. Ann Biomed Eng 1995;23:608–11.

Durka PJ, Blinowska KJ. A unified time–frequency parametrization of EEG. IEEE Eng Med Biol Mag 2001;20(5):47–53.

Durka PJ, Ircha D, Blinowska KJ. Stochastic time–frequency dictionaries for matching pursuit. IEEE Trans Signal Proc 2001;49(3):507–10.

Durka PJ, Szelenberger W, Blinowska K, Androsiuk W, Myszka M. Adaptive time–frequency parametrization in pharmaco EEG. J Neurosci Meth 2002;117:65–71.

Durka PJ, Żygierewicz J, Klekowicz H, Ginter J, Blinowska K. On the statistical significance of event-related EEG desynchronization and synchronization in the time–frequency plane. IEEE Trans on Biomed Eng 2004;51:1167–75.

Evans A, Collins D, Mills S, Brown E, Kelly R, Peters T. 3D statistical neuroanatomical models from 305 MRI volumes. In: Proceedings of the IEEE-Nuclear Science Symposium and Medical Imaging Conference, vol. 95. London: MTP Press; 1993. p. 1813–7.

Evans A, Collins D, Neelin P, MacDonald D, Kamber M, Marrett T. Three-dimensional correlative imaging: applications in human brain mapping. In: Thatcher R, Hallet M, Zeffiro T, John E, Huerta M, editors. Functional neuroimaging: Technical foundations. New York: Academic Press; 1994. p. 145–61.

Galka A, Yamashita O, Ozaki T, Biscay R, Valdés-Sosa P. A solution to the dynamical inverse problem of EEG generation using spatiotemporal kalman filtering. NeuroImage 2004;23:435–53.

Geva A. Biolectric sources estimation using spatio-temporal matching pursuit. Appl Signal Process 1998;5:195–208.

Grave de Peralta-Menendez R, Gonzales-Andino S. Comparisons of algorithms for the localization of focal sources: evaluation with simulated data and analysis od experimental data. IJBEM 2002;4(1).

Grave de Peralta-Menendez R, Gonzales-Andino S, Morand S, Michel C, Landis T. Imaging the electrical activity of the brain: ELECTRA. Human Brain Mapping 2000;9:1–12.

Gribonval R. Sparse decomposition of stereo signals with matching pursuit and application to blind separation of more than two sources from a stereo mixture. In: Proceedings of the International Conference on Acoustics Speech Signal Process. (ICASSP 02). Orlando, Florida, 2002.

Gribonval R. Piecewise linear source separation. In: Proc. SPIE 03. Vol. 5207 Wavelets: Applications in Signal and Image Processing. Sang Diego, California; 2003.

Hadamard J. Lecture on the Cauchy problem in linear partial differential equations. New Haven, CT: Yale University Press; 1923.

Hämäläinen M, Ilmoniemi R. Interpreting magnetic fields of the brain: minimum norm estimates. Med Biol Eng Comput 1994;32:35–42.

Hyvarinen A, Karhunen J, Oja E. Independent component analysis. Wiley; 2001.

Kamiński M, Blinowska K. A new method of the description of the information flow. Biol Cybernetics 1991;65:203–10.

Koles Z. Trends in EEG source localization. Electroenceph Clin Neurophysiol 1998;106:127–37.

König T, Marti-Lopez F, Valdes-Sosa P. Topographic time–frequency decomposition of the EEG. NeuroImage 2001;14:383–90.

Lagerlund T, Sharbrough F, Busacker N. Spatial filtering of multichannel electroencephalographic recordings through principal component analysis by singular value decomposition. J Clin Neurophysiol 1997;14:73–83.

Larsen L, Moe K, Vitiello M, Prinz P. A note on the night-to-night stability of stages 3+4 sleep in healthy older adults: a comparison of visual and spectral evaluations of stages 3+4 sleep. Sleep 1995;18:7–10.

Lopes Da Silva F. EEG analysis: Theory and practice. In: Electroencephalography: Basic principles, clinical applications and related fields. 4th Edition. Williams & Wilkins; 1999. p. 1135–63.

Makeig S. Auditory event-related dynamics of the EEG spectrum and effects of exposure to tones. Electroencephalogr Clin Neurophysiol 1993;86:283–93.

Mallat S. A wavelet tour of signal processing. 2nd Edition. New York: Academic Press; 1999.

Mallat S, Zhang Z. Matching pursuit with time–frequency dictionaries. IEEE Trans. Signal Process. 1993;41:3397–415.

Martínez-Montes E, Valdés-Sosa P, Miwakeichi F, Goldman R, Cohen M, Concurrent. EEG/fMRI analysis by multi-way partial least squares. NeuroImage 2004;22(3):1023–34.

Mazziotta J, Toga A, Evans A, Fox P, Lancaster J. A probabilistic atlas of the human brain: theory and rationale for its development. NeuroImage 1995;2:89–101.

Miwakeichi F, Martínez-Montes E, Valdés-Sosa P, Nishiyama N, Hiroaki M, Yamaguchi Y. Decomposing EEG data into space–time–frequency components using parallel factor analysis. NeuroImage 2004;22(3):1035–45.

Nunez P. Electric fields of the brain. Oxford University Press; 1981.

Pascual-Marqui R. Reply to comments by hämäläinen, ilmoniemi and nunez. en source localization: Discussion of the inverse problem (W. Skrandies, editor). ISBET Newsletter (6)1995;16–28.

Pascual-Marqui R. Standardized low-resolution brain electromagnetic tomography (sloreta): technical details. Meth Findings Exp Clin Pharmacol 2002;24:5–12.

Pascual-Marqui R, Michel C, Lehman D. Low resolution electromagnetic tomography: a new method to localize electrical activity in the brain. Int J Psychophysiol 1994;18:49–65.

Rechtschaffen A, Kales A, editors. A manual of standardized terminology, techniques and scoring system for sleep stages in human subjects. No. 204 in National Institutes of Health Publications. Washington, DC: US Government Printing Office; 1968.

Riera J, Fuentes M. Electric lead field for a piece-wise homogeneous volume conductor model of the head. IEEE Trans on Biomed Eng 1998;45:746–53.

Scherg M, von Cramon D. Evoked dipole source potentials of the human auditory cortex. Electroencephalogr Clin Neurophysiol 1986;65:344–60.

Schmidt D, George J, Wood C. Bayesian inference applied to the biomagnetic inverse problem. Hum Brain Mapp 1999;7:195–212.

Scholz B, Schwierz G. Probability-based current dipole localization from biomagnetic fields. IEEE Trans Biomed Eng 1994;41:735–42.

Talairach J, Tournoux P. Co-Planar stereotaxic atlas of the human brain. New York: Thieme; 1988.

Tallon-Baudry C, Bertrand O, Delpuech C, Pernier J. Oscillatory g-band (30–70 hz) activity induced by a visual search task in humans. J Neurosci 1997;17:722–34.

Tang AC, Pearlmutter BA, Malaszenko NA, Phung DB, Reeb BC. Independent components of magnetoencephalography: Localization. Neural Comput 2002;14:1827–58.

Trujillo-Barreto NJ, Aubert E, Valdés-Sosa P. Bayesian model averaging in EEG/MEG imaging. NeuroImage 2004;21:1300–19.

Wang J, Williamson S, Kaufman L. Magnetic source images determined by a leadfield analysis—the unique minimum-norm least squares estimation. IEEE T Bio-Med Eng 1992;39:231–51.

Yamashita O, Galka A, Ozaki T, Biscay R, Valdés-Sosa P. Recursive penalized least squares solution for dynamical inverse problems of EEG generation. Human Brain Mapping 2004;21:221–35.

Żygierewicz J, Blinowska KJ, Durka PJ, Szelenberger W, Niemcewicz S, Androsiuk W. High resolution study of sleep spindles. Clin Neurophysiol 1999;110(12):2136–47.

Artículo 3.

Matysiak, A., Durka, P.J., Martínez-Montes, E., Barwiński, M., Zwoliński, P., Roszkowski, M., Blinowska, K.J.: Time-frequency-space localization of epileptic EEG oscillations. Acta Neurobiologiae Experimentalis 65, 4, 435-442 (2005).

ACTA NEUROBIOLOGIAE EXPERIMENTALIS

Acta Neurobiol Exp 2005, 65: 435-442

Time-frequency-space localization of epileptic EEG oscillations

Artur Matysiak[1], Piotr J. Durka[1], Eduardo Martinez Montes[2], Marek Barwiński[3,4], Piotr Zwoliński[5], Marcin Roszkowski[5], and **Katarzyna J. Blinowska[1]**

[1]Department of Biomedical Physics, Institute of Experimental Physics, Warsaw University, 69 Hoża St., 00–681 Warsaw, Poland; [2]Cuban Neuroscience Center, Ave 25 #15202 Esquina 158, Cubanacan, Playa, 11600 Havana, Cuba; [3]Institute of Neuroinformatics, Ruhr-University, Universitatsstrasse St 160, 44780 Bochum, Germany; [4]International Graduate School of Neuroscience, Ruhr-University, Universitatsstrasse St. 150, 44780 Bochum, Germany; [5]Department of Neurosurgery, Memorial Child Health Institute, 20 Dzieci Polskich St., 04–736 Warsaw, Poland

Abstract. This paper presents a hybrid method for localization of oscillatory EEG activity. It consists of two steps: multichannel matching pursuit with complex Gabor dictionary, and LORETA inverse solution. Proposed algorithm was successfully applied to the localization of epileptogenic EEG in a single patient.

The correspondence should be addressed to A. Matysiak, Email: amatys@fuw.edu.pl

Key words: EEG, multichannel matching pursuit, inverse solution, LORETA, epilepsy

INTRODUCTION

The essential task for an epileptologist is to localize the epileptic zone. Possible non-invasive and invasive EEG-derivate determination of electric pacemaker is then – in eligible cases – followed by resection of delineated zone. Any possibly reliable mathematical aids are thus very demandable to help in localizing procedures.

In line with these clinical and research needs, there is an increasing interest in the characterization – in time, frequency and space – of structures or activities from the electroencephalographic (EEG) traces (Konig et al. 2001, Miwakeichi et al. 2004). Despite some attempts in using truly multidimensional decomposition methods (Miwakeichi et al. 2004), still the most popular approach has been the combination of methods for bilinear decomposition in two of these dimensions and some other estimation procedure for characterization of the third dimension. Following the general idea proposed by Durka and coauthors (2005), in this study we implement a method based upon two following steps: (i) multichannel adaptive time-frequency parameterization of the EEG time series; (ii) EEG inverse solution.

For the first step we use a multichannel matching pursuit (mmp) (Gribonval 2003) applied to the (analytic) EEG signal, using a dictionary of complex Gabor atoms. The algorithm provides a set of complex weights for each electrode, which define a spatial distribution (topography) on the scalp for given complex atom. This topography is then subjected to source localization (second step), with the use of Low Resolution Electromagnetic Tomography (LORETA) (Pascual-Marqui et al. 1994). This instantaneous inverse solution provides a maximum smoothness for the distribution of primary current density (PCD) inside the brain. Performance of this hybrid algorithm is presented on an epileptic EEG signal from a single patient. Complex Gabor atoms were extracted from the mmp parameterization of the signal, based upon their time-frequency properties corresponding to epileptic oscillatory activity.

Different time-frequency-space localization procedures include e.g., the classical method, relying on spectral integrals (it was compared to the adaptive time-frequency preprocessing by Martinez-Montes and coauthors (2005)). Other method, presented by Geva (1998), uses an mmp algorithm similar to the implementation used in this work, but solves the inverse problem by a linear exhaustive search with sources constrained to a particular grid of the brain and supposed to be single or symmetrical pairs of current dipoles. Another kind of inverse solution, called Source Spectra Imaging (SSI), was used for finding the spectra of the current density distribution after obtaining topographic signatures from three-dimensional decomposition of the spontaneous EEG time-varying spectrum (Martinez-Montes et al. 2004, Miwakeichi et al. 2004).

There were also previous attempts to localize sources of epileptic activity. The method presented by Holmes and coauthors (2004) used LORETA inverse solution for spike components of each spike-wave burst. In this case use of LORETA needs heavy statistical postprocessing. Other method, presented by Worrell and coauthors (2000), used phase-encoded frequency spectral analysis (PEFSA) for characterizing time-frequency structures. It has similar properties as the mmp with complex Gabor dictionaries, but the inverse solution LORETA was done for real weights obtained by projection of the complex weights onto the best-fit line, and in this work we perform LORETA inverse solution for complex weights.

METHODS

Multichannel matching pursuit (mmp)

In this study, multichannel matching pursuit (mmp) procedure is applied to the analytic (Bracewell 1986) signal $\mathbf{S}^{H}_{Ne\times Nt} = \mathbf{S}_{Ne\times Nt} - iH(\mathbf{S}_{Ne\times Nt})$, where H denotes the Hilbert transform performed independently for every channel, and $\mathbf{S}_{Ne\times Nt}$ is the original, real-valued EEG. Mmp decomposes this signal into a linear sum of functions (time-frequency atoms), chosen adaptively from a redundant set called dictionary **D**. In the following we shall denote these atoms as MD Gabors, that is complex multidimensional Gabor functions. MD Gabor is a matrix $\mathbf{M}^{\gamma}_{Ne\times Nt}$ equal to the outer product of transposed vector of complex weights for each channel $W^{\gamma}_{Ne\times 1}$ and normalized 1D complex Gabor function $G^{\gamma}_{1\times Nt}$ (abbrev: 1D Gabor).

$$\mathbf{M}^{\gamma}_{Ne\times Nt} = W^{\gamma}_{Ne\times 1} G^{\gamma}_{1\times Nt} \tag{1}$$

1D Gabor G^{γ} can be characterized by three parameters: time position u, frequency position ω and duration σ,

and the index $\gamma=\{u, \omega, \sigma\}$ represents the set of those three parameters.

$$G^{\gamma}_{1\times Nt} = \frac{2^{1/4}}{\sqrt{\pi}} e^{\pi\frac{(t-u)^2}{\sigma^2}+it\omega} \tag{2}$$

The time is discrete $t = [\delta t...Nt\ \delta t]$. 1D Gabor is normalized i.e., $\|G^{\gamma}\|^2=1$. A complex weight w^{γ}_{e} is a scalar product between 1D Gabor $G^{\gamma}_{1\times Nt}$ and the signal in e^{th} channel $\mathbf{S}^{eH}_{1\times Nt}$.

$$w^{\gamma}_{e} =< S^{eH}, G^{\gamma *} >= \sum_{t=1}^{Nt} s^{eH}_{t} g^{\gamma *}_{t} \tag{3}$$

Finally, the mmp is an iterative procedure, working on the residua $R^{a+1}\mathbf{S}^{H}_{Ne\times Nt}$, left from the signal after substracting results of the previous a iterations. The signal itself is treated as the O^{th} residuum $R^{0}\mathbf{S}^{H}_{Ne\times Nt}$. In each step, the algorithm finds an MD Gabor $\mathbf{M}^{\gamma}_{Ne\times Nt}$, fitting best the residuum:

$$\begin{cases} R^0\mathbf{S}^H_{Ne\times Nt} &= \mathbf{S}^H_{Ne\times Nt} \\ \mathbf{M}^a_{Ne\times Nt} &= \arg\max_{\mathbf{M}^{\gamma}\in\mathbf{D}} \sum_{e=1}^{Ne} |< R^a S^{eH}_{Ne\times Nt}, G^{\gamma *}_{1\times Nt} >|^2 \\ R^{a+1}\mathbf{S}^H_{Ne\times Nt} &= R^a\mathbf{S}^H_{Ne\times Nt} - \mathbf{M}^a_{Ne\times Nt} \end{cases} \tag{4}$$

Linear multichannel decomposition obtained by mmp in matrix notation reads:

$$\mathbf{S}^H_{Ne\times Nt} = \mathbf{W}^T_{Na\times Ne}\mathbf{G}_{Na\times Nt} + R^{Na+1}\mathbf{S}^H_{Ne\times Nt} \tag{5}$$

The main difference between this implementation and the one presented in Durka and coauthors (2005) is that complex atom is now parameterized by only three parameters (time, frequency and duration), and the phase – possibly different in different channels – is contained in the complex weights.

The other difference is that the method presented by Durka and coauthors (2005) lacks exponential convergence properties presented by Mallat and Zhang (1993) and Gribonval (2003). On the other hand, it decays reasonably fast for multichannel EEG signal referenced to the linked ears or some other distant electrode, since in such references multichannel EEG signal tends to be composed of time-frequency structures with similar phases in different channels (Fig. 1). Also, numerical complexity of the algorithm proposed by Durka and coauthors (2005) is lower by a factor equal

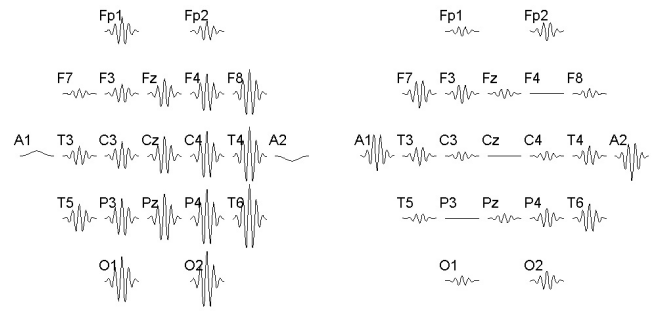

Fig. 1. Heuristic example of a possible EEG waveform, referenced to linked ears (left panel) and an electrode placed on the top of the skull (Cz, right panel). We observe that Cz reference introduces frequency structures in opposite phases in derivations from left/frontal and right/parietal locations.

to number of channels, compared to mmp presented by Gribonval (2003). In this study we use a structured redundant dictionary, that is with given time shift and frequency shift between consecutive Gabor atoms. Time width of all Gabor atoms in the dictionary was constant. The time shift and frequency shift were set to not exceed the value implied by the uncertainty principle.

Low resolution electromagnetic tomography (LORETA)

The standard time-domain EEG forward solution linearly relates scalp multichannel EEG time series $\mathbf{S}_{Ne\times Nt}$ and the primary current density (PCD) time series $\mathbf{J}_{3Nv\times Nt}$. This relation can be written for $\mathbf{S}^H$ and $\mathbf{J}^H = \mathbf{J}\text{-}i\mathcal{H}(\mathbf{J})$

$$\mathbf{S}^H_{Ne\times Nt} = \mathbf{K}_{Ne\times 3Nv}\mathbf{J}^H_{3Nv\times Nt} + \mathbf{E}^H_{Ne\times Nt} \tag{6}$$

where the rows of matrix $\mathbf{J}^H$ correspond to thrice the number of voxel elements $3Nv$, corresponding to the x, y and z components of the PCD vector in each voxel of a grid defined inside the brain, and columns correspond to time samples. The real matrix $\mathbf{K}$, linking the current density with the measurements, is called the lead field matrix and does not depend on time and frequency. It can be calculated by applying Maxwell's equations to a particular head model (Riera and Fuentes 1997). The matrix $\mathbf{E}$ is an additive random element representing unmodeled effects such as the observation noise.

The EEG inverse problem is defined as the estimation of current density time series $\mathbf{J}^H$ from EEG time series $\mathbf{S}^H$ independently for every time point. Mathematically, it is an ill-conditioned (sensitive to noise) and ill-posed problem (non-uniqueness), so additional constraints are required for finding the so-called "inverse solution".

There are several approaches for mathematically solving the problem from Eq. 6. The use of Tikhonov regularization (Tikhonov and Arsenin 1977) and a Bayesian approach (Trujillo-Barreto et al. 2004) have been the most popular. Furthermore, different constraints and prior information about the solution can lead to a different inverse solution. Yet, there is not a "best" inverse solution. However, due to its simple implementation, low computational cost and generally good properties in terms of localization error (Pascual-Marqui et al. 1994), LORETA is the most popular among the distributed inverse solutions.

LORETA assumes that PCD values in neighboring voxels must be similar based on the usually higher interconnectivity of near neurons. This implies the choice of the smoothest distribution of the PCD inside the brain. On the other hand, LORETA does not assume any dependency between different time points, so it is an instantaneous inverse solution.

With the approach used here, we assume that the PCD follows the dynamics of the EEG, since the lead field only affects the spatial dimension. Then, the topographies, defined by the mmp algorithm as corresponding to EEG structures with determined time-frequency properties, can be used as the input of instantaneous inverse solution. This can be seen in another way by comparing Eq. 5 and 6 and establishing the relation between topographies **W** and the PCD signature **J'** for corresponding MD Gabors.

$$\mathbf{W}^{H}_{Ne\times Na} = \mathbf{K}_{Ne\times 3Nv}\mathbf{J}'^{H}_{3Nv\times Nt} + \mathbf{E}'^{H}_{Ne\times Nt} \tag{7}$$

As the input for Eq. 7 consist of complex coefficients, the PCD will also be complex. However, given the properties of the Hilbert transform (Bracewell 1986), the real part of this magnitude will be the real electric current defining localization of the sources of the time-frequency structures represented by MD Gabor.

Experimental data

We present a case of 7 year-old patient, M.K., female, suffering from epilepsy since 3 years. Her seizures started with unilateral simple motor seizures (IA class of the ILAE classification) involving upper part of face (periocular muscles, twitches of eyes) and upper extremity (also twitches, mostly proximal arm). She developed also partial complex fits after some time, seizures soon occurred in clusters, presenting form of Kojevnikov epilepsy (epilepsia partialis continua) lasting for weeks, sometimes months. Various antiepileptic drugs (AED) were not effective, she developed resistance to all conventional and newer AED very soon.

In the following MRI scans we have found slowly progressing characteristic signal of inflammatory process starting within periinsular region of left hemisphere, typical (considering clinical picture) for Rassmusen syndrome (RS), which was the final diagnosis. EEG was always abnormal – however, the picture showed mild generalized pathology (slow waves) of background activity, and occasional ictal discharges of spikes and/or sharp waves in left hemisphere, mostly in centro-frontal region. She has had a lot of AED changes (with no effect at all), she was operated 3 times: first operation was an anterior callosotomy (tractotomy resection of the 2/3 anterior part of the corpus callosum), second was the implantation of NCP-102 vagal nerve neurostimulator, which was set to stimulate intermittently cervical portion of vagal neve (VNS therapy, used in epilepsy treatment since 1997). Both operation failed, we had not achieved any seizure reduction. Typical surgical solution in such cases is hemispherotomy (total disconnection of the whole hemisphere – in this case left), however the procedure is very brutal, resulting of the contralateral hemiplegia, and in this case (left, dominant hemisphere) loss of speech. All those functions were not significantly disturbed, despite some mild Todd paresis after series of seizures. Girl also had very mild mental deterioration, which is typical in RS.

Therefore we decided to make selective resection (third operation) EcoG guided. After wide opening of the left hemisphere skull bone in modification of Yassargil mode we have performed the first ECoG which showed very frequent and marked discharges of spikes and spike-wave complexes within the frontal region (mostly middle and upper frontal gyrus), with spread of discharges to temporal lobe, parietal lobe (postcentral gyrus and even more rostral); after inspection of the temporal lobe we have also found some discharges from deep meso-limbic structures. We decide to resect the 3–4 cm of the temporal lobe (from the tip) with resection of deep structures, as well as the multi-

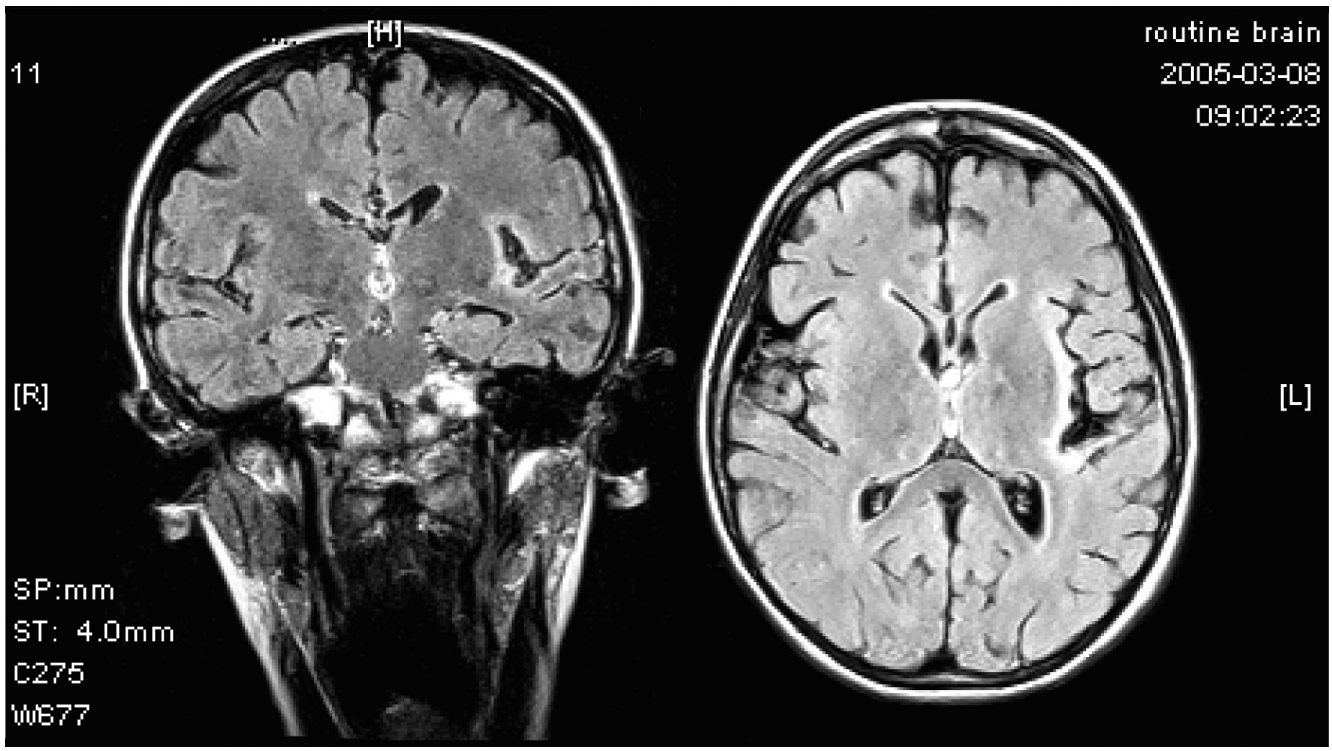

Fig. 2. MRI picture of the periinsular focal abnormality.

focal MST (Multifocal Subpial Transsections) sections of those regions of the hemisphere which shows discharges after the resection. We have ended the operation with almost silent trace of the EEG curve in ECoG. After the operation the girl still has some twitches of the upper part of the face, however seizures are mild and shorter. She does not experiences cluster seizures or status epilepticus.

We assume that progressing character of the RS may come to a stage that hemispherotomy may be the only possible treatment, however – some cases of RS show no such progress.

Software

The mmp implementation uses analytic formula for inner product computations and FFT. The LORETA implementation was developed at Cuban Neuroscience Center and uses three-spherical head model and lead field as defined by Riera and Fuentes (1997).

Both mmp and LORETA used in this study were written in Matlab. They can be downloaded from the EEG.pl portal (http://eeg.pl, Section ”software”). As the inverse solution visualization tool we used BetViewer developed at Cuban Neuroscience Center.

RESULTS

The two-step procedure described in Methods section was applied to EEG signal recorded during epileptic attack of a patient described in Experimantal data section. The epoch length was 8 s and sampling frequency was 256 Hz. The signal was digitally filtered with band pass Butterworth filter (between 1.6 Hz and 40 Hz) in forward and reverse directions. Then it was referenced to the average reference. The redundant dictionary **D** used for mmp decomposition consisted of shifted – in time and frequency – versions of 1D Gabor with one scale s=0.25 s. Time shift was set as Δt=0.125 s, and frequency shift Δf=0.25 Hz.

Inverse solution was found with a version of LORETA algorithm implemented by Cuban Neuroscience Center. This implementation of LORETA is based upon singular value decomposition of the electric lead field for three homogenous concentric spheres model (Riera and Fuentes 1997), previously standardized by the discrete Laplacian operator. The equation for the solution stems from the minimization of the classical LORETA functional and the optimal regularization parameter is found by generalized

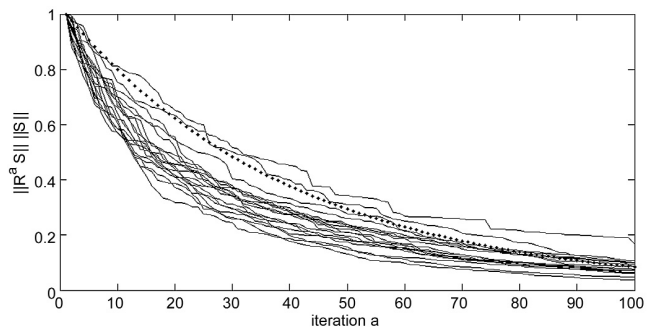

Fig. 3. Signal residuum norm decay for all channels (solid lines) and decay exponential function defined (dotted).

cross-validation technique, although it can be easily modified to maximize any other criteria, such as Akaike Information Criteria, Bayesian Information Criteria, and others.

Figure 3 presents decay of signal residuum's energy for all channels and the plot of a decay exponential function, defined as *EXP(a) = exp(-a/factor)*, where *factor* is chosen such as $EXP(Na) = ||R^{Na}\boldsymbol{S}^{ini}||$. It can be observed that residua decay faster than the corresponding exponential decay function for all but two channels above 50 iterations.

Top panel of Fig. 4 presents the considered EEG signal and a real part of the signal reconstructed from time-frequency atoms (MD Gabors) that were chosen as the epileptic ones. Middle panel presents schematic spatio-time-frequency map obtained for chosen atoms i.e., topographies of absolute values of complex weights are plotted in the corresponding points in the time-frequency plane for every chosen atom. Lower panel 4 presents schematic complex topographies for 8 time-frequency atoms, that is besides topography for given time-frequency atom (as in the middle plot) it shows also phases of complex weights as normalized vectors hooked in the middle of given topography area.

Resulting localization of the generators of chosen time-frequency structures are presented on Fig. 5. Norms of PCD vectors for these structures exhibit consistent activity in the middle and upper frontal gyrus part of the brain. It can be also seen that the PCD vectors flow parallel to the scalp between typical positions of electrode F3 and T5 (Fig. 5). This can be also concluded from the complex topography map of given time-frequency structure (lower panel of Fig. 3) – activity in electrodes F3 and T5 are high but in nearly opposite phases.

DISCUSSION

In described case, patient was operated – she had temporal lobectomy complemented by a multiple subpial transsection (MST) in Morell mode (multiple cuts of the grey matter of hemisphere, disconnecting conjuctions between neurons, done under pia mater). The resection was delineated by electrocorticography (ECoG) which showed broad area of epileptic discharges, mainly in temporal/frontal border, temporal lobe and some parts of parietal lobe. The area of discharges corresponded to the one delineated from the scalp EEG using the procedure presented in this paper. Due to the fact, that some areas of discharges were placed in eloquent zones of brain, only partial lobectomy could be done (Spencer mode topectomy of temporal lobe–resection of the tip of temporal lobe, approx. 3 cm from the pole and resection of deep structures of the temporal lobe); MST method was performed to cut the pathways between the areas that could not be resected. This case shows a desired concordance of the presented mmp/LORETA source localization from interictal scalp EEG discharge areas of ictal discharges seen while performing ECoG.

Despite these promising results it should be stated that our methodology inherits the drawbacks of LORETA inverse solution, as discussed widely in the literature (Pascual-Marqui et al. 1994, Trujillo-Barreto et al. 2004). However it has been shown that the use of a proper time-frequency modeling of the EEG signals can lead to more robust results with the same inverse solution, showing reliable sources even in the absence of a heavy statistical postprocessing of the solutions (Konig at al. 2001).

These results also open different ways to improve performance of this kind of methods. First of all other implementations of multichannel matching pursuit can be used with different dictionaries and different choice of the best atom in each iteration. On the other hand, improvements from the inverse solution point of view can be also achieved, since it is well known that LORETA is really useful only in those cases in which wide areas of the cortex are strongly activated. Likewise, it is almost impossible to recover sources in deep areas such as thalamic and brainstem activations, which are usually reflected in more cortical (but non activated) areas like insulas for example. In this sense the use of other kind of

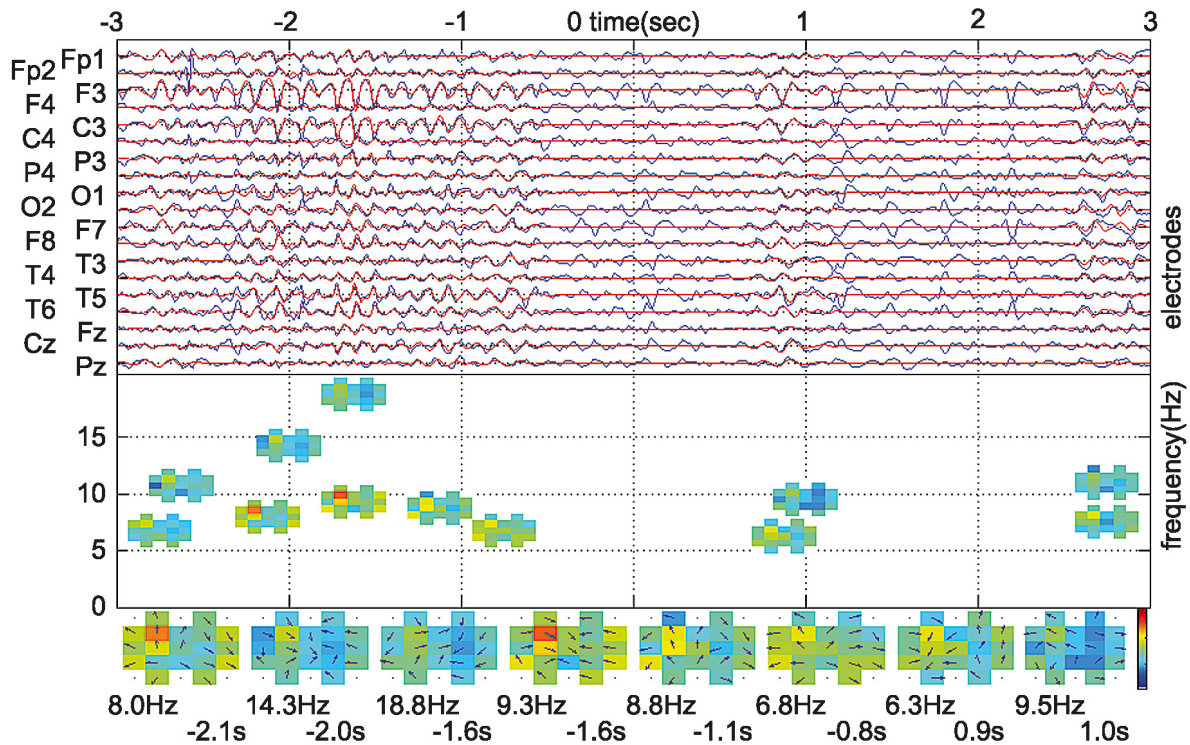

Fig. 4. Top: filtered EEG signal (blue) and real part of signal constructed from time-frequency atoms chosen as epileptic ones (red). Middle: schematic spatio-time-frequency map for chosen atoms. Bottom: schematic complex topographies (amplitudes denoted by colors, phases by arrows) for 8 time-frequency atoms (front of the head upwards).

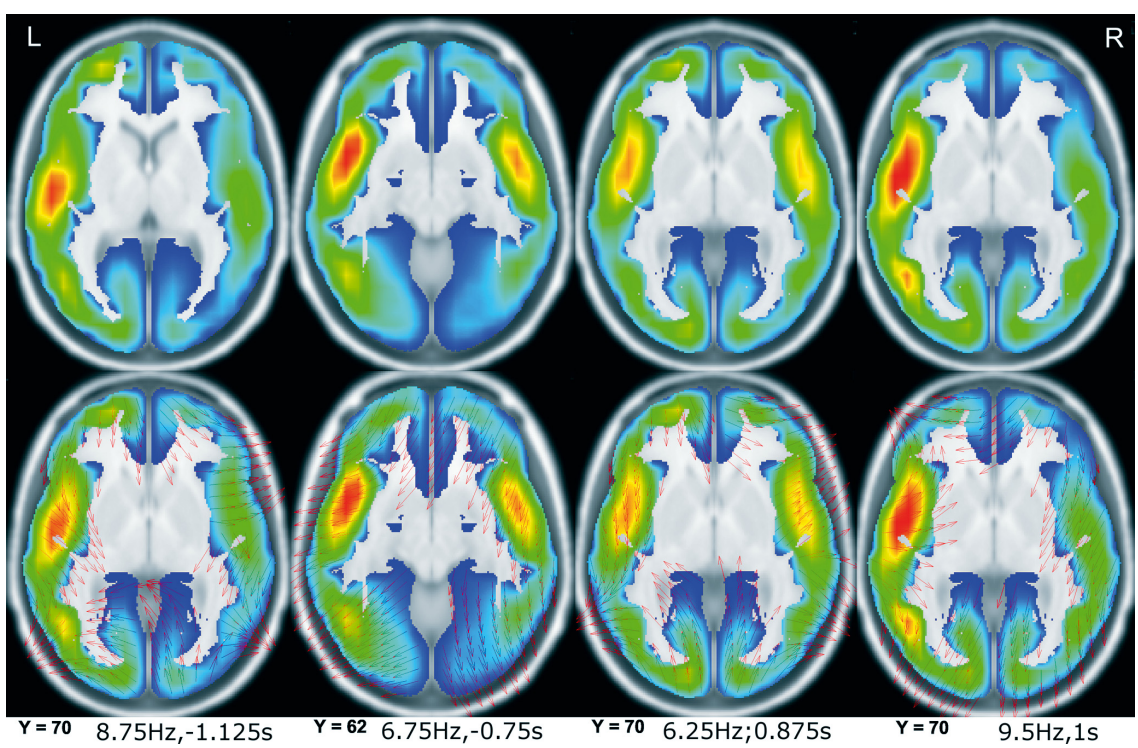

Fig. 5. Norm and normalized directions of the real part of PCD vectors for four time-frequency atoms from Fig. 4 (visualized in BetViewer, developed in Cuban Neuroscience Center, see Software section).

instantaneous inverse solutions based on Bayesian Theory (Trujillo-Barreto et al. 2004) can improve the localization task. Finally, within the same paradigm other EEG inverse solution methods can be used in place of LORETA.

CONCLUSIONS

This work presents the application of a new methodology to the 3D localization of sources of epileptic activity in the brain, based on that introduced in Durka and coauthors (2005). Novelty of the proposed approach consists of using complex Gabor atoms. Its application to a case study demonstrated the desired correspondence between sources obtained by our methodology and those determined by ECoG in surgery. It also showed its ability of recognizing several mixed sources.

REFERENCES

Bracewell RN (1986) The Fourier transform and its applications. McGraw-Hill Book Company.

Durka PJ, Matysiak A, Martinez Montes E, Valdes Sosa P, Blinowska KJ (2005) Multichannel matching pursuit and EEG inverse solutions. J Neurosci Methods 148: 49–59.

Geva AB (1998) Biolectric sources estimation using spatio-temporal matching pursuit. J Applied Signal Proc 5: 195–208.

Gribonval R (2003) Piecewise linear source separation. Proceedings of the SPIE 5207: 297–310.

Holmes MD, Brown M, Tucker DM (2004) Are ”generalized” seizures truly generalized? Evidence of localized mesial frontal and frontopolar discharges in absence. Epilepsia 45: 1568–1579.

Konig T, Marti-Lopez F, Valdes-Sosa P (2001) Topographic time-frequency decomposition of the EEG. Neuroimage 14: 383–390.

Mallat S, Zhang Z (1993) Matching pursuit with time-frequency dictionaries. IEEE Transactions on Signal Processing 41: 3397–3415.

Martinez-Montes E, Valdes-Sosa P, Miwakeichi F, Goldman RI, Cohen MS (2004) Concurrent EEG/fMRI analysis by multi-way partial least squares. Neuroimage 22: 1023–1034.

Martinez-Montes E, Bosch-Bayard J, Matysiak A, Durka P, Rodriguez-Puentes Y (2005) Adaptive time-frequency approximations vs. spectral integrals as preprocessing for EEG inverse solutions [abstract]. Proceedings of the 11th Annual Meeting of the Organization for Human Brain Mapping (available on CD-Rom in Neuroimage, Vol. 26, No.1).

Miwakeichi F, Martinez-Montes E, Valdes-Sosa P, Nishiyama N, Hiroaki M, Yamaguchi Y (2004) Decomposing EEG data into space-time-frequency components using parallel factor analysis. Neuroimage 22: 1035–1045.

Pascual-Marqui RD, Michel CM, Lehman D (1994) Low resolution electromagnetic tomography: A new method to localize electrical activity in the brain. Int J Psychophysiol 18: 49–65.

Riera J, Fuentes ME (1997) Electric lead field for a piecewise homogeneous volume conductor model of the head. IEEE Trans Biomed Eng 45: 746–753.

Tikhonov AN, Arsenin VY (1997) Solutions of Ill-Posed Problems. W.H. Winston, Washington DC.

Trujillo-Barreto NJ, Aubert E, Valdes-Sosa PA (2004) Bayesian model averaging in EEG/MEG imaging. Neuroimage 21: 1300–1319.

Worrell GA, Lagerlund TD, Sharbrough FW, Brinkmann BH, Busacker NE, Cicora KM, O’Brien TJ (2000) Localization of the epileptic focus by low-resolution electromagnetic tomography in patients with a lesion demonstrated by MRI. Brain Topogr 12: 273–82.

Received 1 July 2005, accepted 21 October 2005

Artículo 4.

Miwakeichi, F., Martínez-Montes, E., Valdés-Sosa, P.A., Nishiyama, N., Mizuhara, H., Yamaguchi, Y.: Decomposing EEG data into Space-Time-Frequency Components using Parallel Factor Analysis. Neuroimage 22, 3, 1035-1045 (2004).

ELSEVIER

NeuroImage

www.elsevier.com/locate/ynimg
NeuroImage 22 (2004) 1035–1045

Decomposing EEG data into space–time–frequency components using Parallel Factor Analysis

Fumikazu Miwakeichi,[a,*] Eduardo Martínez-Montes,[b] Pedro A. Valdés-Sosa,[b] Nobuaki Nishiyama,[a] Hiroaki Mizuhara,[a] and Yoko Yamaguchi[a]

[a] *Laboratory for Dynamics of Emergent Intelligence, RIKEN Brain Science Institute, Saitama 351-0198, Japan*
[b] *Neuroscience Department, Cuban Neuroscience Center, Habana, Cuba*

Received 17 July 2003; revised 12 March 2004; accepted 17 March 2004

Finding the means to efficiently summarize electroencephalographic data has been a long-standing problem in electrophysiology. A popular approach is identification of component modes on the basis of the time-varying spectrum of multichannel EEG recordings—in other words, a space/frequency/time atomic decomposition of the time-varying EEG spectrum. Previous work has been limited to only two of these dimensions. Principal Component Analysis (PCA) and Independent Component Analysis (ICA) have been used to create space/time decompositions; suffering an inherent lack of uniqueness that is overcome only by imposing constraints of orthogonality or independence of atoms. Conventional frequency/time decompositions ignore the spatial aspects of the EEG. Framing of the data being as a three-way array indexed by channel, frequency, and time allows the application of a unique decomposition that is known as Parallel Factor Analysis (PARAFAC). Each atom is the tri-linear decomposition into a spatial, spectral, and temporal signature. We applied this decomposition to the EEG recordings of five subjects during the resting state and during mental arithmetic. Common to all subjects were two atoms with spectral signatures whose peaks were in the theta and alpha range. These signatures were modulated by physiological state, increasing during the resting stage for alpha and during mental arithmetic for theta. Furthermore, we describe a new method (Source Spectra Imaging or SSI) to estimate the location of electric current sources from the EEG spectrum. The topography of the theta atom is frontal and the maximum of the corresponding SSI solution is in the anterior frontal cortex. The topography of the alpha atom is occipital with maximum of the SSI solution in the visual cortex. We show that the proposed decomposition can be used to search for activity with a given spectral and topographic profile in new recordings, and that the method may be useful for artifact recognition and removal.

Keywords: Parallel Factor Analysis; EEG space/frequency/time decomposition; Principal Component Analysis; Multiway analysis; Source Spectra Imaging

Introduction

The electroencephalogram (EEG) is the reflection upon the scalp of the summed synaptic potentials of millions of neurons (Lopes da Silva, 1987). Most investigators agree (Lachaux et al., 1999; Varela et al., 2001) that these neurons self-organize into transient networks (“neural masses”) that synchronize in time and space to produce a mixture of short bursts of oscillations that are observable in the EEG record. A statistical description of the oscillatory phenomena of the EEG was carried out first in the frequency domain (Lopes da Silva, 1987) by estimation of the power spectrum for quasi-stationary segments of data. More recent characterizations of transient oscillations are carried out by estimation of the time-varying (or evolutionary) spectrum in the frequency/time domain (Dahlhaus, 1997). These evolutionary spectra of EEG oscillations will have a topographic distribution on the sensors that is contingent on the spatial configuration of the neural sources that generate them as well as the properties of the head as a volume conductor (Nunez, 1993).

The purpose of the present study was to attempt the decomposition of multichannel time-varying EEG spectrum into a series of distinct components or modes. In the parlance of modern harmonic analysis (Chen and Donoho, 2001), we performed a space/frequency/time “atomic decomposition” of multidimensional data. In other words, we assume that each neural mass contributes a distinctive atom to the topographic frequency/time description of the EEG, so that the estimation of these atoms is possible by means of signal-processing techniques. Each atom will be defined by its topography, spectral content, and time profile; in other words, by its spatial, spectral, and temporal signatures. We expect that these extracted atoms ultimately will allow the identification of the corresponding neural masses that produce them.

There is a long history of atomic decompositions for the EEG. However, to date, atoms have not been defined by the triplet spatial, spectral, and temporal signatures but rather pairwise combinations of these components. Some of the current procedures for these analyses are reviewed below.

Space/time atoms: PCA and ICA

Space/time atoms are the basis of both Principal Component Analysis (PCA) and Independent Component Analysis (ICA) as

* Corresponding author. Laboratory for Dynamics of Emergent Intelligence, RIKEN Brain Science Institute, 2-1 Hirosawa, Wako, Saitama 351-0198, Japan. Fax: +81-48-467-6938.
E-mail address: miwakel@brain.riken.go.jp (F. Miwakeichi).
Available online on ScienceDirect (www.sciencedirect.com.)

1053-8119/$ - see front matter © 2004 Elsevier Inc. All rights reserved.
doi:10.1016/j.neuroimage.2004.03.039

applied to multichannel EEG. PCA has been used for artifact removal and to extract significant activities in the EEG (Lagerlund et al., 1997; Soong and Koles, 1995). A basic problem is that atoms defined by only two signatures (space and time) are not determined uniquely. In PCA, orthogonality is therefore imposed between the corresponding signatures of different atoms. This, however, is a rather nonphysiological constraint. Even with this restriction, there is the well-known nonuniqueness of PCA that allows the arbitrary choice of rotation of axes (e.g., Varimax and Quartimax rotations). More recently, ICA has become a popular tool for space/time atomic decomposition (Cichocki and Amari, 2002; Hyvarinen et al., 2001). It avoids the arbitrary choice of rotation (Jung et al., 2001). Uniqueness, however, is achieved at the price of imposing a constraint even stronger than orthogonality, namely, statistical independence. In both PCA and ICA, the frequency information may be obtained from the temporal signature of the extracted atoms in a separate step.

Frequency/time atoms: wavelet analysis

There are many papers on the decomposition of single-channel EEG into frequency/time atoms. For this purpose, the Fast Fourier Transformation (FFT) with sliding window (Makeig, 1993) or the wavelet transformation (Bertrand et al., 1994; Tallon-Baudry et al., 1997) have been employed. In fact, any of the frequency/time atomic decompositions currently available (Chen and Donoho, 2001) could, in principle, be used for the EEG. However, these methods do not address the topographic aspects of the EEG time/frequency analysis.

Space/frequency/time atoms: PARAFAC

Gonzalez Andino et al. (2001) improved previous analyses by analyzing regions of the frequency/time plane where a single dipole model is an adequate spatial description of the signal, thus incorporating topographic information. Topographic frequency/time decomposition of the EEG was introduced by Koenig et al. (2001), which is the first work to estimate atoms characterized simultaneously by a frequency/time and spatial signature. In their analyses, it was possible to extract physiologically significant activity in the EEG. However, in order to achieve a unique decomposition, they imposed the mathematical constraints that the combined frequency/time signatures of all atoms were required to be of minimum norm and the spatial or topographic signatures were required to have maximal smoothness. These constraints have been found to be unnecessary for unique topographic time/frequency decomposition, a fact that has motivated the work described in this paper.

It has long been known, especially in the chemometrics literature, that unique multi-linear decompositions of multi-way arrays of data (more than two dimensions) are possible under very weak conditions (Sidiropoulos and Bro, 2000). In fact, this is the basic argument for Parallel Factor Analysis (PARAFAC). This technique was proposed independently by Harshman (1970, 1972) and by Carroll and Chang (1970) who named the model Canonical Decomposition, and recently has been improved by Bro (1998) who also provided a Matlab toolbox (available as of this writing at: http://www.models.kvl.dk/users/rasmus/). In PARAFAC, for three-way arrays, the data is decomposed as a sum of components (corresponding to our "atoms"), each of which is the tri-linear product of one score vector and two loading vectors (corresponding to our "signatures"). The important difference between PARAFAC and techniques such as PCA or ICA is that the decomposition of multi-way data is unique even without additional orthogonality or independence constraints.

Thus, PARAFAC can be employed for a space/frequency/time atomic decomposition of the EEG. This makes use of the fact that multichannel evolutionary spectra are multi-way arrays, indexed by electrode, frequency, and time. The inherent uniqueness of the PARAFAC solution leads to a topographic time/frequency decomposition with a minimum of *a priori* assumptions.

Here, we use PARAFAC for the purpose of simultaneous space/frequency/time decompositions. Previous applications of PARAFAC to EEG data have analyzed only space/time, and some additional external dimensions provided by subject and drug dose, among other factors (Achim and Bouchard, 1997; Estienne et al., 2001; Field and Graupe, 1991). A special interpretation of this model is also the Topographic Components Model (TCM) (Möcks, 1988a,b), which gives justification for the PARAFAC model in the context of evoked potentials analysis, based on biophysical considerations (Möcks, 1988b). In this field, a relevant proof of the use of TCM over PCA using only synthetic noiseless data was given in Achim and Bouchard (1997).

To illustrate the usefulness of PARAFAC, we applied the decomposition of time-varying EEG spectrum to the comparison of resting EEG to that recorded while the subject performed mental arithmetic. Mental arithmetic produces theta activity in the frontal area and a suppression of alpha activity in the occipital area, while the converse occurs when the eyes are closed in the resting condition (Harmony et al., 1999; Ishihara and Yoshii, 1972; Sasaki et al., 1996). The PARAFAC atomic decomposition should be able to extract these components, localize them correctly, and detect the corresponding level of activity in these bands in each physiological state. Once estimated, the spatial and spectral signatures of the identified atoms may be used to search for similar types of activity in new data sets. Here, this procedure will be called "screening" for the presence of an atom.

Our focus is on space/time/frequency decompositions tailored to the description of oscillatory phenomena. These are not the only interesting phenomena in the EEG, transient activity being another example. The methods described in this paper may be generalized to this application by exchanging the basic dictionary that describes oscillations.

This paper is organized as follows. We first describe the experimental methods. Then, we consider the basic theoretical development of the space/frequency/time atomic decomposition

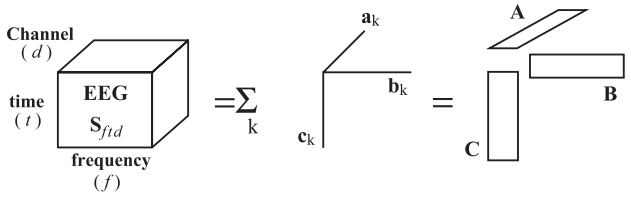

Fig. 1. Graphical explanation of the PARAFAC model. The multichannel EEG evolutionary spectrum **S** is obtained from a channel by channel wavelet transform. **S** is a three-way data array indicated by channel, frequency, and time. PARAFAC decomposes this array into the sum of "atoms". The *k*th atom is the tri-linear product of loading vectors representing spatial ($\mathbf{a}_k$), spectral ($\mathbf{b}_k$), and temporal ($\mathbf{c}_k$) "signatures". Under these conditions, PARAFAC can be summarized as finding the matrices $\mathbf{A} = \{\mathbf{a}_k\}$, $\mathbf{B} = \{\mathbf{b}_k\}$, and $\mathbf{C} = (\mathbf{c}_k)$, which explain **S** with minimal residual error.

and the use of estimated factors to screen for activity in new data segments. The results and discussion follow.

Methods

Data acquisition

Five male right-handed subjects (mean age 25.8 ± 3.96 years) that produced clear theta activities during a mental task were studied in this work. All subjects signed an informed consent form approved by the RIKEN Human Subject Protection Committee before EEG recording. All subjects were required to concentrate, for 3 min, on mental arithmetic (subtraction by serial 7 from 1000) with closed eyes. They were asked the final residual number at the end of the task. The resting EEG with closed eyes was also recorded for comparison. During the recording, we provided no visual nor auditory stimulation for the subjects.

EEG recordings were carried out with a standard 64-channel system (NeuroScan Syn Amps Model 5083) referred to linked earlobes. The EEG data were sampled at 500 Hz and bandpass filtered from 1 to 30 Hz.

Theory

In our application to EEG data, the data matrix $\mathbf{S}_{(N_d \times N_f \times N_t)}$ is the three-way time-varying EEG spectrum array obtained by using the wavelet transformation, where N_d, N_f, and N_t are the number of channels, steps of frequency, and time points, respectively. For the wavelet transformation, a complex Morlet mother function was used (Jensen and Tesche, 2002; Kronland-Martinet and Morlet, 1987; Tallon-Baudry et al., 1997). The energy $S(d,f,t)$ of the channel d at frequency f and time t is given by the squared norm of the convolution of a Morlet wavelet with the EEG signal $v(d,t)$

$$S(d,f,t) = |w(t,f)^{*}v(d,t)|^{2}, \tag{1}$$

where the complex Morlet wavelet, $w(t,f)$ is defined by $w(t,f) = \sqrt{\pi}\sigma_b exp\left(-\left(\frac{t}{\sigma_b}\right)^2\right) * exp(i2\pi ft)$ with σ_b being the-

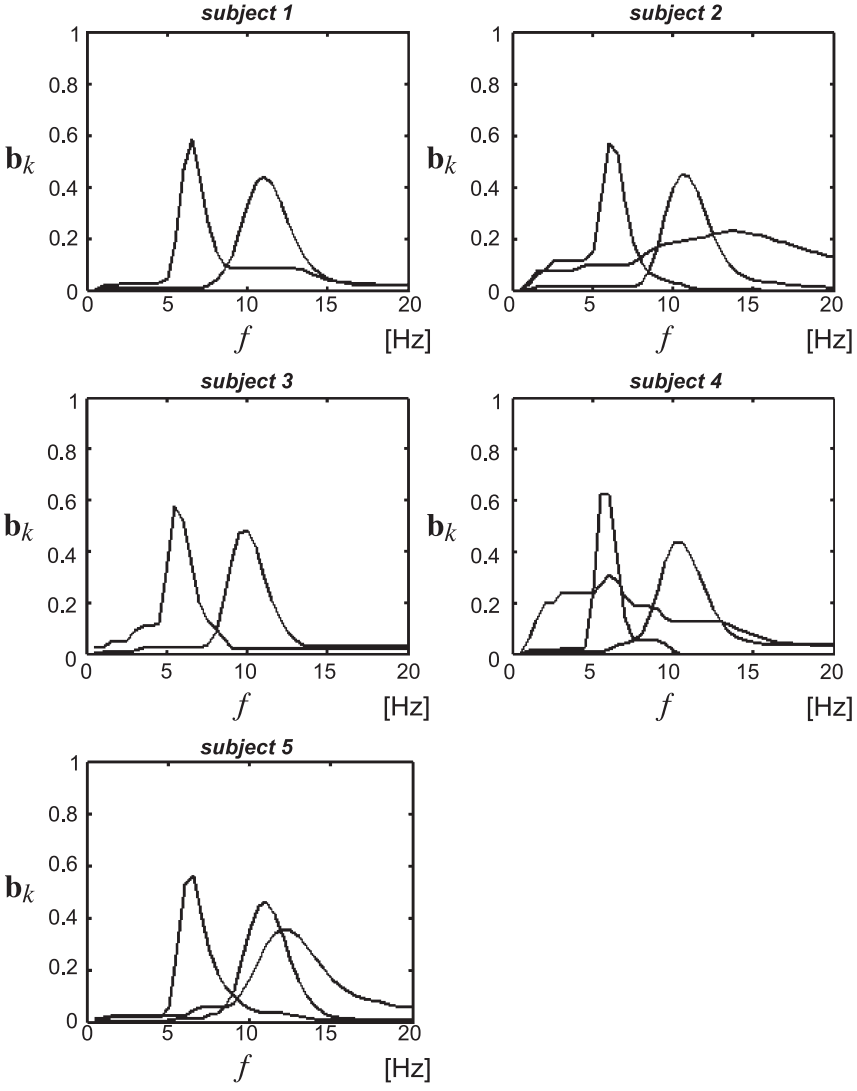

Fig. 2. Spectral signature $\mathbf{b}_k$ of atoms of Parallel Factor Analysis (PARAFAC) for each subject. Note the recurrent appearance of frequency peaks in the theta and alpha bands. The horizontal axis is frequency in Hz and the vertical axis is the normalized amplitude.

bandwidth parameter. The width of the wavelet, $m = 2\pi\sigma_b f$ is set to 7 in this study.

We closely follow here the detailed description of PARAFAC found in Bro (1998). The basic structural model for a PARAFAC decomposition of the data matrix $\mathbf{S}_{(N_d \times N_f \times N_t)}$ of elements S_{dft} is defined as:

$$\hat{S}_{dft} = \sum_{k=1}^{N_k} a_{dk} b_{fk} c_{tk} \tag{2}$$

The problem is to find the loading matrices, **A**, **B** and **C**, whose elements are a_{dk}, b_{fk}, and c_{tk}. In our application, each component k will be designated as an "atom" and the corresponding vectors $\mathbf{a}_k = \{a_{dk}\}$, $\mathbf{b}_k = \{b_{fk}\}$, $\mathbf{c}_k = \{c_{tk}\}$ will be the spatial, spectral, and temporal signatures of each atom (Fig. 1). The uniqueness of the solution is guaranteed when rank **(A)** + rank **(B)** + rank **(C)** $\geq 2N_k + 2$. As can be seen, this is a less-stringent condition than either orthogonality or statistical independence (Sidiropoulos and Bro, 2000). The decomposition (Eq. (2)) is achieved by finding $\min_{a_{dk} b_{fk} c_{tk}} \|\hat{S}_{dft} - \sum_{k=1}^{N_k} a_{dk}\ b_{fk}\ c_{tk}\|$. Since the $\hat{S}_{dft}$ are spectra, this minimization must be carried out under the non-negativity constraint for the loading vectors. This particular variant of PARAFAC has been developed by Bro (1998). PARAFAC produces the vectors $\mathbf{a}_{k(N_d \times 1)}$, which is the kth component loading vector that can be seen as topographical maps, $\mathbf{b}_{k(N_f \times 1)}$ is the spectrum for kth component and $\mathbf{c}_{k(N_t \times 1)}$ is the temporal signature for component k.

The main advantage of this method is that it provides us with a unique decomposition of the time-varying EEG spectrum corresponding to the best model in the least-squares sense. The only indeterminacy in the least-square solution is the order of the atoms and the relative scaling of the signatures. On the other hand, it has also been proved that if the data is approximately tri-linear, then the algorithm will show the true underlying phenomena, if the correct number of components is used and if the signal-to-noise ratio is appropriate (Harshman, 1972; Kruskal, 1976, 1997).

An important point is the selection of the most appropriate number N_k of components. Several methods have been developed for this purpose only (Bro, 1998). The Core Consistency Diagnostic (Corcondia) is an approach that applies especially to PARAFAC models, and has been shown to be a powerful and simple tool for determining the appropriate number of components in multiway models. In this work, we will use not only Corcondia but also the evaluation of systematic variation left in the residuals of the model.

Validation of the method

As described by Harshman (1984) and Bro (1998), the validation of a particular analysis can be seen as part of the analysis itself and can be divided into levels: zero-fit diagnostics (related to data before fitting any model, selection of proper model); one-fit diagnostics (validate the consistency of the model applied); many-fit diagnostics (comparisons between different models, use of statistical inferences on the results). Given some general considerations of the PARAFAC modeling of the time-varying EEG spectrum, we shall make a deeper analysis of the appropriateness of this procedure following these levels and the general guidelines for validating the application of multi-way models given in Bro (1998).

The usual way to assess the multiway (three-way in this case) nature of the data in study is the exploration of results provided by bi-linear analysis of the data. In particular, the application of PCA to the unfolded three-way array will provide a matrix of loadings in which a global behavior can be detected, indicating the existence of dimensional structure in the explored dimensions. For data similar to those treated here, this is clearly shown in Estienne et al. (2001), and with a more complete analysis in Field and Graupe (1991). Another way of assessing the tri-linear structure of the data is by means of the Core Consistency Diagnostic (Corcondia) (Bro, 1998; Estienne et al., 2001). This is a tool provided automatically in the implementation of PARAFAC and other related multi-way algorithms contained in the Matlab Toolbox used here. Corcondia was utilized for successfully demonstrating the presence of multiway structure in our data.

In this work, we have chosen PARAFAC among several multiway models, (e.g., PARAFAC2, PARATUCK2, TUCKER1, TUCKER3) (Bro, 1998). This is an application of Occam's razor as PARAFAC is the simplest and most restricted model. As we only consider it in our analysis, whether other versions of PARAFAC or TUCKER models can give better results in terms of explanation of the systematic variation of the data and interpretability of the results remains an open question.

On the other hand, other drawbacks of the application of PARAFAC model include the need for careful preprocessing of the data and for checking residuals, leverages and other parameters in the search of constant factors, outliers, and degeneracy. We do not detail these problems here, as such analyses appear in the literature, e.g., exhaustive ways of exploring degeneracy and model mis-specifications can be found in Field and Graupe (1991). The Matlab Toolbox used here provided us of these tools for many-fit diagnostics (residuals, leverages, Corcondia, convergence, explained variation).

What is missing in the present study is a rigorous analysis of the uniqueness of the model in our case, but it is well-known that through the use of PARAFAC, uniqueness is almost always present.

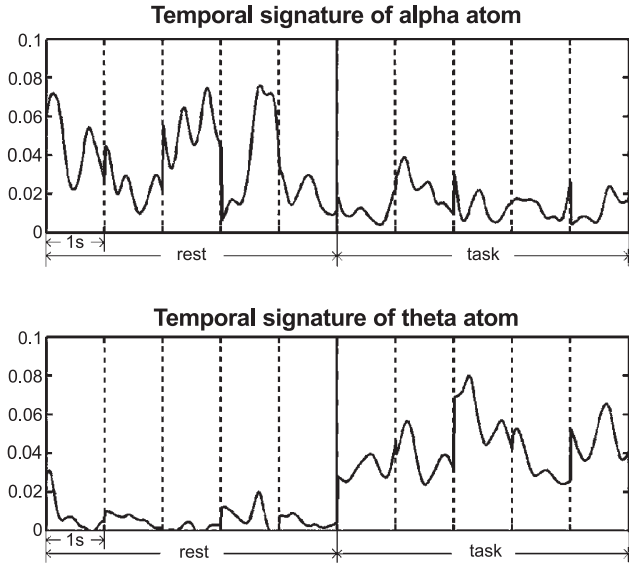

Fig. 3. Temporal signatures, $\mathbf{c}_k$, of theta and alpha atoms of Parallel Factor Analysis (PARAFAC) for a typical subject. The first five segments were chosen randomly from the rest condition; the second five segments were selected so as to contain typical theta bursts. Each segment is 1-s long, containing 100 time frames. The horizontal axis is time t, and the vertical axis is the value of $\mathbf{c}_k$, which is dimensionless.

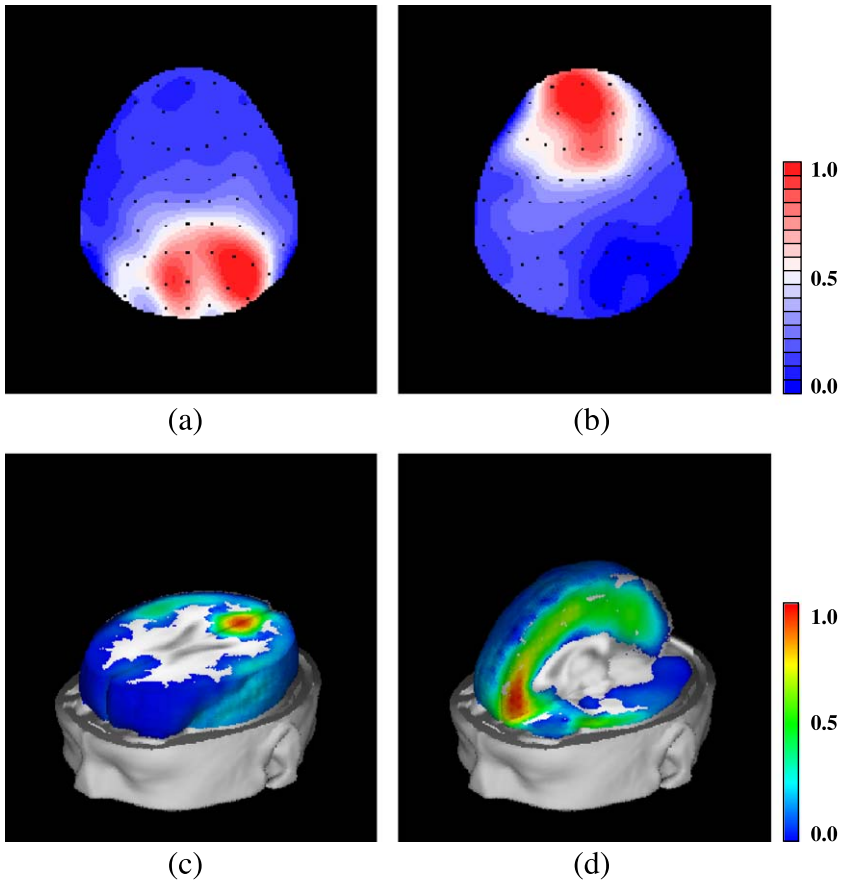

Fig. 4. Spatial signatures, $\mathbf{a}_k$, for the theta and alpha atoms of Parallel Factor Analysis (PARAFAC) of a typical subject. In (a) and (b), each signature is displayed as a topographic map; (c) and (d) are the corresponding Source Spectra Imaging solutions. The cross sections of brain were prepared for better visualization of the maximally activated regions. These are illustrated with a normalized color scale of the magnitude of $\mathbf{J}_k$.

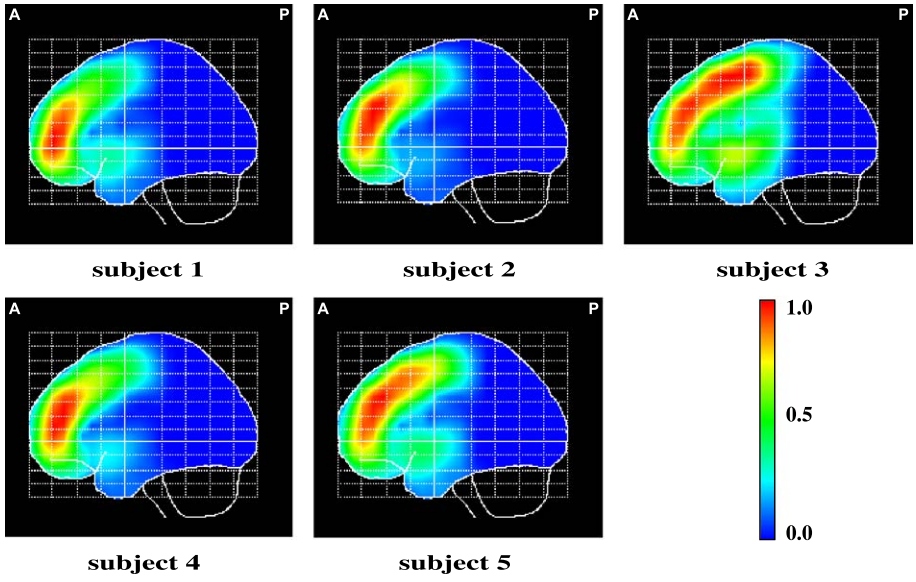

Fig. 5. Maximum-intensity projections of the Source Spectra Imaging solution of the spatial signature, $\mathbf{a}_k$, of the theta atom for each subject.

Although a sufficient condition was given above, usually, uniqueness can be assessed by checking the convergence of the algorithm and the interpretability of the results. A strong sufficient condition, but easier to verify, is that no two loading vectors are linearly dependent.

Screening and artifact detection

PARAFAC can be used not only for extracting significant activities from EEG, but also for searching for the presence of atoms in a new data set, which were not used for estimating the loadings and can be either from the same or from a different subject. If the spatial and spectral signatures of an atom are fixed, they can be used as templates for screening. Formally, after estimating atoms in a training data set, this can be reconstructed as

$$\hat{\boldsymbol{S}} = \mathbf{C}(\mathbf{B} \mid \otimes \mid \mathbf{A})^T, \tag{3}$$

here, $\mathbf{B}|\otimes|\mathbf{A} = [\mathbf{b}_1 \otimes \mathbf{a}_1 \mathbf{b}_2 \otimes \mathbf{a}_2 \ldots \mathbf{b}_{nk} \otimes \mathbf{a}_{nk}]$ is the Khatri-Rao product of **B** and **A**, and represents the convolution of space and frequency. $\mathbf{X}^T$ denotes the transpose of matrix **X**. For the definition of a template, not all atoms are necessary; that is, for the sake of screening, atoms that are not of interest may be eliminated. Let $\mathbf{B}'$ and $\mathbf{A}'$ be fixed spectral and spatial signatures (with some atoms possibly eliminated). The temporal signature, $\mathbf{C}'$, can then be estimated by using least squares in a new data set **X**,

$$\mathbf{C}'^T = (\mathbf{P}^T\mathbf{P})^{-1}\mathbf{P}^T\mathbf{X}; \quad \mathbf{P} = (\mathbf{B}' \mid \otimes \mid \mathbf{A}')^T \tag{4}$$

P can be regarded as a template for screening for the presence of the atoms of interest. The new temporal signature, $\mathbf{C}'$, will then be an estimate of the detected activities corresponding to each atom in the new data set.

If certain atoms obtained by PARAFAC decomposition contain artifact (e.g., eye movements, eye blinking, electromyogram, etc. . .) their space/frequency reconstructions can be used as templates for an artifact detector. The reconstruction, obtained by eliminating the component that corresponds to artifacts, will be an artifact removal method.

Inverse solution for the spatial signatures of atoms: source spectra imaging

Each column $\mathbf{a}_k$ of matrix **A** can be seen as the topography of atom *k*. Thus, it would be desirable to obtain the sources inside the brain that can produce these topographies to highlight more precise anatomical details. The difficulty here is that the spatial signatures are all positive values, as they are the differential topographic

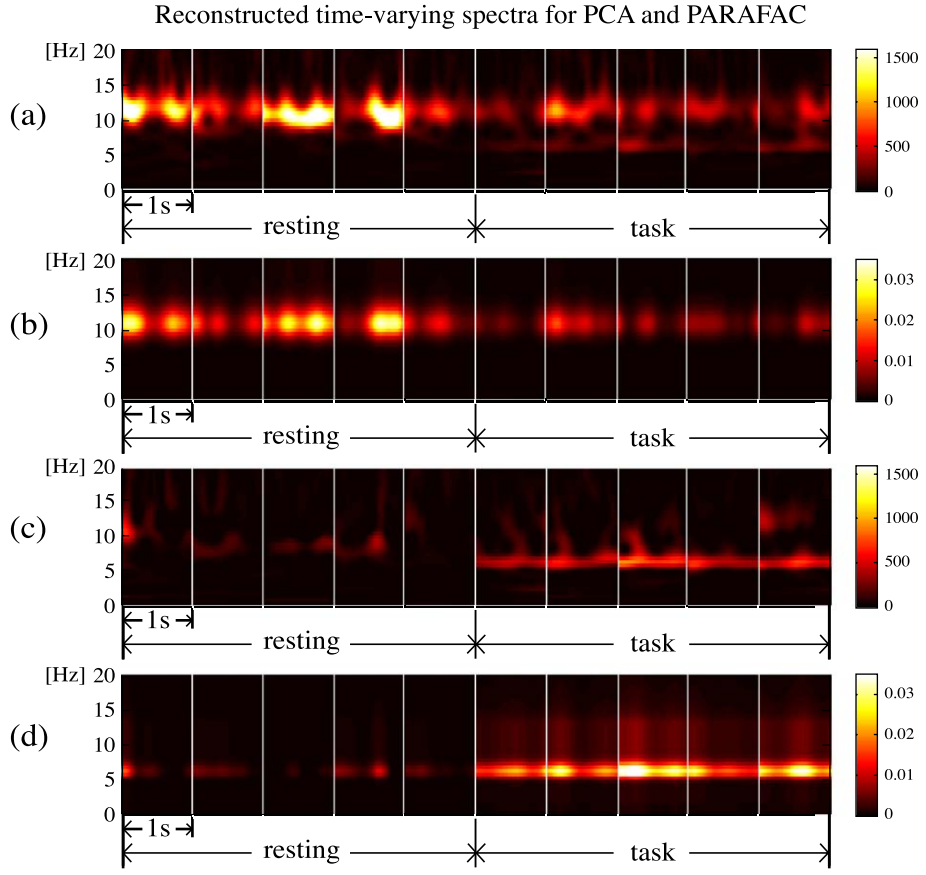

Fig. 6. Panels (a) and (b) illustrate the reconstructed decomposed component by Varimax rotated Principal Component Analysis (PCA) corresponding to the two largest eigenvalues. Panels (c) and (d) are the reconstructed alpha and theta atoms of PARAFAC decomposition in the frequency/time plane, respectively. The first five segments were randomly selected from the resting condition; the second five segments were selected so as to contain typical theta bursts. Each segment is 1-s long and contains 100 time frames.

profiles of EEG spectra, i.e., the variances of complex Fourier coefficients, and therefore the inverse solutions in this case are not the ordinary estimates for the current densities. However, a simple exploratory analysis can be performed in which, under certain assumptions and simplifications, the underlying sources for these topographies can be obtained by an inverse solution. Furthermore, these sources will be shown to be the spectra of electric current densities.

The well-known relation between the electric current densities inside the brain and the electric potentials measured by a set of electrodes on the scalp is:

$$\mathbf{V}_f = \mathbf{K}\mathbf{J}_f \tag{5}$$

Here we have written Eq. (5) directly in the frequency domain, i.e., $\mathbf{V}_{f(N_d \times 1)}$ and $\mathbf{J}_{f(3N_v \times 1)}$ are the vectors of Fourier coefficients of the voltages and electric current density time series, respectively. N_v is the number of voxels of a regular grid inside the brain. The matrix $\mathbf{K}_{(N_d \times 3N_v)}$ is the electric lead field, which is unaffected by the Fourier transformation. As the absolute value of the electric potential has no physical meaning, the average value of voltages was taken as the reference. From Eq. (5), we can find the spectra of voltages as $\alpha = \mathrm{diag}(\mathbf{V}_f\mathbf{V}_f^*)$:

$$\alpha = \mathrm{diag}(\mathbf{K}\mathbf{J}_f\mathbf{J}_f^*\mathbf{K}^T) \tag{6}$$

If we assume that there is no correlation between the current densities in different voxels, i.e., $\mathbf{J}_f\mathbf{J}_f^*$ is a diagonal matrix, we can obtain their spectra as $\gamma = \mathrm{diag}(\mathbf{J}_f\mathbf{J}_f^*)$. Eq. (6) then becomes:

$$\boldsymbol{\alpha} = \boldsymbol{K}^{\cdot\wedge 2}\boldsymbol{\gamma} \tag{7}$$

where $\mathbf{K}^{\cdot\wedge 2}$ indicates the operation of squaring each element of the matrix, $\mathbf{K}$. This represents a linear relation between α (spatial signatures obtained by PARAFAC decomposition), and the spectra of current sources that generate the scalp voltages. For the sake of simplicity, it may be assumed that the spectrum vector of the current density has the same magnitude in all directions for each voxel. Therefore, Eq. (7) may be rewritten as:

$$\boldsymbol{\alpha} = \mathbf{M}\boldsymbol{\mu} \tag{8}$$

Here, matrix $\mathbf{M}_{(N_d \times N_v)}$ was obtained by averaging every three columns of matrix $\mathbf{K}^{\cdot\wedge 2}$, and $\mu_{(N_x \times 1)}$ is the spectrum of current densities for each voxel.

From Eq. (8), the spectra of current sources can be found by an inverse solution procedure. Note here that spectra α and μ are non-negative vectors, allowing us to solve Eq. (8) as a minimum least squares problem under the non-negativity constraint for μ. Eq. (8) is undetermined; thus, we shall constrain the solution to be the smoothest one. In this case, the underlying sources (μ_k) for the topographic signature ($\mathbf{a}_k$) of atom k, can be obtained from

$$\boldsymbol{\mu}_k = \underset{\mu_k \geq 0}{\arg\min} \; |\mathbf{a}_k - \mathbf{M}\boldsymbol{\mu}_k|^2 + \lambda |\mathbf{L}\boldsymbol{\mu}_k|^2 \tag{9}$$

where $\mathbf{L}$ is the discrete Laplacian operator as described in Pascual-Marqui et al. (1994) and λ is a regularization parameter.

In general, we shall call this approximation to the source reconstruction for spectra of voltages the ‘‘Source Spectra Imaging’’ (SSI) solution. Despite the assumption of independence of electric current densities, finding the SSI solution for the spatial signatures implies the a priori assumption of spatial smoothness of the spectrum of current densities. Moreover, for this work, the SSI solution for each atom was obtained by imposing anatomical constraints using the Montreal Neurological Institute Probabilistic Brain Atlas as described in Casanova et al. (2000). This set of

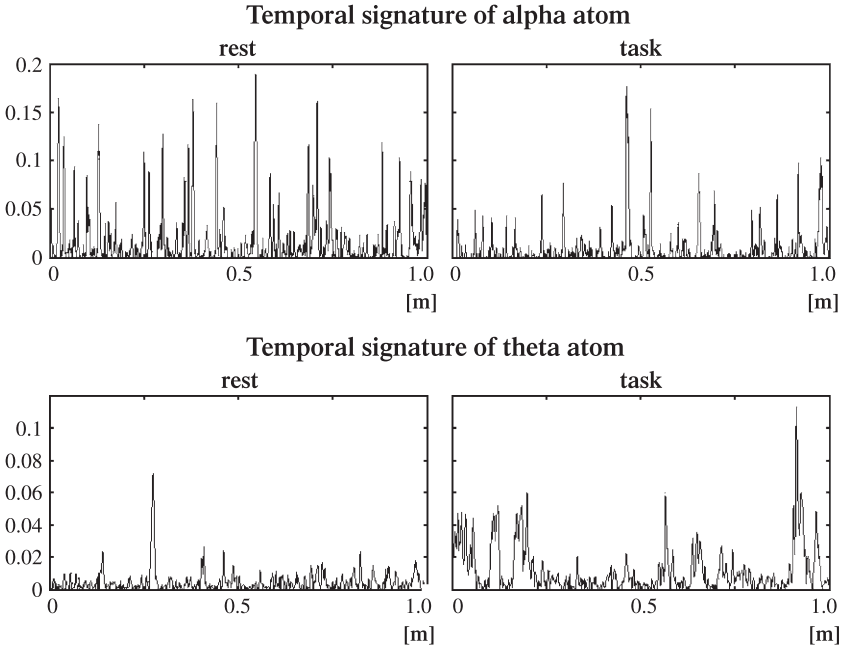

Fig. 7. Theta and alpha activities detected by the screening procedure, based on previously identified spatial and spectral signatures for each component. The screening was applied for 1 min of continuous data sets in the resting and task condition of a new data set of Subject 2. There are more theta bursts and less alpha bursts in the task state, while the converse relationship holds in the resting state.

assumptions has been amply used widely in the so-called distributed inverse solutions, which find the best applicability in the reconstruction of activation of wide areas in the brain. Advantages and shortcomings of these methods have been discussed extensively in the literature (Fuchs et al., 1999; Pascual-Marqui 1995, 1999; Pascual-Marqui et al., 1994).

Results

Parallel Factor Analysis

To evaluate the performance of PARAFAC for extracting alpha and theta activities in EEG, two different states were prepared in a benchmark data set. For this purpose, 10 segments of 1 s each were selected from the wavelet-transformed data (after wavelet transformation the time-varying EEG spectrum data set was subsampled to 100 Hz to reduce the computational cost of PARAFAC). Clear alpha activity is observed continuously during resting and task condition; however, strong theta activity appears only intermittently during task condition. Therefore, five segments were selected randomly from the resting condition and the other five segments were selected from the portions that contain typical theta bursts during the task. The segments were concatenated into the benchmark data set consecutively to form the three dimensional matrix $\mathbf{S}_{(N_d \times N_f \times N_t)}$.

In the PARAFAC decomposition of **S**, two atoms appeared for all subjects with spectral signature peaking in the alpha and theta range (Fig. 2).

The analyzed frequency range was 0.5–20 Hz step by 0.5 Hz, which is sufficient to extract theta and alpha activity. The use of the Corcondia index suggested that in three subjects, these two atoms were sufficient to explain the data set. In two subjects, an additional atom was needed. The Corcondia was more than 90% in all cases (optimally it should be 100%). The alpha and theta peaks were around 11 and 7 Hz, respectively. Subject 1 is typical of those who showed strong alpha and little theta activity during rest conditions. Temporal signatures (Fig. 3) show that during the task condition, this subject produced strong theta activities and reduced alpha activity.

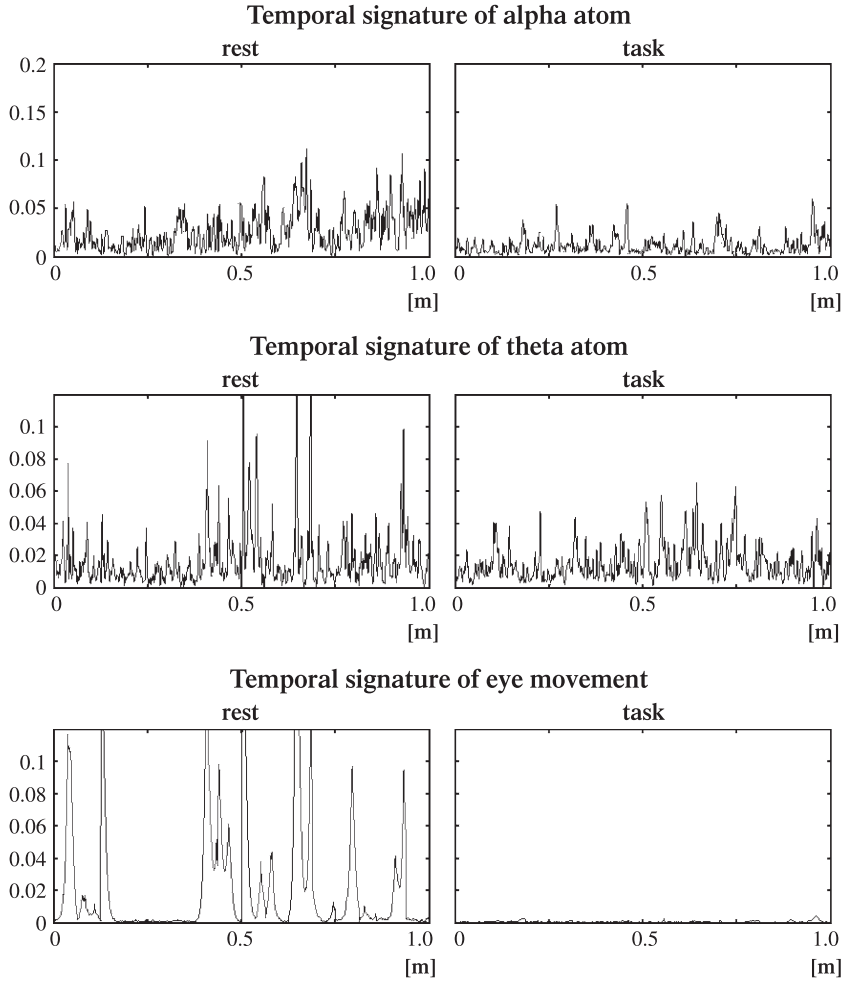

Fig. 8. To train the screening algorithm for the detection of eye movement artifacts, PARAFAC was applied to a data set containing typical theta and alpha activity, as well as eye blinks. Using the spatial and spectral signatures of these three components as a template, we screened 1 min of continuous data sets obtained in the resting condition, which was not used for estimating factors. The data set recorded from Subject 1 contained many eye blink artifacts in the resting condition and fewer in the task condition. On visual inspection of the raw data, it appears that there are more theta bursts during rest than during the task condition. The PARAFAC atomic decomposition showed that this is due to eye blink, as the many peaks in the temporal signature of theta and eye blink atom coincide.

Figs. 4(a) and (b) show the spatial signatures of the alpha and theta atoms as topographic maps for this subject.

The alpha and theta atoms appear in occipital and frontal area, respectively. Figs. 4(c) and (d) are the corresponding SSI solutions for these spatial signatures. The sources for the alpha and theta atoms are in the calcarine sulcus and in the anterior middle frontal cortex, respectively. These spatial distributions were relatively stable for all subjects. Fig. 5 shows the estimated SSI solutions for the spatial signatures of all subjects, corresponding to the theta atom. The activated region had a predominantly frontal distribution in all subjects.

Principal Component Analysis

To compare it with PARAFAC, we also carried out PCA of **S**. For this purpose, the data were transformed into a matrix by unfolding the three dimensional array. Results from our PARAFAC decomposition of **S** were matched with corresponding results obtained by applying PCA to the unfolded data set. Figs. 6(a) and (c) show the reconstructed components in the frequency/time plane that correspond to the two largest eigenvalues of PCA. The first component showed strong alpha activities during the resting condition. The second component shows strong theta activities and reduced alpha activity during the task condition. These components had a marked resemblance to the frequency/time reconstructed plane of the alpha and theta atoms of PARAFAC (Figs. 6(b) and (d)).

The peaks of these activities, as well as the order of appearance of the atoms, were the same in PARAFAC and PCA decompositions. The topographies of the PCA components were also very similar to the spatial signature of the PARAFAC atoms (Figs. 4(a) and (b)).

Screening

Using the screening procedure described above, it was possible to use PARAFAC to search for the presence of atoms in a new data set, which were not used for estimating the loadings. In this study, we consider new data from the same subject and only theta and alpha atoms were of interest. The spatial and spectral signatures for the templates of theta and alpha atoms were estimated by using Subject 2 data as a benchmark. Reconstruction of the temporal signature for new data was carried out by screening 1 min of continuous data in the resting and task conditions. Fig. 7 shows the appearance of pronounced theta bursts and the decrease of alpha bursts in the task state. In the resting state, the theta burst disappeared and the alpha bursts increased.

Artifact detection

If PARAFAC is applied to a data set that contains artifact, some of the atoms will correspond to such activity (e.g., eye blink, eye movement, EMG, etc...). Using these atoms as templates, artifact detection can be carried out by the screening procedure. As an example, PARAFAC was applied first to a training data set from Subject 1 that contained theta and alpha oscillations as well as eye movement artifact (this was assessed empirically by an experienced electrophysiologist). The number of atoms was chosen such they could be identified easily as theta, alpha, and eye movement artifact. Using the spatial and spectral signatures of these three atoms as templates, 1 min of continuous data in resting and task conditions were screened. Fig. 8 shows the corresponding temporal signature of the three atoms for Subject 1.

The data set recorded from this subject contained many eye movement artifacts in the resting condition and far fewer in the task condition. A superficial analysis would lead to the conclusion that there are more theta bursts during the resting than the task condition. However, these are probably due to the presence of artifacts, because there are many coincident peaks in the temporal signatures of the theta and artifact atoms.

Discussion

This paper introduces a new type of space/frequency/time atomic decomposition of the EEG. It takes advantage of the fact that three-way arrays of data may be decomposed into a sum of atoms of which is a trilinear combination of factors or signatures. This decomposition will be unique if the number of atoms is less than half the sum of the ranks of the three matrices formed by concatenating the signatures. The application of this concept to obtain unique space/frequency/time decomposition for the EEG is possible by arranging the multichannel evolutionary spectrum of the EEG in a three-way data array with dimensions indexed by channel, frequency, and time. The underlying theoretical requirement is that of a moderate amount of linear independence for atom topographies, spectra, and time courses. This is a much milder requirement than previous models underlying space/time atomic decompositions (PCA or ICA). This is the first intrinsically unique space/frequency/time atomic decomposition proposed in the literature.

A physiological interpretation of the model presented here is intuitively appealing. It assumes neural sources with a fixed geometrical relation to the sensors that produce oscillatory activity with a fixed spectral whose amplitude is temporally modulated. This model is not a completely general; for example, a frequency-modulated chirp would require a large number of components, such that the rank condition would be violated.

On the other hand, at most three space/frequency/time atoms are necessary for an adequate description of the EEG data analyzed in this paper. The use of the Corcondia index facilitates the selection of the number of components, an issue that is still difficult for most decomposition methods including PCA and ICA. Also, for the data set analyzed in this paper, two of the spectral signatures had a clear and common interpretation as theta and alpha oscillatory activity. Other components were not so constant and were sometimes difficult to interpret. It may be that more a priori information must be built into the model to avoid identification ambiguity. In this regard, PARAFAC shares with ICA the lack of inherent ordering of the extracted components. In the case of ICA, clustering techniques have been applied to identify common modes (Makeig et al., 2002). In the future, this approach might be used also for the space/frequency/time decomposition.

Our work also shows that the temporal signatures of the theta and alpha atoms may be used as indicators of physiological states. A comparison with a PCA-Varimax analysis shows that the results of the latter may sometimes be similar to those of PARAFAC in terms of description of space and frequency/time profiles. PARAFAC, however, provides a more parsimonious description of the data in a qualitatively simpler manner.

An important application of the space/frequency/time atomic decomposition is the screening of new data sets for the presence of particular atoms. In other words, PARAFAC offers the opportunity to screen recordings for bursts of oscillatory activity with a given

topographic and spectral content. The results shown here demonstrate the feasibility of this technique, not only to detect physiological activity but also for the ever-present problem of artifact removal.

One limitation of the implementation of the method presented here is the estimation by the least-squares techniques. Embedding the model in a Bayesian framework would allow more flexibility in incorporating a priori knowledge and a principled testing of different hypotheses about signatures within and between subjects.

Are these results 'real'?

As noted above, it has been proven that if the data is approximately trilinear, if the correct number of components is used, and if the signal-to-noise ratio is appropriate, then the true underlying phenomena will be found with PARAFAC (Harshman 1972; Kruskal, 1976, 1997). Also, there have been examples in which the PARAFAC model coincides with a physical model, e.g., fluorescence excitation–emission, chromatography with spectral detection, and spatiotemporal analysis of multichannel-evoked potentials (Field and Graupe, 1991).

The usual and stronger way to validate the truthfulness of results given by the application of multiway models is by split-half analysis (Harshman, 1984; Harshman and De Sarbo, 1984). Due to the uniqueness of the PARAFAC model, the same loadings must be obtained in the non-split modes from models of any suitable subset of the data. This analysis was not accomplished in this work. Although we do not have definitive proof that our results reflect exactly the real physical phenomena underlying the data, there are some aspects of the method we can lean upon for assessing the robustness of the model.

First, the algorithm is implemented such that we can select different initial values. We obtain the same results by applying the method with initial values given by direct trilinear decomposition of the data as we do by random guesses. Second, changing the convergence criterion over four orders of magnitude did not affect the results. Finally, the interpretability of the results, their agreement with previous studies of this kind of electrophysiological experiment, and their robustness with constraints to the loadings like non-negativity and orthogonality; as well as the small variability among subjects, all give additional evidence in this regard.

From this perspective, we think that PARAFAC space/frequency/time atomic decomposition of multichannel evolutionary spectrum of the EEG can reliably and uniquely extract meaningful and significant physiological activities, although this does not ensure that the results correspond to the physical sources that generated the data. Furthermore, the application of this technique requires careful preprocessing of the data, exploration of outliers and degenerate solutions, use of constraints, selection of appropriate model order, and validation of the results as this cannot be accomplished easily without prior knowledge of, or a theoretical basis for, of the expected results. PARAFAC should be simply considered another promising addition to the Neuroimaging analysis toolkit.

Acknowledgments

The authors want to thank Prof. Mark S. Cohen, Director of Functional MR Imaging, Ahmanson-Lovelace Brain Mapping Center, UCLA School of Medicine, for his very helpful advice and suggestion for this work.

References

Achim, A., Bouchard, S., 1997. Toward a dynamic topographic components model. Electroencephalogr. Clin. Neurophysiol. 103, 381–385.

Bertrand, O., Bohorquez, J., Pernier, J., 1994. Time–frequency digital filtering based on an invertible wavelet transform: an application to evoked potential. IEEE Trans. Biomed. Eng. 41, 77–88.

Bro, R., 1998. Multi-way Analysis in the Food Industry: Models, Algorithms and Applications. PhD Thesis. University of Amsterdam (NL) and Royal Veterinary and Agricultural University (DK).

Carroll, J.D., Chang, J., 1970. Analysis of individual differences in multidimensional scaling via an N-way generalization of 'Eckart-Young' decomposition. Psychometrika 35, 283–319.

Casanova, R., Valdes-Sosa, P., Garcia, F.M., 2000. Frequency domain distributed inverse solution. In: Aine, C.J., Okada, Y., Stroink, G., Swithenby, S.J., Wood, C.C. (Eds.), Biomag 96: Proceedings of the Tenth International Conference on Biomagnetism. Springer Verlag.

Chen, S., Donoho, D., 2001. Atomic decomposition by basis pursuit. SIAM Rev. 43, 129–159.

Cichocki, A., Amari, S., 2002. Adaptive Blind Signal and Image Processing. John Wiley & Sons, Ltd.

Dahlhaus, R., 1997. Fitting time series models to non-stationary processes. Ann. Stat. 25, 1–37.

Estienne, F., Matthijs, N., Massart, D.L., Ricoux, P., Leibovici, D., 2001. Multi-way modelling of high-dimensionality electroencephalographic data. Chemom. Intell. Lab. Syst. 58, 59–71.

Field, A.S., Graupe, D., 1991. Topographic component (Parallel Factor) analysis of multichannel evoked potentials: practical issues in trilinear spatiotemporal decomposition. Brain Topogr. 3, 407–423.

Fuchs, M., Wagner, M., Kohler, T., Wischman, H.A., 1999. Linear and nonlinear current density reconstructions. J. Clin. Neurophysiol. 16, 267–295.

Gonzalez Andino, S.L., Grave de Peralta Menendez, R., Lantz, C.M., Blank, O., Michel, C.M., Landis, T., 2001. Non-stationary distributed source approximation: an alternative to improve localization procedures. Hum. Brain Mapp. 14, 81–95.

Harmony, T., Fernandez, T., Silva, J., et al., 1999. Do specific EEG frequencies indicate different processes during mental calculation? Neurosci. Lett. 266, 25–28.

Harshman, R.A., 1970. Foundations of the PARAFAC procedure: models and conditions for an 'explanatory' multi-modal factor analysis. UCLA Work. Pap. Phon. 16, 1–84.

Harshman, R.A., 1972. Determination and proof of minimum uniqueness conditions for PARAFAC1. UCLA Work. Pap. Phon. 22, 111–117.

Harshman, R.A., 1984. "How can I know if it's 'real'?" A catalog of diagnostics for use with three-mode factor analysis and multidimensional scaling. In: Law, H.G., Snyder, C.W., Hattie, J.A., McDonald, R.P. (Eds.), Research Methods for Multimode Data Analysis. Praeger, New York, pp. 566–591.

Harshman, R.A., De Sarbo, W.S., 1984. An application of PARAFAC to a small sample problem, demonstrating preprocessing, orthogonality constraints, and split-half diagnostic techniques. In: Law, H.G., Snyder, J.A., Hattie, J.A., McDonald, R.P. (Eds.), Research Methods for Multimode Data Analysis. Praeger, New York, pp. 602–642.

Hyvarinen, A., Karhunen, J., Oja, E., 2001. Independent Component Analysis. John Wiley & Sons, Inc.

Ishihara, T., Yoshii, N., 1972. Multivariate analytic study of EEG and mental activity in juvenile delinquents. Electroencephalogr. Clin. Neurophysiol. 33, 71–80.

Jensen, O., Tesche, C.D., 2002. Frontal theta activity in human increased with memory load in a working memory task. Eur. J. Neurosci. 15, 1395–1399.

Jung, T.P., Makeig, S., Westerfield, M., Townsend, J., Courchesne, E., Sejnowski, T.J., 2001. Analysis and visualization of single-trial event-related potential. Hum. Brain Mapp. 14, 166–185.

Koenig, T., Marti-Lopez, F., Valdes-Sosa, P., 2001. Topographic time-frequency decomposition of the EEG. NeuroImage 14, 383–390.

Kronland-Martinet, R., Morlet, J., 1987. Analysis of sound patterns through wavelet transforms. Int. J. Pattern Recogn. Artif. Intell. 1, 273–302.

Kruskal, J.B., 1976. More factors than subjects, test and treatments: an indeterminacy theorem for canonical decomposition and individual differences scaling. Psychometrika 41, 281–293.

Kruskal, J.B., 1977. Three-way arrays: rank and uniqueness of trilinear decompositions, with application to arithmetic complexity and statistics. Linear Algebra Appl. 18, 95–138.

Lachaux, J.P., Rodriguez, E., Martinerie, J., Varela, F.J., 1999. Measuring phase synchrony in brain signals. Hum. Brain Mapp. 8, 194–208.

Lagerlund, T.D., Sharbrough, F.W., Busacker, N.E., 1997. Spatial filtering of multichannel electroencephalographic recordings through principal component analysis by singular value decomposition. J. Clin. Neurophysiol. 14, 73–83.

Lopes da Silva, F., 1987. EEG analysis: theory and practice. In: Neidermeyer, E., Lopes da Silva, F. (Eds.), Electroencephalography. Urban and Schwartzenberg.

Makeig, S., 1993. Auditory event-related dynamics of the EEG spectrum and effects of exposure to tones. Electroencephalogr. Clin. Neurophysiol. 86, 283–293.

Makeig, S., Westerfield, M., Jung, T.-P., et al., 2002. Dynamic brain sources of visual evoked responses. Science 295, 690–694.

Möcks, J., 1988a. Decomposing event-related potential: a new topographic components model. Biol. Psychol. 26, 199–215.

Möcks, J., 1988b. Topographic components model for event-related potentials and some biophysical considerations. IEEE Trans. Biomed. Eng. 35, 482–484.

Nunez, P.L., 1993. Electric Fields of the Brian: The Neurophysics of EEG. Oxford Univ. Press.

Pascual-Marqui, R.D., 1995. Reply to comments by Hamalainen, Ilmoniemi and Nunez. In source localization: continuing discussion of the inverse problem. Skrandies W ISBET Newsletter, vol. 6, pp. 16–28. ISSN 0947-5133.

Pascual-Marqui, R.D., 1999. Review of methods for solving the EEG inverse problem. Int. J. Bioelectromagn. 1, 1.

Pascual-Marqui, R.D., Michel, C.M., Lehmann, D., 1994. Low resolution electromagnetic tomography: a new method for localizing electrical activity in the brain. Int. J. Psychophysiol. 18, 49–65.

Sasaki, K., Tsujimoto, T., Nishikawa, S., Nishitani, N., Ishihara, T., 1996. Frontal mental theta wave recorded simultaneously with megnetroencephalography and electroencephalography. Neuroscience 26, 79–81.

Sidiropoulos, N.D., Bro, R., 2000. On the uniqueness of multilinear decomposition of *N*-way arrays. J. Chemom. 14, 229–239.

Soong, A.C., Koles, Z.J., 1995. Principal-component localization of the sources of the background EEG. IEEE Trans. Biomed. Eng. 42, 59–67.

Tallon-Baudry, C., Bertrand, O., Delpuech, C., Pernier, J., 1997. Oscillatory g-band (30–70 Hz) activity induced by a visual search task in humans. J. Neurosci. 17, 722–734.

Varela, F., Lachaux, J.P., Rodriguez, E., Martinerie, J., 2001. The brainweb: phase synchronization and large-scale integration. Nat. Rev. Neurosci. 2, 229–239.

Artículo 5.

Martínez-Montes, E., Sánchez-Bornot, J.M., Valdés-Sosa, P.A.: Penalized PARAFAC analysis of spontaneous EEG recordings, Statistica Sinica, 18, 4, 1449-1464, (2008). (Supplemental material, Statistica Sinica, 18, 2008, available online).

Statistica Sinica **18**(2008), 1449-1464

PENALIZED PARAFAC ANALYSIS OF SPONTANEOUS EEG RECORDINGS

Eduardo Martínez-Montes, José M. Sánchez-Bornot and Pedro A. Valdés-Sosa

Cuban Neuroscience Center

Abstract: The multidimensional nature of neuroscience data has made the use of multi-way statistical analysis suitable in this field. Parallel Factor Analysis (PARAFAC) is a multidimensional generalization of PCA with the advantage of offering unique solutions. However, imposing physiologically acceptable constraints would improve the interpretation of this type of analysis. In this work we propose a new algorithm called Alternating Penalized Least Squares to estimate PARAFAC solutions using different kinds of soft penalization. The algorithm relies on the recent generalization of modified Newton-Raphson techniques to estimate a multiple penalized least squares model. Applied to semi-synthetic and real spontaneous EEG time-varying spectra, we show that a wide range of sparse and smooth solutions can be found separately, as well as with these two properties combined. Smoothness is usually desired in spectra, and different sparse scenarios are observed in the temporal evolution of physiological intermittent phenomena. The degree of constraints can be tuned through the weighting parameters, whose optimal values can be chosen by means of the cross-validation and Corcondia measures.

Key words and phrases: Dimensionality reduction, EEG, PARAFAC, penalized regression.

1. Introduction

Tools for the analysis of multidimensional data arrays have recently gained popularity in neuroscience (Miwakeichi, Martínez-Montes, Valdés-Sosa, Nishiyama, Mizuhara and Yamaguchi (2004), Morup, Hansen, Herrmann, Parnas and Arnfred (2006) and Beckmann and Smith (2005)). This multi-way analysis is the natural extension of usual multivariate analysis, and it offers several advantages over the well-known bilinear methods for dimensionality reduction, such Principal Component Analysis (PCA) and Independent Component Analysis (ICA). The first advantage is that of more parsimonious and interpretable data models. Another advantage is the achievement of unique decompositions under very mild conditions, without constraining the solutions to be either orthogonal or statistically independent. Several models and algorithms for multi-way analysis have been developed (Bro (1998)). Of particular interest is the PARAFAC model,

first proposed by Harshman (1970) and recently used for the analysis of spontaneous EEG data (Miwakeichi et al. (2004)). The basic model for a PARAFAC decomposition of a three-way data array $\mathbf{X}_{(I\times J\times K)}$ of elements x_{ijk} is:

$$x_{ijk} = \sum_{f=1}^{N_f} a_{if} b_{jf} c_{kf} + \varepsilon_{ijk}, \tag{1.1}$$

where ε_{ijk} represents an error term. The problem is to find the loading matrices, or signatures, $\mathbf{A}$, $\mathbf{B}$ and $\mathbf{C}$, whose elements are a_{if}, b_{jf} and c_{kf}, respectively, with columns corresponding to components (indexed by f) which are also designated as 'atoms' (see Figure 1 of supplemental material online). This model does not suffer from rotational freedom and its only intrinsic indeterminacies are the order of the atoms and the relative scaling of the signatures. These can be solved in practice by choosing the first atom as the one explaining most of the variance, normalizing two of the estimated loadings and scaling the other with the overall explained variance. Therefore, the model is considered to be essentially unique (Stegeman and Sidiropoulos (2007)).

Sufficient conditions for the uniqueness of PARAFAC were given in Harshman (1970), although the most general condition is due to Kruskal (1977). Kruskal´s rank (*k-rank*) of a matrix is the largest number r such that every subset of r columns of the matrix is linearly independent. Uniqueness of the solution is guaranteed when $k\text{-}rank(\mathbf{A}) + k\text{-}rank(\mathbf{B}) + k\text{-}rank(\mathbf{C}) \geq 2N_f + 2$. This is a less-stringent condition than either orthogonality or statistical independence (Sidiropoulos and Bro (2000)). Necessary and sufficient conditions for unique decomposition of higher dimensional arrays are discussed in Stegeman and Sidiropoulos (2007).

Kruskal also showed that if the data conforms to the model, PARAFAC analysis will recover the true underlying phenomena if the correct number of components is used and if the signal-to-noise ratio is appropriate (Kruskal (1977)). To select the appropriate number N_f of components we use the Core Consistency Diagnostic (Corcondia) test (Bro (1998)). This measure takes the value 100% when the data conform exactly to the trilinear model. If Corcondia is lower than 85%, then either too many components have been extracted, the model is misspecified, or gross outliers disturb the model (Bro (1998)). For other details on this issue see Section 1 of the supplemental material (online).

Although other algorithms have been proposed, PARAFAC is most often estimated by Alternating Least Squares (ALS), which offers a good trade-off between computational expense and quality of the solution (Tomasi and Bro (2006)). This consists of simply dividing the parameters into several sets, each being estimated in a least squares sense, conditionally on the remaining parameters. This can be formalized using the following definition.

Definition. Let $\mathbf{A} \in R^{m\times n}$ and $\mathbf{B} \in R^{p\times n}$ be two matrices with columns denoted as $\mathbf{a}_i$ and $\mathbf{b}_i$, $i = 1, \ldots, n$, respectively. Then, the matrix $\mathbf{C} \in R^{mp\times n}$; $\mathbf{C} = \left[\mathbf{a}_1 \otimes \mathbf{b}_1 \cdots \mathbf{a}_n \otimes \mathbf{b}_n\right]$ is called the Khatri-Rao product of $\mathbf{A}$ and $\mathbf{B}$, denoted as $\mathbf{C} = \mathbf{A} \,|\otimes|\, \mathbf{B}$, where $\otimes$ is the Kronecker product.

If the tensor data is reshaped by joining along the second dimension all slices $\mathbf{X}_k$ $(k = 1, \ldots, K)$, we end up with a matrix $\overline{\mathbf{X}}_{\mathbf{A}}^{(I\times JK)}$, and the model can be rewritten in terms of the loadings matrices as $\overline{\mathbf{X}}_{\mathbf{A}}^{(I\times JK)} = \mathbf{A}\,(\mathbf{C} \,|\otimes|\, \mathbf{B})^T + \mathbf{E}_{\mathbf{A}}^{(I\times JK)}$. Here, $\mathbf{E}_{\mathbf{A}}^{(I\times JK)}$ is the error matrix equally rearranged. Similarly, reshaping the original data in such a way that the second (or third) dimension runs along rows and the other two are joined along columns, leads to the following equivalent forms of (1.1):

$$\overline{\mathbf{X}}_{\mathbf{B}}^{(J\times KI)} = \mathbf{B}\,(\mathbf{A} \,|\otimes|\, \mathbf{C})^T + \mathbf{E}_{\mathbf{B}}^{(J\times KI)}; \quad \overline{\mathbf{X}}_{\mathbf{C}}^{(K\times IJ)} = \mathbf{C}\,(\mathbf{B} \,|\otimes|\, \mathbf{A})^T + \mathbf{E}_{\mathbf{C}}^{(K\times IJ)}.$$

The global or general problem in PARAFAC has the loss function

$$\min_{\mathbf{A},\mathbf{B},\mathbf{C}} \left\| \overline{\mathbf{X}}_{\mathbf{A}}^{(I\times JK)} - \mathbf{A}\,(\mathbf{C} \,|\otimes|\, \mathbf{B})^T \right\|^2,$$

where $\|\mathbf{Y}\|$ denotes the Frobenius ($l2$-) norm of a matrix $\mathbf{Y}$, $\|\mathbf{Y}\| = \sqrt{\text{trace}\,(\mathbf{Y}^T\mathbf{Y})}$. With auxiliary matrices $\mathbf{Z}_{\mathbf{A}}^{(JK\times N_f)} = (\mathbf{C} \,|\otimes|\, \mathbf{B})$, $\mathbf{Z}_{\mathbf{B}}^{(KI\times N_f)} = (\mathbf{A} \,|\otimes|\, \mathbf{C})$, and $\mathbf{Z}_{\mathbf{C}}^{(IJ\times N_f)} = (\mathbf{B} \,|\otimes|\, \mathbf{A})$, the ALS algorithm can be expressed as three ordinary least squares (OLS) regressions.

1. Initialize two of the loadings, say $\mathbf{B}$ and $\mathbf{C}$.
2. $\widehat{\mathbf{A}} = \arg\min \left\|\overline{\mathbf{X}}_{\mathbf{A}} - \mathbf{A}\mathbf{Z}_{\mathbf{A}}^T\right\|^2$.
3. $\widehat{\mathbf{B}} = \arg\min \left\|\overline{\mathbf{X}}_{\mathbf{B}} - \mathbf{B}\mathbf{Z}_{\mathbf{B}}^T\right\|^2$.
4. $\widehat{\mathbf{C}} = \arg\min \left\|\overline{\mathbf{X}}_{\mathbf{C}} - \mathbf{C}\mathbf{Z}_{\mathbf{C}}^T\right\|^2$.
5. Repeat Steps 2, 3 and 4 until relative change in fit is smaller than a specified criterion.

Such an algorithm may only improve the fit or keep it the same, driving the loss function to monotonically decrease. Since the problem is a bounded-cost problem (the loss function cannot be less than zero) convergence follows. This property is very attractive, and one of the reasons for the widespread use of ALS. However, the noisy nature of neuroscience data may lead to difficult-to-interpret solutions and, in the worst case, to solutions without physiological interpretation at all. Therefore, the use of appropriate constraints is usually helpful for obtaining clinically and neurophysiologically sound results.

In this context, constraints can be applied as either approximate or exact. In the available implementation of PARAFAC (Andersson and Bro (2000)), only

exact orthogonality, nonnegativity and unimodality of components can be used as constraints, although in theory many others are possible (Bro (1998)). However, in the study of complex systems such as the brain through noisy data, exact constraints are not suitable. Recently, PARAFAC has been estimated through the Expectation-Maximization (EM) algorithm and the Variational Bayesian EM (Morup (2005)). These algorithms imply the use of prior information (approximate constraints) on some or all of the loadings, reducing to ALS when delta functions are used. The use of the Bayesian approach offers a natural way of imposing constraints through prior information and also allows one to address the evaluation of the optimal number of components to extract (e.g. through Automatic Relevant Detection or the Bayesian Information Criterion). However, the implementation of these methods depends strongly on the assumed prior densities for the loadings.

As an alternative, in this work we propose the use of approximate constraints in the ALS approach for a physiologically valid PARAFAC analysis of neuroscience data. Recent advances in the field of least squares regression allow one for the first time to efficiently constrain one or more signatures to be smooth, or sparse, or even to have both these properties. Some of these constraints would be very difficult to deal with in the EM/VBEM approaches and would lead to very slow algorithms. The next section presents the modifications of the ALS algorithm to include penalizations, as well as other details for efficient implementation and estimation of optimal weights for the constraints. Section 3 gives the results of the application of the new method to the analysis of actual and semi-synthetic EEG data, and Section 4 is devoted to the discussion and conclusions of the study.

2. Alternating Penalized Least Squares

Without loss of generality, we focus on the estimation of one of the loadings to be penalized, say $\mathbf{A}$. For this loading, the OLS solution is given by the second step of the ALS algorithm presented above. For simplicity, we write $\overline{\mathbf{X}}_{\mathbf{A}}^{T}$ and $\mathbf{Z}_{\mathbf{A}}$ as $\mathbf{X}$ and $\mathbf{Z}$, respectively. A constraint is introduced by adding a penalization term $P(\mathbf{A})$:

$$\widehat{\mathbf{A}} = \arg\min \left(\left\| \mathbf{X} - \mathbf{Z}\mathbf{A}^{T} \right\|^{2} + \lambda P(\mathbf{A}) \right).$$

The nonnegative parameter λ quantifies the relative importance of the two competing (fit and constraint) terms. Of particular interest is the well-known Ridge regression (Hoerl and Kennard (2000)), where the penalty function is quadratic in $\mathbf{A}$, having the general form $P(\mathbf{A}) = \|\mathbf{L}_1\mathbf{A}\mathbf{L}_2\|^2$, with $\mathbf{L}_1$ and $\mathbf{L}_2$ being two operators that operate on the columns and rows of $\mathbf{A}$ respectively. The choice of the first or second order difference operator for $\mathbf{L}_1$ ($\mathbf{L}_2$) is aimed

at the imposition of smoothness along rows (columns) of the coefficients matrix (Timmerman and Kiers (2002)). Alternatively, $P(\mathbf{A})$ can be a non-convex penalty function characterized by having a singularity at the origin and which leads to sparse solutions (Fan and Li (2001)). In this line, some penalizers are the Least Absolute Shrinkage Selection Operator (Lasso) (Tibshirani (1996)), which uses the *l1*-norm of $\mathbf{A}$, so $P(\mathbf{A}) = \|\mathbf{A}\|_1$; a variant called the "Fusion Lasso" (Land and Friedman (1996)), with $P(\mathbf{A}) = \|\mathbf{L}\mathbf{A}\|_1$, where $\mathbf{L}$ is the first order difference operator; and the Smooth Clipped Absolute Deviation (SCAD) (Fan (1997)), with a more complicated definition for the penalty function. Also, some particular combinations of penalties have been introduced, such as the "Fused Lasso" (Tibshirani, Saunders, Rosset, Zhu and Knight (2005)), which combines typical penalties of Lasso and Fusion Lasso; and Elastic Net (Enet) (Zou and Hastie (2005)) combining *l1*-norm penalties (Lasso) and quadratic penalties (Ridge). A general expression for this penalty is $P(\mathbf{A}) = \mu_1 \|\mathbf{L}_1\mathbf{A}\|_1 + \mu_2 \|\mathbf{L}_2\mathbf{A}\|^2$, where $\mu_i, (i = 1, 2)$ is the weight for the *l(i)*-norm term. These strategies are suitable in problems where group behavior is searched for in some of the coefficients. A compendium of different non-convex penalizers and their application to neuroscience data can be found in Valdés-Sosa, Sánchez-Bornot, Vega-Hernández, Melie-García, Lage-Castellanos and Canales-Rodríguez (2006).

For estimating penalized linear regression models with the use of non-convex penalties, (which are not algebraically treatable), we used the Local Quadratic Approximation (LQA) algorithm (Fan and Li (2001)). It unifies nearly all variable selection techniques into an easy-to-implement iterative application of Ridge regression, and retains the convergence properties of the Newton-Raphson algorithm (Hunter and Li (2005)). Recently, our group has developed a generalized LQA variant to tackle the estimation of a penalized least squares model with combinations of different types of penalties (Sánchez-Bornot, Martínez-Montes, Lage-Castellanos, Vega-Hernández and Valdés-Sosa (2008)). This is called Multiple Penalized Least Squares (MPLS) and, for a PARAFAC loading, is established as

$$\widehat{\mathbf{A}} = \arg\min \left(\left\| \mathbf{X} - \mathbf{Z}\mathbf{A}^T \right\|^2 + \sum \lambda_l P_l(\mathbf{A}) \right), \tag{2.1}$$

where $l = 1, \ldots, N_l$, indexes the penalty functions and corresponding weighting parameters. This loss function cannot be separated into contributions from columns of $\mathbf{A}$ (rows of $\mathbf{A}^T$), thus each column has to be estimated conditionally on the others using a backfitting algorithm (Hastie and Tibshirani (1990)). Mathematically, if we set $\mathbf{T}_f = \mathbf{X} - \sum_{f' \neq f} \mathbf{z}_{f'} \mathbf{a}_{f'}^T$, then the loss function for the f-th atom $\mathbf{a}_f$ can be written as $\|\mathbf{T}_f - \mathbf{z}_f \mathbf{a}_f^T\|^2 + \sum \lambda_l P_l(\mathbf{A})$, where $\mathbf{z}_f$ is the f-th column of $\mathbf{Z}$. The solution to this problem is not necessarily the overall solution of (2.1) in the least squares sense. However, this formulation is very useful in

practice due to the following lemma, whose proof can be found in Section 2 of the supplemental material (online).

Lemma 1. *Consider the minimization subject to any constraint of the loss function of a multiple penalized linear regression model for a row* $\mathbf{a}^T$: $\min(\|\mathbf{T} - \mathbf{z}\mathbf{a}^T\|^2 + \sum \lambda_l P_l(\mathbf{a}))$. *The solution is that of* $\min \|\alpha - \mathbf{a}\|^2 + \sum \overline{\lambda}_l P_l(\mathbf{a}))$, *where* α *is the solution of the unconstrained problem* $\alpha = \arg\min(\|\mathbf{T} - \mathbf{z}\alpha^T\|^2) = \mathbf{T}^T\mathbf{z}/\mathbf{z}^T\mathbf{z}$, *and* $\overline{\lambda}_l = \lambda_l/\mathbf{z}^T\mathbf{z}$.

This result allows for a fast computation of each atom which compensates for the slowness of the iterative backfitting process. Moreover, it is possible to use different constraints for each atom separately. The APLS algorithm can then be summarized as follows.

1. Initialize the loadings: $\mathbf{A}_0$, $\mathbf{B}_0$ and $\mathbf{C}_0$.
2. Iterate until convergence the following steps (iteration t).
3. Estimate $\widehat{\mathbf{A}}_t = backfitting(\overline{\mathbf{X}}_\mathbf{A}, \mathbf{A}_{t-1}, \mathbf{B}_{t-1}, \mathbf{C}_{t-1}, P_\mathbf{A})$.
4. Estimate $\widehat{\mathbf{B}}_t = backfitting(\overline{\mathbf{X}}_\mathbf{B}, \mathbf{A}_{t-1}, \mathbf{B}_{t-1}, \mathbf{C}_{t-1}, P_\mathbf{B})$.
5. Estimate $\widehat{\mathbf{C}}_t = backfitting(\overline{\mathbf{X}}_\mathbf{C}, \mathbf{A}_{t-1}, \mathbf{B}_{t-1}, \mathbf{C}_{t-1}, P_\mathbf{C})$.

($P_\mathbf{A}$, $P_\mathbf{B}$ and $P_\mathbf{C}$ summarize multiple penalties on $\mathbf{A}$, $\mathbf{B}$ and $\mathbf{C}$, respectively.)

Backfitting Algorithm: $\widehat{\mathbf{A}} = backfitting(\overline{\mathbf{X}}_\mathbf{A}, \mathbf{A}, \mathbf{B}, \mathbf{C}, P_\mathbf{A})$.

(i) For each column $\mathbf{a}_f$, $\mathbf{b}_f$ and $\mathbf{c}_f$ of $\mathbf{A}$,$\mathbf{B}$ and $\mathbf{C}$, respectively, compute $\mathbf{z}_f = \mathbf{c}_f \otimes \mathbf{b}_f$ and $\alpha_f = (\overline{\mathbf{X}}_\mathbf{A} - \sum_{f' \neq f} \mathbf{z}_{f'} \mathbf{a}_{f'}^T)^T \mathbf{z}_f / \mathbf{z}_f^T \mathbf{z}_f$.

(ii) Estimate $\widehat{\mathbf{a}}_f = \arg\min(\|\alpha_f - \mathbf{a}_f\|^2 + P_\mathbf{A})$.

(iii) Repeat (i) and (ii) until convergence.

Finally, two important issues should be mentioned. First, each iterative step (penalized least squares) of the backfitting algorithm is approximated by iterative ridge regressions using LQA to guarantee its global convergence. This ensures the convergence of the backfitting (Ansley and Kohn (1994)), improving the fit or keeping it the same. Therefore, similar to ALS, since the loss function is non-negative, the whole algorithm converges at least to a local minima. On the other hand, in some cases PARAFAC is known to depend strongly on initial loadings. For the ALS algorithm, several options have been used for obtaining initial estimates ranging from random guesses to direct trilinear decomposition (Bro (1998)). A common option has been to use several runs with initial guesses to ensure convergence to a unique solution. We follow this approach in the case of synthetic data, although for real data we always start from the unconstrained PARAFAC solution, which ensures that penalized loadings will resemble the original ones.

Second, we have to set values for the weighting parameters for each penalty function that allow a continuous control over the corresponding constraint. Automatic selection of optimal values can be found by generalized cross-validation (GCV) (Golub, Heath and Wahba (1979)), or information criteria such as Akaike's (Akaike (1974)) or Schwartz's Bayesian Information Criterion (Schwartz (1978)). In this work we compute solutions with different values for the weighting parameters and review corresponding values of the logarithm of GCV (logGCV), and the Corcondia measure, for identifying an 'optimal' solution. In the case of using several penalty functions, this can lead to a computationally expensive approach. Thus, for the case of the Enet penalty, we follow a different approach that consists of using only a few pairs of values for μ_1 and μ_2 such that $\mu_1 + \mu_2 = 1$, and finding the optimal weighting parameter common for both terms through inspection of log GCV and Corcondia. The former is logGCV$= \log(\widehat{\sigma}^2) - \log(1 - df/N)$, where $N = IJK$ is the number of data elements, $\widehat{\sigma}^2 = \|\mathbf{X} - \widehat{\mathbf{X}}\|^2/(N - df)$ is an estimate of the error variance component, and df is the effective number of parameters (degrees of freedom), which is very difficult to compute for nonlinear models and non-quadratic penalties. Here, we approximate df by the sum of each loading's degrees of freedom. This approximation is also used in the backfitting process for each atom, as proposed by Hastie and Tibshirani (1990), Chapters 2 and 6.

3. Constrained Decomposition of EEG Data

3.1. Ordinary PARAFAC

The data used in this study is the time-varying spectrum of a resting-state EEG recording of 16 bipolar derivations. This is a three-dimensional array of 208 320 elements, indexed by 16 derivations, 124 frequencies and 105 time points, that can be subject to PARAFAC analysis as is schematically shown in Figure 1 of the supplemental material (online). The estimated loadings correspond to spatial, spectral and temporal signatures, respectively. More details about these data set and their preprocessing for PARAFAC can be found in the supplemental material (online), and in Martínez-Montes, Valdés-Sosa, Miwakeichi, Goldman and Cohen (2004)

Unconstrained PARAFAC decomposition via ALS was performed, and examination of Corcondia, residual errors, and explained variance allowed us to determine the appropriate number of components as three. Figure 1 shows the three atoms extracted for the spatial, temporal and spectral loadings. The latter allows the identification of the present rhythms in the data, namely alpha (solid line), theta (dot line), and gamma (dash line) atoms. Note that temporal signatures show different behaviors, being quite constant for the gamma atom, and showing intermittent activity for the alpha and theta atoms. The spatial

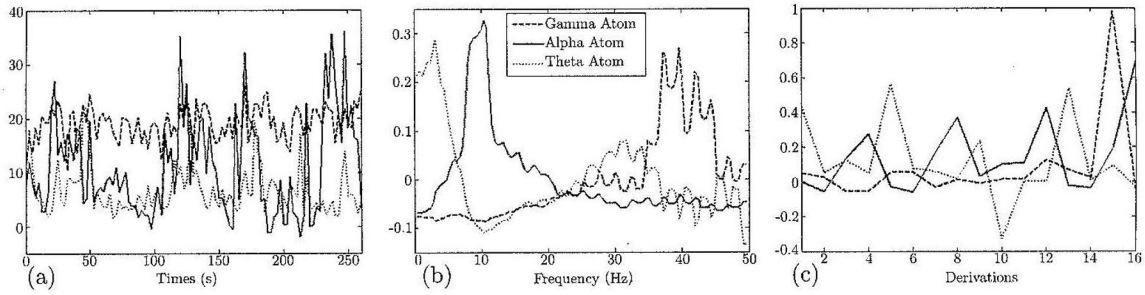

Figure 1. Unconstrained PARAFAC decomposition via ALS of the time-varying spectra of resting-state EEG. (a) Temporal signatures (b) Spectral signatures (c) Spatial signatures. The three atoms extracted are identified according to the classical band classification as alpha (8-12Hz), theta (4-8Hz), and gamma (>30Hz) from the spectral loadings. The spectral and spatial signatures are normalized and the temporal retains the scale of the data. Figure in color in the online version.

loadings are more difficult to interpret in this view and are not of interest in this paper, although the representation on the scalp is shown in Figure 2 of the supplemental material (online).

3.2. Smoothness

Although the main spectral peaks of the three atoms are clearly distinguished (Figure 1b), this is not always the case, and oscillations or roughness of the spectrum sometimes make it difficult to interpret. To overcome this, we imposed several degrees of smoothness on one spectral loading ($P(\mathbf{B}) = \|\mathbf{L}_2\mathbf{B}\|^2$, $\mathbf{L}_2$ being the second difference operator) while leaving the other two loadings unconstrained. Figure 2a-e show the spectral signatures for different values of the corresponding weighting parameter. As can be seen, the higher the weighting parameter, the smoother the signatures for all atoms. The 'optimal' value for this parameter is $\lambda = 1$ in terms of minimization of the GCV, the residual sum of squares (RSS) and the relative distances to unconstrained solution, as well as maximization of the Corcondia measure, as shown by Table 1 of the supplemental material (online). However, the RSS and logGCV obtained for the unconstrained PARAFAC decomposition are lower, which might be explained by its uniqueness, i.e., the constraint pulls the solution far from the least squares one. On the other hand, Figure 2f shows the spectral signatures obtained by requiring smoothness and non-negativity simultaneously, illustrating the feasibility of combining this kind of soft constraint with the hard constraint already used in PARAFAC (Bro (1998)).

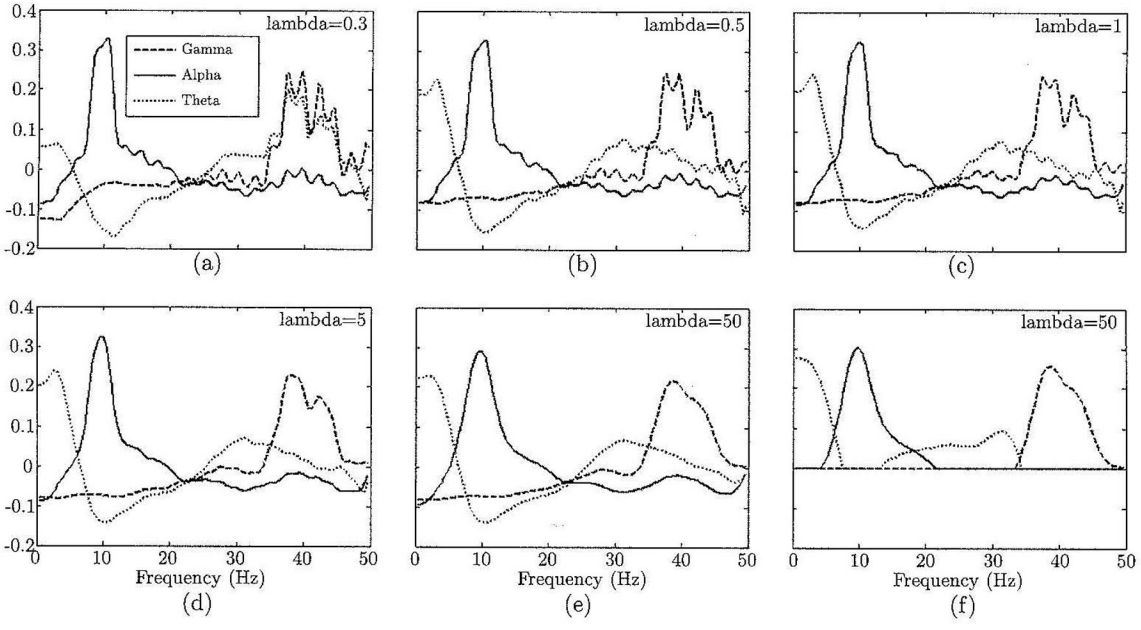

Figure 2. Spectral signatures constrained to be smooth, obtained by PARAFAC via APLS. (a)−(e) Spectral loadings with different degree of smoothness (see value of lambda, the smoothing parameter). (f) Spectral loadings constrained to be smooth and non-negative. Values of logGCV and Corcondia are shown in Table 1 of the supplemental material (online). Figure in color in the online version.

3.3. Sparsity and group behavior

EEG data and other neuroimages often show intermittent activity. For example, epileptic spikes are very localized in time, spontaneous rhythms usually alternates periods of high and low amplitudes, and experimental block designs give the amplitude of oscillations a box-like appearance. Having this in mind, we simulated the three scenarios for a temporal signature that are shown in the top row of Figure 3. The first is theoretically suitable for the use of Lasso penalization since it shows very sparse signatures (Figure 3a top). The second shows non-zero values in groups, within which all points have the same value (Figure 3b top) so, theoretically, this is the ideal situation for applying the Fusion Lasso penalization. Finally, the third also shows signatures with group behavior, but now with smooth variations in values inside a group (Figure 3c top), which is suitably tackled by penalizations combining smoothness and sparsity, such as Elastic Net. With these simulated temporal signatures and the unconstrained spatial and spectral loadings, we recomposed the three-dimensional data and added some white noise (signal-to-noise ratio of 20 dB). The bottom row of Figure 3 shows the unconstrained PARAFAC decomposition of this semi-synthetic data. Note that in all cases there is a good correspondence (Corcondia>99%), but the sparse nature of the real signatures (many zero values) cannot be recovered.

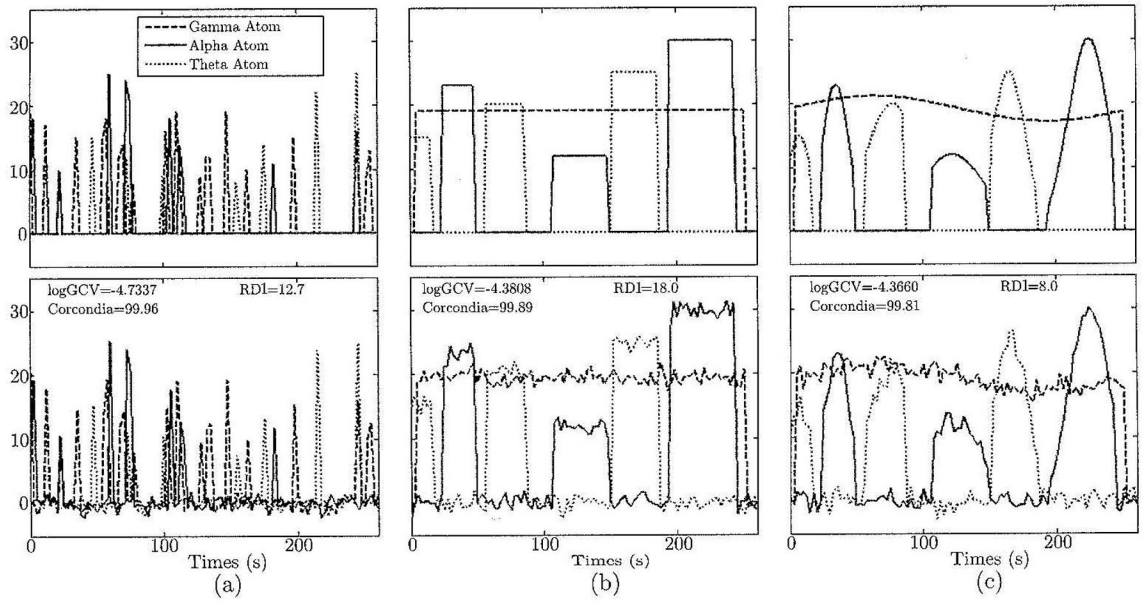

Figure 3. Simulated temporal signatures for the three atoms (top), and those obtained by unconstrained PARAFAC (bottom). Logarithm of Generalized Cross Validation (logGCV) function and relative distance (RD1) to the real loadings are also shown. (a) Lasso scenario; only some time points are activated. (b) Fusion Lasso scenario; each signature is a box-like function. (c) Elastic Net scenario; only a few patches are activated, but this activation is smooth inside the patch. Figure in color in the online version.

Penalized PARAFAC analyses with different constraints on the temporal signature, and without constraining the other two loadings, were performed. Figure 4a shows the temporal loading obtained by using a Lasso penalization ($P(\mathbf{C}) = \|\mathbf{C}\|_1$) for the first scenario (Figure 3a). Here, the optimum value (minimum logGCV) for the weighting parameter is 0.1, which also produces the lowest relative distance to the real loading, i.e., the one resembling the real loading most accurately. This plot for other values of the weighting parameter and corresponding logGCV, Corcondia, and relative distances are shown in the top row of Figure 3 of the supplemental material (online). Similarly, Figure 4b shows the temporal signatures obtained by using Fusion Lasso penalization ($P(\mathbf{C}) = \|\mathbf{L}_1\mathbf{C}\|_1$, $\mathbf{L}_1$ being the first difference operator) on the second simulated data set (Figure 3b). The value $\lambda = 0.9$ seems to be optimal, having the highest Corcondia, the lowest logGCV, and the lowest relative distance to the real loading. The temporal loadings estimated for different values of λ are shown in the middle row of Figure 3 of the supplemental material (online). Finally, in Figure 4c the temporal signatures estimated with the use of Enet penalization ($P(\mathbf{C}) = \mu_1 \|\mathbf{L}_1\mathbf{C}\|_1 + \mu_2 \|\mathbf{L}_2\mathbf{C}\|^2$) on the third simulated data set (Figure 3c) are shown. Enet solutions were found using a first order difference operator for the

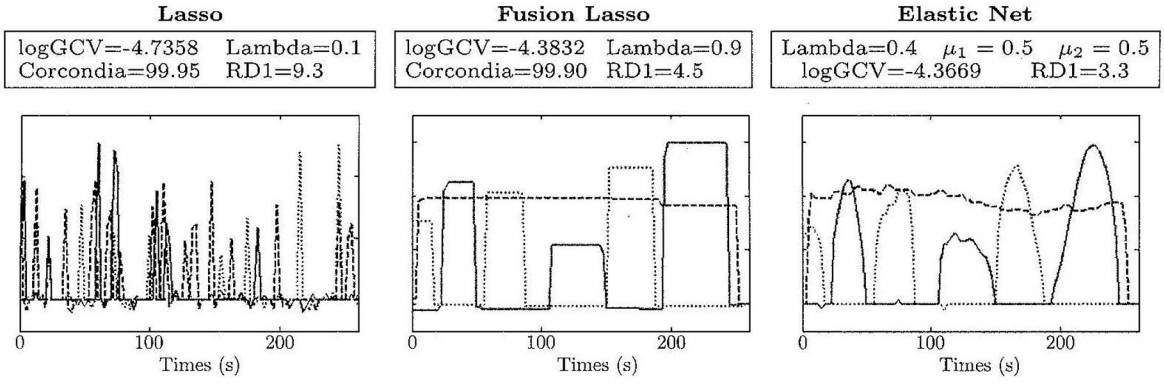

Figure 4. Estimated temporal signatures for the three atoms using constrained PARAFAC with corresponding penalization for the three simulated scenarios. Values of optimum lambda, logarithm of GCV, Corcondia (except for Enet), and relative distance to real temporal signature (in percent) are shown. Solid line represents the Alpha atom, dotted line represents the Theta atom, and dashed line the Gamma atom. Figure in color in the online version.

l1-norm term and a second order difference operator for the *l2*-norm term. Different values of the parameter λ were explored for three different pairs of weights $(\mu_1, \mu_2) = \{(0.9, 0.1);\ (0.5, 0.5);\ (0.1, 0.9)\}$. Solutions with the lowest logGCV in each case are shown in the bottom row of Figure 3 of the supplemental material (online). Since values of logGCV and Corcondia (not shown) are almost the same in the three cases, in Figure 4c we present the solution with $\mu_1 = \mu_2 = 0.5$ as best, based only on the relative distance to the real loading. The slowest computed solution took around 2.5 minutes to converge.

3.4. Combining smoothness and sparsity

Finally, we explored the three types of sparse constraints on the temporal signature of the real data. Additionally, smoothness was required for the spectral loading in order to test the ability of the proposed algorithm to simultaneously impose different types of constraints to different loadings. Figure 5 shows three PARAFAC decompositions corresponding to the use of the Lasso, the Fusion Lasso and the Enet penalizations on the temporal loading, and Ridge (with a second order difference operator) on the spectral loading. The 'optimal' solutions were selected as those with minimum logGCV, also taking into account the Corcondia measure. All decomposition converged in less than 4 minutes.

The discussed properties of each penalty used can be easily distinguished. In the first case (Figure 5a, top), the signatures are sparser, since more coefficients are set to zero. In the second case (Figure 5b, top), there are some flat periods, and in the third (Figure 5c, top), the groups of coefficients with nonzero values

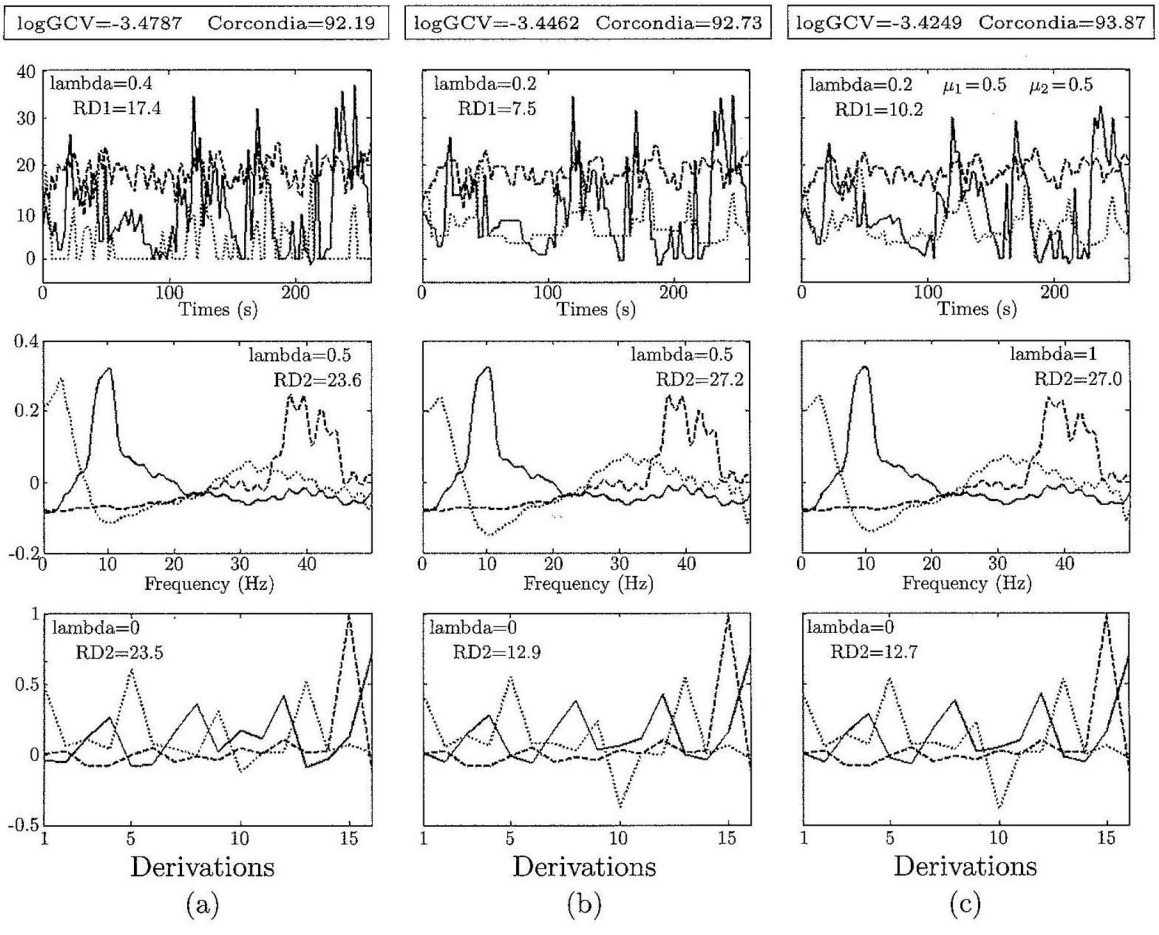

Figure 5. Estimated temporal (top), spectral (middle), and spatial (bottom) signatures for the three atoms using constraints for temporal and spectral loadings in real data. a) Lasso penalization (sparsity) on the temporal loading; b) Fusion Lasso penalization (sparsity on the first differences); c) Enet penalization (combination of sparsity and smoothness) with first and second order difference operators in the *l1*-norm and *l2*-norm terms, respectively. In all cases the smoothness constraint (using the second order difference operator) was required on the spectral loading. Corresponding optimal values for lambda, logGCV, Corcondia, and relative distances to unconstrained loadings (in percent) are shown. Solid line represents the Alpha atom, dotted line represents the Theta atom, and dashed line the Gamma atom. Figure in color in the online version.

show a smoother behavior. In all cases, the theta atom seems to be the one most reactive to the imposed constraint, and the gamma atom the one least reactive. Spectral loadings are almost the same as presented in Figure 2 with a corresponding smoothing parameter, and the spatial loadings closely resemble the unconstrained one shown in Figure 1c. This can be considered as evidence of a small influence of penalization in one loading on the remaining loadings.

Moreover, it can be of help in reducing the time needed for performing this kind of analysis, since one can first explore the optimal values for the weighting parameters in separate constrained analysis for the loadings, and then look for the optimal set of parameters for the conjoint analysis in a small neighborhood.

4. Conclusions

In this work we have proposed a methodology for imposing constraints on loadings in a PARAFAC decomposition. The combination of a multiple penalized linear regression algorithm and the alternating least squares philosophy has given rise to what we have called the Alternating Penalized Least Squares algorithm.

Although the idea of constraining the loading matrices in a PARAFAC regression is not new, to our knowledge, this is the first time that such a general algorithm is proposed, allowing the use (together with the usual constraints of orthogonality, nonnegativity, and others) of a wide range of unexplored penalties and combinations of penalties. This is particularly important in neuroscience, when the complex and noisy nature of the data makes the use of prior information unavoidable.

In our exploration, PARAFAC via APLS was useful for imposing smoothness on the spectral loading of the time-varying spectrum of real spontaneous EEG recording. It was equally successful in estimating different kinds of temporal evolutions that are common in neuroscience experimental designs. They range from very sparse signatures with only a few nonzero 'appearances' in time, to other group behavior such as box-like and piece-wise smooth functions. We found that the true simulated loadings are better recovered with the use of appropriate constraints than with the unconstrained solution. On the other hand, though the degree of constraint can be tuned by hand, we found that the use of GCV and the Corcondia measure can help in selecting an optimal solution. Constraining different loadings simultaneously did not affect the optimal values of the weighting parameters. This can reduce time of computation if they are selected in faster, separated analysis.

The proposed approach inherits some of the virtues and drawbacks of unconstrained PARAFAC. Among the former, the most attractive is the uniqueness of solution under very mild conditions. In this sense, the use of constraints can even help in those cases in which the noise level of the data restricts the convergence. Among the latter, we can mention the strong dependency on initial estimates, as well as the appearance of highly correlated atoms known as degeneracy. Again the use of constraints, when needed, can be helpful in avoiding degeneracy, and initial estimates for loadings can be obtained from the unconstrained solution. We conjecture that APLS provides more robust solutions than the ordinary ALS, although a more thorough study on this issue should be carried out in the future.

On the other hand, the use of a backfitting procedure can make the overall algorithm slower, although the efficient implementation through LQA and the use of Lemma 1 (Section 2) compensate for this effect. The computational time of the algorithm proposed depends on the chosen weighting parameters, usually being lower when optimum values are used. In our analysis, the slowest case converged in no more than 10 minutes, although the average computational time was around 2-3 minutes for actual data, and about a minute for synthetic data. Some approaches developed for speeding up the ALS algorithm in PARAFAC, such as Candelinc (Carroll, Pruzansky and Kruskal (1980)) and the use of QR-decompositions, could also be implemented in the context of the proposed algorithm.

Several issues remain unexplored and will be the subject of future work. First, the extension of the algorithm to use different penalization for each atom might allow for the extraction of, e.g., temporal evolutions with different properties for different rhythms in the same decomposition. Second, the use of statistical techniques such as bootstrapping for assessing the significance of findings is needed. Third, other approaches, such as the use of the Variational Bayesian framework, can be of help for selecting the optimal penalized decompositions. Finally, it should be mentioned that the APLS algorithm can also be applied in the context of other multidimensional models, such as Tucker, Parafac2, and multi-way Partial Least Squares (Bro (1998)).

Acknowledgement

Authors gratefully acknowledge Mayrim Vega-Hernández, Agustín Lage-Castellanos and Lester Melie-García for their useful comments and for detailed revision of the manuscript.

References

Akaike, H. (1974). A new look at the statistical model identification. *IEEE Trans. Automat. Control* **19**, 716-723.

Andersson, C. A. and Bro, R. (2000). The N-way Toolbox for MATLAB. *Chemometrics Intell. Lab. Syst.* **52**, 1-4.

Ansley, C. F. and Kohn, R. (1994). Convergence of the backfitting algorithm for additive models. *J. Austral. Math. Soc. Ser. A* **57**, 316-329.

Beckmann, C. F. and Smith, S. M. (2005). Tensorial extensions of independent component analysis for multisubject FMRI analysis. *NeuroImage* **25**, 294-311.

Bro, R. (1998). Multi-way Analysis in the Food Industry: Models, Algorithms and Applications. Ph.D. Thesis, University of Amsterdam and Royal Veterinary and Agricultural University, Denmark.

Carroll, J. D., Pruzansky, S. and Kruskal, J. B. (1980). Candelinc: A general approach to multidimensional analysis of many-ways arrays with linear constraints on parameters. *Psychometrika* **45**, 3-24.

Fan, J. (1997). Comments on 'Wavelet in Statistics: A Review.' by Antoniadis. J. Italian Statist. Assoc. **6**, 131-138.

Fan, J. Q. and Li, R. Z. (2001). Variable selection via nonconcave penalized likelihood and its oracle properties. *J. Amer. Statist. Assoc.* **96**, 456, 1348-1360.

Golub, G., Heath, M. and Wahba, G. (1979). Generalized cross-validation as a method for choosing a good ridge parameter. *Technometrics* **21**, 215-223.

Harshman, R. A. (1970). Foundations of the PARAFAC procedure: models and conditions for an 'explanatory' multi-modal factor analysis. *UCLA Work. Pap. Phon.* **16**, 1-84.

Hastie, T. and Tibshirani, R. (1990). *Generalized Additive Models.* Chapman and Hall, London.

Hoerl, A. E. and Kennard, R. W. (2000). Ridge Regression: biased estimation for nonorthogonal problems. *Technometrics* **42**, 80-86.

Hunter, D. R. and Li, R. (2005). Variable selection using MM algorithms. Ann. Statist. **33**, 1617-1642.

Kruskal, J. B. (1977). Three-way arrays: rank and uniqueness of trilinear decompositions, with application to arithmetic complexity and statistics. *Linear Algebra Appl.* **18**, 95-138.

Land, S. and Friedman, J. (1996). Variable fusion: a new method of adaptive signal regression. Technical Report. Department of Statistics, Stanford University, Stanford.

Martínez-Montes, E., Valdés-Sosa, P. A., Miwakeichi, F., Goldman, R. and Cohen, M. (2004). Concurrent EEG/fMRI analysis by multi-way partial least squares. Neuroimage **22**, 1023-1034.

Miwakeichi, F., Martinez-Montes, E., Valdés-Sosa, P. A., Nishiyama, N., Mizuhara, H. and Yamaguchi, Y. (2004). Decomposing EEG data into space-time-frequency components using Parallel Factor Analysis. Neuroimage **22**, 1035-1045.

Morup, M. (2005). Analysis of brain data using multi-way array models on the EEG. Msc Thesis, Technical University of Denmark.

Morup, M., Hansen, L. K., Herrmann, C. S., Parnas, J. and Arnfred, S. M. (2006). Parallel Factor Analysis as an exploratory tool for wavelet transformed event-related EEG. *NeuroImage* **29**, 938-947.

Sánchez-Bornot, J. M., Martínez-Montes, E., Lage-Castellanos, E., Vega-Hernández, M. and Valdés-Sosa, P. A. (2008). Uncovering sparse brain effective connectivity: a voxel-based approach using penalized regression. *Statist. Sinica* **18**, 1501-1518.

Schwartz, G. (1978). Estimating the dimension of a model. *Ann. Statist.* **6**, 461-464.

Sidiropoulos, N. D. and Bro, R. (2000). On the uniqueness of multilinear decomposition of N-way arrays. *J. Chemometr.* **14**, 229-239.

Stegeman, A. and Sidiropoulos, N. D. (2007). On Kruskal's uniqueness condition for the Candecomp/Parafac decomposition. *Linear Algebra Appl.* **420**, 540-552.

Tibshirani, R. (1996). Regression shrinkage and variable selection via the lasso. *J. Roy. Statist. Soc. Ser. B* **58**, 267-288.

Tibshirani, R., Saunders, M., Rosset, S., Zhu, J. and Knight, K. (2005). Sparsity and smoothness via the fused lasso. *J. Roy. Statist. Soc. Ser. B* **67**, 91-108.

Timmerman, M. E. and Kiers, H. A. L. (2002). Three-way component analysis with smoothness constraints. *Comput. Statist. Data Anal.* **40**, 447-470.

Tomasi, G. and Bro, R. (2006). A comparison of algorithms for fitting the PARAFAC model. *Comput. Statist. Data Anal.* **50**, 1700-1734.

Valdés-Sosa, P. A., Sánchez-Bornot, J. M., Vega-Hernández, M., Melie-García, L., Lage-Castellanos A. and Canales-Rodríguez, E. (2006). Granger Causality on Spatial Manifolds: applications to Neuroimaging. Chapter 18 in *Handbook of Time Series Analysis: Recent Theoretical Developments and Application.* (Edited by Björn Schelter, Matthias Winterhalder and Jens Timmer). Wiley-VCH, Weinheim.

Zou, H. and Hastie, T. (2005). Regularization and variable selection via the elastic net. *J. Roy. Statist. Soc. Ser. B* **67**, 301-320.

Neurostatistics Department, Cuban Neuroscience Center, Havana, Cuba.

E-mail: eduardo@cneuro.edu.cu

Neurostatistics Department, Cuban Neuroscience Center, Havana, Cuba.

E-mail: bornot@cneuro.edu.cu

Neurostatistics Department, Cuban Neuroscience Center, Havana, Cuba.

E-mail: peter@cneuro.edu.cu

(Received April 2007; accepted March 2008)

Penalized PARAFAC analysis of spontaneous EEG recordings

Eduardo Martínez-Montes, José M. Sánchez-Bornot, Pedro A. Valdés-Sosa

Neurostatistics Department, Cuban Neuroscience Center.

Supplemental Material

1. Determination of the model order in PARAFAC

Determining the correct number of components in a PARAFAC decomposition is a difficult task, in which experience and prior knowledge on the data to be analyzed is very useful. Although no flawless method exists for this purpose, a few different approaches have been used so far. One is the use of residual analysis (or a Scree-plot), similarly applied to bilinear methods such as Principal Component Analysis. On one hand, if systematic variation is left in the residuals, it is an indication that more components can be extracted. On the other hand one can plot the number of components versus the percentage variance explained by the model or the residuals. Then, only those components explaining large percentage of the variance are considered relevant. Another method is the Split-half analysis, which consists in randomly splitting the data in two halves and fit a PARAFAC model to each of them. Due to the uniqueness, the decomposition will be the same only if the correct number of components is used (Bro (1998)). Another approach is the use of cross-validation (CV) (see e.g. Louwerse, Smilde and Kiers (1999)) and evaluation of information criteria such as Bayesian Information Criteria (BIC) (Morup, Hansen, Herrmann, Parnas and Arnfred (2006)). Finally, other more sophisticated methods have been developed such as the Add-one-Up (Chen, Liu, Cao and Yu (2001)) and the Core Consistency Diagnostic (Corcondia), which apply especially to PARAFAC models (Bro (1998)).

In this paper we use the Corcondia measure, together with the analysis of residual variance. This measure is based on the fact that the PARAFAC model can be seen as a particular case of a more general model known as Tucker 3,

whose structural equation is as follows:

$$x_{ijk} = \sum_{d=1}^{N_d} \sum_{e=1}^{N_e} \sum_{f=1}^{N_f} a_{id} b_{je} c_{kf} g_{def} + \varepsilon_{ijk}$$

The properties and usefulness of this model are extensively described in Bro (1998). For our purposes we only need to show that the main differences of this model with PARAFAC are i) that the loading matrices can have different number of components (N_d, N_e and N_f respectively) and ii) the existence of the so-called 'core array' $\mathbf{G}_{(N_d \times N_e \times N_f)}$ (with elements g_{def}), which allows for modelling weighted combinations of the loading matrices. Then, this model reduces to PARAFAC when $N_d = N_e = N_f$ and $\mathbf{G}$ is the superidentity three dimensional array (i.e. it has zeroed elements apart from those elements in the superdiagonal which are ones).

After having fitted a PARAFAC model to the data **X,** verification that the trilinear structure is appropriate can be obtained by calculating the core array of a Tucker 3 model for the same data using the estimated loading matrices by PARAFAC. This estimation is made by least squares regression and if PARAFAC is valid, then this estimated core array $\mathbf{G}$ should resemblance the superidentity array $\mathbf{T}$. A simple way to assess if the model structure is reasonable is therefore to monitor the distribution of superdiagonal and off-superdiagonal elements of $\mathbf{G}$, which can be summarized in a single parameter (Core Consistency) defined as:

$$Core\ Consistency = 100 \left(1 - \frac{\sum_{d=1}^{N_d} \sum_{e=1}^{N_e} \sum_{f=1}^{N_f} (t_{def} - g_{def})^2}{\sum_{d=1}^{N_d} \sum_{e=1}^{N_e} \sum_{f=1}^{N_f} g_{def}^2} \right)$$

This is a general measure of the trilinearity of the data, taking the value 100% in the ideal case in which the data conform exactly to the trilinear model. If this is not the case (e.g. if Corcondia is lower than 85%) then either too many components have been extracted, the model is misspecified, or gross outliers disturb the model (Bro (1998)). Among the advantages of the use of this measure is that there is no need for prior assumptions on the distribution of residuals neither to estimate degrees of freedom (as in using information criteria such as CV, BIC). Despite its simplicity, this measure has been shown to be a very powerful tool in assessing the real number of components in several fields of application of the PARAFAC model (Bro and Kiers (2003), Miwakeichi, Martínez-Montes,

Valdés-Sosa, Nishiyama, Mizuhara and Yamaguchi (2004), Morup (2005), Morup, Hansen, Herrmann, Parnas and Arnfred (2006)).

2. Lemma 1 and its proof.

Lemma 1. Consider the minimization of the loss function of a multiple penalized linear regression model for a row $\mathbf{a}^T$, subject to any constraint: $\min\left(\left\|\mathbf{T}-\mathbf{z}\mathbf{a}^T\right\|^2+\sum\lambda_l P_l(\mathbf{a})\right)$. The solution to this problem is equivalent to $\min\left(\left\|\boldsymbol{\alpha}-\mathbf{a}\right\|^2+\sum\overline{\lambda}_l P_l(\mathbf{a})\right)$, where $\boldsymbol{\alpha}$ is the solution of the unconstrained problem: $\boldsymbol{\alpha}=\arg\min\left(\left\|\mathbf{T}-\mathbf{z}\boldsymbol{\alpha}^T\right\|^2\right)=\mathbf{T}^T\mathbf{z}/\mathbf{z}^T\mathbf{z}$, and $\overline{\lambda}_l=\lambda_l/\mathbf{z}^T\mathbf{z}$.

Proof.

Let $\boldsymbol{\alpha}=\mathbf{T}^T\mathbf{z}/\mathbf{z}^T\mathbf{z}$ and $\mathbf{H}=\mathbf{T}-\mathbf{z}\boldsymbol{\alpha}^T$. Then $\min\left(\left\|\mathbf{T}-\mathbf{z}\mathbf{a}^T\right\|^2+\sum\lambda_l P_l(\mathbf{a})\right)=$
$=\min\left(\left\|\mathbf{H}+\mathbf{z}\boldsymbol{\alpha}^T-\mathbf{z}\mathbf{a}^T\right\|^2+\sum\lambda_l P_l(\mathbf{a})\right)=\min\left(\left\|\mathbf{H}+\mathbf{z}(\boldsymbol{\alpha}-\mathbf{a})^T\right\|^2+\sum\lambda_l P_l(\mathbf{a})\right)=$
$=\min\left(\|\mathbf{H}\|^2+2trace(\mathbf{H}^T\mathbf{z}(\boldsymbol{\alpha}-\mathbf{a})^T)+\mathbf{z}^T\mathbf{z}\left\|\boldsymbol{\alpha}-\mathbf{a}\right\|^2+\sum\lambda_l P_l(\mathbf{a})\right)$. Since $\|\mathbf{H}\|^2$ does not depend on $\mathbf{a}$ (constant term), $\mathbf{H}^T\mathbf{z}=0$, and $\mathbf{z}^T\mathbf{z}$ is a non-negative scalar, then we can divide the function by $\mathbf{z}^T\mathbf{z}$ and define $\overline{\lambda}_l=\lambda_l/\mathbf{z}^T\mathbf{z}$ to finally get:

$\min\left(\left\|\mathbf{T}-\mathbf{z}\mathbf{a}^T\right\|^2+\sum\lambda_l P_l(\mathbf{a})\right)=\min\left(\left\|\boldsymbol{\alpha}-\mathbf{a}\right\|^2+\sum\overline{\lambda}_l P_l(\mathbf{a})\right)$.■

3. Data description and preproccesing

The data chosen for the study consist of an EEG recording on 16 bipolar derivations (Fp2-F8, F8-T4, T4-T6, T6-O2, O2-P4, P4-C4, C4-F4, F4-Fp2; Fp1-F7, F7-T3, T3-T5, T5-O1, O1-P3, P3-C3, C3-F7, F7-Fp1) for a subject in resting state. The corresponding time-varying spectra are computed with the use of Thomson multitaper method (Thomson (1982)). Then, we end up with a three dimensional data set of 208 320 elements, indexed by 16 derivations, 124 frequencies and 105 time points, that can be subject to PARAFAC analysis as is schematically shown in figure 1 of this supplemental material. Other details about the data can be found in Goldman, Stern, Engel and Cohen (2002).

This data was used previously, together with fMRI data for a concurrent analysis using multi-way Partial Least Squares (Martínez-Montes, Valdés-Sosa, Miwakeichi, Goldman and Cohen (2004)) where only the spectral loading obtained by unconstrained PARAFAC decomposition via ALS was reported. Ex-

amination of Corcondia, residual errors and explained variance allowed to determine the appropriate number of components as 3. Here we followed the same preprocessing carried out in that work. Firstly, three outlier time points were identified by the analysis of leverages and removed for subsequent analysis. Secondly, the data was centered along the frequency dimension and scaled through time and space. Finally, the spectral and spatial loadings were normalized while the temporal one kept the scale of the data. In the same way the physical magnitude (microvolts squared) can be assigned to any of the loadings indistinctly, therefore, in this paper we will refer to values of the loadings as energy of the data and omit labels on y-axes of figures.

4. Supplemental figures and Tables

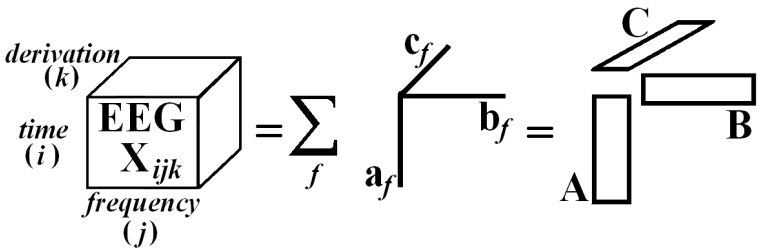

Figure 1. Schematic representation of PARAFAC decomposition. The time-varying EEG spectrum is decomposed as a sum of atoms, each being the outer (tensor) product of signatures corresponding to dimensions. Matrices $\mathbf{A}$, $\mathbf{B}$ and $\mathbf{C}$ contain atoms as columns.

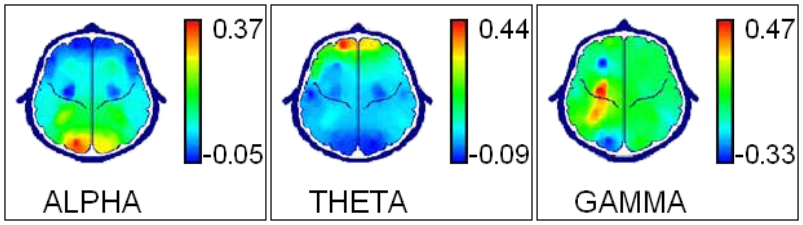

Figure 2. Topographical representation of spatial signatures of the three atoms obtained with unconstrained PARAFAC decomposition. Reproduced from Martínez-Montes, Valdés-Sosa, Miwakeichi, Goldman, and Cohen (2004), (their figure 6). The values in the colorbar represents normalized energy.

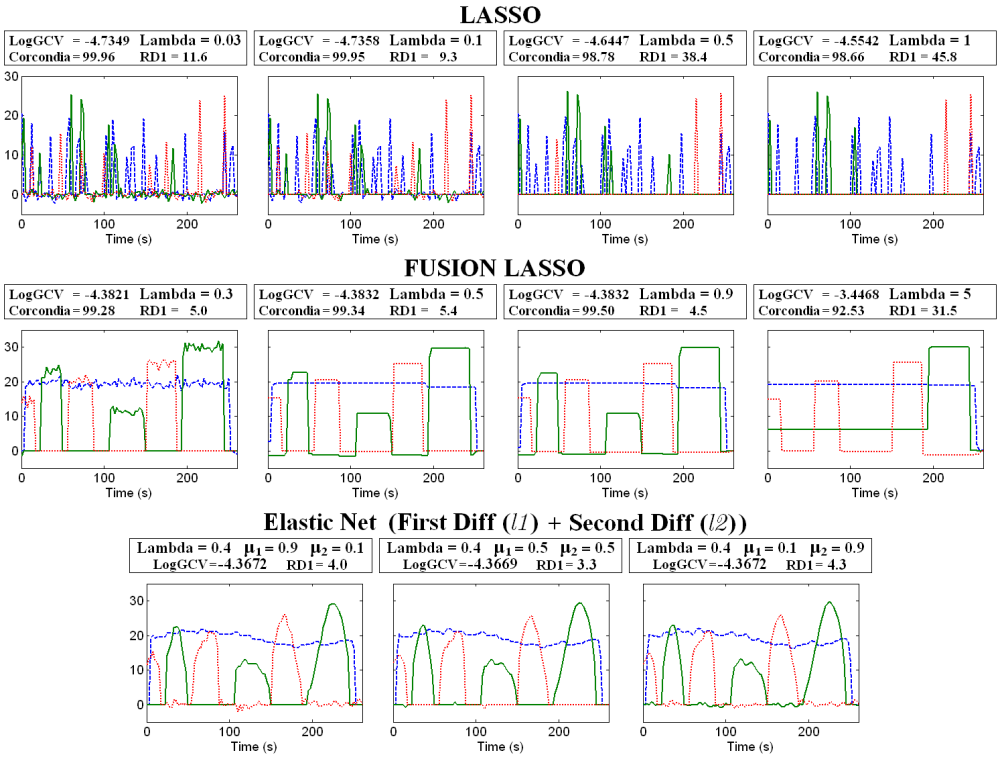

Figure 3. Temporal loadings obtained using different penalizers for the three simulated scenarios presented in figure 3 of the manuscript. In all cases, corresponding values of lambda, logarithm of GCV, Corcondia and relative distances are shown. Green solid line represents the Alpha atom, red dotted line represents the Theta atom and blue dashed line the Gamma atom. Top row: using Lasso penalization for the first simulated scenario (figure 3a of the manuscript), with different weighting parameters. Corcondia was above 99% in all cases, since the data is by construction trilinear, though noisy. However, according to logGCV the optimum value for the weighting parameter is 0.1, which also have the lowest relative distance to the real loading. Middle row: using Fusion Lasso penalization with different values of lambda on the second simulated data (figure 3b of the manuscript). The value $\lambda = 0.9$ seems to be optimal, having the highest Corcondia, the lowest logGCV and the lowest relative distance to the real loading. Bottom row: using Enet penalization on the third simulated scenario (figure 3c of the manuscript). Enet solutions were found using a first order difference operator for the *l1*-norm term and a second order difference operator for the *l2*-norm term. Different values of the parameter λ were explored for three different pairs of weights (μ_1 for *l1*-norm term and μ_2 for the *l2*-norm term) and the solution with the lowest logGCV is

presented. The optimal weighting parameter was the same for the three choices of pairs of weights μ_1 and μ_2. Also, values of logGCV and Corcondia (not shown) are almost the same in the three cases and we could select the solution with $\mu_1 = \mu_2 = 0.5$ as the best one based only on the relative distance to the real loading.

Table 1. Parameters of interest for comparing PARAFAC decompositions obtained with different degrees of smoothness for the spectral loadings. Note that among constrained solutions, lambda=1 gives the lowest GCV, RSS and relative distances, while the highest Corcondia.

lambda	0	0.3	0.5	1	5	10	50
logGCV	-3.4581	-3.4138	-3.4493	**-3.4559**	-3.4385	-3.3850	-3.2426
Corcondia	93.43	75.04	93.24	**93.48**	92.59	92.18	90.96
RSS	6512.67	6821.23	6571.55	**6527.91**	6642.44	7008.00	8080.08
df	735.0	549.9	734.9	734.8	734.1	733.2	726.3
Time (s)	0.23	405.36	453.62	140.80	108.11	95.46	90.71
Niter	4	7	14	**6**	6	6	6
RD 1 (%)	0	33.54	9.68	**5.67**	5.75	5.79	8.20
RD 2 (%)	0	81.45	33.21	**28.65**	31.36	32.69	40.67
RD 3 (%)	0	55.26	3.62	**2.43**	5.92	7.91	13.56

Legend: lambda = smoothing parameter; logGCV = logarithm of Generalized Cross Validation function evaluated at lambda; Corcondia = Core Consistency Diagnostic; RSS = residual sum of squares; df = degrees of freedom; Time = time of computation, in seconds; Niter = number of iterations needed for convergence; RD 1 = relative distance between estimated temporal signature and temporal signature of the unconstrained PARAFAC decomposition, in percent. This is defined as the ratio between the norm of the difference between constrained and unconstrained loadings and the norm of the constrained loading. RD 2 and RD 3 = idem to RD 1 but for spectral and spatial loadings respectively.

References

Bro, R. (1998). Multi-way Analysis in the Food Industry: Models, Algorithms and Applications. Ph.D. Thesis. University of Amsterdam and Royal Veterinary and Agricultural University, Denmark.

Bro, R. and Kiers, H. A. L. (2003). A new efficient method for determining the number of components in PARAFAC models. J.Chemometr. 17, 274-286.

Chen, Z. P., Liu, Z., Cao, Y. C. and Yu, R. Q. (2001). Efficient way to estimate the optimum number of factors for trilinear decomposition. Anal Chim. Acta 444, 295-307.

Goldman, R. I., Stern, J. M., Engel, J. and Cohen, M. S. (2002). Simultaneous EEG and fMRI of the alpha rhythm. NeuroReport 13, 18, 2487-2492.

Louwerse, D. J., Smilde, A. K. and Kiers H. A. L. (1999). Cross-validation of multiway component models. J. Chemometr. 13, 491-510.

Martínez-Montes, E., Valdés-Sosa, P. A., Miwakeichi, F., Goldman, R., and Cohen, M. (2004). Concurrent EEG/fMRI Analysis by Multi-way Partial Least Squares. Neuroimage 22, 3 1023-1034.

Miwakeichi, F., Martínez-Montes, E., Valdés-Sosa, P. A., Nishiyama, N., Mizuhara, H., and Yamaguchi, Y. (2004). Decomposing EEG data into space-time-frequency components using Parallel Factor Analysis. Neuroimage 22, 3, 1035-1045.

Morup, M. (2005). Analysis of brain data using multi-way array models on the EEG. Msc Thesis. Technical University of Denmark.

Morup, M., Hansen, L. K., Herrmann, C. S., Parnas, J. and Arnfred, S. M. (2006). Parallel Factor Analysis as an exploratory tool for wavelet transformed event-related EEG. NeuroImage 29, 3, 938-947.

Thomson, D. J. (1982). Spectrum estimation and harmonic analysis. Proc. IEEE 70, 1055-1096.

Artículo 6.

Martínez-Montes, E., Vega-Hernández, M., Sánchez-Bornot, J.M., Valdés-Sosa, P.A.: Identifying complex brain networks using penalized regression methods. Journal of Biological Physics 34, 3-4, 315-323 (2008).

J Biol Phys (2008) 34:315–323
DOI 10.1007/s10867-008-9077-0

ORIGINAL PAPER

Identifying Complex Brain Networks Using Penalized Regression Methods

Eduardo Martínez-Montes · Mayrim Vega-Hernández · José M. Sánchez-Bornot · Pedro A. Valdés-Sosa

Received: 14 January 2008 / Accepted: 11 April 2008 /
Published online: 5 July 2008

Abstract The recorded electrical activity of complex brain networks through the EEG reflects their intrinsic spatial, temporal and spectral properties. In this work we study the application of new penalized regression methods to i) the spatial characterization of the brain networks associated with the identification of faces and ii) the PARAFAC analysis of resting-state EEG. The use of appropriate constraints through non-convex penalties allowed three types of inverse solutions (Loreta, Lasso Fusion and ENet L) to spatially localize networks in agreement with previous studies with fMRI. Furthermore, we propose a new penalty based in the Information Entropy for the constrained PARAFAC analysis of resting EEG that allowed the identification in time, frequency and space of those brain networks with minimum spectral entropy. This study is an initial attempt to explicitly include complexity descriptors as a constraint in multilinear EEG analysis.

Keywords Information Entropy · PARAFAC · EEG inverse problem · Multiple penalized least squares model · Complex brain networks

1 Introduction

The complexity of neuronal networks is clearly apparent in their dynamics, which is driven by the activity and interaction of a large number of neurons in each network. This has created the need for developing advanced statistical tools that deal with a huge amount of data, especially where the main challenge is the analysis of neuroimaging data in which the number of hidden parameters to estimate is much greater than the number of observations. Major examples are the cases of the well-known inverse problem of Electroencephalography (EEG) [1], the dimensionality reduction (time–frequency, principal and independent components, parallel factor) analysis of EEG [2–4], and the estimation of connectivity

E. Martínez-Montes (✉) · M. Vega-Hernández · J. M. Sánchez-Bornot · P. A. Valdés-Sosa
Neurostatistics Department, Cuban Neuroscience Center, Ave. 25, esq 158, #15202, Cubanacán, Havana, Cuba PO Box: 6414
e-mail: eduardo@cneuro.edu.cu

patterns from functional Magnetic Resonance Imaging (fMRI) time series [5]. Despite some attempts to model nonlinear aspects of these complex scenarios [6], the use of linear models is the most popular approach and still demonstrates its capacity of dealing with new facets of neuroscience problems [7, 8]. In this context, very often one has to use different sources of knowledge (anatomical, physiological) about the parameters of interest to achieve interpretable results, which has made the use of the Bayesian framework and penalized least squares (PLS) regression, two of the most appealing approaches.

PLS models have been addressed as multivariate linear regressions with regularization with efficient and flexible techniques to solve variable selection problems. Interestingly, the use of non-convex penalty functions (non-quadratic, continuous and with a singularity at the origin) has been proposed to obtain sparse and stable solutions [9], such as the Least Absolute Shrinkage Selection Operator (Lasso) [10] and the Smoothed Clipped Absolute Deviation [9], which also produces unbiased estimators. Moreover, this approach can be extended to use any combination of penalties, leading to solutions sharing properties such as smoothness and sparseness, e.g. Elastic Net (ENet) [11] combines a Lasso-type penalty term and a quadratic penalty term. These nonlinear models are estimated by modified Newton–Raphson algorithms such as the Local Quadratic Approximation [9] and the Minorization–Maximization [12], which are based on an iterative estimation of (Ridge) quadratic regression and have recently been generalized to deal with multiple penalty terms simultaneously, i.e. to tackle the Multiple Penalized Least Squares (MPLS) model [13].

In this work we present the application of this methodology to the spatial characterization of the brain networks associated with the identification of faces and to the Parallel Factor Analysis (PARAFAC) of resting-state EEG. The PARAFAC analysis of the time-varying spectra of the multichannel EEG allows for an identification of brain networks responsible for spontaneous rhythms, characterizing them simultaneously in time, frequency and space. In both cases we explore the usefulness of different non-convex penalties already described in the literature. Further, we propose a new penalty based on the Information Entropy to be applied in the identification of neuronal networks with minimum spectral entropy in the spontaneous EEG.

2 Materials and Methods

2.1 MPLS Model and Entropy–Ridge Penalty

Consider the multivariate linear regression model: $\mathbf{y}=\mathbf{X}\boldsymbol{\beta}+\mathbf{e}$, where $\boldsymbol{\beta}$ is the vector of parameters to estimate; $\mathbf{y}$ the data vector; $\mathbf{X}$ the given design matrix and $\mathbf{e}$ the vector of independent and identically distributed random errors. Then, the MPLS model for $\boldsymbol{\beta}$ is stated as:

$$\hat{\boldsymbol{\beta}} = \arg\ \min\left\{(\mathbf{y}-\mathbf{X}\boldsymbol{\beta})^T(\mathbf{y}-\mathbf{X}\boldsymbol{\beta}) + \sum \lambda_m p_m(\boldsymbol{\beta})\right\} \quad (1)$$

where the sum is over $m=1,\ldots,N$ penalties, which impose different kinds of constraints through $p_m(\boldsymbol{\beta})$, with corresponding weighting parameters λ_m. In this work we will use the following penalty functions: (1) Ridge, which is the usual l_2-norm of the vector of coefficients and produces stable and non-sparse solutions; (2) Lasso, which is the l_1-norm of the vector of coefficients and produces very sparse solutions; (3) Lasso Fusion [14], which is the l_1-norm of the application of the first differences operator on the coefficients and produces sparse solutions with piece-wise flat behavior; (4) ENet, which is a sum of an l_1-norm term and an

l_2-norm term, producing sparse solutions with piece-wise smooth behavior. These penalty functions are defined in the second column of Table 1, and their plots are depicted in Fig. 1.

When $\boldsymbol{\beta}$ can be considered as a probability density function (pdf), i.e. when it is normalized to unity, the Information Entropy is defined as $H(\boldsymbol{\beta}) = -k\sum \beta_j \ln \beta_j$, with j= 1,…,n and k is a positive constant [15]. This measure will be maximum for $\beta_j = 1/n; \forall j$ and minimum ($H(\boldsymbol{\beta})$=0) when $\beta_l = 1$ and $\beta_j = 0; \forall j \neq l$. Therefore it is a measure of the "peakness" of the pdf. If we use this measure as a penalty in MPLS, we are constraining the solution to have minimum Entropy, i.e. to be the sharpest one. Note that this penalty differs from the so called entropy-penalty or l_0 penalty, defined as the l_0-norm of the parameters to estimate [9].

According to the conditions given by [9], modified to cope with our model in equation 1, a penalty function of the form $p(\boldsymbol{\beta}) = \sum \bar{p}(\beta_j)$ with β_j>0, produces (1) sparse solutions iff $\min\{\bar{p}'(\beta_j)/2 + \beta_j\} > 0$ and (2) unbiased solutions iff $\bar{p}'(\beta_j) = 0$ for β_j=1. It is easy to find that the penalty function $H(\boldsymbol{\beta})$ produces sparse solutions if k<2 but does not satisfy the unbiasedness condition. However, it is easy to derive a sparse and unbiased estimator with the use of a penalty which combines the Entropy with a Ridge penalizer, of the form:

$$p(\boldsymbol{\beta}) = -\sum \left(\beta_j \ln \beta_j - \beta_j^2 \big/ 2\right).$$

In effect, for each element β_j, $\arg\min\left\{\bar{p}'(\beta_j)/2 + \beta_j\right\} = 1/3$, which leads to fulfill condition 1 since $\bar{p}'(1/3)/2 + 1/3 = (\ln 3)/2 > 0$. On the other hand, $\bar{p}'(\beta_j = 1) = -\ln(1) - 1 + 1 = 0$, thus fulfilling condition 2. We will call this function the Entropy–Ridge penalty and its shape is shown in Fig. 1.

2.2 Spatial Localization of Neural Sources

The inverse problem (IP) of the EEG consists in the identification of the neural current sources inside the brain generating the voltage field measured over an array of sensors distributed on the scalp surface. The mathematical relation between these voltages ($\mathbf{y}$) and the Primary Current Density (PCD, $\boldsymbol{\beta}$) can be written as a system of linear equations:

$$\mathbf{y} = \mathbf{K}\boldsymbol{\beta} + \boldsymbol{\varepsilon} \tag{2}$$

where $\boldsymbol{\varepsilon}$ represents the experimental noise and $\mathbf{K}$ is known as the electric lead field: a matrix that comprise the geometrical and electrical properties of the model assumed for the head. This system is highly underdetermined since the number of unknown generators inside the brain is much higher than the number of sensors. Therefore, there is no unique solution and the IP is ill-posed.

The additional (prior) information or constraints used for obtaining a unique solution characterizes each of the known inverse solutions [1]. Also, different approaches have

Table 1 Some inverse solutions derived from MPLS model

Name	$\sum \lambda_m p_m(\boldsymbol{\beta})$	Inverse solution
Ridge	$\lambda \boldsymbol{\beta}^{\mathrm{T}} \mathbf{Q}^{\mathrm{T}} \mathbf{Q} \boldsymbol{\beta}$	If **Q**=**I**→Minimum Norm; if **Q**=**L**→Loreta
Lasso	$\lambda \sum \lvert \mathbf{q}_j \boldsymbol{\beta} \rvert$	If **Q**=**I**→Lasso; if **Q**=**L**→Lasso Fusion
ENet	$\lambda_1 \boldsymbol{\beta}^{\mathrm{T}} \mathbf{R}^{\mathrm{T}} \mathbf{R} \boldsymbol{\beta} + \lambda_2 \sum \lvert \mathbf{q}_j \boldsymbol{\beta} \rvert$	If **Q**=**R**=**I**→ENet; if **Q**=**R**=**L**→ENet L

Q ($\mathbf{q}_j$ as j-th row) and **R** are linear operators. **I** is the identity matrix, and **L** a discrete version of Laplacian operator. ENet stands for Elastic Net.

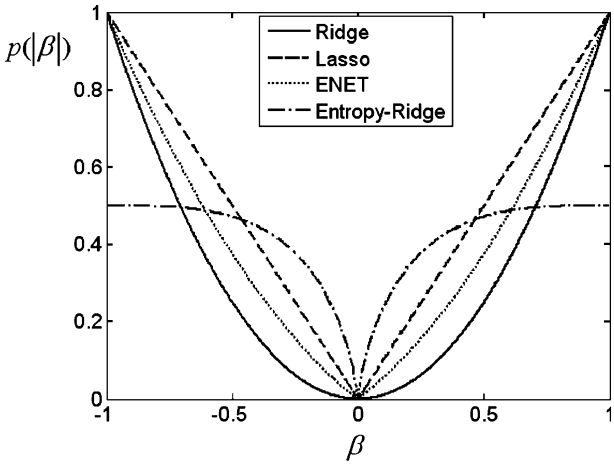

Fig. 1 Penalty functions: Ridge (*solid*), Lasso (*dash*), ENet (*dot*), Entropy–Ridge (*dot-dash*)

been used (Bayesian, Dipole fitting) but the most popular is the regularization, which is equivalent to a PLS regression. Therefore, the IP can be formulated as a general MPLS model in the form of equation 1, where the lead field is the design matrix. This formulation encompasses several known inverse solutions as particular cases, e.g. Minimum Norm and Low Resolution Electromagnetic Tomography (Loreta, see Table 1 and [1]). On the other hand, the use of non-convex penalty functions allows to obtain new types of inverse solutions [16], whose performance is explored here in the source analysis of face recognition. As a first approximation, optimal values for λ_m will be found by generalized cross-validation [17].

2.3 Penalized PARAFAC

The multidimensional nature of neuroscience data has made the use of multiway statistical analysis suitable in this field. Many bidimensional approaches such as Independent and Principal Components Analysis (PCA) are very popular but offer non-interpretable results when higher dimensional structure is hidden in the data. PARAFAC analysis is a generalization of PCA to deal with multidimensional data. For example, the EEG time-varying spectra is a three dimensional array ($\mathbf{Y}_{(I\times J\times K)}$), indexed by channels, time points and frequencies [4]. The PARAFAC model is then stated as:

$$y_{ijk} = \sum a_{if} b_{jf} c_{kf} + \varepsilon_{ijk}$$

where a_{if}, b_{jf} and c_{kf} are the elements of loading matrices $\mathbf{A}_{(I\times F)}$, $\mathbf{B}_{(J\times F)}$ and $\mathbf{C}_{(K\times F)}$, respectively, and ε_{ijk} represents the noise. The sum is over $f=1,\ldots,F$, which represents components or atoms. For each component the corresponding columns of **A**, **B** and **C** define the spatial (topographic), temporal and spectral signatures respectively. The spectral signatures show the frequency content of the present activities and allow the identification of brain rhythms. The corresponding spatial and temporal signatures give the topographic map and dynamics of the neuronal networks producing those rhythms.

The main advantage of PARAFAC is that the decomposition is unique (up to a scale factor or permutation of components) under very mild conditions without requiring orthogonality or independence among components [18]. However, physiologically acceptable constraints are of help in the interpretation of results. The matrix formulation of PARAFAC allows the estimation of the loading matrices via the Alternating Least Squares (ALS) algorithm [18], in which, iteratively, each loading is (least squares-) estimated conditionally on the others. Substituting each least squares step in ALS by an MPLS regression allows us to introduce different types of constraints in the PARAFAC decomposition.

In the case of the time-varying spectra of the EEG, we have explored the use of smoothness constraints for the spectral loading, with the Ridge penalty, using a Laplacian operator [19]. Here we further use the ENet L (ENet using a Laplacian operator, see Table 1) and the Entropy–Ridge penalties in the estimation of spectral signatures. The former is aimed to find sparse spectra with smooth patches in the relevant frequencies, while the latter would imply to constraining the loadings to have minimum spectral Entropy, which can be interpreted as finding those functional brain networks with a well-defined frequency of oscillation. This is possible since the spectral signatures obtained from PARAFAC are normalized to unity as a scaling convention to deal with the scale indeterminacy.

3 Results

3.1 Source Localization of Face Recognition

The analyzed data set corresponds to an experiment in which subjects are presented with images of faces or non-faces followed by a mask image after 30 ms. They are required to respond if a face was presented or not. This kind of experiment evokes a voltage transient that appears in the EEG as a negative peak around 170 ms after presentation of the stimulus and is known as N170 peak. The amplitudes of this peak for each electrode form a topography, corresponding to vector **y** in equation 2. Sources of the evoked N170 peak were sought separately for the topographies corresponding to correct and incorrect responses (averaged across 80 trials), as well as for the differential topography (correct minus incorrect) with the use of Loreta, Lasso Fusion and ENet L (Table 1) methods. Note that the map found in the case of differential topography with these nonlinear inverse methods is not necessarily the difference between the maps found from correct and incorrect topographies. Since the PCD is a vector field, the Hotelling's T^2 statistic [20] was computed across 10 subjects for each condition and for the difference between them.

Figure 2 shows the maximum intensity projection in the coronal view of the estimated Hotelling's T^2 images by the three methods for each condition: correct response (top row), incorrect response (middle row) and differential topography (bottom row). Significant activations for the correct and incorrect detection of faces were found in the right inferior and superior temporal gyrus, in the middle frontal gyrus (right and left) and in the right middle occipital gyrus, although with different degree of activation. These areas are in agreement with previous fMRI studies on the conscious perception of faces [21]. Significant differential sources were located mainly in the right inferior temporal and middle occipital gyri.

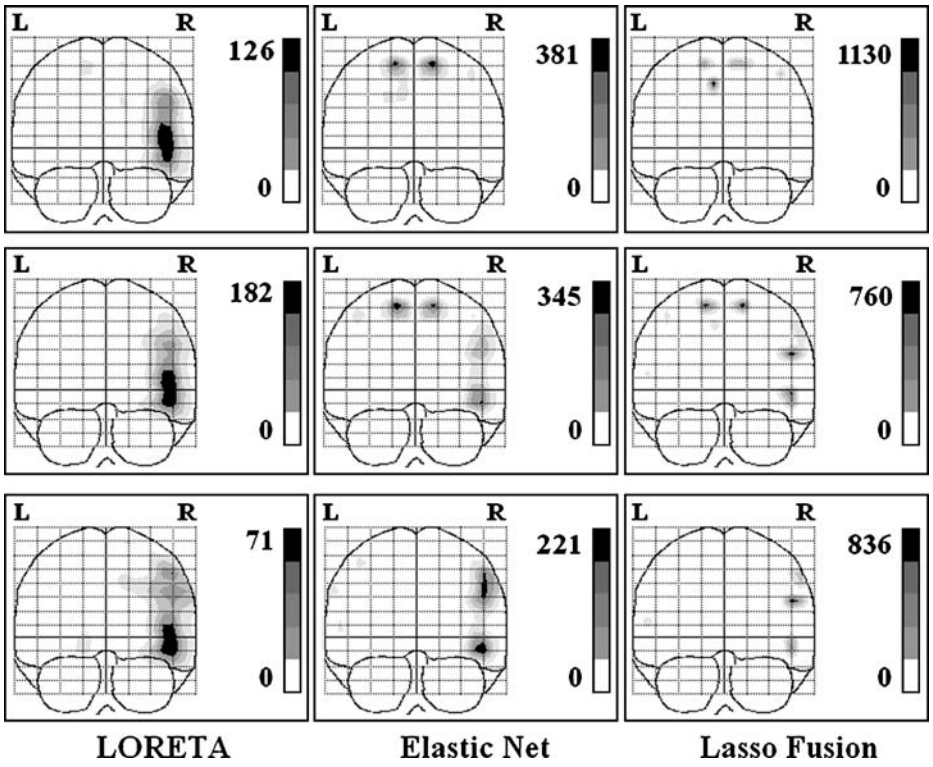

Fig. 2 Hotelling's T^2 images of sources of evoked N170 peak corresponding to topographic maps of correct face detection (*upper panel*), incorrect face detection (*middle panel*), and the difference between correct and incorrect detection (*bottom panel*)

On the other hand, it can be seen that the use of l_1-norm (Lasso Fusion) allows for much more concentrated (sparser) solutions, dividing the usual low resolution image given by Loreta in several sources. ENet L, in turn, offers solutions with intermediate degree of sparseness and smoothness (that can be tuned through the regularization parameters) and which are more physiologically plausible.

3.2 Penalized PARAFAC Analysis of Resting EEG

The time-varying spectral density of a resting-state EEG was obtained with Thomson's multitaper method, organized as a three-dimensional array (indexed by channels, time points and frequencies) and decomposed by unconstrained and constrained PARAFAC into three components with corresponding topographic, temporal and spectral signatures [22]. The latter allowed the identification of spontaneous brain rhythms. Figure 3a shows unconstrained spectral loadings which, although presenting clear main peaks, have negative values and some oscillating behavior that might be due to fitting residual noise. Figure 3b presents the smoother loadings given by constrained PARAFAC using a Ridge penalty with a Laplacian operator.

Figure 4a shows the piece-wise smooth spectral loading as estimated by using an ENet penalty, and Fig. 4b the sparser loadings obtained with the Entropy–Ridge penalty. The three constrained versions are more reasonable and physiologically sound options for the

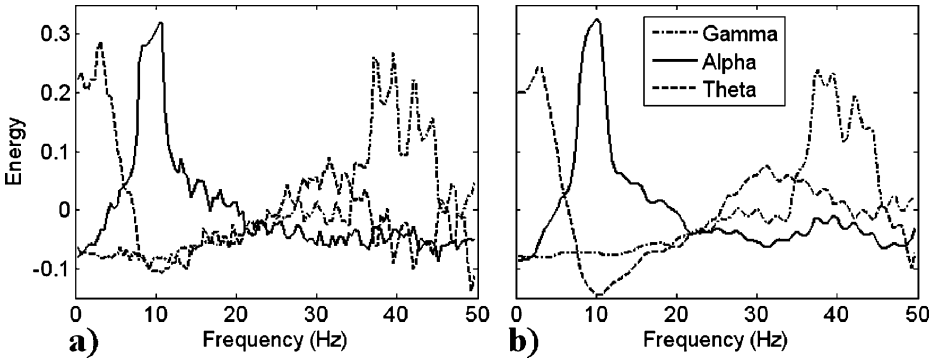

Fig. 3 Spectral signatures found by: **a**) unconstrained PARAFAC, **b**) PARAFAC with MPLS using a Ridge penalty. Components are identified as alpha (*solid*), theta (*dash*) and gamma (*dot-dash*)

interpretability of the results than the unconstrained signatures. However, Ridge and ENet solutions do not avoid the negative values and the oscillating behavior for frequencies far from the main peak.

4 Conclusions

In this work we have applied a general statistical tool, MPLS, to the identification of neuronal networks. This approach allows the use of known as well as yet unexplored types of constraints in neuroscience (even in a combined way), that can represent better the physiological or physical knowledge of complex brain activity.

As a first example of the usefulness of the methodology, three inverse solutions (Loreta, Lasso Fusion and ENet L) found sources in agreement with previous studies with fMRI. In addition, it was shown that by combining l_1- and l_2-norm terms, ENet L offers solutions with intermediate levels of blurring between Loreta (too smooth) and Lasso Fusion (too sparse). However, this method strongly depends on the selection of optimal regularization parameters. Therefore, further research on the use of appropriate (nonlinear) methods is

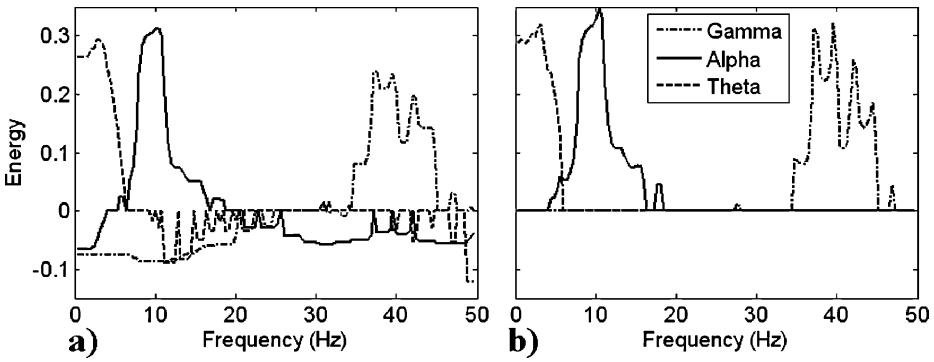

Fig. 4 Spectral signatures found by: **a**) PARAFAC with MPLS using ENet penalty, **b**) PARAFAC with MPLS using Entropy–Ridge penalty. Components are identified as alpha (*solid*), theta (*dash*) and gamma (*dot-dash*)

needed. In general, the formulation of the EEG inverse problem in terms of an MPLS model, offers the possibility of exploring a wide range of new kind of inverse solutions.

On the other hand, application of MPLS to PARAFAC analysis can also lead to more interpretable results. In this work, we proposed a new penalty based in the Information Entropy of the EEG spectral density that allowed the estimation of non-negative and piece-wise smooth spectral loadings with PARAFAC. This is interpreted as the identification in time, frequency and space of those brain networks with minimum spectral Entropy, i.e. whose dynamics shows oscillations in a very well-defined frequency band. Since the PARAFAC decomposition is unique, weighting parameters can be tuned to obtain different degrees of constraint. However, future work is needed on the selection of their optimal values using cross-validation or other information criteria.

In general, this study can be considered as an initial attempt to include the complexity of the brain activities of interest as a constraint in the analysis of the neuroimaging data reflecting them. The use of other measures of complexity as constraints (with penalized regression methods) in the search of complex brain networks should also be carried out. This approach can be of importance in the study of other types of cognitive and pathological activity, such as epilepsy and Alzheimer's disease, where changes in complexity might reflect the functional or health state of the brain.

Acknowledgments The authors thank Mark Cohen and Jhoanna Pérez-Hidalgo-Gato for kindly providing the data of the resting EEG and face identification experiment used in this study.

References

1. Pascual-Marqui, R.D.: Review of methods for solving the EEG inverse problem. Int. J. Bioelectromagn. **1**, (1), 75–86 (1999)
2. Durka, P.J., Blinowska, K.J.: A unified time–frequency parametrization of EEG. IEEE Eng. Med. Biol. **20**, (5), 47–53 (2001)
3. Makeig, S., Westerfield, M., Jung, T.P., Enghoff, S., Townsend, J., Courchesne, E., Sejnowski, T.J.: Dynamic brain sources of visual evoked responses. Science **295**, 690–694 (2002)
4. Miwakeichi, F., Martínez-Montes, E., Valdés-Sosa, P.A., Nishiyama, N., Mizuhara, H., Yamaguchi, Y.: Decomposing EEG data into space–time–frequency components using Parallel Factor Analysis. Neuroimage **22**, (3), 1035–1045 (2004)
5. Harrison, L., Penny, W.D., Friston, K.: Multivariate autoregressive modeling of fMRI time series. Neuroimage **19**, 1477–1491 (2003)
6. Freiwald, W.A., Valdés, P.A., Bosch, J., Biscay, R., Jiménez, J.C., Rodríguez, L.M., Kreiter, A.K., Singer, W.: Testing non-linearity and directness of interactions between neural groups in the macaque inferotemporal cortex. J. Neurosci. Methods **94**, 105–119 (1999)
7. Friston, K.J., Holmes, A.P., Worsley, K.J., Poline, J.P., Frith, C.D., Frackowiak, R.S.J.: Statistical parametric maps in functional imaging: a general linear approach. Hum. Brain Mapp. **2**, (4), 189–210 (1994)
8. Kiebel, S.J., Tallon-Baudry, C., Friston, K.J.: Parametric analysis of oscillatory activity as measured with EEG/MEG. Hum. Brain Mapp. **26**, 170–177 (2005)
9. Fan, J.Q., Li, R.Z.: Variable selection via nonconcave penalized likelihood and its oracle properties. J. Am. Stat. Assoc. **96**, 1348–1360 (2001)
10. Tibshirani, R.: Regression shrinkage and variable selection via the lasso. J. R. Stat. Soc. Ser. B **58**, 267–288 (1996)
11. Zou, H., Hastie, T.: Regularization and variable selection via the elastic net. J. R. Stat. Soc. Ser. B **67**, 301–320 (2005)
12. Hunter, D.R., Li, R.: Variable selection using MM algorithms. Ann. Stat. **33**, 1617–1642 (2005)
13. Valdés-Sosa, P.A., Sánchez-Bornot, J.M., Vega-Hernández, M., Melie-García, L., Lage-Castellanos, A., Canales-Rodríguez, E.: Granger causality on spatial manifolds: applications to neuroimaging. In: Schelter, B., Winterhalter, M., Timmer, J. (eds.) Handbook of Time Series Analysis: Recent Theoretical Developments and Applications, pp. 461–492. Wiley-VCH, Weinheim (2006)

14. Land, S., Friedman, J.: Variable fusion: a new method of adaptive signal regression. Technical Report. Department of Statistics, Stanford University, Stanford (1996)
15. Shannon, C.E.: A mathematical theory of communication. Bell Syst. Tech. J. **27**, 379–423, 623–656 (1948)
16. Vega-Hernández, M., Sánchez-Bornot, J.M., Lage-Castellanos, A., Martínez-Montes, E., Valdés-Sosa, P.A.: Penalized regression methods for solving the EEG inverse problem. NeuroImage **27**(1) (2006) (CD-ROM)
17. Golub, G.H., Heat, M., Wahba, G.: Generalized cross-validation as a method for choosing a good ridge parameter. Technometrics **21**, 215–223 (1979)
18. Bro, R.: Multi-way analysis in the food industry: Models, algorithms and applications. PhD thesis, University of Amsterdam and Royal Veterinary and Agricultural University, Denmark, (1998)
19. Martínez-Montes, E., Sánchez-Bornot, J.M., Valdés-Sosa, P.A.: Generalized penalized PARAFAC analysis of EEG time series. NeuroImage, **36**(S1), (2007) (CD-ROM)
20. Mardia, K., Kent, J., Bibby, J.: Multivariate analysis. Academic Press, San Diego, CA (1979)
21. Kanwisher, N., McDermott, J., Chon, M.M.: The fusiform area: a module in human extrastriate cortex specialized for face perception. J. Neurosci. **17**, 4302–4311 (1997)
22. Martínez-Montes, E., Valdés-Sosa, P.A., Miwakeichi, F., Goldman, R.I., Cohen, M.S.: Concurrent EEG/fMRI analysis by multi-way partial least squares. NeuroImage **22**, (3), 1023–1034 (2004)

Artículo 7.

Martínez-Montes, E., Valdés-Sosa, P.A., Miwakeichi, F., Goldman, R.I., Cohen, M.S.: Concurrent EEG/fMRI Analysis by Multi-way Partial Least Squares. Neuroimage, 22, 3, 1023-1034 (2004). (Erratum in: Neuroimage 26, 3, 973 (2005)).

ELSEVIER

NeuroImage

www.elsevier.com/locate/ynimg
NeuroImage 22 (2004) 1023–1034

Concurrent EEG/fMRI analysis by multiway Partial Least Squares

Eduardo Martínez-Montes,[a,*] Pedro A. Valdés-Sosa,[a] Fumikazu Miwakeichi,[b] Robin I. Goldman,[c] and Mark S. Cohen[d]

[a] *Neurophysics Department, Cuban Neuroscience Center, Havana, Cuba*
[b] *Laboratory for Dynamics of Emergent Intelligence, RIKEN Brain Science Institute, Wako, Saitama, Japan*
[c] *Hatch Center for MR Research, Columbia University, New York, NY 10032, USA*
[d] *Ahmanson-Lovelace Brain Mapping Center, UCLA, Medical School, Los Angeles, CA 90095, USA*

Received 17 July 2003; revised 12 March 2004; accepted 17 March 2004

Data may now be recorded concurrently from EEG and functional MRI, using the Simultaneous Imaging for Tomographic Electrophysiology (SITE) method. As yet, there is no established means to integrate the analysis of the combined data set. Recognizing that the hemodynamically convolved time-varying EEG spectrum, S, is intrinsically multidimensional in space, frequency, and time motivated us to use multiway Partial Least-Squares (N-PLS) analysis to decompose EEG (independent variable) and fMRI (dependent variable) data uniquely as a sum of "atoms". Each EEG atom is the outer product of spatial, spectral, and temporal signatures and each fMRI atom the product of spatial and temporal signatures. The decomposition was constrained to maximize the covariance between corresponding temporal signatures of the EEG and fMRI. On all data sets, three components whose spectral peaks were in the theta, alpha, and gamma bands appeared; only the alpha atom had a significant temporal correlation with the fMRI signal. The spatial distribution of the alpha-band atom included parieto-occipital cortex, thalamus, and insula, and corresponded closely to that reported by Goldman et al. [NeuroReport 13(18) (2002) 2487] using a more conventional analysis. The source reconstruction from EEG spatial signature showed only the parieto-occipital sources. We interpret these results to indicate that some electrical sources may be intrinsically invisible to scalp EEG, yet may be revealed through conjoint analysis of EEG and fMRI data. These results may also expose brain regions that participate in the control of brain rhythms but may not themselves be generators. As of yet, no single neuroimaging method offers the optimal combination of spatial and temporal resolution; fusing fMRI and EEG meaningfully extends the spatio-temporal resolution and sensitivity of each method.

Keywords: N-PLS; EEG/fMRI fusion; PARAFAC; Multiway analysis; SSI; SITE

Introduction

The armamentarium of the neuroscientist now includes tools with spatial resolution ranging from centimeters to microns and temporal resolution from years to nanoseconds. Even so, no single tool provides an optimal combination of spatial and temporal resolution, and there generally exists a tradeoff in which improvement in one dimension of resolution requires compromises in the other (Churchland and Sejnowski, 1988). Extending our understanding of the functional architecture of the human brain necessarily requires a rational combination of multiple methods. Particularly attractive is the fusion of the superb temporal resolution of electroencephalography (EEG) or magnetoencepalography (MEG), with the excellent contrast and spatial resolving power of functional MRI (fMRI). Several methods of integration have been reported (Horwitz and Poeppel, 2002), each with its own approaches to analysis.

Under the assumption that the response of the brain to a set of stimuli or conditions is the same when acquired at different times, several groups (Babiloni et al., 2001; Baillet et al., 2001; Singh et al., 1998) have attempted the analysis of EEG and fMRI data, gathered separately. While this approach is not without problems (Gonzalez-Andino et al., 2001; Ioannides, 1999), there is increasing evidence that adequate modeling of multimodal data will allow the estimation of the underlying neural processes with simultaneously high spatial and temporal resolution (Trujillo et al., 2001).

More recently, methods have been described for the concurrent collection of EEG and fMRI data (Goldman et al., 2000). These methods make possible the study of dynamic relationship between fluctuations in the blood oxygenation level dependent (BOLD) signal and the properties of the electrical activity recorded on the scalp. Here, the fMRI and EEG data each necessarily provide evidence of the same underlying brain activity, although the extent to which they are measuring the same signals, or even signals from the same processes, is indeterminate.

In a method they have called Simultaneous Imaging for Tomographic Electrophysiology, or SITE, Goldman et al. (2002) created tomograms of the brain regions whose fMRI signal changes were associated with variations in alpha band power. In that work, 16 bipolar EEG channels were recorded under the eyes-closed resting state that is well known to produce elevated alpha wave activity. To match the EEG and the fMRI time courses, they then convolved the

* Corresponding author. Neurophysics Department, Cuban Neuroscience Center, Avenue 25, Esq. 158, #15202, PO Box 6412, 6414 Cubanacán, Playa, Havana, Cuba. Fax: +53-7-208-6707.
E-mail address: eduardo@cneuro.edu.cu (E. Martínez-Montes).
Available online on ScienceDirect (www.sciencedirect.com.)

1053-8119/$ - see front matter © 2004 Elsevier Inc. All rights reserved.
doi:10.1016/j.neuroimage.2004.03.038

measured alpha power at each time point with an a priori hemodynamic response model (Cohen, 1997) and calculated the correlation between the fluctuations of alpha activity and the BOLD time course at each voxel. Alpha activity was defined as the broad band spectral power in the frequency range 8–12 Hz calculated over the 2.5-s period needed to acquire each MRI volume and averaged over the occipital derivations (*T6-O2*, *O2-P4*, *T5-O1*, *O1-P3*). Positive correlations were found in thalamic voxels as well as in the insula, while negative correlations predominated in the parieto-occipital cortex. Thus, these correlation maps showed extended thalamocortical structures implicated in the generation of this EEG rhythm. A deeper analysis of these results, however, leads to further questions.

Traditionally, the EEG has been decomposed into a series of fixed broad spectral bands (delta, theta, alpha, beta, gamma, ...) based more on history and discovery than on a theoretical framework. This approach, although computationally convenient, may obscure the fact that the sources of each of these characteristic oscillations may or may not be unique (Szava et al., 1994). It has been shown that the EEG can be analyzed as a partially overlapping spectral components defined with high-frequency resolution (Pascual-Marqui et al., 1988); each spectral component being interpreted as reflecting the activity in a given oscillatory network. We seek here to associate each of these components with the BOLD-fMRI activity. In keeping with standard terminology in time–frequency decompositions (Chen et al., 2001), these components will be designated as "atoms".

While strong prior information suggests that the scalp locations best associated with alpha power fluctuations may well be near the occipital electrodes, other spectral components may have a more subtle or distributed relationship to scalp topography. Under these more general circumstances, it may be better to have a more data-driven means to estimate the linear combination of EEG measurements (or derivations) that correlate optimally with BOLD. Such estimates are likely to result in greater statistical power for the detection of EEG–fMRI relationships. Similarly, it might be desirable to look at the correlation of the EEG with a calculated optimum linear combination of all BOLD signals, rather than with each voxel separately.

Essentially, our goal has been to seek methods that best explain the spatio-temporal relationships between fMRI and the oscillatory components of the EEG without first forming a priori hypotheses as to which characteristics of the EEG are likely be of most interest. These considerations led us to search for methods of atomic decomposition of the EEG and methods for correlating the output of this decomposition with the fMRI data. There are a lot of well-known methods for data reduction of the EEG. Among them, Principal Components Analysis (PCA), Independent Components Analysis (ICA), and dictionary-based decompositions have been the most explored. They have been applied only to two-dimensional data. As the time-varying EEG spectrum is, in fact, a three-dimensional array (electrode pairs, frequencies, and time), it cannot be expressed conveniently as a matrix. The decomposition of such a multidimensional data has been better accomplished by a generalization of the Singular Value Decomposition known as Parallel Factor Analysis (PARAFAC) (Harshman, 1970), a tool that has been used previously in the analysis of evoked potentials (Field and Graupe, 1991) and pharmacological studies using high-dimensionality EEG data (Estienne et al., 2001). The most interesting advantage of the PARAFAC model is that it provides a unique decomposition without imposing orthogonality or independence constraints to the components. It is also valued for being a parsimonious and "easily interpretable" model (Bro, 1998).

Several calibration methods (Principal Components Regression, ridge regression) can be used for correlating the EEG decomposition and the fMRI data. Although some general guidelines have been given for establishing a hierarchy among them (Kiers, 1991), there is not definitive calibration method that one can stick to, since its correct application depends strongly on the behavior of the data considered. In a straightforward application of any of these methods (e.g., Principal Components Regression), one could use the EEG spectral power estimates (principal components of time-varying EEG spectrum), for different time segments, as the independent variable to be correlated with the fMRI. This procedure in two steps (decomposing and correlating) does not ensure that we are finding the optimal relationship between the EEG and the fMRI because decomposition is based on nonphysiological assumptions (e.g., it is unreasonable to expect that the activities of individual neural generators to be mutually orthogonal). Therefore, we should search for a method that is capable of simultaneously extracting EEG spectral components or atoms (and their scalp landscapes) having maximal temporal covariance with certain BOLD profiles. One possible candidate for such a multimodal analysis is Partial Least-Squares (PLS) regression, introduced in fMRI analysis by McIntosh et al. (1996). In PLS, the fMRI data are treated as a matrix (voxels by time). PLS identifies those linear combinations of fMRI voxels that have maximal temporal covariance with linear combinations of a second matrix of independent variables, measured at the same time points. The method hinges on calculating the Singular Value Decomposition (SVD) of the covariance matrix between the fMRI and independent variables. This method has been used for spatio-temporal analysis of event-related potentials (Lobaugh et al., 2001) and simultaneous EEG and MEG data (Düzel et al., 2003).

Fortunately, the PLS technique has been extended by Bro (1996) to deal with multidimensional data, obtaining a new model known as Multiway Partial Least Squares or just N-PLS. This model consists essentially of decomposing the independent and dependent data into multilinear models such that the score vectors from these models have pairwise maximal covariance. The multilinear decomposition is made in the same way as PARAFAC, thus inheriting both advantages and limitations of that model.

In this paper, the N-PLS model will be introduced for decomposing the EEG into a sum of atoms each with a specific spatial, temporal, and spectral factors or "signatures". Simultaneously, the fMRI data will be decomposed into the same number of atoms, each the product of spatial and temporal signatures, in such a way that the latter will have maximal covariance with the EEG temporal signature. The source localization of the EEG spatial signature (topography) of each atom will be examined, allowing separate analysis of the tomographic distribution of the EEG sources (what we will call sources of the "EEG rhythm") and those tomographic sources obtained as the fMRI tomograms that we interpret as the "brain rhythm" generating system. It should be noted that we have limited our consideration to oscillatory components of the EEG. While important, they do not exhaust the list of interesting phenomena that might possibly relate to the fMRI. Transient waveforms, for example, are not optimally described in the time–frequency framework. In principle, the methods developed here may be extended to consider this situation.

Methods

Consider a matrix, $\mathbf{F}_{(N_s \times N_t)}$, of the fMRI data ($N_s$ voxels, N_t time points) that is recorded simultaneously with the EEG time series from N_d electrodes. Further, define the EEG signal recorded during each TR (the period needed to collect an MRI volume) as a "segment." In the present case, the time-varying EEG spectrum, $\mathbf{S}(\omega)_{(N_d \times N_t)}$ (ω being the frequency), for N_t segments, was estimated via the Thomson multitaper method (Thomson, 1982). Let **s** be a reference EEG time signal, formed by selecting a linear combination, **a**, of the EEG electrode power in a given band of frequencies Ω, which was then filtered by the hemodynamic response, **H**:

$$\mathbf{s}_{(1\times N_t)} = \mathbf{a}^T_{(1\times N_d)} \sum_{\omega\in\Omega} \mathbf{S}(\omega)_{(N_d\times N_t)} \mathbf{H}_{(N_t\times N_t)} \quad (1)$$

where the symbol, $\mathbf{a}^T$, represents the transpose of vector **a**. Then, the correlations between the fMRI matrix and the reference EEG signal: $\mathbf{r}_{(N_s \times 1)}$= corr(**F**, **s**) are mapped.

In the analysis performed by Goldman et al. (2002), they chose an ad hoc linear combination, **a** (an occipital electrode set), and frequency band (8–12 Hz) for finding the reference EEG time signal. We will extend this analysis to estimate the optimal linear combination of electrodes, and a particular spectral window defining an optimal frequency band $\sum_{\omega\in\Omega} \mathbf{b}(\omega)\mathbf{S}(\omega)$. Finally, we will estimate a suitable linear combination, $\mathbf{u}^T_{(1 \times N_s)}$ of the elements of the fMRI matrix to be correlated with a particular EEG time signal.

Parallel Factor Analysis

Recognizing that the time-varying EEG spectrum may be expressed conveniently as a three-dimensional array makes possible the use of Parallel Factor Analysis (PARAFAC) (Carroll and Chang, 1970; Harshman, 1970), a generalization of Principal Component Analysis (PCA) for dealing with multidimensional data. With PARAFAC, the time-varying EEG spectrum is decomposed (in a least-squares sense) into trilinear components, or atoms, each being the product of a spatial, spectral and temporal factors, or signatures.

Unlike PCA, PARAFAC has no rotational freedom; therefore, the decomposition is unique, even without any orthogonality constraints. It has been shown that if the data are approximately trilinear, the correct number of components is used, and the signal-to-noise ratio is adequate, then the PARAFAC algorithm will show the true underlying phenomena (Kruskal, 1976, 1977). Moreover, PARAFAC provides a unique data-determined linear combination, i.e., a reference time signal, to correlate with the fMRI data. The use of PARAFAC in analyzing three-dimensional EEG data, (space, frequency, time) is described in a companion paper (Miwakeichi et al., 2004).

Then, applied to the time-varying EEG spectrum, which is expressed as a three-dimensional matrix $\mathbf{S}_{(N_d \times N_w \times N_t)}$, PARAFAC decomposition establishes an element-wise trilinear model for these data:

$$\hat{S}_{dwt} = \sum_{k=1}^{N_k} a_{dk} b_{wk} c_{tk} + \varepsilon_{dwt} \quad (2)$$

where d, w, and t designate electrode pairs, frequency, and time, respectively, and the term ε_{dwt} represents the error. The total number of components is N_k, each of which is designated by index k. Our problem is to find the so-called "loading matrices", **A**, **B**, and **C** whose N_k columns are the loading vectors $\mathbf{a}_{k(N_d \times 1)}$, $\mathbf{b}_{k(N_w \times 1)}$, and $\mathbf{c}_{k(N_t \times 1)}$ of elements a_{dk}, b_{wk}, and c_{tk} respectively.

We can fit the model expressed in Eq. (2) by finding

$$\min_{a_{dk} b_{wk} c_{tk}} \left|\left| S_{dwt} - \sum_{k=1}^{N_k} a_{dk} b_{wk} c_{tk} \right|\right|^2.$$

The interpretation of the loading vectors is as follows: $\mathbf{a}_k$ is the spatial signature of the kth atom, which is a representative topographic map, or linear combination of electrodes; $\mathbf{b}_k$ is the spectral signature for the kth atom and $\mathbf{c}_k$ is the temporal signature, or time course, for atom k. The only indeterminacies in the least-square solution are the order of components and the scaling of loading vectors. Thus, centering and scaling of the data are needed before decomposition, as is a convention for the signs and scale of the loadings. For PARAFAC, the resulting spectral and spatial loadings are normalized, while the non-normalized loading will be the temporal factor, reflecting the scale of the data.

It is important to select the most appropriate number, N_k, of components. The Core Consistency Diagnostic (Corcondia) is an approach for so doing that applies especially to PARAFAC models, and has been shown to be a powerful and simple tool for determining the appropriate number of components in multiway models (Bro, 1998). In this work, we use not only Corcondia but also the evaluation of the systematic variation left in the model's residuals.

PARAFAC has been extensively used in chemometrics, psychometrics, and econometrics. In the field of spatio-temporal analysis of Event-Related Potentials, PARAFAC has been shown to be formally equivalent to the Topographic Components Model (TCM) (Möcks, 1988a,b). Field and Graupe (1991) offered some general guidelines for the correct exploration of EEG data with PARAFAC. The basic pitfall of the application of PARAFAC is that the data are actually not trilinear, and, hence, a careful preprocessing and analysis of the results most be done for assessing the validity of the model.

Multiway Partial Least-Squares Regression

Despite being a useful tool for data explorations and to find a unique reference EEG time signal, the PARAFAC analysis leaves two important questions unanswered:

a) Which frequency components are related to the fMRI signal?
b) What is the optimal linear combination of EEG electrodes to correlate with the fMRI?

Partial Least-Squares regression is an automatic procedure to find the linear combination that maximizes the temporal correlation between the EEG and fMRI data (de Jong and Phatak, 1997; Martens and Naes, 1989). This method is similar to Principal Components Regression (PCR), where the independent variable is decomposed into a set of scores, and the dependent variable is regressed on these scores instead of the original variable. The main difference being that in PLS regression, both independent and dependent variables are decomposed such that these scores have maximal covariance; that is, the relevant variations of the independent variable for predicting the dependent variable are emphasized. An extension of the PLS regression model to three-way data was proposed by Ståhle (1989). Later, Bro (1996) developed a general multiway PLS (N-PLS) regression model that was shown

to be optimal according to the theory of PLS and had a particular case numerically equivalent to that of Ståhle. N-PLS seeks in accordance with the philosophy of PLS to describe the covariance of the dependent and independent variables. This is achieved by fitting multilinear models simultaneously for independent and dependent variables and for a regression model relating the two decomposition models. On the other hand, as covariance is the product of the correlation and the variances, these three measures actually are maximized collectively.

According to Bro (1996), the model is known as N-PLS or Multilinear PLS in general, and the specific model to be used in this work is called tri-PLS2. This follows from its having a three-way decomposition for the independent variable (*tri*), which will be the time-varying EEG spectrum, and a two-way or bilinear decomposition for the dependent variable (*2*), corresponding to the fMRI data. This can be considered as a form of PARAFAC decomposition constrained by additional conditions of maximal covariance with certain BOLD components. The structural model can be expressed as:

$$\hat{S}_{dwt} = \sum_{k=1}^{N_k} a_{dk} b_{wk} c_{tk} + e_{dwt}$$

$$\hat{F}_{st} = \sum_{k=1}^{N_k} u_{sk} v_{tk} + \varepsilon_{st}$$

where ε_{st} and e_{dwt} are elements of noise matrices and the index, s, represents the voxels or grid points inside the brain. These decomposition models are estimated iteratively, component-wise, by finding a set of normalized vectors, $\mathbf{a}_k$, $\mathbf{b}_k$, and $\mathbf{u}_k$ such that the least-squares score vectors, $\mathbf{c}_k$ and $\mathbf{v}_k$, have maximal covariance. It is worth underscoring that the N-PLS model is unique, as it consists of successively estimated one-atom models, each of which is itself always unique. On the other hand, note that the EEG data must first be preprocessed, both by removing muscle and motion artifacts, replacing them by linear interpolation of the data, and by convolution of the EEG spectrum with the hemodynamic impulse response function (Cohen, 1997). A graphical representation of the tri-PLS2 method is shown in Fig. 1.

The interpretation of loading vectors is straightforward. The spectral signature of the EEG for the k atom, $\mathbf{b}_k$, will allow the identification of those brain rhythms whose time-varying envelopes has maximal covariances with the BOLD signal. The spatial signature of the fMRI for atom k, $\mathbf{u}_k$, is a tomographic map (which is not a correlation map) showing those BOLD signals whose time courses are correlated maximally with the EEG. Finally, the spatial signature of the EEG, $\mathbf{a}_k$, is a representative topography of atom k, extracted by asking for the maximal temporal correlation between EEG and fMRI.

The decomposition is made component-wise; that is, for each component (atom), a rank-one model is built of both the independent variable 3D matrix **S**, and the dependent variable 2D fMRI matrix, **F**. These models are then subtracted from the original data, and a new atom of signatures is found from the residuals. The calculation for one atom of the tri-PLS2 model is developed in detail in Appendix A. As in PARAFAC, a convention about signs and scale is needed. In this case, the non-normalized factors will be the temporal signatures of both the EEG and the fMRI data, while the other signatures are normalized. Signs were assigned to ensure that the correlation between fMRI and EEG temporal signatures for the alpha atom were positive. Moreover, in this work, it is important to obtain smooth images as atoms of the spatial signature of the fMRI. For the sake of simplicity, the raw data can be presmoothed and the same smoothed signatures will be obtained from the decomposition (Bro, personal communication). Therefore, the raw fMRI data are presmoothed to obtain smoothed atoms for the spatial signature of fMRI. Smoothing consisted of applying the nearest neighbor moving average three times to the raw fMRI data.

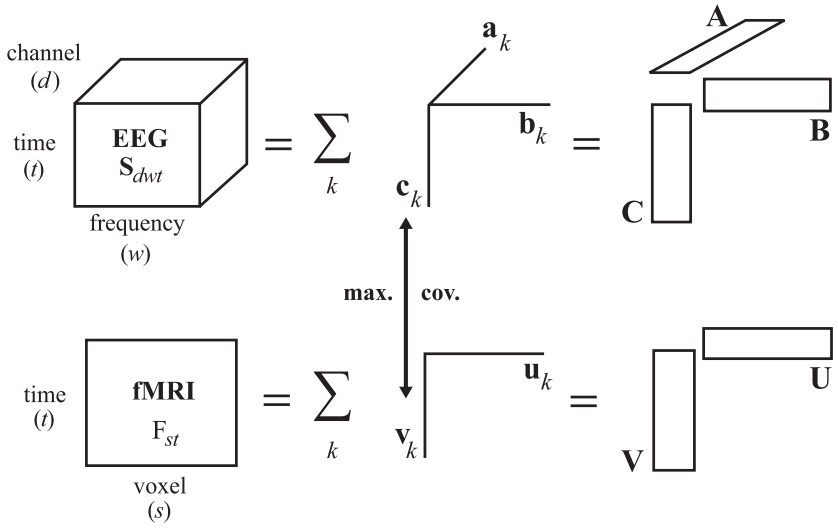

Fig. 1. Tri-PLS2 diagram. The time-varying EEG spectrum is represented as a three-dimensional array indexed by time (t), frequency (w), and channel (d). The fMRI matrix is indexed by time and voxels (s). Both data are decomposed into a sum of atoms or components. Each EEG atom have spatial ($\mathbf{a}_k$), spectral ($\mathbf{b}_k$), and temporal ($\mathbf{c}_k$) signatures. fMRI atoms have a spatial ($\mathbf{u}_k$) and temporal ($\mathbf{v}_k$) signature. The extraction of atoms is performed simultaneously by constraining the temporal signatures to have maximal covariance. Joining all atoms for each signature allows them to be expressed in matricial notation, obtaining corresponding matrices **A**, **B**, **C**, **V**, **U**.

Assessment of N-PLS model

The advantages of N-PLS over bilinear methods are that it is much more parsimonious, easier to interpret, and less prone to noise. This advantages hold even over nonlinear calibration models (e.g., feedforward neural networks) because they are bilinear in the decomposition of the independent variable and the nonlinearity is introduced only in the relation of this decomposition with the dependent variable. Another advantage is that the algorithm is faster than other multilinear decomposition methods (e.g., PARAFAC) due to the relatively few parameters to estimate and particularly, because the tri-PLS algorithm boils down to eigenvalue problems.

However, this model has its own pitfalls. The basic problem is the appropriateness of the trilinear model. As this is a data-dependent question, there is not a general and straightforward answer. If there is no any a priori knowledge about the three-way nature of a given data, one could try different methods to see which one describes the data best. In the case of several methods fitting the data equally well, one should choose the simplest model and in this regard multilinear models are preferred over bilinear ones. On the other hand, although it has been shown that models like N-PLS seldom fail to converge and offer degenerate solutions (Bro, 1998), these are problems that can arise in multiway methods and should be taken into account in the exploration of the data.

In practice, it is convenient to apply a PARAFAC decomposition to the EEG data before applying tri-PLS2 model. This initial exploration will allow to assessing the appropriateness of the trilinear model for the time-varying EEG spectrum, to identify possible outliers in the data, and the estimation of the number of significant atoms present in the data. The implementation of PARAFAC used in this work is contained in a Matlab Toolbox developed by Bro and available on the web. It provides several diagnostic tools, such as Corcondia, residuals plots, leverages plots, convergence, and explained variance of the data, among others.

As said above, the appropriate number of components was obtained with the residual analysis and the Corcondia index. This index was also used for assessing the trilinear structure of the data as shown in Estienne et al. (2001). The analysis of leverages allowed to detecting four outliers in the time mode. These four time windows (or segments) were discarded from the data for subsequent analysis. We also removed some constant signature (nonphysiologically meaningful) in the frequency mode by an adequate centering across this mode. Furthermore, comparison between the loadings of the time-varying EEG spectrum decomposition provided by PARAFAC and those provided by tri-PLS will validate (at a preliminary level) the truthfulness of the results obtained. A detailed explanation about the use of the diagnostic tools for this exploratory analysis and discussion of the reliability of PARAFAC model can be found in Bro (1998) and Miwakeichi et al. (2004).

Source localization analysis

The spatial signature for the time-varying EEG spectrum, $\mathbf{a}_k$, may be analyzed further by source reconstruction methods, such as Low-Resolution Electromagnetic Tomography (LORETA) (Pascual-Marqui et al., 1994) to find those underlying electrical sources that are correlated temporally with the BOLD signal. However, LORETA cannot be applied directly since $\mathbf{a}_k$ is not derived from voltages but rather from the power spectra of voltages. Therefore, in this case, we developed a procedure that allows the estimation of the spectra of the EEG sources on the basis of the spectra of the observed voltages. We shall call this type of source localization "Source Spectra Imaging" (SSI). This is based on the following assumptions:

- There is no spatial correlation between scalp voltage measurements.
- There is no spatial correlation between electric current densities inside the brain.
- The source spectra (variances of current densities in frequency domain) to be estimated will be the smoothest one in space.
- The source spectra is the same in the x, y, and z directions.

The detailed formulation for obtaining this inverse solution can be found in a companion paper (Miwakeichi et al., 2004). It must be emphasized that the assumptions behind this inverse solution can classify it as a distributed inverse solution, whose pitfalls and drawbacks have been extensively described in the literature (Fuchs et al., 1999; Pascual-Marqui, 1999).

Moreover, the EEG data analyzed in this work corresponds to voltages measured in an array of 16 bipolar pairs; therefore, to find the SSI solution, the problem of transforming these bipolar measurements into unipolar voltages must be addressed. We must thus construct the matrix $\mathbf{M}$ that transforms the spatial signatures of the EEG, $\mathbf{a}_k^{\text{uni}}$, obtained (ideally) from a unipolar array, into those measured from bipolar recordings (Eq. (3)). A partial representation of matrix $\mathbf{M}$ is given in Eq. (4). Then, $\mathbf{a}_k^{\text{uni}}$ is estimated by multiplying Eq. (3) by the Moore-Penrose pseudo-inverse of matrix $\mathbf{M}$.

$$\mathbf{a}_k = \mathbf{M}\mathbf{a}_k^{\text{uni}} \tag{3}$$

$$\boldsymbol{M} = \begin{array}{cccccccc} Fp2 & \dots F7 & F8 & \dots O2 & \dots T4 & \dots T6 & \\ 1 & \dots 0 & -1 & \dots 0 & \dots 0 & \dots 0 & Fp2-F8 \\ 0 & \dots 0 & 1 & \dots 0 \dots & -1 & \dots 0 & F8-T4 \\ \vdots & \vdots & \vdots & \vdots & \vdots & \vdots & \vdots \\ 0 & \dots 0 & 0 \dots & -1 & \dots 0 \dots & 1 & T6-O2 \\ \dots & \dots & \dots & \dots & \dots & \dots & \vdots \end{array} \tag{4}$$

Further, with this method, we can visualize the spatial signatures of the EEG obtained by tri-PLS2 decomposition (which would correspond to the bipolar topographies) as a topographic map on the head. Finally, it is noteworthy that these topographic maps, and their SSI solutions, are essentially dimensionless, as the former is normalized as part of the scale convention for the tri-PLS2 model.

Statistical inference

Our first inferential problem is to determine whether there is a significant correlation between the time courses of the EEG and fMRI. This can be tested readily by permutation of the time

segments in the time-varying EEG spectrum, which will destroy any temporal correlation between the EEG and fMRI data (Galán et al., 1997). This procedure is not appropriate, however, if there is any autocorrelation in the time series of the EEG data. Using the ARFIT toolbox for Matlab (Schneider and Neumaier, 2001), we fitted an autoregressive model of order 2 (selected automatically by Schwarz's criterion) to the time course of time-varying EEG spectrum. With this information, we applied a block bootstrap method, which is adequate in the case of weak dependence of observations (time points in this case). The method consists of resampling with replacement, using blocks of consecutive time points instead of individual time points. The length of the blocks was chosen to be great enough to preserve the original dependence, so that the empirical distribution of statistics for blocks will resemble that for the original time points (Davison and Hinkley, 1997). On the other hand, it is also desirable to have as many blocks as possible. In our case, we use nonoverlapping blocks of length $l = 2p+1$; $p = 2$ being the order of the autoregressive model. Thus, by applying the tri-PLS2 method for N resampled series, we obtained N different decompositions into atoms of corresponding signatures for each modality. The correlation coefficients between the EEG and corresponding fMRI time courses for each atom were then computed. From the 95th percentile of the empirical distribution of these correlations, we established a significance level for testing of the original correlation.

Our second inferential problem is to determine which voxels in the spatial signature of the fMRI are significantly different from zero. This is important for identifying brain regions that contribute to a particular EEG-fMRI temporal correlation. Thus, for this problem, we used a simple jackknife resampling procedure (Davison and Hinkley, 1997) from which a pseudo t image was constructed. In this specific case, the jackknifed estimate was obtained as follows: the leave-one-out spatial signatures ($\mathbf{u}_i$; $i = 1 \ldots N_t$) of the fMRI were created by leaving out time points one at a time and applying the tri-PLS2 model to the truncated data. The jackknife pseudo observations were then computed as:

$$\boldsymbol{u}_i^* N_t \boldsymbol{u} - (N_t - 1)\boldsymbol{u}_i; \quad i = 1 \ldots N_t$$

where $\mathbf{u}$ is the fMRI spatial signature corresponding to the complete data. This equation holds for all components although we have eliminated the subscript k for simplicity. Using the mean of the pseudo observations ($\bar{\boldsymbol{u}}^* = \frac{1}{N_t}\sum_{i=1}^{N_t} \boldsymbol{u}_i^*$) and the standard deviations $\left(\sigma_{u^*} = \sqrt{\frac{1}{N_t}\sum_{i=1}^{N_t}(\boldsymbol{u}_i^* - \bar{\boldsymbol{u}}^*)^2}\right)$, the pseudo $\mathbf{t}$ image for each atom can be computed as $\mathbf{t}_{\text{image}} = \sqrt{N_t}\frac{\bar{\boldsymbol{u}}^*}{\sigma_{u^*}}$.

Experimental data

The EEG was sampled at 200 Hz from an array of 16 bipolar pairs, (*Fp2-F8*, *F8-T4*, *T4-T6*, *T6-O2*, *O2-P4*, *P4-C4*, *C4-F4*, *F4-Fp2*; *Fp1-F7*, *F7-T3*, *T3-T5*, *T5-O1*, *O1-P3*, *P3-C3*, *C3-F7*, *F7-Fp1*), with an additional channel for the EKG and scan trigger. The fMRI time series was measured in six slice planes (4 mm, skip 1 mm) parallel to the AC–PC line, with the second from the bottom slice through AC–PC. More details about this data set can be found in Goldman et al. (2002). In the work presented here, we have analyzed five simultaneous EEG/fMRI recordings from three different subjects. Informed consent was obtained from all volunteers based on a protocol approved previously by the UCLA Office for the Protection of Research Subjects.

Results

Both PARAFAC and N-PLS techniques were applied to the recorded data sets, and yielded similar results for all subjects. There was no statistical inference about differences among subjects, so, for the purpose of this paper, we present representative data from a single subject. As a first exploration of the data, a PARAFAC model was fitted to the time-varying EEG spectrum. The appropriate number of components for this model was chosen using Corcondia (see above). The model was fitted using direct trilinear decomposition for its initial values.

Three significant atoms or components, characterized by their spectral signature, were extracted by PARAFAC (Fig. 2A). It is

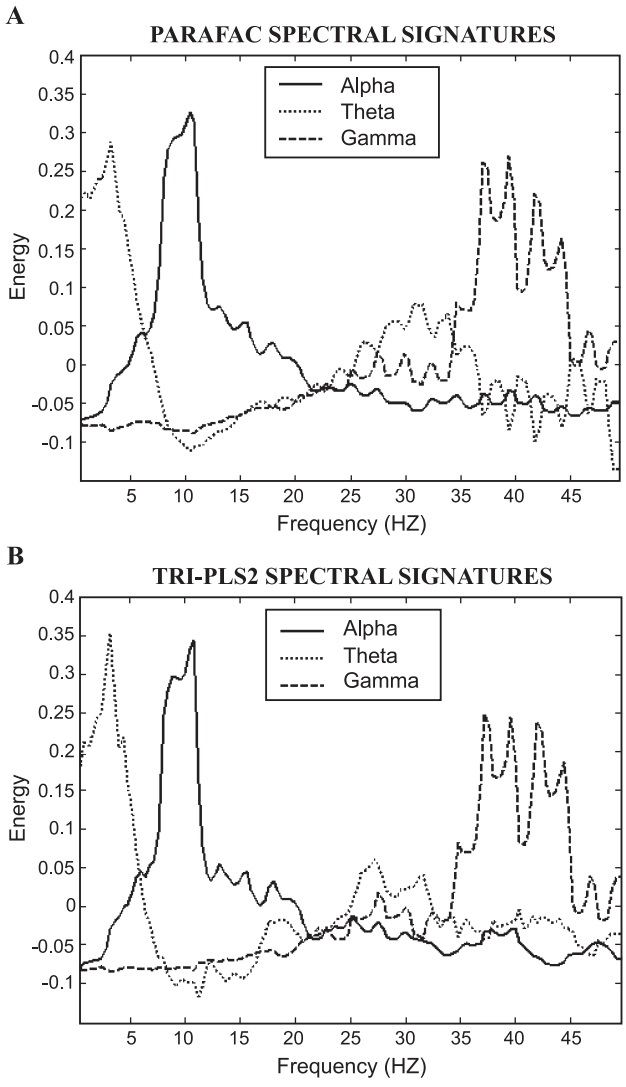

Fig. 2. Spectral signatures of the EEG decomposition. (A) Spectral signatures obtained from PARAFAC decomposition of the time-varying EEG spectrum. Three atoms were extracted. The first has a spectral peak around 10 Hz, corresponding to the well-known alpha rhythm. The second has a spectral peak around 4 Hz, which is a value usually assigned to theta activity. The third atom corresponds to a fast activity with spectral peaks from 35 to 45 Hz, in the gamma range. (B) Spectral signatures of the time-varying EEG spectrum, obtained from the tri-PLS2 model. Three atoms or components were extracted. These spectra resemble strongly those obtained from PARAFAC decomposition.

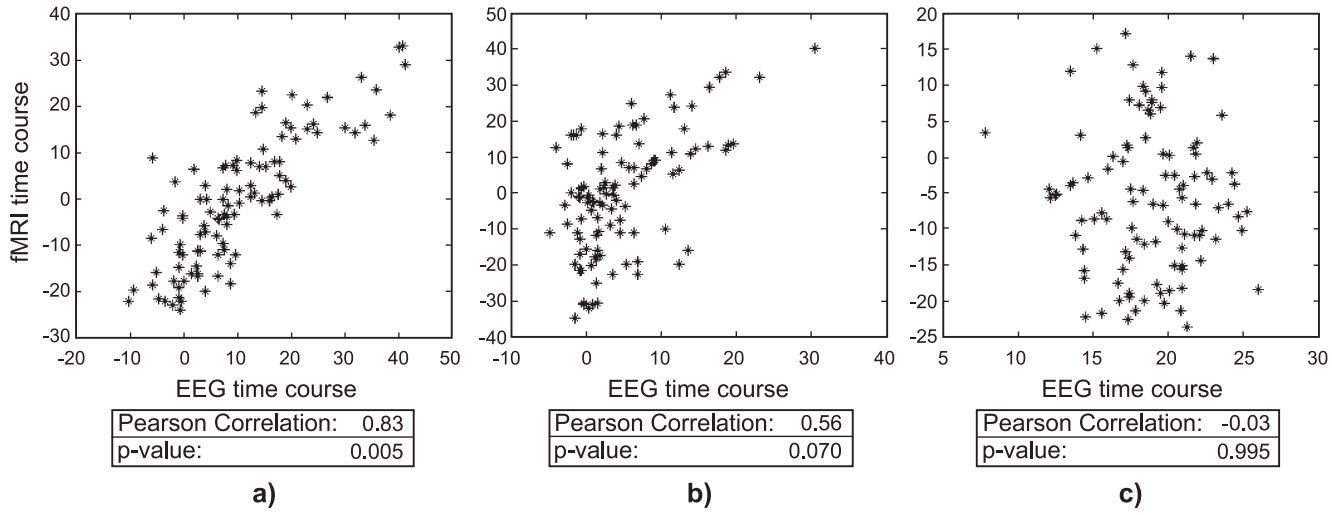

Fig. 3. Scatter plot of fMRI temporal signature against EEG temporal signature. (a) Alpha atom. A nearly linear positive dependence can be seen. The Pearson correlation value is 0.83, corresponding to $P = 0.005$. (b) Theta atom. The linear dependence between the EEG time course and fMRI time course has a positive correlation value of 0.56. However, it is not significant, $p = 0.07$. (c) Gamma atom. There is no clear linear dependence.

easy to recognize the alpha atom with its peak near 10 Hz. A slower theta activity peak is also present with a maximum around 4 Hz, as is a gamma peak in the range from 35 to 45 Hz. The Corcondia for this fit was around 93%, and the explained variation of the data was 53.5%. Moreover, PARAFAC allowed identification of outliers in the temporal signature, which were eliminated from the data for subsequent PARAFAC and posterior analyses.

Using this information, the N-PLS model was applied for only three atoms. In Fig. 2B, the spectral signatures for all atoms are shown, and they resemble strongly the spectra found by PARAFAC decomposition. Fig. 3 shows scatter plots of the temporal signatures of the fMRI vs. the EEG separately for each atom. The alpha and theta activities seem to have clearly positive correlations, but gamma activity does not. The Pearson correlation values are shown for each activity band. Supporting the visual impression, correlations were highest for the alpha atom. By using the 1000 samples of the block bootstrap test described previously, only the alpha atom presents a correlation value with probability lower than 0.05. The theta atom has a non-negligible correlation value, whose empirical probability is slightly higher than the predetermined theoretical significance level of 0.05.

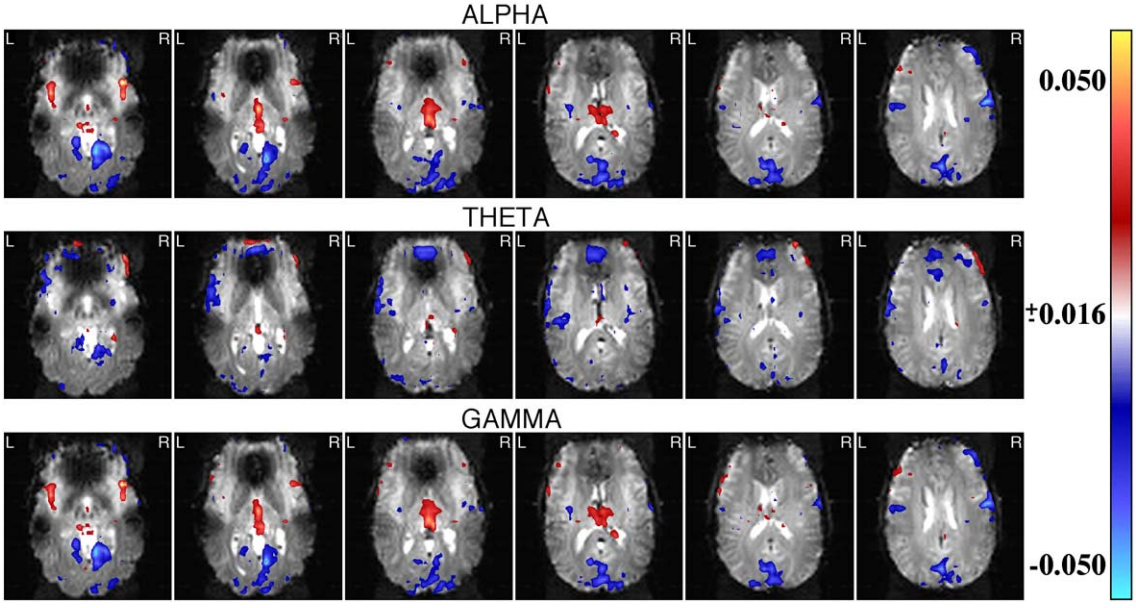

Fig. 4. fMRI spatial signatures for the three atoms. All images were plotted following a color scale from −0.05 to 0.05. However, the components have different minimum and maximum values. Alpha and Gamma atoms have a maximum of 0.055 and a minimum value of −0.066. Theta atom has a maximum value of 0.037 and a minimum of −0.066. The threshold was chosen conveniently to 0.016 for better visualization of the areas with higher values.

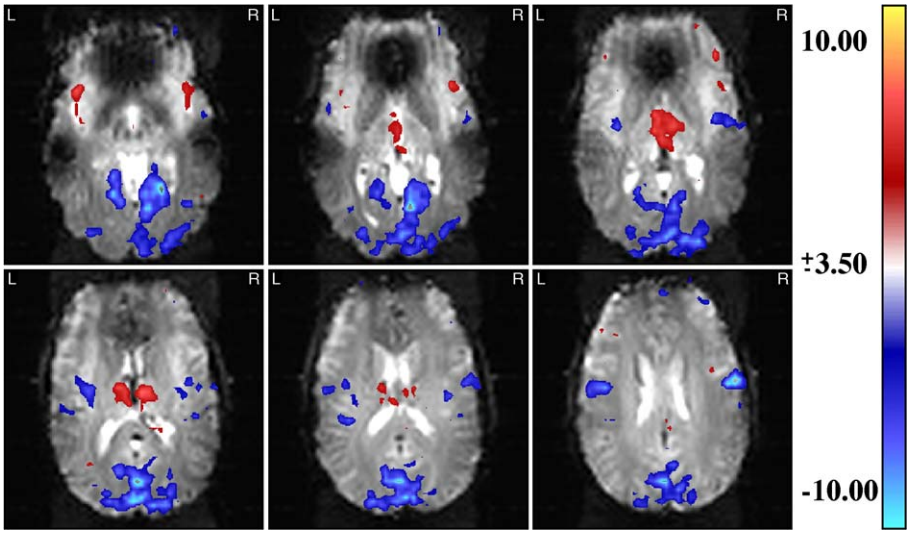

Fig. 5. Jackknifed pseudo *t* image for the fMRI spatial signature of the alpha rhythm atom. The jackknife procedure consisted of leaving out temporal points one at a time and applying the tri-PLS2 model to the truncated data. Then, a *t* value was calculated for each voxel and the resulting image was thresholded to a significance value of ±3.5. Blue regions (anterior median occipital, lateral occipital, occipital pole, and left and right temporal superior) represent those areas with significantly negative temporal correlation with EEG. Thalamus and insula are red representing a significant positive correlation between EEG and fMRI time courses.

Fig. 4 shows the spatial signature of the fMRI decomposition: the $\mathbf{u}_k$ vectors. These are shown as tomograms in which those regions that have negative temporal correlation between EEG and fMRI are blue and those that have positive temporal correlation appear in red. For the alpha atom, the fMRI spatial signature shows positive activation of thalamus and insula, while occipital and superior temporal regions are activated negatively. The theta atom showed predominantly negative activation of anterior cingulate and occipital regions, while the gamma atom resembles the alpha component. For testing the robustness of this type of image, a pseudo *t* image of the alpha atom was calculated, it being the only atom having a significant temporal correlation with the EEG. This image is shown in Fig. 5, and was achieved by the jackknife procedure described above. In this figure, blue regions, (anterior median occipital, lateral occipital, occipital pole, and left and right temporal superior) represent those areas with significant negative

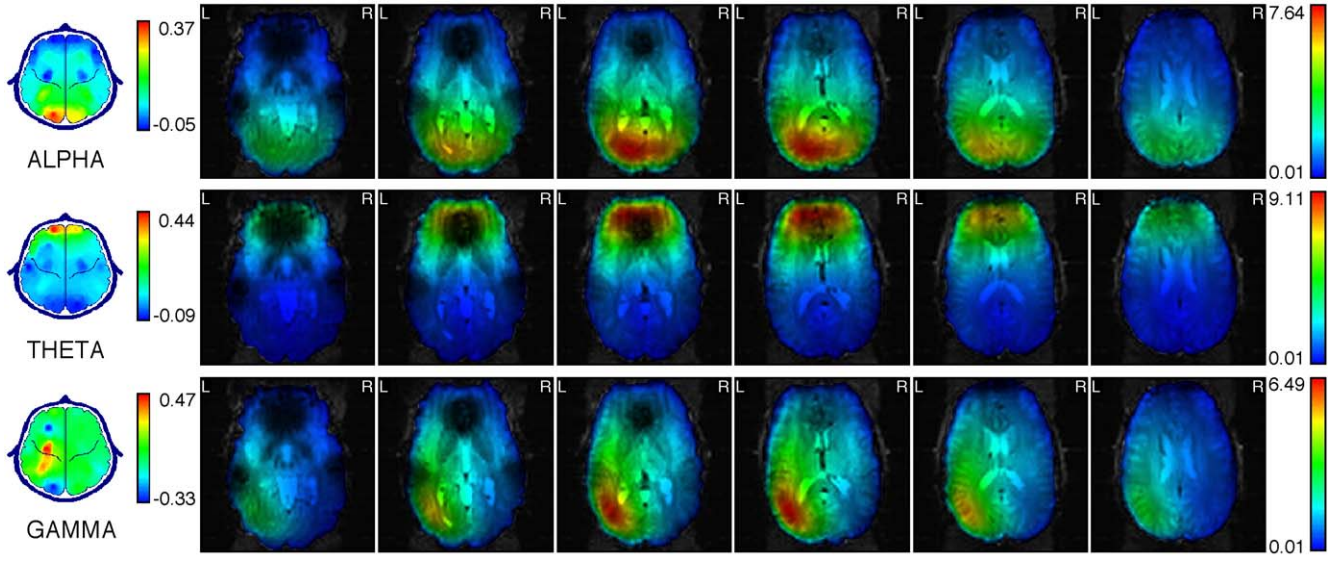

Fig. 6. Spatial signatures of the EEG and its SSI solutions. The topographical representation of spatial signatures of the EEG is shown at the far left. This map was calculated by pseudo-inverting the matrix that transforms topographies from unipolar recordings into those obtained with bipolar derivations. The alpha atom shows higher values at posterior regions, the theta topography has higher values located in frontal regions, and the gamma atom shows maximum values in the left parieto-temporal area. The corresponding SSI solutions are to the right. Maximum activation for the alpha component is located in the occipital area, with higher activation in the left hemisphere. Theta sources are in the anterior cingulate region, and the activated region for the gamma atom is located in the parieto-temporal area. Units for inverse solutions are ignored because energy values for the topographies are plotted and have been normalized as part of the N-PLS algorithm.

temporal correlation with the EEG. The areas corresponding to thalamus and insula are red, representing a significant positive correlation between EEG and fMRI time courses.

From the spatial signature, $\mathbf{a}_k$, of the time-varying EEG spectrum, we estimated those regions inside the brain that contribute to the EEG and that are correlated temporally with fMRI. Fig. 6 shows the topographies or EEG spatial signatures, and their corresponding SSI solutions (current density spectra) for each atom. The topography of the alpha atom shows higher values at posterior regions; the theta topography has higher values in frontal regions, and the gamma atom shows maximum topographic values in the left parieto-temporal area. The Source Spectra Imaging solution for the alpha component showed its maximum activation in the occipital area, with higher activation in the left hemisphere. Sources for theta atom are in the anterior cingulate region, and the activated region for the gamma atom is in the parieto-temporal area.

Discussion

This paper introduces a new method, trilinear Partial Least Squares (tri-PLS2), for the analysis of concurrent EEG/fMRI recordings. This is the first use of Partial Least-Squares techniques to carry out multimodal neuroimaging fusion. Our objective is to identify the coherent systems of neural oscillators that contribute to the spontaneous EEG. Doing so requires the solution of three related problems: (i) decomposing the EEG, in the space–frequency–time domain, into a set of components or atoms, (ii) establishing the relation of these EEG components to concurrent BOLD fluctuations, and (iii) analyzing the sources of the EEG atoms. We shall consider each of these problems in turn. At the outset it should be stressed that the two phenomena—EEG and BOLD—evolve over very different time scales. In fact, we shall be analyzing the *evolutionary spectrum* (Priestley, 1965) of the EEG, a concept based on a locally stationary modeling of the electroencephalogram (Dahlhaus, 1997). It is only the *envelope* of the waves usually analyzed by electroencephalography that will be matched to BOLD.

Atomic decomposition of the EEG

The analysis of the *evolutionary spectrum* of the EEG produces a three-dimensional data array (space–frequency–time). The first choices that come to mind for the decomposition of this array are either Principal Components Analysis (PCA) or Independent Components Analysis (ICA), a set of techniques that have received much recent attention. We decided to avoid these methods, however, for two reasons: First, they achieve a unique decomposition into atoms only by imposing arbitrary mathematical constraints (orthogonality and independence, respectively), and second, these methods are targeted toward two-dimensional arrays (matrices). In our situation, this means "unfolding" the data, stacking the time and frequency components along one dimension, and thereby destroying their distinction; keeping these different dimensions separate seems a much better alternative. A first attempt at a space–frequency–time atomic decomposition was reported in a paper by Koenig et al. (2001). In their method, the decomposition is carried out in several stages; first by the identification of time–frequency atoms, and then by the estimation of distinct topographies that are stable over time. This separation into two stages of analysis is not conceptually necessary, and in fact is not optimal.

Our trilinear method based on Parallel Factor Analysis, introduced in the present paper, allows space–frequency–time estimation in a single step, by minimization of an explicit objective function. The resulting decomposition is intrinsically unique and specifies atoms that are defined as spectral components that vary over time and have a specific topography. A more detailed description of the combined use of PARAFAC, and distributed inverse solutions for in vivo imaging of neural oscillatory systems, is the subject of a companion paper (Miwakeichi et al., 2004). A consistent finding in all data sets analyzed was the appearance of three components whose peaks were within the traditional theta, alpha, and gamma bands. Thus, when looking at the relations of the EEG with BOLD, it is potentially important not to constrain the analysis to a single frequency band, as was done by Goldman et al. (2002), although the present data do not show strong fMRI correlation with the EEG signal in the other bands.

It is remarkable that the restriction of maximal correlation with the BOLD signal produces spectra that are practically the same as those obtained by the PARAFAC decomposition. Based on the diagnostic tools, the physiological interpretability, and the replicability among several data sets, we can say that these are meaningful results, although we cannot ensure that they correspond with the real underlying physical phenomena. Therefore, it can be concluded that we have obtained robust and physiologically meaningful results with the use of tri-PLS algorithm.

Relating EEG atoms to the BOLD signal

As shown here, it is possible to constrain the trilinear EEG atomic decomposition further by requiring maximal temporal correlation with the BOLD signal, a procedure that extends the classical Partial Least-Squares technique. It is important to say that the correlation found between both temporal signatures was assessed by a block bootstrap method, which is a strong diagnostic tool for obtaining reliable results. Furthermore, the spatial signature of the fMRI was also statistically validated with the use of a jackknife procedure. These kind of diagnostic tools provide additional evidence on the robustness of the model assumed, i.e., about how well the properties of the data fit the assumptions of the model.

The alpha component has a temporal relation to the BOLD signal that is significant. The regional distribution of the fMRI spatial factor corresponds closely to that described by Goldman et al. (2002), for alpha activity, thus confirming their conclusions. Since the correlation between the EEG and BOLD temporal factors are positive, it becomes clear that the image shown in Fig. 5 is equivalent to the correlation map presented by that group. In particular, there is a positive relation between thalamic and insular BOLD activity and the EEG time course for alpha component. On the other hand, the BOLD signals within parieto-occipital and somatosensory cortices are related inversely to EEG. This latter negative correlation is probably due to a decrease in the amplitude of the EEG in activated cortex in this band, resulting from the temporal resynchronization of the postsynaptic potentials of the involved neural circuits.

The extracted theta component showed moderate temporal correlations that did not reach the pre-established 0.05 level of statistical significance. An examination of the spatial distribution

of the fMRI spatial signature for this atom shows a frontal activation. It is tempting to speculate that this component corresponds to a frontal midline theta rhythm that has not been adequately resolved due to the limited spatial coverage of the brain by the fMRI protocol used. The gamma component was not correlated with the recorded BOLD signal. Once again, we cannot exclude the possibility that better spatial coverage of the brain might reveal such correlations. Further, we can speculate that gamma fluctuations might relate to dynamic and transient assemblies of systems of brain activation (Tallon-Baudry and Bertrand, 1999) that are not stable throughout the recording period.

Analyzing the sources of the EEG atoms

A strength of both PARAFAC and tri-PLS2 is that they identify definite topographic patterns that can be subjected to source localization. These inverse solutions interpreted together with the fMRI spatial factors provide new information on the sources of EEG rhythms.

The Source Spectra Imaging solution for the alpha component reveals activation predominantly in the parieto-occipital region. This corresponds with results on the origins of alpha rhythm that have been reported previously, both using a frequency domain dipole solution (Valdés-Sosa et al., 1998) as well as frequency domain distributed solutions (Casanova et al., 2000). An interesting fact is that the thalamus shows very little activation, in contrast to the high positive correlation found by Goldman et al. (2002), and confirmed by the tri-PLS2 fMRI spatial signature.

This dissociation between the sources of the spatial signature of the EEG atoms and the spatial signature of the fMRI of the alpha atom is likely due to the negligible contribution of the primary current sources of thalamic neurons to the scalp EEG. In this case, the observed correlations between thalamic BOLD and EEG must be indirect. For example, the thalamus is probably correlated negatively with the parieto-occipital cortex, which seems to be the location of the generators of the ''EEG alpha rhythm''. Because the BOLD signal in this region is also correlated negatively with the alpha EEG spectrum, this would explain a positive correlation between alpha power and thalamic metabolic activity as an indirect effect through parieto-occipital cortex. In the terminology of Friston et al. (1996), there is a functional connectivity between the EEG and thalamus, but the effective connectivity path would not be direct, being mediated instead by the parieto-occipital cortex. Thus, according to the definitions given here, insula, thalamus, and parieto-occipital cortex are generators of the ''alpha brain rhythm'' while only parieto-occipital cortex contribute to the ''EEG alpha rhythm''. We note that the analyses presented in this paper do not allow the distinction of whether a structure belonging to a rhythm generating system oscillates in that frequency range. It seems unlikely that joint EEG/fMRI recordings can resolve the extent of phasic, versus tonic, participation in a brain rhythm of a structure that does not produce a measurable EEG. In other words, there is still invisible information for an EEG/fMRI fusion analysis, namely, the fine temporal characteristics of those areas that are invisible in the scalp EEG. In future planned experiments, it may be possible to resolve this issue through conjoint fMRI and depth electrode studies.

The tri-PLS2 method introduced in this paper is an example of multimodal image fusion, which takes advantage of the spatial resolution of the fMRI, as well as the temporal resolution of the EEG. This data analytic approach is capable of parsimoniously determining which EEG components are significant in the final analyses, and of revealing new features of the data by differentiating regions exposed within the fMRI data from those indicated solely through inverse solutions using the EEG. We are pursuing a number of improvements to enhance the integration of both types of data modalities by this method. In the first, we are developing a variant of tri-PLS2 that will estimate the spatial components, not on the scalp topography, as is done now, but instead directly in the source space. This would integrate source localization into the procedure rather than applying it as a postprocessing step for the topographies of the EEG atoms. Additionally, the autocorrelation of both the EEG and BOLD time series will be taken into account, whereas the model presented here ignores this information. Finally, it may well be that there are interactions between time, topography, and frequency spectrum that the current algorithm cannot account for.

Acknowledgments

The authors want to thank Dr. Eduardo Aubert from the Cuban Neuroscience Center for his important collaboration on handling MRI images used in this paper. Also, for their support and continuous comments on this work, we thank Nelson Trujillo, Lester Melie, and Ernesto Palmero from the Neurophysics Department of the Cuban Neuroscience Center. MSC is supported for this work under NIH DA15549 and DA13054.

Finally, we appreciate and thank Prof. Yoko Yamaguchi, head of the Laboratory for Dynamics of Emergent Intelligence of the RIKEN Brain Science Institute, for her hospitality and support for the successful conclusion of this work.

Appendix A. Tri-PLS2 algorithm

To calculate an atom of the tri-PLS2 model, we rewrite the model for dependent and independent variables taking only one atom, k, into account. Here the independent variable is the time-varying EEG spectrum, convolved previously with the hemodynamic response function, which is a three-way array $\mathbf{S}$. The dependent variable is the fMRI 2D matrix $\mathbf{F}$. The structural models then are

$$\hat{S}_{dwt} = a_{dk} b_{wk} c_{tk} \tag{A.1}$$

and

$$\hat{F}_{st} = u_{sk} v_{tk}. \tag{A.2}$$

The score vectors are those dependent on time (temporal signatures), i.e., $\mathbf{c}_k = (c_{1k},\ldots,c_{tk},\ldots,c_{N_{tk}})^T$ and $\mathbf{v}_k = (v_{1k},\ldots,v_{tk},\ldots,v_{N_{tk}})^T$; the others are also called the weights (spatial and spectral signatures of the EEG, spatial signature of the fMRI). The indices $t = 1,\ldots, N_t$, $w = 1,\ldots, N_w$, $d = 1,\ldots, N_d$ and $s = 1,\ldots, N_s$ represent time, frequency, channels, and voxels, respectively. For given weight vectors, the least-squares solution for determining the score vectors are:

$$c_{tk} = \sum_{w=1}^{N_w} \sum_{d=1}^{N_d} S_{dwt} a_{dk} b_{wk} \tag{A.3}$$

and

$$v_{tk} = \sum_{s=1}^{Ns} F_{st} u_{sk}. \tag{A.4}$$

Our problem is to find a set of normalized weight vectors, $\mathbf{a}_k$, $\mathbf{b}_k$, and $\mathbf{u}_k$, which produce score vectors, $\mathbf{c}_k$ and $\mathbf{v}_k$, having maximal covariance. The objective function to be maximized is:

$$\max_{\mathbf{a}_k,\mathbf{b}_k,\mathbf{u}_k} \left[\sum_{t=1}^{N_t} c_{tk} v_{tk} \middle| c_{tk} = \sum_{w=1}^{N_w} \sum_{d=1}^{N_d} S_{dwt} a_{dk} b_{wk} \wedge v_{tk} = \sum_{s=1}^{N_s} F_{st} u_{sk} \right] \tag{A.5}$$

For simplicity, the restriction of normalization on the weight vectors is not made explicit. Eq. (A.5) is not strictly correct because there is no correction for degrees of freedom, but as this correction is constant for a given atom, it will not affect the maximization. Eq. (A.5) also does not express the covariance if **S** and **F** have not been centered.

The next procedure is performed in two ways. First, Eq. (A.5) could be taken to:

$$\max_{\mathbf{a}_k,\mathbf{b}_k} \left[\sum_{t=1}^{N_t} \sum_{w=1}^{N_w} \sum_{d=1}^{N_d} S_{dwt} v_{tk} a_{dk} b_{wk} \right] = \max_{a_k,b_k} \left[\sum_{w=1}^{N_w} \sum_{d=1}^{N_d} z_{dwt} a_{dk} b_{wk} \right], \tag{A.6}$$

where $z_{dwk} = \sum_{t=1}^{N_t} S_{dwt} v_{tk}$ are the elements of an auxiliary matrix, $\mathbf{Z}_k$. If one writes Eq. (A.6) in matrix notation, the equation will become:

$$\max_{\mathbf{a}_k,\mathbf{b}_k} [\mathbf{b}_k^T \mathbf{Z}_k \mathbf{a}_k] \Rightarrow (\mathbf{b}_k, \lambda_k, \mathbf{a}_k) = \mathrm{SVD}(\mathbf{Z}_k, 1). \tag{A.7}$$

In other words, the weight vectors, $\mathbf{a}_k$ and $\mathbf{b}_k$ can be computed from the first component of a singular value decomposition of $\mathbf{Z}_k$ [SVD($\mathbf{Z}_k$, 1)]. This follows directly from the properties of SVD.

Second, substituting in Eq. (A.5) the corresponding score vector for the dependent variable:

$$\max_{\mathbf{u}_k} \left[\sum_{t=1}^{N_t} \sum_{s=1}^{N_s} F_{st} c_{tk} u_{sk} \right] = \max_{u_k} \left[\sum_{s=1}^{N_s} y_{sk} u_{sk} \right], \tag{A.8}$$

where $y_{sk} = \sum_{t=1}^{N_t} F_{st} c_{tk}$ are the elements of an auxiliary vector $\mathbf{y}_k$. Since $\mathbf{u}_k$ is restricted to be normalized, the maximum value of the expression (A.8) is reached when $\mathbf{u}_k$ is a unit vector in the same direction as $\mathbf{y}_k$. Therefore, the solution is:

$$\mathbf{u}_k = \frac{\mathbf{y}_k}{\|\mathbf{y}_k\|} = \frac{\mathbf{F}^T \mathbf{c}_k}{\|\mathbf{F}^T \mathbf{c}_k\|} \tag{A.9}$$

On the other hand, through the models of the data sets given in Eqs. (A.1) and (A.2), the prediction model between **S** and **F** is found by using a regression model for the so-called inner relation (established for the loadings matrices, i.e., for all atoms at the same time):

$$\mathbf{V} = \mathbf{CX} + \mathbf{E}_v.$$

This expression ensures that the maximum covariance restriction holds, and allows prediction of new samples of dependent variables. As the different atoms for score vectors are not always orthogonal, all of these atoms must be taken into account in calculating regression coefficients. The regression thus leads to:

$$\mathbf{x}_k = (\mathbf{C}^T \mathbf{C})^{-1} \mathbf{C}^T \mathbf{v}_k. \tag{A.10}$$

Finally, we can summarize the algorithm as follows:

1. Center **S** and **F**.
2. Let $\mathbf{v}_k$ equal a column in **F**.
3. Atom $k = 1$.
4. Compute matrix $\mathbf{Z}_k$ using **S** and $\mathbf{v}_k$.
5. Determine $\mathbf{a}_k$ and $\mathbf{b}_k$ from Eq. (A.7).
6. Calculate $\mathbf{c}_k$ from Eq. (A.3).
7. Compute $\mathbf{u}_k$ from Eq. (A.9).
8. Compute $\mathbf{v}_k$ from Eq. (A.4).
9. If the results converge, continue. Otherwise go to step 4.
10. Do the regression, finding $\mathbf{x}_k$ from Eq. (A.10).
11. $\mathbf{S}_t = \mathbf{S}_t - c_{tk} \mathbf{b}_k \mathbf{a}_k^T$ (for all t) and $\mathbf{F} = \mathbf{F} - \mathbf{C}\mathbf{x}_k \mathbf{u}_k^T$.
12. $k = k + 1$. Repeat from 4 until **F** is properly described.

References

Babiloni, F., Babiloni, C., Carducci, F., Angelone, L., Del Gratta, C., Romani, G.L., Rossini, P.M., Cincotti, F., 2001. Linear inverse estimation of cortical sources by using high resolution EEG and fMRI priors. IJBEM 3, 1.

Baillet, S., Leahy, R.M., Singh, M., Shattuck, D.W., Mosher, J.C., 2001. Supplementary motor area activation preceding voluntary finger movements as evidenced by magnetoencephalography and fMRI. IJBEM 3, 1.

Bro, R., 1996. Multi-way calibration. Multi-linear PLS. J. Chemom. 10, 47–61.

Bro, R., 1998. Multi-way Analysis in the Food Industry: Models, Algorithms and Applications. PhD Thesis. University of Amsterdam (NL) and Royal Veterinary and Agricultural University (DK).

Carroll, J.D., Chang, J., 1970. Analysis of individual differences in multidimensional scaling via an N-way generalization of '*Eckart–Young*' decomposition. Psychometrika 35, 283–319.

Casanova, R., Valdés-Sosa, P.A., García, F., Aubert, E., Riera, J., Korin, W., Lins, O., 2000. Frequency domain distributed inverse solutions. In: Aine, C.J., Okada, Y., Stroink, G., Swithenby, S.J., Wood, C.C. (Eds.), Biomag 96, Proceedings of the 10th International Conference on Biomagentism. Springer-Verlag, New York (ISBN:0387989153).

Chen, S., Donoho, D., Saunders, M., 2001. Atomic decomposition by basis pursuit. SIAM Rev. 43 (1), 129–159.

Churchland, P.S., Sejnowski, T.J., 1988. Perspectives on cognitive neuroscience. Science 242 (4879), 741–745.

Cohen, M.S., 1997. Parametric analysis of fMRI data using linear systems methods. NeuroImage 6 (2), 93–103.

Dahlhaus, R., 1997. Fitting time series models to non-stationary processes. Ann. Stat. 25, 1–37.

Davison, A.C., Hinkley, D.V., 1997. In: Gill, R., Ripley, B.D., Ross, S., Stein, M., Williams, D. (Eds.), Bootstrap Methods and Their Application. Cambridge Univ. Press, UK.

de Jong, S., Phatak, A., 1997. Partial least squares regression. Recent advances in total least squares techniques and errors—in variables modeling. In: Van Huffel, E. (Ed.), SIAM, Philadelphia.

Düzel, E., Habib, R., Schott, B., Schoenfeld, A., Lobaugh, N., McIntosh, A.R., Scholz, M., Heinze, H.J., 2003. A multivariate, spatiotemporal analysis of electromagnetic time–frequency data of recognition memory. NeuroImage 18, 185–197.

Estienne, F., Matthijs, N., Massart, D.L., Ricoux, P., Leibovici, D., 2001. Multi-way modelling of high-dimensionality electroencephalographic data. Chemom. Intell. Lab. Syst. 58, 59–71.

Field, A.S., Graupe, D., 1991. Topographic component (Parallel Factor) analysis of multichannel evoked potentials: practical issues in trilinear spatiotemporal decomposition. Brain Topogr. 3 (4), 407–423.

Friston, K.J., Frith, C.D., Fletcher, P., Liddle, P.F., Frackowiak, R.S.J., 1996. Functional topography: multidimensional scaling and functional connectivity in the brain. Cereb. Cortex 6, 156–164.

Fuchs, M., Wagner, M., Kohler, T., Wischman, H.A., 1999. Linear and nonlinear current density reconstructions. J. Clin. Neurophysiol. 16 (3), 267–295.

Galán, L., Biscay, R., Rodríguez, J.L., Pérez Abalo, M.C., Rodríguez, R., 1997. Testing topographic differences between event related brain potentials by using non-parametric combinations of permutation tests (published erratum appears in Electroencephalogr. Clin. Neurophysiol. 107(1998 Nov)(5): 380–381). Electroencephalogr. Clin. Neurophysiol. 102 (3), 240–247.

Goldman, R.I., Stern, J.M., Engel, J., Cohen, M.S., 2000. Acquiring simultaneous EEG and functional MRI. Clin. Neurophysiol. 111, 1974–1980.

Goldman, R.I., Stern, J.M., Engel, J., Cohen, M.S., 2002. Simultaneous EEG and fMRI of the alpha rhythm. NeuroReport 13 (18), 2487–2492.

Gonzalez-Andino, S.L., Blanke, O., Lantz, G., Thut, G., Grave de Peralta, R., 2001. The use of functional constraints for the neuroelectromagnetic inverse problem: alternatives and caveats. IJBEM 3, 1.

Harshman, R.A., 1970. Foundations of the PARAFAC procedure: models and conditions for an 'explanatory' multi-modal factor analysis. UCLA Work. Pap. Phon. 16, 1–84.

Horwitz, B., Poeppel, D., 2002. How can EEG/MEG and fMRI/PET data be combined? Hum. Brain Mapp. 17, 1–3.

Ioannides, A.A., 1999. Problems associated with the combination of MEG and fMRI data: theoretical basis and results in practice. In: Yoshimoto, T., Kotani, M., Kuriki, S., Karibe, H., Nakasato, N. (Eds.), Recent Advances in Biomagnetism. Tohoku University. Press, Sendai, pp. 133–136.

Kiers, H.A.L., 1991. Hierarchical relations among three-way methods. Psychometrica 56, 449–470.

Koenig, T., Martí-López, F., Valdés-Sosa, P.A., 2001. Topographic time–frequency decomposition of the EEG. NeuroImage 14, 383–390.

Kruskal, J.B., 1976. More factors than subjects, test and treatments: an indeterminacy theorem for canonical decomposition and individual differences scaling. Psychometrika, 41.

Kruskal, J.B., 1977. Three-way arrays: rank and uniqueness of trilinear decomposition with applications to arithmetic complexity and statistics. Linear Algebra Appl. 18, 95–138.

Lobaugh, N.J., West, R., McIntosh, A.R., 2001. Spatiotemporal analysis of experimental of experimental differences in event-related potential data with partial least squares. Psychophysiology 38, 517–530.

Martens, H., Naes, T., 1989. Multivariate Calibration. Wiley, Chichester.

McIntosh, A.R., Bookstein, F.L., Haxby, J.V., Grady, C.L., 1996. Spatial pattern analysis of functional brain images using Partial Least Square. NeuroImage 3, 143–157.

Miwakeichi, F., Martínez-Montes, E., Valdés-Sosa, P.A., Mizuhara, H., Nishiyama, N., Yamaguchi, Y., 2004. Decomposing EEG data into space–time–frequency components using parallel factor analysis. NeuroImage 22, 1035–1045.

Möcks, J., 1988a. Decomposing event-related potentials: a new topographic components model. Biol. Psychol. 26, 199–215.

Möcks, J., 1988b. Topographic components model for event-related potentials and some biophysical considerations. IEEE Trans. Biomed. Eng. 35, 482–484.

Pascual-Marqui, R.D., 1999. Review of methods for solving the EEG inverse problem. Int. J. Bioelectromagn. 1 (1), 75–86.

Pascual-Marqui, R.D., Valdés-Sosa, P.A., Alvarez, A., 1988. A parametric model for multichannel EEG spectra. Int. J. Neurosci. 40, 89–99.

Pascual-Marqui, R.D., Michel, C.M., Lehmann, D., 1994. Low resolution electromagnetic tomography: a new method for localizing electrical activity in the brain. Int. J. Psychophysiol. 18, 49–65.

Priestley, M.B., 1965. Evolutionary spectra and non-stationary processes. J. R. Stat. Soc., Ser. B Stat. Methodol. 27, 204–237.

Schneider, T., Neumaier, A., 2001. Algorithm 808: ARfit—A Matlab package for the estimation of parameter and eigenmodes of multivariate autoregressive models. ACM Trans. Math. Softw. 27 (1), 58–65.

Singh, M., Patel, P., Al-Dayeh, L., 1998. fMRI of brain activity during alpha rhythm. Int. Soc. Mag. Res. Med. 3, 1493.

Ståhle, L., 1989. Aspects of analysis of three-way data. Chemom. Intell. Lab. Syst. 7, 95–100.

Szava, S., Valdés-Sosa, P.A., Biscay, R., Galán, L., Bosch, J., Clark, I., Jímenez, J.C., 1994. High resolution quantitative EEG analysis. Brain Topogr. 6, 211–219.

Tallon-Baudry, C., Bertrand, O., 1999. Oscillatory gamma activity in humans and its role in object representation. Trends Cogn. Sci. 3 (4), 151–162.

Thomson, D.J., 1982. Spectrum estimation and harmonic analysis. Proc. IEEE 70, 1055–1096.

Trujillo, N.J., Martínez, E., Melie, L., Valdés, P.A., 2001. A Symmetrical Bayesian Model for fMRI and EEG/MEG Neuroimage Fusion. IJBEM 3, 1.

Valdés-Sosa, P.A., Bosch, J., Virués, T., Aubert, E., Fermín, E., González, E., 1998. EEG source frequency domain SPM. NeuroImage 7 (4), 636.

ELSEVIER

NeuroImage

www.elsevier.com/locate/ynimg
NeuroImage 26 (2005) 973

Corrigendum

Corrigendum to "Concurrent EEG/fMRI analysis by multiway partial least squares" [NeuroImage 22 (2004) 1023–1034]

Eduardo Martínez-Montes,[a,*] Pedro A. Valdés-Sosa,[a] Fumikazu Miwakeichi,[b] Robin I. Goldman,[c] and Mark S. Cohen[d]

[a]*Neurophysics Department, Cuban Neuroscience Center, Havana, Cuba*
[b]*Laboratory for Dynamics of Emergent Intelligence, RIKEN Brain Science Institute, Wako, Saitama, Japan*
[c]*Hatch Center for MR Research, Columbia University, New York, NY 10032, USA*
[d]*Ahmanson-Lovelace Brain Mapping Center, UCLA, Medical School, Los Angeles, CA 90095, USA*

Received 22 February 2005; accepted 22 February 2005
Available online 31 March 2005

Some of the mathematical expressions were found to have errors. These errors do not change the conclusions of the paper.

The expression in the last paragraph of the subsection "Statistical Inference," page 1028, first column, should read:

$$\mathbf{u}_i^* = N_t\mathbf{u} - (N_t - 1)\mathbf{u}_i; \qquad i = 1..N_t$$

Furthermore, the equations following this one, which appear within the text of this last paragraph, do not concur with the notation followed in the rest of the paper: nonitalic uppercase bold letters represent matrices and nonitalic lowercase bold letters represent vectors. Thus, the last sentence of the subsection "Statistical Inference" should read:

"Using the mean of the pseudo observations $\left(\bar{\mathbf{u}}^* = \frac{1}{N_t}\sum_{i=1}^{N_t}\mathbf{u}_i^*\right)$ and the standard deviations $\left(\sigma_{\mathbf{u}^*} = \sqrt{\frac{1}{N_t}\sum_{i=1}^{N_t}(\mathbf{u}_i^* - \bar{\mathbf{u}}^*)^2}\right)$, the pseudo **t** image for each atom can be computed as $\mathbf{t}_{image} = \sqrt{N_t}\frac{\bar{\mathbf{u}}^*}{\sigma_{\mathbf{u}^*}}$."

DOI of original article: 10.1016/j.neuroimage.2004.03.038.
* Corresponding author.
E-mail address: eduardo@cneuro.edu.cu (E. Martínez-Montes).
Available online on ScienceDirect (www.sciencedirect.com).

doi:10.1016/j.neuroimage.2005.02.019

ANEXO B. LISTA DE ABREVIATURAS Y ACRÓNIMOS

BMA	Del inglés, Bayesian Model Averaging
BOLD	Del inglés, Blood Oxigenation Level Dependent
CI	Componentes Independientes
CP	Componentes Principales
Corcondia	Del Inglés, Core Consistency Diagnostic
DCP	Densidad de Corriente Primaria
DCRE	Dinámica Cerebral Relacionada a Eventos
EEG	Electroencefalograma o electroencefalografía
EM	Del inglés, Expectation-Maximization
IRMf	Imágenes de Resonancia Magnética funcional
ITC	Del inglés, Intertrial Coherence
Lasso	Del ingles, Least Absolute Shrinkage Selection Operator
LORETA	Del inglés, LOw Resolution Electromagnetic TomogrAphy
MCA	Mínimos Cuadrados Alternantes
MCP	Mínimos Cuadrados Parciales
MCPT	Mínimos Cuadrados Parciales Tensorial
MMP	Del inglés, Multichannel Matching Pursuit
MP	Del inglés, Matching Pursuit
PARAFAC	Del inglés, Parallel Factor
PRE	Potencial Relacionado a Eventos

RPF	Restablecimiento Parcial de Fase
VARETA	Del inglés, VAriable Resolution Electromagnetic TomogrAphy
VBEM	Del inglés, Variational Bayes Expectation-Maximization

ANEXO C. GLOSARIO DE TÉRMINOS INGLÉS-ESPAÑOL

Término en inglés	Equivalente en español usado en la Tesis
Time (phase)-locked activity	Actividad bloqueada en tiempo [Artículo 1].
Background (ongoing) activity	Actividad de fondo [Artículo 1].
Induced activity	Actividad inducida [Artículo 1].
n-way analysis, multiway analysis	Análisis multidimensional [Bro 1998].
n-way array	Arreglo n-dimensional o tensor de orden n [Bro 1998].
Spatial, spectral, temporal signatures or loadings	Características o factores espaciales, espectrales, temporales. Vectores o tensores de primer orden obtenidos en la descomposición multidimensional, PARAFAC o MCPT [Bro 1998].
Intertrial Coherence	Coherencia Interensayo. Medida matemática de la uniformidad de la distribución de fases de coeficientes complejos [Makeig y col. 2002, Artículo 1].
Cross-talk	Cross-talk. Obtención de componentes que muestran mezcla de actividades en una descomposición PARAFAC [Bro 1998, Beckmann 2005].
Degeneracy	Degeneración. Obtención de factores en PARAFAC con alta correlación entre distintas componentes [Bro 1998].
Redundant dictionary	Diccionario redundante o sobrecompleto. Conjunto de funciones que forman una base sobrecompleta [Artículo 2].
EEG resting state	EEG en estado de reposo. EEG registrado en un estado de reposo físico con ojos cerrados [Artículo 7].

Electrocorticogram, ECoG	Electrocorticograma. Medición del potencial eléctrico en electrodos insertados directamente en la corteza cerebral durante cirugía [Artículo 3].
Outliers	Elementos atípicos. Aunque no existe una definición matemática rigurosa, estos son elementos que están distantes numéricamente del resto de los datos.
Spectral Entropy	Entropía espectral. Entropía Informacional de la densidad espectral del EEG, vista como función de distribución de probabilidad [Artículo 6].
Information Entropy	Entropía Informacional. Entropía definida por Shannon en la Teoría de la Información [Shannon 1948].
Sparse	Esparcidas. Se dice que una función es esparcida si toma valor cero en la mayor parte de su dominio. Un vector es esparcido si la mayor parte de sus elementos son nulos.
Time-varying EEG spectrum	Espectro variante en el tiempo del EEG. Consiste en el espectro estimado (con la Transformada de Fourier u otro método) en segmentos consecutivos de EEG [Artículo 7].
Epileptic spikes	Espigas epilépticas. Tipo de actividad eléctrica usual en los pacientes epilépticos que se caracteriza por ser un pico de voltaje de duración muy corta.
Phase-locking factor	Factor de bloqueo de fase. Medida matemática que sirve de estadígrafo en el test de Rayleigh de uniformidad de fases. Es matemáticamente igual al ITC [Tallon-Baudry y col. 1996].
Box-like function	Función de pulso rectangular [Artículo 5].
Non-convex function	Función no convexa. [Artículo 5].
L1-norm, L2-norm	Función norma L1 y norma L2 [Artículo 5].
Sleep spindles	Husos de sueño. Oscilación corta (1-3 s) y de frecuencia entre 7 y 14 Hz que aparece en el EEG registrado durante el sueño [Anderer y col. 2001].

Topographic time-frequency method	Método tiempo-frecuencia topográfico [Koenig y col. 2001].
Alternating least squares	Mínimos Cuadrados Alternantes [Bro 1998].
Alternating penalized least squares	Mínimos Cuadrados Alternantes Penalizados [Artículo 5].
Multiway (multilinear) partial least squares (NPLS)	Mínimos Cuadrados Parciales Tensorial (MCPT) [Bro 1996].
Multiple penalized least squares model	Modelos de mínimos cuadrados penalizados múltiples [Artículo 5].
PARAFAC screening	Monitoreo o exploración con PARAFAC. Análisis PARAFAC con uno o dos factores fijos para la búsqueda de la actividad definida por estos [Artículo 4].
Event-related potential, evoked potential (ERP)	Potencial relacionado a evento (PRE) [Artículo 1].
Signal-to-noise ratio	Relación señal-ruido. Razón entre una medida de la varianza o energía de la señal y de su ruido. Se utiliza fundamentalmente para simular datos ruidosos [Artículos 1 y 5].
Partial phase resetting (PPR)	Restablecimiento parcial de fase (RPF) [Makeig y col. 2002].
Second trigonometric momento	Segundo momento trigonométrico [Mardia 1972].
Inverse solutions, source localization methods	Soluciones inversas, métodos de localización de fuentes [Artículos 2 y 3].
Test of equality of eigenvalues	Test de igualdad de autovalores de una matriz [Mardia 1976].
Tomograms, tomographic maps	Tomogramas, mapas tomográficos. Mapas de alguna magnitud directamente en voxeles definidos en el cerebro [Goldman y col. 2002, Artículo 7].

Short Time Fourier Transform	Transformada de Fourier de Tiempo Corto. Transformación de Fourier a segmentos de la señal que son usualmente multiplicados por funciones "ventanas" con una localización temporal definida [Makeig 1993].
Voxel	Voxel. Elemento de volumen en que se divide el cerebro para asignar magnitudes cuantificadas como imágenes de resonancia magnética funcional y densidad de corriente primaria.
Wavelet	Wavelet. Es un tipo de función oscilatoria que puede ser trasladada en tiempo y dilatada (modulada en frecuencia) [Tallon-Baudry y col. 1997].

ANEXO D. PRESENTACIONES EN EVENTOS CIENTÍFICOS

1. Martínez-Montes, E., Trujillo-Barreto, N., Goldman, R., Cohen, M., Valdés-Sosa, P.A. Trilinear Partial Least Squares Analysis for EEG-fMRI fusion. Human Brain Mapping 2002, Sendai, Japón, Junio 2-6, 2002.
2. Martínez-Montes, E., Trujillo-Barreto, N., Goldman, R., Cohen, M., Valdés-Sosa, P.A. Trilinear Partial Least Squares Analysis for EEG-fMRI fusion. Bioinformatics Cuba-UK. Universidad de la Habana, Diciembre 16-19, 2002.
3. Martínez-Montes, E., Trujillo-Barreto, N., Goldman, R., Cohen, M., Valdés-Sosa, P.A. Multi-way Partial Least Squares Analysis for concurrent EEG-fMRI recordings. Workshop on Brain Dynamics. Centro de Neurociencias de Cuba, Ciudad Habana, Febrero 17-21, 2003.
4. Miwakeichi, F., Martínez-Montes, E., Valdés-Sosa, P.A., Nishiyama, N., Mizuhara, H., Yamaguchi, Y. Parallel Factor Analysis can extract significant activities in multichannel EEG. 9th International Conference on Functional Mapping of the Human Brain, Nueva York, Junio 19-22, 2003.
5. Goldman R.I., Martínez-Montes E., Valdés-Sosa P.A., Cohen M.S. Convergent evidence for distributed sources of alpha rhythm. Neuroscience 2003: Annual meeting of the Society for Neuroscience, Washington, USA, Noviembre 8-12, 2003.
6. Martínez-Montes, E., Trujillo-Barreto, N., Goldman, R., Cohen, M., Valdés-Sosa, P.A. Trilinear Partial Least Squares Analysis for EEG-fMRI fusion. 6th International Conference on Operative Research. Universidad de la Habana, Septiembre 15-19, 2003.

7. El-Deredy, W., Martínez-Montes, E., Lage-Castellanos, A., Bringas, M.L., Valdés-Sosa, P.A. Phase resetting? Consequences on subsequent stimulus processing. 12th Annual Meeting of the Organization for Human Brain Mapping, Florencia, Italia, Junio 11-15, 2006.
8. Martínez-Montes, E., Sánchez-Bornot, J.M., Valdés-Sosa, P.A. Generalized Penalized PARAFAC analysis of EEG time series. 13th Annual Meeting of the Organization for Human Brain Mapping, Chicago, USA, Junio 10-14, 2007.
9. Martínez-Montes, E., Sarmiento-Pérez, R., Sánchez-Bornot, J.M., Valdés-Sosa, P.A. Information Entropy-based penalty for PARAFAC analysis of resting EEG. 1st International Conference on Cognitive Neurodynamics, Shanghai, China, Noviembre 17-21, 2007.
10. Martínez-Montes, E., Cuspineda, E., El-deredy, W., Sánchez-Bornot, J.M., Lage-Castellanos, A., Valdés-Sosa, P.A. Exploring event related brain dynamics with test on complex valued time-frequency representations. 4th Congress of the Cuban Society and First Ibero-American Workshop on Clinical Neurophysiology, Varadero, Cuba, Marzo 11–14, 2008.
11. Martínez-Montes, E., Valdés-Sosa, P.A. Exploring changes in phase of EEG oscillations with tests on complex valued time-frequency representations [abstract]. Presented at the 14th Annual Meeting of the Organization for Human Mapping, June 15-19, 2008, Melbourne, Australia. Available on CD in NeuroImage.
12. Martínez-Montes, E., Sánchez-Bornot, J.M., Valdés-Sosa, P.A. Penalized PARAFAC analysis of resting-state EEG. 4th Congress of the Cuban Society and

First Ibero-American Workshop on Clinical Neurophysiology, Varadero, Cuba, Marzo 11–14, 2008.

13. El-deredy, W., Martínez-Montes, J.M., Valdés-Sosa, P.A. Phase resetting and event related potentials: the controversy continues. 10th International Conference on Cognitive Neuroscience, Bodrum, Turkey, Septiembre 1-5, 2008.